Role of Tissue Inhibitor of Metalloproteinase 4 (TIMP4) and TIMP3 in Vascular Diseases

by

Mei Hu

A thesis submitted in partial fulfillment of the requirements for the degree of

Doctor of Philosophy

Department of Physiology
University of Alberta

ABSTRACT

Atherosclerosis and aortic aneurysms are two major vascular diseases, and extracellular matrix (ECM) plays an important role in both as a non-cellular component of the aortic wall that also regulates vascular cell behavior and function. Atherosclerosis is a major contributor to cardiovascular complications and has been significant healthcare burden worldwide. It is a chronic inflammatory disease characterized by accumulation of lipids and ECM in the arterial wall. Tissue inhibitor of metalloproteinases (TIMPs) can impact atherosclerotic plaque deposition by regulating vascular ECM turnover, infiltration of inflammatory cells, and plaque stability. Aortic aneurysm is a permanent localized dilation of the vessel characterized by the degradation of aortic ECM, elevated matrix metalloproteinases (MMPs) activities and localized inflammatory responses. TIMPs play an important regulatory role in the pathogenesis of aortic aneurysms through modulating MMP activities. Both thoracic and abdominal aortic aneurysms (TAAs & AAAs) progress irreversibly with a high risk of fatal dissection or rupture, and invasive surgical repair is currently the only treatment available due to the lack of drug-based treatment.

TIMPs include 4 family members. Abnormal expression of TIMP1, TIMP2 and TIMP3 has been found in patients with atherosclerosis. However, the role of TIMP4 in atherosclerosis has not been reported so far. Therefore, we first investigated the role of TIMP4 in atherosclerosis. Mice lacking low-density lipoprotein receptor (*Ldlr*) and *Timp4* (*Ldlr*$^{-/-}$/*Timp4*$^{-/-}$) were fed high fat (HFD) or regular laboratory diet. After 3 or 6 months, HFD-fed male and female *Ldlr*$^{-/-}$/*Timp4*$^{-/-}$ mice exhibited higher plaque density in the abdominal aorta (but not in the thoracic aorta) compared to *Ldlr*$^{-/-}$ mice. Although plasma lipid and cholesterol levels were lower in *Ldlr*$^{-/-}$/*Timp4*$^{-/-}$-HFD mice, cholesterol content in the abdominal aorta was higher along with elevated inflammatory cytokines,

MMP activities, macrophage-like smooth muscle cells (SMCs) in *Ldlr*$^{-/-}$/*Timp4*$^{-/-}$-HFD compared to *Ldlr*$^{-/-}$-HFD mice. *In vitro*, oxidized LDL markedly increased CD68 expression, reduced SMC markers, increased lipid uptake and reduced cholesterol efflux protein ABCA1 in *Ldlr*$^{-/-}$/*Timp4*$^{-/-}$ compared to *Ldlr*$^{-/-}$ SMCs from abdominal, but not thoracic aorta. TIMP4 expression in the abdominal aorta and its corresponding SMCs was ~2-fold higher than in the thoracic aorta and thoracic SMCs; TIMP4 levels decreased following HFD. *Timp4*-deficiency in bone marrow-derived macrophages did not alter their foam cell formation capacity in response to oxidized LDL treatment.

Considering the link between atherosclerosis and AAA, I then investigated the susceptibility of *Timp4*-deficient abdominal aorta to AAA and the role of atherosclerosis in this susceptibility. I established a hypercholesterolemic aneurysm model in *Ldlr*$^{-/-}$ or *Ldlr*$^{-/-}$/*Timp4*$^{-/-}$ mice by using HFD and Angiotensin II (Ang II). We found despite more plaque deposition in the abdominal aorta, the incidence and severity of AAA in *Ldlr*$^{-/-}$/*Timp4*$^{-/-}$ mice was much less than in *Ldlr*$^{-/-}$ mice.

Accordingly, I next investigated if *Timp4*-deficiency reduced susceptibility to aortic aneurysm by subjecting the *Timp4*$^{-/-}$ mice to a different model of aortic aneurysm (peri-adventitial elastase-induced-AAA or TAA). I also used *Timp3*$^{-/-}$ mice in parallel to compare the impact of TIMP4 loss to the absence of another TIMP in these models. I found that loss of TIMP3, but not TIMP4, exacerbated TAA and AAA severity in males and females. *Timp3*$^{-/-}$ mice exhibited more increased proteinase activity and SMC phenotypic switching post-AAA and -TAA compared to the parallel WT and *Timp4*$^{-/-}$ groups. *Timp3*$^{-/-}$ mice exhibited increased infiltration of inflammatory cells in the media post-AAA, but in the adventitia post-TAA. Consistent with this observation, *Timp3*$^{-/-}$ mice showed impaired intimal barrier integrity following AAA, but a greater adventitial neovascularization post-TAA. *Timp4*$^{-/-}$ and WT mice responded similarly to TAA and AAA

induction. In healthy human aorta specimens, TIMP3 was detected in media and intima in the abdominal aorta, and additionally in the adventitia in the thoracic aorta; and decreased in these regions in AAA and TAA specimens. TIMP4 levels remained unchanged in these specimens.

In summary, this research has demonstrated that TIMP4 protects against plaque deposition in the abdominal aorta independent of plasma cholesterol levels. However, loss of TIMP4 did not increase susceptibility to aortic aneurysm in the hyperlipidemic model or the elastase model indicating that *Timp4*-deficiency increases susceptibility to atherosclerosis but not to aortic aneurysm, whereas *Timp3*-deficiency exacerbated aortic aneurysm, highlighting the disease-specific function of different TIMPs in the vasculature.

PREFACE

This thesis is the original work by Mei Hu. All work in the thesis was conducted in Dr. Zamaneh Kassiri's laboratory in Heritage Medical Research Center, 474, Department of Physiology, University of Alberta, Edmonton, AB, Canada. Human diseased aortic specimens were procured from patients who underwent open surgical repairs for abdominal aortic aneurysm or bicuspid aortic valve-associated aeropathy at the Grey Nuns Hospital and University of Alberta Hospital, Edmonton, AB. Non-diseased human aortas were obtained through the Human Organ Procurement and Exchange (HOPE) program (Alberta, Canada) from donors. Informed and signed consents were obtained from all participants. The study protocols were approved by the Human Research Ethics Review Process (HERO) at the University of Alberta.

All animal procedures were performed according to the ARRIVE (Animal Research: Reporting of *in vivo* Experiments) guidelines, and in accordance with the guidelines of Animal Care and Use Committee (ACUC) and the Canadian Council of Animal Care (CCAC). The protocol numbers for atherosclerosis and aneurysm animal studies in this dissertation are AUP1362 and AUP1273, respectively.

A version of Chapter 3 of this dissertation has been published as Hu M, Jana S, Kilic T, Wang F, Shen M, Winkelaar G, Oudit GY, Rayner K, Zhang DW, Kassiri Z. Loss of TIMP4 (Tissue Inhibitor of Metalloproteinase 4) Promotes Atherosclerotic Plaque Deposition in the Abdominal Aorta Despite Suppressed Plasma Cholesterol Levels. *Arterioscler Thromb Vasc Biol*. 2021 Jun;41(6):1874-1889. I was responsible for most of the data collection and analysis, as well as the manuscript composition and revision. Drs. S Jana, F Wang, M Shen and T Kilic helped with data collection, Dr. G Winkelaar provided human aorta samples, Drs. GY Oudit GY, K Rayner and DW

Zhang provided critical feedback and input. Dr. Z Kassiri was the supervisory author and was involved with concept formation, manuscript composition and supervised the project.

A version of Chapter 5 of this dissertation has been submitted to a peer-reviewed journal (Arteriosclerosis, Thrombosis, and Vascular Biology) with Hu M, Meganathan I, Kassiri Z. Loss of TIMP3, but not TIMP4, exacerbates thoracic and abdominal aortic aneurysm. I was responsible for most of the data collection and analysis, as well as the manuscript composition. Dr. I Meganathan helped with human aortic endothelial culture and permeability assay. Dr. Z Kassiri was the supervisory author and was involved with manuscript composition and supervised the project.

A version of Appendix A of this dissertation has been published as Hu M, Hiroyasu S, Granville DJ, Kassiri Z. Implications of Sm22α-Cre expression in keratinocytes and unanticipated inflammatory skin lesion in a model of atherosclerosis. Am J Physiol Heart Circ Physiol. 2022 Sep 1;323(3):H528-H534. I was responsible for all the data collection and analysis, as well as the manuscript composition and revision. Dr. Hiroyasu S and Dr. Granville DJ provided critical feedback and input. Dr. Z Kassiri was the supervisory author and was involved with manuscript composition and supervised the project.

DEDICATIONS

I dedicate this dissertation to my family, my parents, my brother, and my boyfriend for all the love, support, companionship, and encouragement they have given throughout the long academic journey.

ACKNOWLEDGMENTS

I would like to express my most sincere gratitude and high regard to my supervisor, Dr. Zamaneh Kassiri. I am grateful for her patient guidance and assistance for my PhD research, and for all her support in terms of time, ideas, and funding to make my PhD program progress smoothly. Her enthusiasm and perseverance in research will also continue to inspire me to pursue a better future.

I am grateful for the support and contribution from many distinguished professors at the University of Alberta, University of Ottawa, University of British Columbia and Osaka Metropolitan University Graduate School of Medicine. I want to express my greatest thanks to my committee members, Dr. Dawei Zhang and Dr. Allan G. Murray, for their advice, insights, and guidance on my PhD projects; to my reading course advisor and candidacy examiner, Dr. Francis Plane, and to my candidacy examiner, Dr. Nadia Jahroudy, for their recognitions and supports of my PhD research. I would also like to thank Dr. Gavin Y. Oudit for providing the human tissue and scientific assistance, and to Dr. Dawei Zhang, Dr. Gerrit Winkelaar, Dr. Katey Rayner, Dr. Sho Hiroyasu and Dr. David J. Granville for their contributions to my manuscripts. I also admire their rigorous research attitudes and approachable working styles, which will benefit me for the rest of my life.

I also would like to sincerely thank all the members in Dr. Kassiri`s lab. They provided great collaboration and help along the way, the time we have spent together has been valuable and unforgettable.

Last but not least, I would like to gratefully acknowledge the financial support provided by the China Scholarship Council (CSC) that supported me from 2017-2021. None of this would have been possible without the financial support of my country.

TABLE OF CONTENTS

ABSTRACT ii

PREFACE v

DEDICATIONS vii

ACKNOWLEDGMENTS viii

TABLE OF CONTENTS ix

LIST OF TABLES xiv

LIST OF FIGURES xv

LIST OF ABBREVIATIONS xvii

CHAPTER 1 ..... ***1***

INTRODUCTION ***1***

1.1. Prologue 2

1.2. Aorta Anatomy and Physiology 3

1.2.1. Structure and function of aorta 3

1.2.2. Different cell types in the aortic wall 5

1.2.3. Vascular ECM structure and properties 8

1.2.4. Regional heterogeneity within the aorta 10

1.3. TIMPs: basic structure and activity 12

1.3.1. Origin and general function 12

1.3.2. Structure, expression, and targets 13

1.3.3. Activities independent of metalloproteinase inhibition 15

1.3.4. TIMP-knockout phenotypes in mice 16

1.4. Physiological Remodeling of Vascular ECM 18

1.5. Atherosclerosis 19

1.5.1. The formation of atherosclerotic plaque 20

1.5.2. Reverse cholesterol transport in atherosclerosis 22

1.6. Aortic Aneurysm 23

1.6.1. Abdominal aortic aneurysm 23

1.6.2. Thoracic aortic aneurysm 25

1.6.3. Management and treatment of aortic aneurysm 28

1.6.4. Rodent models of abdominal and thoracic aortic aneurysm 30

1.7. Atherosclerosis and Aortic Aneurysms 31

1.8. ECM Remodeling in Vascular Diseases 32

1.8.1. ECM remodeling in atherosclerosis 32

1.8.2. ECM remodeling in aortic aneurysm 33

1.9. The Roles of TIMPs in Vascular Diseases 34

1.9.1. TIMPs in atherosclerosis 35
1.9.2. TIMPs in aortic aneurysm 37
1.10. TIMPs in Therapeutics 39
1.11. Characterization of TIMP4 and Its Role in Vascular Diseases 40
1.11.1. Structure, regulation, function 40
1.11.2. Role in cancer progression and heart diseases 41
1.11.3. Role in vascular diseases 42
1.12. Characterization of TIMP3 and Its Role in Vascular Diseases 44
1.12.1. Structure, regulation, and targets 44
1.12.2. Function in ECM remodeling, inflammatory, angiogenesis and apoptosis 45
1.12.3. Multifaced role of TIMP3 in aortic aneurysm 46
1.13. Rationale 48
1.14. Hypotheses and Objectives 49
CHAPTER 2 51
MATERIALS AND METHODS 51
2.1. Antibodies 52
2.2. Other Reagents 52
2.3. Human Control (non-diseased) and Diseased Aortic Specimen Procurement 54
2.4. Experimental Animal Care, Breeding and Genotyping 55
2.5. Experimental Mouse Model of Atherosclerosis 57
2.6. Angiotensin II Pump Implantation 58
2.7. Induction of Abdominal Aortic Aneurysm and Thoracic Aortic Aneurysm by Peri-adventitial Application of Elastase 59
2.8. Tissue and Plasma Collection 61
2.9. *En face* Oil Red-O (ORO) Staining, Lipid Deposition Visualization and Quantification 62
2.10. Cholesterol, Lipid and Lipoprotein Measurements in Plasma and Aortic tissue 63
2.11. Morphometric and Immunofluorescent Analyses of the Aorta 64
2.12. Filipin Staining and Visualization of Unesterified Cholesterol 65
2.13. BODIPY Staining and Detection of Neutral Lipid Deposits in Tissue and SMCs 65
2.14. In Situ Gelatin Zymography 66
2.15. Gelatin Zymography 67
2.16. *In vivo* Evans Blue Permeability Assay 67
2.17. *En Face* Immunostaining for VE-cadherin 68
2.18. Macrophage Isolation and Culture 69
2.19. Smooth Muscle Cell Isolation and Culture 70

2.20. Immunofluorescent Staining for Trans-differentiation of SMCs to Macrophage-Like Cells, and Macrophages to Foam Cells 70
2.21. Primary Human Aortic Endothelial Cell Culture and siRNA Transfection 71
2.22. *In vitro* Endothelial Cell Permeability Assay 72
2.23. RNA Extraction and Quantitative Real-time PCR 73
2.24. Protein Extraction and Immunoblotting Analysis 75
2.25. Beads-based Multiplex Cytokine Protein Array 76
2.26. Statistics 77
CHAPTER 3 78
ROLE OF TIMP4 IN ATHEROSCLEROSIS 78
3.2. Introduction 80
3.3. Methods 81
3.3.1. Human Abdominal Aorta Specimens 81
3.3.2. Animals 81
3.3.3. Tissue and plasma collection 82
3.3.4. *En face* Oil Red-O (ORO) staining, lipid deposition visualization and quantification 83
3.3.5. Cholesterol, lipid and lipoprotein measurements in plasma and aortic tissue 83
3.3.6. Morphometric and immunofluorescent analyses of the aorta 84
3.3.7. Filipin staining and visualization of unesterified cholesterol for aorta 84
3.3.8. BODIPY staining and detection of neutral lipid deposits in aortic tissue and primary SMCs 85
3.3.9. In situ gelatin zymography 85
3.3.10. Macrophage isolation and culture 85
3.3.11. Smooth muscle cell isolation and culture 86
3.3.12. Immunofluorescent staining for trans-differentiation of SMCs to macrophage-like cells, and macrophages to foam cells 86
3.3.13. RNA extraction and quantitative real-time PCR 87
3.3.14. Protein extraction and immunoblotting analysis 87
3.3.15. Beads-based multiplex cytokine protein array 87
3.3.16. Statistics 88
3.4. Results 88
3.4.1. *Timp4*-deficiency increases plaque deposition in the abdominal but not in the thoracic aorta 88
3.4.2. High fat-induced rise in plasma cholesterol and TG is suppressed in mice lacking TIMP4 93
3.4.3. Adverse aortic remodeling and higher cholesterol content in the abdominal aorta of *Ldlr*$^{-/-}$*/Timp4*$^{-/-}$-HFD mice 94
3.4.4. Increased inflammation detected in the abdominal aorta of *Ldlr*$^{-/-}$*/Timp4*$^{-/-}$-HFD mice 96
3.4.5. Loss of TIMP4 increases protease activity in the abdominal aorta 99
3.4.6. Regional expression profile of TIMPs in the aorta and aortic SMCs 101
3.4.7. Loss of TIMP4 does not increase transformation of macrophages to foam cells 102
3.4.8. Timp4-deficiency renders SMCs more prone to transformation to macrophage-like cells 105
3.4.9. Atherosclerotic abdominal aortas from patients show reduced TIMP4 with increased lipid deposition 110
3.5. Discussion 113
3.6. Conclusion 115
CHAPTER 4 117

ROLE OF TIMP4 IN ATHEROSCLEROSIS-RELATED AORTIC ANEURYSM 117

4.1. Introduction 118

4.2. Methods 119

4.2.1. Experimental animals and procedures 119
4.2.2. Angiotensin II pump implantation 119
4.2.3. *En face* Oil Red-O (ORO) staining 119
4.2.4. Histological staining 120

4.3. Results 120

4.3.1. Less severe aortic aneurysm developed in *Ldlr*$^{-/-}$/*Timp4*$^{-/-}$ mice after Ang II infusion 120
4.3.2. More atherosclerotic plaque deposited in *Ldlr*$^{-/-}$/*Timp4*$^{-/-}$ abdominal aorta 120
4.3.3. *Timp4*-deficiency ameliorated adverse ECM remodeling and the development of Ang II-mediated aneurysm 121

4.4. Discussion 123

CHAPTER 5 125

ROLE OF TIMP4 VERSUS TIMP3 IN AAA AND TAA 125

5.1. Introduction 127

5.2. Methods 128

5.2.1. Human control (non-diseased) and aneurysmal thoracic and abdominal aorta specimen procurement 128
5.2.2. Animals 129
5.2.3. Induction of abdominal aortic aneurysm and thoracic aortic aneurysm by peri-adventitial application of elastase 129
5.2.4. Aorta collection and imaging 130
5.2.5. Morphometric and immunofluorescent analyses of human and mouse aorta 130
5.2.6. In situ zymography 131
5.2.7. Gelatin zymography 131
5.2.8. *In vivo* Evans blue permeability assay 132
5.2.9. *En face* immunostaining for VE-cadherin 132
5.2.10. Primary human aortic endothelial cell culture, siRNA transfection and *in vitro* permeability Assay 132
5.2.11. RNA and protein extraction and analyses 133
5.2.12. Statistics 133

5.3. Results 134

5.3.1. Loss of TIMP3, but not TIMP4, Exacerbates AAA and TAA 134
5.3.2. SMC Transformation and Increased Proteinase Activity in *Timp3*$^{-/-}$ Aneurysmal Aorta 138
5.3.3. Different Pattern of Inflammation in *Timp3*$^{-/-}$ Aortic Wall following AAA vs TAA 143
5.3.4. *Timp3*-deficiency Increased Intimal Permeability in AAA, and Increased Peri-adventitial Vascularization in TAA 145
5.3.5. TIMP3 is Significantly Decreased in AAA, but Increased in TAA Specimens from Patients 150

5.4. Discussion 152

CHAPTER 6 156

DISCUSSION 156

6.1. Important findings 157

6.1.1. Plasma cholesterol levels are not the sole indicator of atherosclerosis risk 157

6.1.2. TIMP4 protects abdominal aorta SMCs from transforming to macrophage-like cells in hyperlipidemic conditions....158
6.1.3. TIMP4 is one of the factors underlying the regional heterogeneity of the aorta....159
6.1.4. TIMP3 maintains aortic EC barrier integrity by preserving adhesion molecules in aortic aneurysm....160
6.1.5. TIMP3 has a region-specific function in the aorta....162
6.2. Clinical significance of abdominal aortic atherosclerosis....162
6.3. Perspectives of developing TIMP3 or TIMP4 mutants as potential therapeutic strategies for vascular diseases....163
CHAPTER 7....165
LIMITATIONS AND FUTURE DIRECTIONS....165
7.1. Limitations....166
7.1.1. Limitations of mouse models for understanding human atherosclerosis....166
7.1.2. Experimental TAA and AAA model....167
7.2. Future Directions....167
7.2.1. To further validate the cell-specific function of TIMP4 in vascular disease....167
7.2.2. To further explore the underlying mechanism by which *Timp4*-deficiency impedes Ang II induced-AAA....168
REFERENCES....169

LIST OF TABLES

TABLE 1. 1 REGIONAL HETEROGENEITY WITHIN THE AORTA 12
TABLE 1. 2 A SUMMARY OF THE GENERAL PROPERTIES OF THE FOUR HUMAN TIMPS 15
TABLE 1. 3 MOUSE PHENOTYPES RESULTING FROM DELETION OF INDIVIDUAL TIMP GENES 16
TABLE 1. 4 COMPARISON OF THORACIC AND ABDOMINAL AORTIC ANEURYSM 29
TABLE 1. 5 GENES ASSOCIATED WITH HERITABLE THORACIC AORTIC DISEASE IN HUMANS 29
TABLE 1. 6 RODENT MODELS OF ABDOMINAL AND THORACIC AORTIC ANEURYSM 31
TABLE 1. 7 TIMPS IN ATHEROSCLEROSIS AND AORTIC ANEURYSMS 38
TABLE 2. 1 PRIMARY ANTIBODY DILUTION IN DIFFERENT APPLICATIONS 52
TABLE 2. 2 CLINICAL INFORMATION FOR THE HUMAN AORTA SPECIMENS 54
TABLE 2. 3 INFORMATION OF EXPERIMENTAL MICE 55
TABLE 2. 4 PCR REACTIONS FOR *TIMP3, TIMP4* AND *LDLR* MUTATIONS 56
TABLE 2. 5 PRIMERS FOR *TIMP4*, *LDLR* AND *TIMP3* PCR REACTIONS 57
TABLE 2. 6 NUTRIENT INFORMATION OF TD.88137 CALORIES DIET 57
TABLE 2. 7 MOUSE ASSAY IDS FOR THE GENES THAT WERE MEASURED BY TAQMAN REAL-TIME PCR 74

LIST OF FIGURES

FIGURE 1. 1 DIAGRAM OF ABOUT THE AORTA. 5

FIGURE 2. 1 FLOW CHART FOR BREEDING OF HETEROZYGOUS *LDLR*$^{-/-}$/ *TIMP4*$^{-/-}$ DOUBLE KNOCK OUT MICE IN 3 GENERATIONS. 56

FIGURE 2. 2 THE PERCENTAGE WEIGHT GAIN OF *LDLR*$^{-/-}$ AND *LDLR*$^{-/-}$/*TIMP4*$^{-/-}$ MICE AFTER 3-MONTH OR 6-MONTH HFD. 58

FIGURE 3. 1 *TIMP4* (TISSUE INHIBITOR OF METALLOPROTEINASE 4)-DEFICIENCY LEADS TO INCREASED PLAQUE DEPOSITION IN THE ABDOMINAL BUT NOT THE THORACIC AORTA DESPITE LOWER PLASMA CHOLESTEROL AND TRIGLYCERIDE IN MALE MICE. 90

FIGURE 3. 2 *TIMP4*-DEFICIENCY IN FEMALE MICE LEADS TO MORE PLAQUE DEPOSITION IN THE ABDOMINAL BUT NOT THE THORACIC AORTA. 91

FIGURE 3. 3 WILDTYPE (WT) AND *TIMP4*-DEFICIENT (*TIMP4*$^{-/-}$) MICE DO NOT DEVELOP ATHEROSCLEROTIC PLAQUES AFTER 6 MONTHS OF HFD FEEDING. 92

FIGURE 3. 4 *LDLR*$^{-/-}$/*TIMP4*$^{-/-}$ MICE HAVE LESS PLAQUE DEPOSITION IN THE AORTIC SINUS. 92

FIGURE 3. 5 ABDOMINAL AORTA IN *LDLR*$^{-/-}$/*TIMP4*$^{-/-}$ MICE SHOW ADVERSE REMODELING ASSOCIATED WITH PLAQUE BUILD-UP AND HIGHER CHOLESTEROL CONTENT. 95

FIGURE 3. 6 HIGHER PLAQUE DENSITY IN *LDLR*$^{-/-}$/*TIMP4*$^{-/-}$ MICE IS ASSOCIATED WITH GREATER INFLAMMATION IN THE ABDOMINAL AORTA AFTER 3-MO HIGH-FAT DIET (HFD). 97

FIGURE 3. 7 *LDLR*$^{-/-}$/*TIMP4*$^{-/-}$ MICE HAVE LESS INFLAMMATION IN THE AORTIC SINUS. 98

FIGURE 3. 8 SYSTEMIC INFLAMMATORY PROFILE IN PLASMA. 99

FIGURE 3. 9 PROTEASE ACTIVITY IS INCREASED IN THE ABDOMINAL AORTA OF HIGH-FAT DIET (HFD)-FED *LDLR*$^{-/-}$/*TIMP4*$^{-/-}$ MICE. 100

FIGURE 3. 10 REGINAL EXPRESSION PROFILE OF THE 4 TIMPS (TISSUE INHIBITOR OF METALLOPROTEINASES) IN THE AORTA AND AORTIC SMOOTH MUSCLE CELLS. 102

FIGURE 3. 11 *TIMP4*-DEFICIENCY DOES NOT ENHANCE THE FORMATION OF MACROPHAGE-DERIVED FOAM CELLS. ... 104

FIGURE 3. 12 PRIMARY ABDOMINAL *LDLR*$^{-/-}$/*TIMP4*$^{-/-}$ AORTIC SMOOTH MUSCLE CELLS HAVE A HIGHER POTENCY IN TAKING UP LIPIDS AND ACQUIRE A "MACROPHAGE-LIKE" PHENOTYPE. 107

FIGURE 3. 13 EXPRESSION LEVEL OF MACROPHAGES, LIPID UPTAKE RECEPTORS AND TRANSPORTERS AND TIMPS IN IN ABDOMINAL AORTIC SMCS AFTER OXLDL TREATMENT. 108

FIGURE 3. 14 THORACIC AORTA SMOOTH MUSCLE CELLS FROM *LDLR*$^{-/-}$/*TIMP4*$^{-/-}$ MICE DO NOT SHOW ENHANCED POTENCY IN LIPID UPTAKE COMPARED TO *LDLR*$^{-/-}$ MICE. 109

FIGURE 3. 15 EXPRESSION OF TIMP4 (TISSUE INHIBITOR OF METALLOPROTEINASE 4) IS DECREASED IN ATHEROSCLEROTIC ABDOMINAL AORTA FROM PATIENTS. 111

FIGURE 3. 16 EXPRESSION OF TIMP4, LIPIDS AND MACROPHAGES IN ATHEROSCLEROTIC HUMAN ABDOMINAL AORTA. 112

FIGURE 4.1 *TIMP4*-DEFICIENCY ALLEVIATED THE AAA FORMATION IN RESPONSE TO ANG II IN HYPERCHOLESTEROLEMIC MICE. 122
FIGURE 5. 1 LOSS OF TIMP3 (TISSUE INHIBITOR OF METALLOPROTEINASE 3) BUT NOT TIMP4 GREATLY EXACERBATES ELASTASE-INDUCED AAA AND TAA. 135
FIGURE 5. 2 TIMP3-DEFICIENCY GREATLY EXACERBATES ELASTASE-INDUCED EXPANSION OF AORTIC ANEURYSMS IN FEMALE MICE. 136
FIGURE 5. 3 *TIMP3*$^{-/-}$ MICE EXHIBIT A GREATER PERIADVENTITIAL FIBROSIS FOLLOWING AAA BUT NOT TAA. 137
FIGURE 5. 4 AORTIC ANEURYSM IN TIMP3-DEFICIENT MICE IS ASSOCIATED WITH GREATER SMOOTH MUSCLE CELL LOSS COMPARED TO *TIMP4*$^{-/-}$ OR WT. 140
FIGURE 5. 5 TIMP3 DEFICIENCY RESULTS IN A GREATER INCREASE IN PROTEASE ACTIVITIES IN AAA AND TAA. 141
FIGURE 5. 6 TAQMAN MRNA EXPRESSION OF MMPS AND TIMPS IN THE THORACIC AORTA AND ABDOMINAL AORTA WITH OR WITHOUT ANEURYSMS IN THE MALE MICE. 142
FIGURE 5. 7 DEFICIENCY OF TIMP3 RESULTED IN MARKEDLY INCREASED ACCUMULATION OF INFLAMMATORY CELLS IN THE MEDIA OF AAA, AND ADVENTITIA OF TAA. 144
FIGURE 5. 8 *TIMP3*-DEFICIENCY COMPROMISED THE ENDOTHELIAL BARRIER IN ANEURYSMAL ABDOMINAL AORTA. 147
FIGURE 5. 9 INCREASED DENSITY OF ADVENTITIAL VASA VASORUM IN *TIMP3*$^{-/-}$-TAA. 148
FIGURE 5. 10 TIMP3 DEFECT DID NOT AFFECT THE ENDOTHELIAL PERMEABILITY OF TAA AND THE ADVENTITIAL VASCULARIZATION OF AAA. 149
FIGURE 5. 11 DIFFERENTIAL EXPRESSION PATTERN OF TIMP3 & TIMP4 IN HEALTHY & ANEURYSMAL ABDOMINAL AND THORACIC AORTA SPECIMENS FROM PATIENTS. 151

LIST OF ABBREVIATIONS

AAA	Abdominal aortic aneurysm
ABCA1	ATP-binding cassette transporter A1
ABCG1	ATP-binding cassette transporter G1
ACE	Angiotensin converting enzyme
ACUC	Alberta Animal Care and Use Committee
ADAM	A disintegrin and metalloproteinase
ADAMTS	A disintegrin and metalloproteinase with thrombospondin motif
AGTR	Angiotensin II receptor
ALK1	Activin receptor-like kinase 1
Ang II	Angiotensin II
ANOVA	Analysis of variance
ApoB-100	Apolipoprotein B-100
ApoE	Apolipoprotein E
ARBs	Angiotensin-II receptor blockers
ARCL1B	Autosomal recessive cutis laxa type 1B
ARRIVE	Animal Research: Reporting of *in vivo* Experiment
AT2R	Ang II type 2 receptor
BAPN	β-aminopropionitrile
BAV	Bicuspid aortic valve
BMM	Bone marrow macrophage
BSA	Bovine serum albumin

CCAC	Canadian Council of Animal Care
CCL	C-C motif chemokine ligand
CD	Cluster of Differentiation
cDNA	Complementary deoxyribonucleic acid
CNS	Central nervous system
cGMP	Cyclic guanosine monophosphate
CSF	Colony-stimulating factor
CXCL	C-X-C motif chemokine ligand
DAPI	4′,6-diamidino-2-phenylindole dihydrochloride
DF20	DMEM/F12 medium supplemented with 20% FBS
DMEM	Dulbecco's modified eagle medium
EC	Endothelial cell
ECM	Extracellular matrix
EDS	Ehlers-Danlos syndrome
EGF	Epidermal growth factor
EGFR	Epidermal growth factor receptor
ERK 1/2	Extracellular signal-regulated protein kinase 1/2
ET-1	Endothelin-1
EVAR	Endovascular aneurysm repair
FAK	Focal adhesion kinase
FBS	Fetal Bovine Serum
FITC	Fluorescein isothiocyanate
FPLC	Fast-protein liquid chromatography

GAGs	Glycosaminoglycan
G-CSF	Granulocyte colony-stimulating factor
GM-CSF	Granulocyte-macrophage colony-stimulating factor
HAoEC	Human Aortic Endothelial Cell
HBSS	Hanks' balanced salt solution
HDL	High-density lipoprotein
H&E	Hemotoxylin and eosin
HFD	High-fat diet
HGF	Hepatocyte growth factor
HOPE	Human Organ Procurement and Exchange
HPRT	Hypoxanthine-guanine phosphoribosyltransferase
HREB	Hearth Research Ethics Board
HTAAD	Hereditary thoracic aortic aneurysm and dissection
IB	Immunoblotting
ICAM-1	Intercellular adhesion molecule 1
ICC	Immunocytochemistry
IHC	Immunohistochemistry
IL	Interleukin
INF- γ	Interferon gamma
IOD	Integrated optical density
LRP	LDL receptor related protein
JAM-A	Junction-associated molecule-A
JNK	Jun NH(2)-terminal kinase

KCL	Potassium chloride
KDa	Kilodalton
KTs	Keratinocytes
LDL	Low-density lipoprotein
LDLR	Low-density lipoprotein receptor
LDS	Loeys-Dietz syndrome
LIF	Leukemia inhibitory factor
LOX	Lysyl oxidase
LOX1	Lectin-like oxidized LDL receptor 1
LRP1	LDL receptor-associated protein 1
LTBP	Latent transforming growth factor β-binding protein
LV	Left ventricular
Mac-2	Macrophage-2
MCP-1	Monocyte chemotactic protein 1
M-CSF	Macrophage colony-stimulating factor
MHY11	Myosin heavy chain-11
MI	Myocardial infarction
MIP-1α	Macrophage inflammatory protein 1-alpha
MMP	Metalloproteinase
MSF	Marfan Syndrome
MSR1	Macrophage scavenger receptor 1
MT-MMP	Membrane-type metalloproteinases
NO	Nitric oxide

OCT	Optimal cutting temperature
OLR1	oxidized low-density lipoprotein receptor 1
ORO	Oil Red-O
oxLDL	Oxidized LDL
PBS	Phosphate-buffered saline
PDGF	Platelet-derived growth factor
PFA	Paraformaldehyde
PGs	Proteoglycans
PMA	Phorbol ester
PPE	Porcine pancreatic elastase
PSR	Picrosirius red
RCT	Reverse cholesterol transport
RFU	Relative fluorescent unit
RPM	Revolutions per minute
RT	Room temperature
SGS	Shprintzen-Goldberg syndrome
α-SMA	Smooth muscle alpha-actin
SM22	Smooth muscle 22
SMC	Smooth muscle cell
SM-MHC	Smooth muscle myosin heavy chain
SP	Sulfated polysaccharide
SPF	Specific pathogen-free
SR-A1	Scavenger receptor class

SR-B1	Scavenger receptor B1
TAA	Thoracic aortic aneurysm
TAC	Trans aortic constriction
TAAD	Thoracic aortic aneurysm dissection
TACE	Tumor necrosis factor-α converting enzyme
TGFβ	Transforming growth factor beta
TIMP	Tissue inhibitors of matrix metalloprotein
TNFα	Tumor necrosis factor alpha
TNFR	Tumor necrosis factor receptor
UTR	Untranslated region
VAF	Viral antibody-free
VCAM-1	Vascular cell adhesion protein 1
VE-cadherin	Vascular endothelial cadherin
VEGF	Vascular endothelial growth factor
VEGFR	Vascular endothelial growth factor receptor
VLDL	Very low-density lipoprotein
VSMC	Vascular smooth muscle cell
VVG	Verhoeff-Van Gieson
WT	Wild type

CHAPTER 1

INTRODUCTION

1.1. Prologue

Atherosclerosis is the underlying cause of cardiovascular disease as well as playing an important role in stroke, chronic kidney disease and peripheral arterial diseases. The cardiovascular disease, primarily myocardial infarction and stroke are the leading cause of mortality and disability worldwide, and although therapies targeting risk factors have significantly reduced clinical events, their progress has stagnated, and a huge economic burden from cardiovascular disease remains [1]. Aortic aneurysm another vascular complication, is an irreversible dilation and structural disruption of aortic wall that predisposes to the potentially fatal consequence of dissection or rupture. However, no drug therapy has been shown to be beneficial in controlling aneurysms or clinic events [2, 3]. TIMPs (tissue inhibitors of metalloproteinases) are a group of endogenous inhibitors of metalloproteinase that can regulate ECM (extracellular matrix) remodeling and affect vascular cells and cell-cell interactions by controlling metalloproteinase proteolytic activity. Atherosclerotic plaques are predominantly composed of various cells and matrices, and degradation of ECM components is characteristic of aortic aneurysm. Abnormal ECM remodeling and degradation owing to elevated matrix metalloproteinases (MMPs) were strongly associated with the development of atherosclerosis and aortic aneurysm [4, 5]. The alterations in TIMP and MMP expression in vascular disease have also been reported in many groups [6-9]. However, the specific mechanisms underlying the role of TIMP in the progression of vascular diseases have not been explored in depth. It has been shown that TIMP4 specifically affects lipid metabolism and regulates smooth muscle cell (SMC) proliferation, while its direct role in atherosclerosis and aortic aneurysms remains unclear. TIMP3 has the broadest spectrum against metalloproteinases and is therefore a master regulator of ECM proteolysis and ectodomain shedding. Considering the

regional heterogeneity of aortic aneurysm formation and development, the different roles of TIMP3 and TIMP4 in the thoracic versus abdominal aortic aneurysm also needs to be investigated.

1.2. Aorta Anatomy and Physiology

The aorta is the main artery that carries oxygenated blood from the heart to the rest of the body. It can be anatomically divided into thoracic and abdominal aorta at the aortic hiatus of the diaphragm. Thoracic aorta can be further divided into aortic root, ascending thoracic aorta, aortic arch and descending thoracic aorta. Abdominal aorta can be divided into suprarenal and infrarenal abdominal aorta. (**Figure 1.1 A**) Aortic root is the portion attached to the heart and contains aortic valves located at the left ventricular outlet. The ascending aorta follows and is the first segment of the aorta. The ascending aorta then arches to left forming the arch of the aorta. The descending aorta is a continuation of aortic arch and ends at the branch where it divides into two common iliac arteries.

1.2.1. Structure and function of aorta

The aortic valves (also known as aortic semilunar valves) permit ejection of blood from the heart into aorta but prevent backflow to left ventricular (LV). They consist of three crescent moon-shaped cusps: the left coronary (left posterior), right coronary (anterior) and non-coronary cusps (right posterior), named for their relationship to the coronary arteries supplying blood to the myocardium. (**Figure 1.1 B**) The aortic arch gives off three major arteries on the superior aspect that supply blood to the head and neck. The descending thoracic aorta is a continuation of the aortic arch, which lies along the left side of spine and gives off many small arteries as it descends. The

abdominal aorta is the direct continuation of the thoracic aorta after it crosses the diaphragm, it is located anterior to the vertebral body and adjacent to the inferior venous cava. There are several major arteries branching from abdominal aorta that supply all organs in the abdomen, including mainly anterior visceral branches (celiac trunk, superior and inferior mesenteric arteries) and paired visceral branches (suprarenal and renal arteries). Based on the location of kidney, the abdominal aorta is also divided into suprarenal and infrarenal abdominal aorta.

The wall of aorta consists of three tunics: tunica intima, tunica media and tunica adventitia. **(Figure 1.1 C)** Tunica intima is the thinnest layer, made up by a monolayer of endothelial cells (EC), a thin layer of basement membrane or basal lamina, a fine network of connective tissue, and a distinct sheet of elastic fibers known as the internal elastic lamina. The basement membrane anchors the endothelium on the connective tissue. The internal elastic lamina forms the boundary between tunica intima and media. The entire layer of intima is permeable, facilitating diffusion of materials between the tunics. Endothelium in tunica intima also integrates physical and neurohumoral signals to regulate vascular tone. The tunica media is comprised of layers of smooth muscle cells (SMC) supported by substantial elastic fibers in a circular wavy arrangement, and a framework of collagenous fibers that bind the tunica media to the intima and adventitia. Separating the tunica media from the tunica adventitia is the external elastic lamina. Tunica media is mainly responsible for vasoconstriction and regulation of the internal diameter. Tunica adventitia is a connective tissue layer, composed primarily of collagen fibers that harbor nerves, lymphatics, and tiny blood vessels, also known as the vasa vasorum. The primary function of tunica adventitia is to restrain the aorta from excessive tensile stretch and recoil.

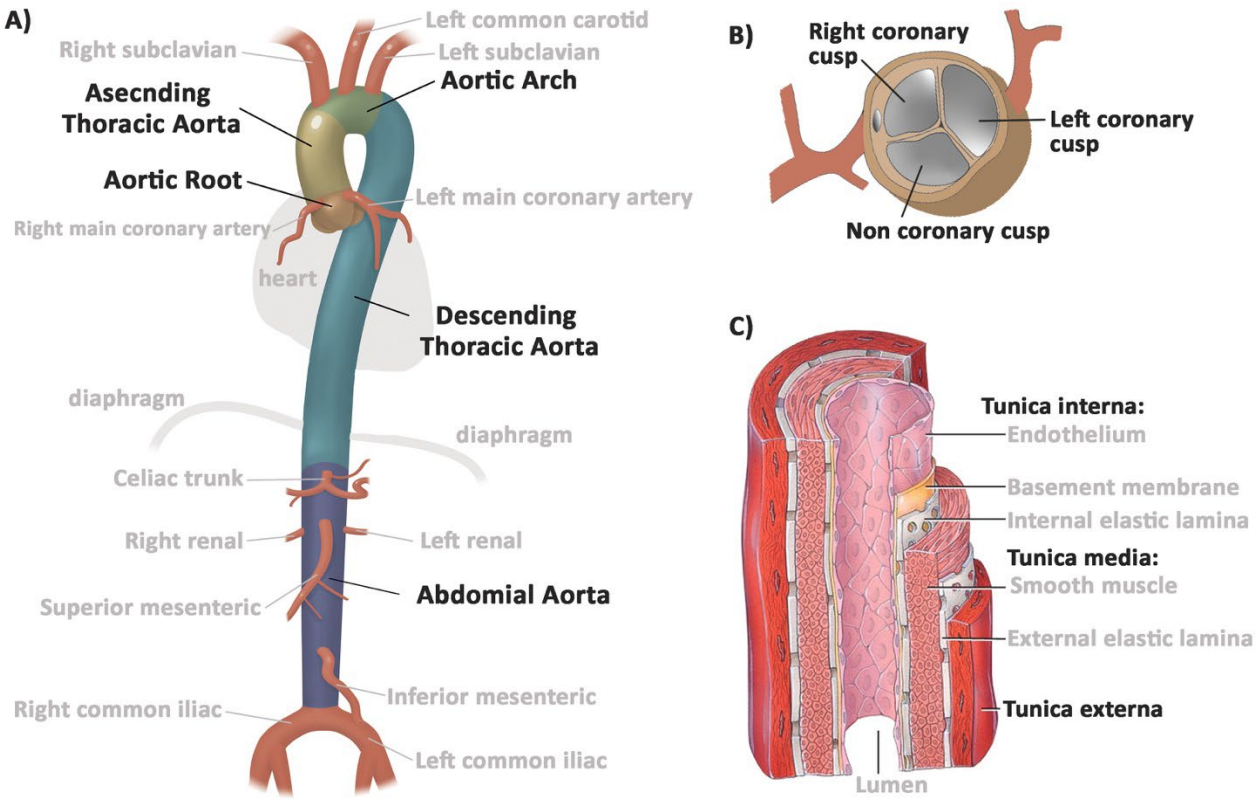

FIGURE 1. 1 DIAGRAM OF ABOUT THE AORTA.

(A) Aorta and its principal branches. (B) Superior view of aortic valve in transverse panel. (C) Structure of aortic wall.

1.2.2. Different cell types in the aortic wall

Different cell types reside in aortic tissue, mainly endothelial cells (ECs), vascular smooth muscle cells (VSMCs), fibroblasts, and progenitor cells. These cells along with the vascular extracellular matrix (ECM), make up the different layers of aortic wall. Cells in the vascular system exhibit varying degrees of plasticity and can undergo remarkable phenotypic and functional changes to adapt to different environmental changes.

The endothelium, or tunica intima is a continuous monolayer of flattened squamous cells that lines the inner surface of the entire vascular tree. This continuous endothelial layer provides an uninterrupted barrier between the blood and the remainder of the vessel wall. Signals or substances

can be exchanged across EC barrier through several ways such as paracellular and transcellular transport [10]. Endothelial barrier integrity and vascular permeability are governed by intercellular junctions, including adherens junctions and tight junctions, which connect adjacent ECs and create the barrier. VE-cadherin is the main component of adherens junction, and tight junctions is mainly composed of members of claudin and junction-associated molecule (JAM) families, occludin, and other adhesion molecules. The phosphorylation of connexins and focal gap formation underlies the mechanism by which endothelial permeability increases in response to various modulators [11]. The primary function of EC is achieved by the production of a variety of factors that regulate vascular tone, vessel wall inflammation, angiogenesis, coagulation and anticoagulation. Functional ECs are sentinels of cardiovascular health. First and foremost, ECs are an important source of vasoactive mediators in arteriae, including vasodilators and vasoconstrictors defined based on their modulation of VSMCs, which also suggests a huge control of ECs over the regulation of vascular tone. Among them, nitric oxide (NO) and endothelium-derived hyperpolarization factors (EDHF) are potent vasodilators released by ECs in large arterial, and endothelin-1 (ET-1) is the most potent vasoconstrictor. In addition, ECs are major participants and regulators of vascular host defense and inflammation by releasing and interacting with a variety of inflammatory mediators [12]. Activated ECs by the inflammatory mediators [e.g., thrombin, bradykinin, interleukin (IL)-1, and tumor necrosis factor (TNF)] increase adhesion molecule expression, cause intercellular gap, increase leukocyte adhesion and trafficking [13]. Furthermore, the intact and functional endothelium is both an anti-inflammatory and an antithrombotic surface, due to the expression of multiple antiplatelet and anticoagulant agents. Another general feature of ECs is induction of neo-angiogenesis. Angiogenesis is a process of de-novo growth of blood vessels by sprouting ECs from existing vasculature, which is regulated by the angiogenic factors, such as vascular endothelial growth factor (VEGF), and involves EC proliferation, degradation of the vascular ECM and EC

migration. The angiogenic response correlates with the degree of inflammatory infiltration of immune cells in the aortic wall [14] and plays a critical role in the development and rupture of aortic aneurysms and atherosclerosis [15-17].

The SMCs are spindle-shaped with an elongated nucleus, they are predominantly localized in the tunica media and embedded circumferentially in the layers of elastic and collagenous fibers. The primary function of SMC is to maintain vascular tone and resistance, and to regulate blood pressure and blood flow distribution through vasoconstriction and vasodilation. Healthy SMCs are in a quiescent and contractile state, presenting an elongated, spindle-like morphology and a "hills and valleys" growth pattern *in vitro*. However, triggered by environmental cues, SMCs can transition between several phenotypic states accompanied by changes in morphology and function. The shift of SMC from a contractile state to a synthetic state is an extensively studied phenotypic switching characterized by the increase in proliferation and migration properties, a critical process that triggers arterial remodeling in response to various stimuli associated with vascular injury and diseases, such as aortic aneurysm, post-angioplasty restenosis and atherosclerosis [18]. These synthetic or differentiated SMCs down-regulate SMC markers [e.g., ACTA2/smooth muscle alpha-actin (α-SMA), transgelin/SM22 alpha, MYH11/smooth muscle myosin heavy chain (SM-MHC)] and secrete ECM proteins. In the progress of atherosclerosis, SMC also undergoes a phenotypic switch characterized by the expression of markers of alternative cell types. Those markers usually are related to a specific state and function carried out by the cell, for example, macrophage-like SMCs have a variety of receptors for lipid uptake and become foam cells by phagocytosis of lipids. Francis's laboratory suggested that ~40% of CD68-positive cells in advanced human coronary atherosclerosis are SMC- rather than leukocyte-originated [19].

The tunica adventitia is home to a series of cell populations, of which fibroblasts are the predominant resident population. Fibroblasts appear as plump spindle-shaped with flat and oval

nuclei, and primarily participate in vascular structural support [20]. Notably, fibroblasts can be activated in response to various external stimuli and differentiate into αSMA-expressing myofibroblast, which is morphologically characterized as large spindle-shaped stellate cells. The myofibroblast is capable of contractility, migration and synthesizing ECM [20], and plays a pivotal role in vascular remodeling, repair, inflammation, neointimal hyperplasia and fibrosis [21-23]. Those activated adventitial fibroblasts are observed to be involved in the development of pulmonary hypertension, atherosclerosis, and aortic aneurysm [24, 25]. The adventitial niche also contains a number of progenitor/stem cells, they are essential for vascular development and maintaining vessel homeostasis [26]. The progenitor cells are mostly latent, and can differentiate into a variety of cells and migrate to the site of injury to participate in vascular repair, remodeling and endothelial regeneration [27, 28].

1.2.3. Vascular ECM structure and properties

Extracellular matrix is a noncellular component of the aorta which is mainly synthesized and secreted by vascular SMCs in the media and FBs in the adventitia. ECM proteins link together to form a support network contributing to the mechanical and chemical characteristics of tissues important for vascular plasticity, strength, and cell activity. The major ECM proteins involved in these processes are elastin, collagens, proteoglycans (PGs)/glycosaminoglycan (GAGs), fibronectin and several other glycoproteins, among which elastin and collagen are dominant.

Elastin is one of the earliest ECM proteins synthesized by vascular SMCs and secreted as tropoelastin monomers that coacervate onto a scaffold of fibrillin-rich microfibrils where tropoelastin molecules are aligned and eventually cross-linked through the help of various matrix molecules [e.g. fibulins, lysyl oxidases (LOXs), latent transforming growth factor β-binding

proteins (LTBP)] forming mature elastic fibers [29]. Elastic fibers are arranged in concentric layers called elastic lamina in aortic media, which counterbalance the biomechanical forces and confer the distensibility and recoil properties for the aorta. Each elastic laminae is alternately connected with a concentric ring of SMC layer through the binding of elastin extensions and SMC surface integrins, forming the elastin-contractile unit that enables a coordinated response of the mechanical stress imposed on the aorta from the pulsatile blood flow [30].

The major collagens in aorta are collagen type I and III, which are mainly responsible for the tensile strength and stiffness of the aortic wall to withstand the blood pressure. The collagen type I and III are classic fibril-forming collagens assembled from polypeptide alpha-chains. Three polypeptide alpha-chains are assembled into a procollagen triple helical which are matured as tropocollagen triple helix in endoplasmic reticulum through post-translational modification, the tropocollagen is enzymatically cross-linked by lysyl oxidase families to form collagen microfibrils, which are further organized and assembled into long collagen fibers [31]. In addition to their mechanical properties of the aortic wall, elastic fibers and fibrillar collagens can directly interact with vascular cells via various integrins and other proteins to modulate the adhesion, proliferation, and migration of SMCs [32-36].

PGs are glycosylated proteins with covalently attached GAG chains found in all layers of the aorta. They comprise the non-fibrillar fraction of the ECM, fill the extracellular space not occupied by the fibrillar ECM, provide structural and mechanical support for the aortic wall, and interact with various molecules (integrins, growth factors, cytokines, etc.) to mediate signaling responses of vascular cells [5]. Fibronectin is a dimeric glycoprotein in ECM that is expressed on the surface of vascular cells and becomes part of the ECM as fibronectin fibrils, a process that requires activation via binding of integrin receptors [37]. In the vascular ECM, fibronectin links other fibers and matrix proteins forming an integrated matrix and influences intracellular signaling transduction

via interacting with integrins [38]. Laminins are heterotrimeric glycoproteins that make up the constituents of the basement membranes. Integrins are the important adhesion receptors on vascular cells binding collagens, laminin and fibronectin in the vessel wall that promote cell adhesion to the ECM. Other structural ECM proteins, such as fibrillin, fibulin, and thrombospondin also play important roles during vascular wall development and remodeling.

1.2.4. Regional heterogeneity within the aorta

Aorta is the largest vessel in the body and is responsible for transporting oxygen and nutrients to organs throughout the body. To ensure optimal mechanical operation for the aorta [39], the aortic wall differs in morphology, structure, mechanical properties and embryology in the region above and below the diaphragm (**Table 1.1**). The deviations in mechanical properties along the aorta are primarily due to the disparities in structural composition, specifically by the changes in elastic lamellar unit and collagen mass.

The overall appearance of aortic canal is much thicker in the ascending and thoracic segments than in the abdominal segment, with thickness decreasing slightly downward in the thoracic region while remaining constant in the abdominal aorta. Similar to the external dimensions, the inner diameter of aorta steadily decreases with distance from the aortic root. Therefore, the ratio of wall thickness to lumen diameter remains almost constant throughout the aorta, which results in uniform wall stress in the thoracic and abdominal aortas under physiologic conditions [40].

The thickness and composition of three tunica layers are uneven and vary in thoracic and abdominal aorta. The tunica intima accounts for <1% of the total wall thickness and remains uniform along the aorta, whereas the thickness of tunica adventitia is negligible in the thoracic aorta but increases considerably along the abdominal aorta [5]. Comprised of numerous elastin

lamellar that determine the thickness of the entire wall, the medial layer has the greatest variation and diversity between thoracic and abdominal aorta. The thickness of tunica media increases from birth to adulthood, and the postnatal increase in the thoracic aorta is mainly due to the synthesis of many additional lamellar units, whereas in abdominal aorta this expansion is achieved by widening in each lamellar unit [40]. The additional synthesized units explain the increased elastin content in the thoracic aorta, which allows a higher distensibility favoring the higher pulse required for the aorta close to the heart. Hence, tension per lamellar unit is elevated in the adult abdominal aorta [40, 41], despite the estimated wall stress is constant in both segments throughout growth. Additionally, the amount of collagen, that provides strength and limits stretch under high pressure, remains approximately constant with distance from the heart [42], resulting in a lower ratio of elastin-to-collagen in the abdominal compared with the thoracic aorta. Furthermore, in the human aorta, the thoracic aorta contains a vascularized external zone distributed by vasa vasorum and an avascular inner medial zone, whereas the entire abdominal aorta is normally devoid of the vasa vasorum [43]. The vasa vasorum provides additional supply to the outside region in the thoracic aorta, whereas the avascular area obtains oxygen and nutrients from the blood through direct trans-intimal diffusion. Differences in mechanical properties, matrix composition, oxygen and nutrient delivery to the cells in the thoracic and abdominal aortic media likely contribute to the variations identified in vascular remodeling, as well as the region-specific heterogeneity of aortic diseases, such as atherosclerosis and aortic aneurysm [44]. Lastly, embryonic development of VSMC also differs in the thoracic and abdominal aortic regions, with ascending thoracic SMC originating from secondary heart field and cardiac neural crest, descending thoracic SMC originating from somites precursors while progenitor of abdominal SMC deriving from the splanchnic mesoderm, which also shows distinct responses to various biophysical stimuli [45-47].

Table 1. 1 Regional heterogeneity within the aorta

	Thoracic Aorta	Abdominal Aorta
Morphology	Thicker aortic wall Larger aortic diameter (outer and inner)	Thinner aortic wall Smaller aortic diameter (outer and inner)
Structure	Thicker media layer with more lamellar units and SMC Grows by synthesis of additional lamellar units Greater ratio of elastin-to-collagen content Vascularized outer zone of aorta with vasa vasorum	Thinner media layer with fewer lamellar units and SMC Grows by widening in each lamellar unit Lower ratio of elastin-to-collagen content Avascular outer region
Mechanics	Greater distensibility TAA breaking stress greater than AAA [44]	Increased stiffness Increased tension per lamellar unit AAA breaking stress lower than TAA [44]
Embryology	Ascending: secondary heart field and cardiac neural crest; Descending thoracic: somites [47]	Derived from splanchnic mesoderm [47]
Atherosclerosis	A low likelihood of fatty streak progression from fatty streak to atheroma [48]	High likelihood of lesion progression from fatty streak to high-grade lesions [48]

Abbreviations: SMC, smooth muscle cell; TAA, thoracic aortic aneurysm; AAA, abdominal aortic aneurysm.

1.3. TIMPs: basic structure and activity

1.3.1. Origin and general function

As the name implies, tissue inhibitors of metalloproteinases are a group of endogenous inhibitors of metalloproteinase activity. A total of four mammalian TIMPs were identified between 1985 and 1996. Their homologs are also distributed in different species of the animal kingdom, including vertebrates and invertebrates [49]. Four TIMPs are designated as TIMP-1, -2, -3 and -4. TIMP1 was discovered by Docherty and colleagues in 1985 as an inhibitor of metalloproteinases [50]. Human TIMP2 was cloned in 1990, TIMP3 in 1992, and TIMP4 in 1996 [51].

TIMPs regulate diverse biological processes, including ECM remodeling and the activity of growth factors and their receptors by inhibiting the activity of metalloproteinases. Metalloproteases are the most diverse class of catalytic enzymes in the human body, characterized by the requirement of a divalent metal ion for their catalytic activity. They are synthesized as inactive zymogens with a pro-domain that must be removed for activation. The metalloproteases mainly include 23 matrix

metalloproteases (MMPs; can be secreted or membrane-anchored), 13 disintegrin metalloproteases from ADAMs (a disintegrin and metalloproteinase family, membrane- anchored), and 19 ADAMs with thrombospondin motifs (ADAMTSs, secreted). Activated metalloproteinases are inhibited by TIMPs in a 1:1 molar stoichiometry. These endogenous proteins can inhibit all MMPs and selectively inhibit members of the ADAM and ADAMTS families. Each TIMP can target multiple enzymes, and each metalloproteinase has large protein substrates that regulate cell surface receptors and control the extracellular environment. Thus, TIMP-mediated inhibition plays an important role in the control of extracellular tissue homeostasis and cellular function.

1.3.2. Structure, expression, and targets

TIMPs are proteins of 207-224 amino acids with a molecular weight of about 23-25 kilodaltons (KDa). They share approximately 40% identity in amino acid sequence, with TIMP2 and TIMP4 showing the highest degree of similarity to each other, with 50% identity. All mammalian TIMPs have two distinct structural domains, each folded and stabilized by three disulfide bonds. One is the amino-terminal structural domain (also known as N-terminus) of about 125 amino acid residues, and one is the carboxyl-terminal structural domain (also known as C-terminus) of about 65 residues. The N-terminal region is highly conserved in all TIMPs, and it contains the inhibitory capacity of metalloproteases. The C-terminus appears to mediate other non-inhibitory interactions, notably involved in the formation of the proenzyme complex. All TIMPs have a crystal-like structure and display a wedge-shaped appearance. The residues of the N-terminal structural domain form a ridge on the wedge-shaped protein, which inserts into the active site of the metalloprotease, thereby inhibiting its active function.

Although they inhibit the proteolytic activity of MMPs, TIMPs differ in many ways, including regulation of expression, solubility, inhibition spectrum and interaction with pro-MMPs **(Table 1.5)**. TIMP1 gene is highly inducible at the transcriptional level in response to many cytokines and hormones [52, 53]. Similarly, expression of the TIMP3 is induced in response to several stimuli. Mutations in this gene have been shown to be associated with the autosomal dominant disease Sorsby's fundus dystrophy [54]. In contrast, TIMP2 gene is constitutively expressed. However, the regulation of TIMP4 expression has not been determined. TIMP1, TIMP2 and TIMP4 proteins are secreted and exist in soluble form, whereas TIMP3 is largely incorporated into the tissue matrix. TIMP1 and TIMP3 contain N-linked glycans and have glycosylated forms [55]. TIMP1 and TIMP2 are ubiquitously present in tissues and body fluids, whereas TIMP3 is tissue restricted. The expression pattern of TIMP4 appears to be different and more tissue specific than other TIMPs, as it is found mainly in the brain, adipose tissue, heart, ovary, and skeletal muscle.

TIMP1 inhibits almost all MMPs but is a poor inhibitor of some membrane-type metalloproteinases (MT-MMP, these MMPs contain a transmembrane C-terminal domain that anchors the enzyme to the cell surface), including MT1-MMP, MT2-MMP, MT3-MMP and MT5-MMP [56]. TIMP1, TIMP2, and TIMP4 each inhibit only a few ADAMs and ADAMTS (TIMP1 inhibits ADAM10 and ADAMTS4, TIMP2 inhibits ADAMTS4, and TIMP4 inhibits ADAM17, ADAM28 and ADAMTS4). TIMP3, however, has the broadest spectrum of metalloproteinase inhibition, including all MMPs, multiple ADAMs (ADAM10, ADAM12, ADAM17, ADAM19, ADAM28 and ADAM33) and ADAMTSs (ADAMTS1, ADAMTS2, ADAMTS4, and ADAMTS5).

TIMPs also bind to the zymogen form of MMP (pro-MMP), but instead of inhibiting it, they are involved in regulating the activation process of MMP. TIMP1 binds preferentially to pro-MMP9, TIMP3 binds to either pro-MMP2 or pro-MMP9, whereas TIMP2 and TIMP4 bind to pro-

MMP2. Among them, TIMP2 plays a key role in the activation of cell surface pro-MMP2. In this process, TIMP2 binds to the active site of MT1-MMP, which subsequently binds to pro-MMP2 to form a ternary complex. If this occurs in the vicinity of a second free MT1-MMP, the second MT1-MMP then hydrolyzes the pre-fragment of MMP2 to initiate activation of the protease [57].

1.3.3. Activities independent of metalloproteinase inhibition

TIMPs are proposed to be multifunctional proteins with multiple biological activities. In addition to an inhibitory role against metalloproteinases, other functions have been reported in numerous studies, including regulation of cell proliferation, differentiation, cell migration and invasion, anti- and pro-apoptosis, and anti-angiogenesis. Some of these functions have been indirectly attributed to the inhibition of metalloproteinases because it affects cell-matrix interactions and ECM turnover, thus indirectly affecting cell survival (e.g. removal of anchorage-dependent cells from association with the ECM leads to apoptosis or cell death [58]). However, several other activities have been found to be independent of metalloproteinase inhibition. TIMPs-mediated cell growth or proliferation is identified as a direct cellular effect that can be mediated by a putative receptor. CD63 was found as a cell surface binding partner for TIMP1, and the TIMP1-CD63-integrin β1 complex subsequently activates focal adhesion kinase (FAK), PI3-K and ERK pathways, thus turning on survival signals [59, 60]. Integrin was found to be a receptor for TIMP2, and interaction of TIMP2 with this integrin abolished angiogenic factor-induced endothelial cell proliferation. A more detailed description of this aspect can be found in Keith Brew et al [49, 61-64].

Table 1. 2 A summary of the general properties of the four human TIMPs

	TIMP1	TIMP2	TIMP3	TIMP4
Chromosomal location: human	Xp11.3	17q25.3	22q12.3	3p25.2
Amino acid length	207	220	211	224
Molecular masses (KDa)	23.2	24.4	24.1	25.5
Protein localization	Soluble	Soluble/cell surface	ECM	Soluble/cell surface
Expression	inducible	constitutive	inducible	inducible
Pro-MMP interactions	Pro-MMP9	Pro-MMP2	Pro-MMP2/9	Pro-MMP2
MMPs inhibition	Weak for MT1, 2, 3, 5-MMP	All	All	All
ADAMs inhibition	ADAM10; ADAMTS4	ADAMTS4	ADAM10, 12, 17, 19, 28, 33; ADAMTS1, 2, 4, 5	ADAM17, 28; ADAMTS4
Receptor-binding	CD63, CD88 LRP-1	α3β1 integrin, LRP1	EFEMP1, VEGFR2 AGTR1, LRP1, SP	
Identified signaling pathway	Receptor unknown, ↑PTEN-signaling	↑ α3β1 -integrin/Shp1 signaling	VEGF-receptor-2; Angiotensin II type 2 receptor	unknown

The main information in the table is adapted from the references in Brew et al [49, 61].

Abbreviation: AGTR, Angiotensin II receptor; EFEMP, EGF-containing fibulin-like extracellular matrix protein; LRP, LDL receptor related protein; VEGFR, vascular endothelial growth factor receptor; SP, sulfated polysaccharide.

1.3.4. TIMP-knockout phenotypes in mice

Through extensive studies in mice lacking specific TIMP genes, the biological role of these TIMP molecules have been investigated and their function in the pathophysiology and progression of several diseases has been elucidated. **Table 1.6** summarizes the phenotypes observed in individual TIMP-deficient mice.

Table 1. 3 Mouse phenotypes resulting from deletion of individual TIMP genes

Genotype	Phenotype	PMID
***Timp1*$^{-/-}$**	Delayed the formation of compact myelin in CNS	21508247
	Revealed severe myelin pathology in experimental autoimmune encephalomyelitis	17148673
	Abolished spontaneous remyelination	32071226
	Impaired learning and memory	16860884
	Exhibited rapid onset thermal and mechanical hypersensitivity at the site of inflammation	31616247
	Reduced long-term repopulation capacity of hematopoietic stem cells	21521782
	Impaired learning and memory	16860884
	Reduced serum progesterone levels and abnormal uterine morphology in female mice	12488323; 11732988
	Decreased adipose tissue weight in high fat diet induced obesity	12574803

	Hyperphagia and hyperphagia and obesity in female mice feeding with standard chow-diet	19036876
	Enhanced estrogen-induced uterine wet-weight gain/edema	14568914
	Improved the rate of infection clearance after Pseudomonas aeruginosa corneal infection	15618213
	Developed an allergic asthma phenotype induced by ovalbumin	18955015; 28992358
	Enhanced airway re-epithelialization and reduced lumen obliteration	18385523; 16388023
	Amplified acute lung injury in the alveolar compartment	15947421
	Reduced hepatic stellate cell proliferation and the development of liver fibrosis	21300026
	Reduced fibrosis in the liver lobe after bile duct ligation	23755201
	Protected against diet-induced hepatic steatosis and glucose intolerance	26168159
	Impeded metastasis of pancreatic cancer cells to the liver	27506299
	Impaired acute inflammation and attenuated development of fibrosis in colitis	27194531
	Changed in LV geometry	10652195
	Ameliorated coxsackievirus B3-mediated myocarditis	18055551
	Exacerbated adverse left ventricular remodeling after myocardial infarction	15598866; 12388239; 14630637
	Promoted cerebral aneurysm progression with the increased enzyme activity of MMPs	17569872
	Failure to mature and adapt the vascular network to ischemia or changes in flow	27430487
Overexpression	Relieved experimental allergic encephalomyelitis symptoms	20558576
	Failure to substantially modify pulmonary fibrotic disease in mice	18178676
***Timp2*$^{-/-}$**	Impairment of pro-MMP2 activation by MMP14	10827176; 10827175
	Prohibited neuronal differentiation and neurite outgrowth *in vivo*	15901773
	led to β-cell exhaustion in male, promoted nutritionally induced obesity in both sexes	21285317
	Exhibited motor dysfunction (reduced hindlimb extension and shortened gait)	16216006
	Accelerated osteoarthritis development via promotion of angiogenesis	22664108
	Reduced myogenesis *in vivo*	17678891
	Reduced renal tubulointerstitial fibrosis through increasing MMP2 activation	23760282
	Enhanced hypertrophy and exacerbated LV diastolic dysfunction in response to Ang II	24692173
	Exacerbated cardiac dysfunction and remodeling after pressure overload	21986284
	Caused adverse post-MI myocardial remodeling	20056917
	Promoted cerebral aneurysm progression with the increased enzyme activity of MMPs	17569872
	Exacerbated renovascular remodeling in Ang II-induced hypertension	24077247
***Timp3*$^{-/-}$**	Impaired cognitive function	19806081
	Resistance to Fas-mediated neuronal cell death after mild ischemia	17962815
	Reduced tumor number and total volume in obesity-associated hepatocarcinogenesis	31292722
	Impacted innate immunity by dysregulating cleavage of TNF and its receptors	16393953
	Promoted the differentiation of macrophages into proinflammatory (M1) cells	23742180
	Enhanced metastatic dissemination to multiple organs by melanoma and lymphoma cells	16702949
	Delayed the growth of early, but not advanced tumor cells	25807548
	Increased inflammatory response to intra-articular antigen-induced arthritis	15920158
	Exhibited enhanced energy expenditure through thermogenesis	24736588
	Caused Sorsby Fundus Dystrophy	7894485; 18295466
	Promoted pathologic VEGF-mediated angiogenesis in the choroid	21282576; 19478078;18408187
	Led to pathological neovascularization in oxygen-induced retinopathy	23299479
	Accelerated epithelial apoptosis in mammary tissue	11560952
	Impaired bronchiole branching morphogenesis	14499643
	Spontaneous air space enlargement and impaired lung function	11560951
	Disrupted alveologenesis during lung development	19128402
	Promoted inflammation following acute lung injury	20008147
	Increased pulmonary compliance in response to lipopolysaccharide-induced sepsis	15805139
	Led to chronic hepatic inflammation and failure of liver regeneration	15322543

	Exhibited metabolic dysfunction and promoted microbiota-driven hepatic steatosis	27373162
	Caused hepatic steatosis and adipose tissue inflammation	19027012
	Enhanced ADAM17-dependent EGFR signaling and TNFR1 dictates hepatocyte apoptosis	20628198
	Enhanced interstitial nephritis and fibrosis	19406980
	Enhanced apoptotic response and renal tubulointerstitial fibrosis	23760282
	Exacerbated diabetic nephropathy	23401241; 23797704; 22896043
	Led to dilated cardiomyopathy and dysfunction	15262835; 16037568
	Promoted neonatal mouse cardiomyocyte proliferation via EGFR/JNK/SP-1 signaling	19211917
	Caused myocardial fibrosis and heart failure by deregulation of TGFbeta1 and TNF signaling	19625257
	Exacerbated iron overload-mediated cardiomyopathy and liver disease	29373036
	Exacerbated LV adverse remodeling, LV rupture, and dilated cardiomyopathy post-MI	20675565; 17945252
	Exacerbated myocardial fibrosis and LV diastolic dysfunction in response to Ang II	24692173
	Led to adverse structural remodeling of the arterial ECM in response to Ang II	23524300
Overexpression	Protected from insulin resistance, glucose intolerance, and non-alcoholic steatohepatitis	22228717
	Impaired release of TNF-alpha and myogenic gene expression	20682640
***Timp4*$^{-/-}$**	Exacerbated diastolic dysfunction, and worsened myocardial hypertrophy and fibrosis	24842912
	Increased post-MI mortality duo to left ventricular rupture	20516072
	Had no changed in blood pressure after Ang II perfusion	3531724
	Decreased survival due to adverse ECM accumulation after left ventricular pressure overload	16294222
	Impaired lipid absorption and ameliorated the HFD-induced obesity	28740132

Abbreviations: ADAM17, a disintegrin and metalloprotease 17; Ang II, angiotensin II; CNS, central nervous system; ECM, extracellular matrix; EGFR, epidermal growth factor receptor; HFD, high fat diet. HGF, hepatocyte growth factor; JNK, jun NH(2)-terminal kinase; MI, myocardial infarction; MMP, matrix metalloproteinase; Timp, tissue inhibitor of metalloproteinase; TNF, tumor necrosis factor; TNFR, tumor necrosis factor receptor; VEGF, vascular endothelial growth factor; LV, left ventricular.

1.4. Physiological Remodeling of Vascular ECM

The composition and integrity of the ECM are key determinants of the physical properties of the aortic wall. The normal vascular ECM is a highly dynamic structural network that undergoes continuous physiological remodeling in the form of matrix synthesis and degradation in response to multiple physiological or pathophysiological stimuli. Several protease families are involved in the degradation process, including metalloproteinases (MMPs, matrixins), ADAM, ADAMTS, plasminogen activators, and plasmin [5, 65-67].

MMPs are the predominant proteases involved in vascular ECM remodeling. They are a family of zinc-containing endopeptidases consisting of 23 enzymes known for their ECM degradation function and are also involved in the cleavage of numerous proteins. These enzymes can be

classified into different groups based on their structure or preferred substrates and are referred to as collagenases (MMP-1, 8, 13 and 18), gelatinases [gelatinase A (MMP2) and gelatinase B (MMP9)], laminases (MMP3 and MMP10), matrilysins (MMP7 and MMP26) and membrane-bound MMPs (MT1-MMP/MMP14, MT2-MMP/MMP15, MT3-MMP/MMP16, MT4-MMP/MMP17 and MT5-MMP/MMP24). The MMPs family degrades all vascular ECM components, including collagen and elastin, which are essential for the structural integrity of the vessel wall and are also important substrates for MMPs. MMPs participate in vascular tissue remodeling during injury repair and angiogenesis and affect vascular cell behaviors such as EC function and SMC contraction, proliferation, and migration [68, 69].

In normal physiological vascular remodeling, the activity of MMPs is mainly regulated by TIMPs inhibition. Factors that promote vascular remodeling, such as chronic changes in hemodynamics, vascular injury, inflammatory cytokines, and reactive oxygen species, increase the production and activation of MMPs, which are derived mainly from vascular SMCs, fibroblasts, ECs, and inflammatory cells, ultimately disrupting the balance between MMPs and TIMPs and increasing actual activity of MMP, leading to excessive vascular matrix disruption as well as abnormal ECM turnover [70]. Abnormal ECM remodeling leads to various vascular pathological processes, including tissue degeneration and fibrosis, which are closely associated with atherosclerosis and aortic aneurysm.

1.5. Atherosclerosis

Atherosclerosis is a chronic vascular disease characterized by the formation of plaque in the aortic wall. Organs with plaque formation in the arteries develop clinical diseases including ischemic heart diseases, stroke, and peripheral vascular diseases. These cardiovascular diseases

principally myocardial infarction and cerebral stroke are the leading cause of mortality and disability worldwide and impose huge health and economic burdens across the global [1]. Atherosclerotic lesions can develop slowly throughout life and are largely irreversible, although some studies suggested that some degree of plaque regression can be achieved [71, 72]. Therefore, the most important clinical goals are prevention and early diagnosis. Current atherosclerosis treatments focus on lowering blood lipids and targeting other traditional risk factors for cardiovascular diseases, such as hypertension, smoking, diabetes, and obesity. Among them, statins are the most prescribed to lower cholesterol, however, discontinuation and nonadherence due to a range of side effects, have stagnated its benefits [73, 74]. Anti-inflammatory therapies targeting interleukin-1β (IL-1β) for the treatment of atherosclerosis also face many challenges [75, 76]. Consequently, a better and more comprehensive understanding of the disease could create more opportunities for the development of precision medicine and new treatments.

1.5.1. The formation of atherosclerotic plaque

The endothelial cells in the intima function as a selectively permeable barrier and form the frontline defense for plaque deposition. The shape and alignment of ECs in regions of arterial branching or curvature are affected by disturbed flow, exhibiting permeability to macromolecules such as low-density lipoprotein (LDL), and are therefore preferential sites for lesion formation [77, 78]. The apolipoprotein B-100 (apoB-100) molecule serving as a ligand for LDL receptor (LDLR) is proposed to be the major atherogenic ingredient in lipoproteins. In addition to well-known LDL, other apoB-containing lipoprotein particles, such as remnant lipoprotein particles derived from triglyceride-rich lipoprotein (chylomicrons and very-low-density lipoprotein) [79, 80] and lipoprotein(a) [81], can also contribute to atherosclerosis initiation. Native apoB100-containing

lipoproteins are taken up by the endothelium via the receptor mediated transcytosis associated with scavenger receptor B1 (SR-B1) [82] and activin receptor-like kinase 1 (ALK1) [83], as well as caveolin-1/caveolae-mediated transcytosis [84], and are accumulated in intima region of preferred sites. The absorbed lipoproteins are subsequently trapped through interacting with vascular ECM particularly proteoglycans, promoting the retention and deposition of lipids in the sub-endothelium space [85, 86]. This results in an activation of the overlying EC by a still poorly understood mechanism but likely involving the generation of proinflammatory oxidized lipids, such as oxidized phospholipids or oxidized LDL. The activated ECs express adhesion molecules including selectins, vascular cell adhesion protein 1 (VCAM-1) and intercellular adhesion molecule 1 (ICAM-1), chemotactic proteins including monocyte chemotactic protein 1 (MCP1) and growth factors including macrophage colony-stimulating factor (M-CSF), that mediate the recruitment, trafficking, and migration of blood leukocytes into intima, followed by leukocytes proliferation and differentiation into macrophages. These macrophages in turn, internalize the lipoproteins via macropinocytosis, phagocytosis and scavenger receptor-mediated uptake [including lectin-like oxidized LDL receptor 1 (LOX1), SR-A1, and CD36], giving rise to cholesterol ester engorged "foam cells" and activating pro-inflammatory signaling [87]. Over time, lipids and foam cells continue to accumulate, and other leukocytes, particularly T cells, enter the lesion and a lot of proinflammatory cytokines and chemokines including IL-1, IL-6, and TNF, C-C motif chemokine ligand [CCL]-2 and CCL5 are secreted resulting in enhanced inflammatory response. Simultaneously, the foam cells die to contribute to necrotic cores consisting of cellular debris and cholesterol. Also, SMCs transform from a contractile to a proliferative state and migrate to the region underlying the EC layer, forming a "fibrous cap" containing ECM that protects the lesion from rupture. Notably, growing evidence indicates that SMC can also differentiate into macrophage-like cells that give rise to foam cells (even accounting for a large proportion of total

foam cells) and osteochondrogenic cells that deposit calcium phosphate salts [88, 89]. At last, the primary endpoint of this series of events is myocardial infarction resulting from coronary thrombosis triggered by lesion rupture or endothelial erosion [90].

1.5.2. Reverse cholesterol transport in atherosclerosis

The lipid-scavenging cells cannot limit the uptake of lipids and rely on reverse cholesterol transport (RCT) to maintain cellular cholesterol homeostasis. This RCT during atherosclerosis is defined as the process by which cholesterol moves out of foam cells in plaques, enters the circulation, and returns to the liver for excretion in feces [91]. The relationship of RCT to atherosclerosis is associated with the function of high-density lipoprotein (HDL), which served as an “acceptor” for cholesterol efflux from lesions. The RCT begins with the removal of free (unesterified) cholesterol from the foam cells that are of SMC or macrophage origin via the cholesterol pumps ATP-binding cassette transporter A1 (ABCA1) and ATP-binding cassette transporter G1 (ABCG1). The effluxed free cholesterol binds to nascent HDL (a form of lipid-poor apoA-I) and is modified by cholesterol acyltransferase into cholesteryl ester. SR-B1 on macrophage was also proposed to facilitate the efflux of free cholesterol to mature HDL particles via passive diffusion [92]. The plaque-derived HDL cholesterol can be directly taken up by liver through binding the receptor SR-BI or transferred to VLDL and LDL, following uptake by liver LDLR. Finally, this cholesterol is excreted into bile and ultimately in feces. Loss function of ABCA1 or ABCG1 in macrophages accelerated atherosclerosis [93-95]. SR-B1 overexpression in the liver decreased atherosclerosis [96], whereas partial loss of macrophage SR-B1 increased atherosclerosis [97]. The RCT, therefore, is considered an important target to inhibit the progression of atherosclerosis and even to promote its regression.

1.6. Aortic Aneurysm

Aortic aneurysm is a permanent and irreversible localized dilation of the vessel exceeding the normal diameter by more than 50%. The dilation is caused by disruption of the aortic wall combined with unfavorable tissue remodeling, including endothelial damage in intima, SMC loss and ECM degradation in the media, and ECM degradation in the adventitia. Aortic aneurysm tends to expand asymptomatically until a catastrophic event occurs such as dissection or rupture. The risk of aortic rupture in aged patients is estimated to be as high as 32.5% for abdominal aortic aneurysms (AAA) greater than 5 cm in diameter and 5% for thoracic aortic aneurysm (TAA) [98, 99], resulting in up to 200,000 deaths worldwide each year [100]. **(Table 1.2)** To date, there is no proven efficient medical treatment to prevent aortic aneurysm progression or clinic events [100, 101]. Invasive endovascular and open repair are the only definitive treatments to stabilize large aneurysms [102, 103], but provide no significant therapeutic benefits for the small asymptomatic aortic aneurysm [104, 105]. Therefore, a better understanding of the underlying mechanisms of the aortic aneurysm is needed to guide effective drug therapies in retarding aneurysm progression.

Aortic aneurysm is subdivided anatomically into the TAA and AAA. Although TAA and AAA share many common characteristics, including physical appearances, proteolytic degradation of elastic fibers and degradative remodeling of ECM, they are distinct diseases with different epidemiology, risk factors, etiologist, histopathological features and genetic molecular (**Table 1.2**).

1.6.1. Abdominal aortic aneurysm

AAA represents aortic enlargement with a diameter of 3.0 cm or larger in any segment of the aorta below the diaphragm, with the infrarenal aorta being the most common site of formation. The regional heterogeneity of aortic structure as described above and the unique hemodynamic characteristics of the infrarenal aorta might help to explain why this region is the preferred location for AAA [106]. The incidence of AAA is approximately 2.5-6.5 per 1000 person-years in western countries, which is more prevalent compared to TAA [107]. AAA is prevalent in the elderly population, mainly in men, with a prevalence of 1.0% to 14.2% and 0.2% to 6.4% in women [108]. Although the prevalence of AAA is higher in men, women have been reported to have a faster growth rate and a 4-fold higher risk of rupture [98]. Cigarette smoking is the risk factor most strongly associated with AAAs, followed by age, sex, hypertension, hypercholesterolemia, and atherosclerosis [109]. Genetics also influence AAA formation and growth **(Table 1.2)**. However, no gene defects associated with AAA have been identified [110].

AAA is characterized by structural deterioration of the aortic wall with degraded medial elastin, VSMCs loss, and accumulation and activation of inflammatory cells [111-114]. The pathogenic mechanism of AAA is complex and not fully understood, genetic, environmental, hemodynamic, and molecular all contribute to the development of aneurysms. The main factors in AAA pathogenic mechanism are atherosclerosis, inflammation, and proteolytic imbalance.

Most AAAs are found in patients with advanced atherosclerosis, which is therefore considered to be the underlying cause of AAAs [115]. This is outlined further below. A hallmark of AAA histopathology is the massive infiltration of inflammatory cells in the arterial wall, involving essentially all the classical cellular components of inflammation. Neutrophile occurs in the early stages of experimental AAA formation but is transient. Depletion of circulating blood neutrophils has been found to greatly limit the formation of experimental AAA in animals [116]. Monocytes and macrophages are relatively abundant and consistent in the progression of AAA. Monocytes

and macrophage with diverse origins and phenotypes have critical and differential roles in the initiation, progression, and healing of the aneurysmal process [117]. Mast cells also have been reported to participate in AAA pathogenesis [118-120]. These inflammatory cells in the aneurysmal wall as a major source of cytokines, chemokines, reactive oxygen species and proteolytic enzymes [such as MMPs and cysteine proteases) induce aortic SMC apoptosis, neoangiogenesis, aortic wall remodeling and degradation leading to AAA formation and evolution. However, current clinical trials targeting inflammation or immune response have shown no significant effects on AAA growth or clinical events [2].

In addition to inflammation, ECM remodeling associated with proteolytic degradation is another critical pathogenic role in AAA. An imbalance between the amount of the MMPs and their inhibitors is responsible for the excessive proteolytic degradation. MMPs are a type of proteolytic enzyme whose activity is augmented in aortic aneurysm, as evidenced by analysis of aneurysmal tissue from animals and humans. The increase in MMPs and a decrease in TIMPs lead to the breakdown of collagen and elastin in the ECM as well as apoptosis of VSMCs. This results in the weakening and destruction of the normal aortic wall architecture, leading to the formation of dilated vessels and the development of aneurysms. Likewise, no efficacy of an MMP inhibitor drug has been reported [121].

1.6.2. Thoracic aortic aneurysm

TAA represents the dilation of one or more aortic portions that occur above the diaphragm, including the aortic root, ascending aorta, aortic arch, and descending aorta. It is most common in the ascending aorta, followed by the descending thoracic aorta, and rare in the aortic arch and thoracoabdominal region [122]. The incidence of TAA is about 10.4 per 100,000 patient-years,

much lower than that of AAA [123]. However, since TAAs are majorly asymptomatic and not easy to screen until acute thoracic aortic aneurysm dissection (TAAD) or rupture occurs. Thus, the rate of rupture-associated mortality is much higher than in patients with AAA. The prevalence of TAA is 1.3-8.9% in men and 1.0-2.2% in women [124]. but similar to AAA, TAA also grows faster in women and has a nearly 3-fold higher risk of rupture than in men **(Table 1.2)** [98]. Unlike AAA which commonly occurs in old age, TAA often occurs at a young age due to strong genetic influences [125]. TAAs can be categorized as familial syndromic or non-syndromic forms, associated with bicuspid aortic valve (BAV) and sporadic forms. Gene mutations cause both familial and isolated cases of heritable TAA diseases. Whereas sporadic TAA shares similarities with AAA in terms of risk factors and pathogenesis, mainly related to aging, hypertension, smoking, and male gender, and is often accompanied by atherosclerosis, inflammatory infiltration, and elevated MMP activity [126].

Approximately 30% of cases of familial TAAs are associated with an underlying mutation in a specific genetic variant, and of the 53 TAA/TAAD-related genes uncovered to date, the majority encode proteins involved in the ECM, SMC contraction, or the canonical transforming growth factor (TGF)-β signaling pathway**.** The genes associated with heritable thoracic aortic disease in humans are summarized in **Table 1.3**. Marjolijn Renard et al. applied the semi-quantitative ClinGen framework to evaluate putative gene-disease relationships between these candidate genes and hereditary thoracic aortic aneurysm and dissection (HTAAD), and identified 11 genes associated with HTAAD (ACTA2, COL3A1, FBN1, MYH11, SMAD3, TGFB2, TGFBR1, TGFBR2, MYLK, LOX, PRKG1) **(Table 1.3)** [127, 128]. The heterogeneity of TAA in gene mutations complicates mechanistic studies using human tissues or animal models. Furthermore, although genetic mutations have been found to also influence AAA formation, there is little overlap

in genetic mutations between AAA and TAA, reflecting fundamental differences in their pathophysiology.

Pathological feature of patient TAAs is mostly characterized as cystic or mucoid medial degradation, that is histologically manifested as elastic fiber fragments or loss, SMC depletion, proteoglycan deposition and increase in MMP activity [86].

Vascular structure remodeling associated with the degradation of ECM plays a central role in TAA. Gene variants in structural proteins of the aortic wall clearly make an important contribution to the pathogenesis of the syndrome and sporadic TAA. *Fibrillin 1*, the pathogenic gene of Marfan Syndrome (MFS), is an ECM glycoprotein that assembles to form microfibrils and the formation of elastic fibers. It also binds to the large latent TGF binding protein that sequesters TGFβ within matrix in an inactive (or latent) form. It has been reported *fibrillin 1* mutation led to the aberrant activation of TGFβ and its downstream pathways contributing to pathogenesis in MFS [129].

Mutations in genes encoding SMC contractile proteins predispose individuals to TAA, suggesting that smooth muscle function plays a critical role in TAA, but the mechanism is unknown. ACTA2 encodes the smooth muscle-specific isoform of α-actin (α-SMA), which forms the thin filament of the SMC contractile unit. MYH11 encodes the smooth muscle myosin heavy chain, that forms the thick filament of the SMC contractile unit. MYLK encodes the myosin light chain kinase, a ubiquitously expressed kinase, which can phosphorylate myosin regulatory light chains to facilitate myosin interaction with actin filaments to produce SMC contractile activity. Mutations in these genes disrupt the SMC contractile structural unit and affect SMC force generation which may be a major driver of TAAs and dissection [128]. In addition, SMC phenotype transition [130, 131], alterations in SMC signaling and mechanosensing may also be implicated in the pathogenesis of TAA [128].

MMPs play a nonnegligible role in the remodeling of TAA, but they are far less studied than AAA. Increased levels of MMPs (especially MMP2 and MMP9) have been found in TAA patients and animal models [132]. MMPs are involved in both the degradation and adaptive remodeling of ECM in the development of TAA. MMP2-deletion increased Ang II–induced TAA by suppressing the TGFβ pathway and the de novo synthesis of ECM, but MMP2-deletion protected against CaCl2-induced TAA through inhibiting aberrant ECM degradation [133].

Along with MMPs, there is also evidence of inflammation in TAA, but it is less pivotal than that in AAA and the mechanism for the induction of inflammation in TAA is not well defined.

1.6.3. Management and treatment of aortic aneurysm

To date, there are no effective pharmacological treatments to prevent and limit the occurrence and progression of aortic aneurysms. Current management options for patients with aortic aneurysms include follow-up monitoring, lifestyle changes (e.g., smoking cessation), pharmacologic management, surgery, and endovascular stenting. For small to medium-sized asymptomatic aneurysms use the cardiovascular risk management and pharmacologic stabilization of AAA such as antihypertensives (beta-blockers), antibiotics, lipid-lowering agents (statins), protease inhibition (doxycycline), angiotensin-converting-enzyme inhibitors, angiotensin receptor blockers, and antithrombotic regents. Unfortunately, none of these drugs have been shown in clinical trials to be beneficial in controlling aneurysms [2, 3]. Open surgery or percutaneous endovascular aneurysm repair (EVAR) is the only effective treatment for AAA and TAA when the risk level of aneurysm rupture meets certain criteria. EVAR has long-term durability issues and high reintervention rates, while open repair has high perioperative mortality and complications

[134]. Hence, a better understanding of aneurysm pathogenesis could provide new clues and directions for the development of effective drug treatments.

Table 1. 4 Comparison of thoracic and abdominal aortic aneurysm

	TAA	AAA
Locations	Aortic root, ascending aorta, aortic arch, thoracic descending aorta	Abdominal descending aorta (suprarenal aorta, infrarenal aorta)
Epidemiology	Incidence: 10.4 per million patient-year [123] Prevalence: 1.3–8.9% in men and 1.0–2.2% in women [124] Ruptured: 5% at 5 cm, 9% at 6 cm, and 16% at 7 cm [98]	Incidence: 2500-6500 per million patient-year [107] Prevalence: 1.0-14.2% in men and 0.2-6.4% in women [108] Ruptured: 9.4% for 5.5 to 5.9 cm, 10.2% for 6.0 to 6.9 cm, and 32.5% for 7.0 cm or more [99]
Sex-difference (presentation)	Women more rapid TAA growth and a 3-fold higher risk of rupture [135]	Women more rapid AAA growth and a 4-fold higher risk of rupture [136]
Risk factors	Gene, BAV; Aging, hypertension, cigarette smoking, and male sex	Cigarette, aging, male, hypertension, hypercholesterolemia, and atherosclerosis
Genetic predisposition	COL3A1, EFEMP2, ELN, FBN1, FBN2, LOX, ACTA2, FLNA, MYH11, MYLK, PRKG1, SMAD3, SMAD4, SKI, TGFB2, TGFBR1, TGFBR2 [127]	SORT1, CDKN2B-AS1, ERG, AC012065.7/LDAH, MEPE, CDKN1A, ADAMTS8, CRISPLD2, CTAGE1 [137]
Pathological characteristics	Medial elastic fiber fragments or loss, SMC depletion, proteoglycan deposition and increase in MMP activity	Degraded medial elastin, VSMCs loss, and accumulation and activation of inflammatory cells
Management	Follow-up surveillance, smoking cessation; Medical treatment: control hypertension and hypercholesterolemia, β-blocker, statin, ACE inhibitor, ARBs, antithrombotic regents; Surgical options: endovascular stenting, open repair.	

Abbreviations: TAA, thoracic aortic aneurysm; AAA, abdominal aortic aneurysm; BAV, bicuspid aortic valve; COL3A1, procollagen type III α1; EFEMP, EGF containing fibulin extracellular matrix protein; ELN, Elastin; FBN1/2, fibrillin-1/2; LOX, lysyl oxidase; ACTA2, smooth muscle actin α2; FLNA, filamin A; MYH11, smooth muscle myosin heavy chain 11; MYLK, myosin light chain kinase; PRKG1, protein kinase CGMP-dependent 1; SMAD3/4, suppressor of mothers against decapentaplegic 3/4; TGFB2, transforming growth factor beta 2; TGFBR1/2, transforming growth factor-beta receptor type 1/2; SORT1, sortilin 1; CDKN2B-AS1, CDKN2B Antisense RNA 1; LDAH, lipid droplet-associated serine hydrolase; MEPE, matrix extracellular phosphoglycoprotein; CDKN1A, cyclin dependent kinase inhibitor 1A; ADAMTS8, ADAM with thrombospondin type 1 motif 8; CRISPLD2, cysteine rich secretory protein LCCL domain containing 2; CTAGE1, cutaneous T cell lymphoma-associated antigen 1. MMP, metalloproteinase; (V)SMC, (vascular) smooth muscle cell; β-blocker, beta-adrenergic blocking agents; ACE, angiotensin converting enzyme; ARBs, angiotensin-II receptor blockers.

Table 1. 5 Genes Associated with Heritable Thoracic Aortic Disease in Humans

Gene Symbol	Protein	Phenotype (Syndrome, OMIM ID)	*Risk categories	Pathways impacted
COL3A1	Procollagen type III α1	EDS type IV (#130050)	Definitive	ECM
EFEMP2	EGF containing fibulin-like extracellular matrix protein 2 (fibulin-4)	ARCL1B	Moderate	ECM
ELN	Elastin	Cutis laxa syndrome	Limited	ECM

FBN1	Fibrillin-1	MFS (#154700)	Definitive	ECM
FBN2	Fibrillin 2	CCA	Moderate	ECM
LOX	Lysyl oxidase	Aortic aneurysm familial thoracic, 10 (#617168)	Strong	ECM
ACTA2	Smooth muscle actin α2	Aortic aneurysm familial thoracic, 6 (#611788)	Definitive	SMC contraction
FLNA	Filamin A	Cardiac valvular dysplasia	Limited	SMC contraction
MYH11	Smooth muscle myosin heavy chain 11	Aortic aneurysm familial thoracic, 7 (#613780)	Definitive	SMC contraction
MYLK	Myosin light chain kinase	Aortic aneurysm familial thoracic, 7 (#613780)	Definitive	SMC contraction
PRKG1	Protein kinase cGMP dependent type 1	Aortic aneurysm familial thoracic, 8 (#615436)	Strong	SMC contraction
SMAD3	Mothers against decapentaplegic drosophila homolog 3	LDS 3 (#613795)	Definitive	TGFβ
SMAD4	Mothers against decapentaplegic drosophila homolog 4	JPS/HHT	Limited	TGFβ
SKI	SKI protooncogene	SGS	Limited	TGFβ
TGFB2	TGFβ2	LDS 4 (#614816)	Definitive	TGFβ
TGFBR1	TGFβ receptor type I	LDS 1 (#609192)	Definitive	TGFβ
TGFBR2	TGFβ receptor type II	LDS 2 (#610168)	Definitive	TGFβ

**Risk categories，Semi-quantitative assessment of gene-disease relationships into qualitative categories ("definite", "strong", "moderate" or "limited" et,al.). Definitive and Strong genes are established to predispose to heritable thoracic aortic disease. Moderate and Limited genes are potentially important in terms of proper diagnosis in an individual with thoracic aortic enlargement, but these genes do not carry significant risk for progression to acute aortic dissections. Uncertain or unproven genes are not listed in the table above, and more comprehensive information can be found from the primary references of Pinard, et al. [128] and Renard, et al. [127].*

Abbreviations: EDS, Ehlers-Danlos syndrome; ECM, extracellular matrix; ARCL1B, Autosomal recessive cutis laxa type 1B; MFS, Marfan syndrome; CCA, Congenital contractural arachnodactyly; SMC, smooth muscle cell. TGFβ, transforming growth factor beta; cGMP, cyclic guanosine monophosphate; LDS, Loeys-Dietz syndrome; JPS/HHT, Juvenile polyposis syndrome/ Hereditary hemorrhagic telangiectasia; SGS, Shprintzen-Goldberg syndrome.

1.6.4. Rodent models of abdominal and thoracic aortic aneurysm

In parallel, several experimental models of aortic aneurysms have been developed, using various genetically modified animals to understand the molecular mechanisms underlying aortic aneurysms. Current common mouse models for abdominal and thoracic aortic aneurysms include chemically induced, genetically modified, and a combination of both. Most of these experimental models share some of the characteristics of human aortic aneurysms, such as media degradation, SMC loss, inflammatory infiltration, thrombosis, and atherosclerosis. (**Table 1.4**) Although they do not fully mimic the clinical features of this disease in humans, these models help to gain insight

into the pathogenesis of this disease and can be utilized to discover novel therapies for aortic aneurysms.

Table 1. 6 Rodent models of abdominal and thoracic aortic aneurysm

Model induction	*Characteristics	Aortic aneurysms	Ref.
Ang II + *ApoE*$^{-/-}$/*Ldlr*$^{-/-}$	Suprarenal aorta; MD, I, T, A	AAA	[138, 139]
$CaCl_2$ (Peri-adventitial application)	Infrarenal aorta; MD, I	AAA	[140]
$CaPO_4$ (Peri-adventitial application)	Infrarenal aorta; MD, I	AAA	[141]
Elastase (Intraluminal perfusion)	Infrarenal aorta; MD, I	AAA	[142]
Elastase (Peri-adventitial application)	Infrarenal aorta; MD, I	AAA	[143]
Elastase (Peri-adventitial application) + BAPN	Infrarenal aorta; MD, I, T, R	AAA	[144, 145]
Elastase (Peri-adventitial application) + Anti-TGFβ	Infrarenal aorta; MD, I, T, R	AAA	[146]
Lox$^{-/-}$	Thoracic aorta; MD	TAA	[147]
Fbln4^{SMKO}	Ascending aorta; MD, I	aTAA	[148]
Fbn1$^{mgR/mgR}$	Aortic root and ascending aorta; MD, I	aTAA	[149, 150]
Tgfbr1$^{M318R/+}$, *Tgfbr2*$^{G357W/+}$	Aortic root; MD	aTAA	[151]
Smad3$^{-/-}$	Aortic root and ascending aorta; MD, I, R	aTAA	[152]
$CaCl_2$ (Peri-adventitial application)	Thoracic aorta; MD, I	TAA	[153]
Elastase (Peri-adventitial application)	Thoracic aorta; MD, I	TAA	[154]
Ang II + *MMP2*$^{-/-}$	Thoracic aorta; MD	TAA	[133]
Ang II+BAPN	Thoracic aorta; MD, I, R	TAA	[155]
ApoE$^{-/-}$/*Ldlr*$^{-/-}$ + HFD	Arch, thoracic, abdominal aorta; MD, I, A	aTAA + TAA + AAA	[156, 157]
Ang II + BAPN (pump perfusion)	Thoracic and abdominal aorta; MI, I	TAA + AAA	[158]
Smad4$^{SMA-cre}$	Thoracic and abdominal aorta; MD, I, R	TAA + AAA	[159]
Tsukuba hypertensive mice + high salt	Thoracic and abdominal aorta; MD, R	TAA + AAA	[160]
Deoxycorticosterone acetate + high salt/ aldosterone	Thoracic and abdominal aorta; MD, I	TAA + AAA	[161]

Abbreviation: AAA, abdominal aortic aneurysm; Ang II, angiotensin II; ApoE, apolipoprotein E; BAPN, β-aminopropionitrile; Fbn1, fibrillin-1;Gata, GATA-binding protein; GM-CSF, granulocyte-macrophage colony-stimulating factor; HFD, high fat diet; Ldlr, low-density lipoprotein receptor; Lox, lysyl oxidase; MMP, matrix metalloproteinase; Nos, nitric oxide synthase; PBS, phosphate-buffered saline; PPE, porcine pancreatic elastase; Robo, roundabout guidance receptor; TAA, thoracic aortic aneurysm; Tgfbr; transforming growth factor β receptor. aTAA, ascending thoracic aortic aneurysm.
**MD indicates medial degeneration; I, inflammatory components; T, thrombus; R, rupture; A, atherosclerosis.*

1.7. Atherosclerosis and Aortic Aneurysms

Patients with AAAs frequently have atherosclerosis. Both diseases affect same sites of the aorta (such as infrarenal abdominal aorta), share traditional risk factors (including smoking, hypertension and hypercholesterolemia) [162, 163], and exhibit similar pathophysiological mechanisms, such as inflammatory cell infiltration, arterial remodeling, shear stress changes and thrombosis formation [115]. Atherosclerosis has been considered the underlying cause of AAA, which was widely termed as "atherosclerotic aneurysm". One possibility is that atherosclerosis-driven inflammation underlies AAA. A large number of immune cells enter the aortic wall from the atherosclerotic plaque, leading to apoptosis and phenotypic changes of SMCs that can impair the matrix-producing and matrix-repair capacity, and proteases released by inflammatory cells can induce the degradation of vascular elastic fibers [100]. Another mechanism suggests that an AAA develops as a pathological response of outward remodeling to aortic atherosclerosis. Adequacy of outward remodeling in compensating for progressive plaque growth and flow-limiting stenosis can promote SMC apoptosis and medial thinning, leading to expansion of aortic wall and AAA formation [164]. However, the current data from animal and human studies on the role of atherosclerosis in AAA is controversial, and drugs aimed at limiting atherosclerosis are not beneficial to slow the growth of AAAs [100]. One Tromsø study has demonstrated that AAA formation is not caused by atherosclerosis [165]. Agmon et al. have reported that atherosclerosis had little effect on descending aortic dilation in the population [166]. Therefore, atherosclerosis might be important in the development of some AAAs, but its role in AAA needs to be further elucidated.

1.8. ECM Remodeling in Vascular Diseases

1.8.1. ECM remodeling in atherosclerosis

Elastin and collagen are highly expressed in the aortic ECM. Decreased elastin disrupts the vascular elasticity, and fragments of elastin promote inflammatory aggregation leading to further vascular damage and is therefore a predisposing factor for the progression of atherosclerosis [167]. Collagen accumulation is characteristic of atherosclerotic plaques. The synthesis of different types of collagens increases dramatically in the early stages of atherosclerosis formation. It is estimated that collagen accounts for 60% of the proteins in calcified plaques [168]. Collagen also constitutes the fibrous cap, which provides tensile strength and thus stabilizes the plaque. Specific components of the ECM, such as Proteoglycans and hyaluronanm, can regulate different key events in the pathogenesis of atherosclerosis. Proteoglycans (i.e. versican) interact with lipoproteins to cause their retention in aortic wall and the initiation of atherosclerosis [169]. Hyaluronan contributes to neointimal hyperplasia and promotes inflammation during atherosclerosis [170]. Accumulation of proteoglycans and hyaluronic acid was found at sites of plaque erosion and was associated with acute coronary thrombosis [170-172].

1.8.2. ECM remodeling in aortic aneurysm

Elastin and collagen provide significant structural support for the aorta. Elastin-contractile units confer the contractile function of aortic wall [173]. Whereas loss of elastin matrix causes the initiation and expansion of aortic aneurysm. Fragmentation of elastic fibers is a featured biomarker of aortic aneurysms. Alteration in collagen architecture and homeostasis can also affect the mechanical property of aortic wall leading to aneurysm growth and ultimate rupture [111, 174]. Abnormalities in some specific ECM components compromising aortic structural integrity and biomechanical stress have been identified as the main mechanisms of TAA development. Mutations in the FBN1 gene disrupt fibrillin-1 in the elastin-contractile unit predisposing to

heritable MFS which is often associated with the development of TAA and dissection [175]. Mutations in the COL3A1 gene, affecting the synthesis and structure of the pro a1 (III) chain of collagen type III, predisposes to the vascular-type Ehlers–Danlos syndrome characterized by TAA and dissection. Lysyl oxidases (LOXs) are extracellular copper enzymes that catalyze the cross-linking of elastin and collagen and stabilize the elastic lamellae and collagen fibers, mutations in LOX have been identified that cause TAA and dissection in both humans and animals [176, 177]. Increased levels of proteoglycan have been detected frequently in the degenerative media of thoracic AAD tissue [178].

1.9. The Roles of TIMPs in Vascular Diseases

All the ECM components implicated in vascular diseases are substrates for metalloproteinases. Metalloproteinases in vascular tissue are mainly regulated by endogenous TIMPs. Therefore, the role of TIMP in the pathogenesis of vascular diseases is mainly reflected in the effects on ECM structure through the regulation of various metalloproteinase activities. In addition, TIMPs can directly or indirectly affect vascular cells and cell-cell interactions by inhibiting the shedding of cell surface proteins. The imbalance of TIMP and MMP may lead to pathological vascular remodeling and vascular disease. In atherosclerotic lesions, decreased TIMP levels contribute to MMP-mediated excessive matrix degradation leads to plaque instability. Decreased TIMP levels also lead to excessive hydrolysis of the elastic lamina and promote aneurysm formation. However, increased expression of TIMP may also indicate a staged compensatory response due to excessive tissue matrix destruction. The effects of alterations in the respective gene levels of TIMPs on atherosclerosis and aneurysms can be seen in **Table 1.7**.

1.9.1. TIMPs in atherosclerosis

The balance of TIMPs and MMPs plays a key role in the pathogenesis of atherosclerosis development and plaque fibrous cap rupture. The MMP family includes interstitial collagenases (e.g., MMP1, MMP8 and MMP13) that specialize in the initial cleavage of the protease-resistant fibrillar collagens that impart strength to the fibrous cap of atherosclerotic plaques. Other members (e.g., gelatinases, MMP9) catalyze the further breakdown of collagen fragments. Their increased activity is therefore closely related to plaque destabilization and is responsible for acute plaque rupture [179-183]. Stromelysin-1 (MMP3) and one of the gelatinases (gelatinase B, or MMP9) also break down elastin, an extremely important structural component of aortic media [184]. Increased expression of MMPs (MMP1, 2, 3, 9) has been identified in plaques' shoulders and regions of foam cell accumulation of human atherosclerotic plaques [185]. Unstable coronary syndromes have been found closely associated with increased numbers of MMP9-positive macrophages, that contribute to matrix degradation and the progression of acute cardiovascular events [186]. TIMP inhibits the activity of these enzymes under normal as well as pathologic conditions. Experimental manipulation of TIMP production has suggested that this protein plays a significant role in limiting plaque progression and rupture.

TIMP1 is mainly produced by vascular fibroblasts, SMCs and macrophages, and its expression is influenced by stimuli such as inflammatory cytokines. Interleukin-8 mediated downregulation of TIMP1 expression in cholesterol-loaded human macrophages [187]. This regulation allows a balance that may favor proteolytic activity in macrophage-rich regions. Equally, previous study has shown that *Timp1*-deficiency is associated with macrophage-rich lesions accompanied by active proteinases and medial destruction [188]. A decreased MMP9/TIMP1 ratio has been found to be related with plaque instability and severity of coronary atherosclerosis [189]. In contrast,

overexpression of TIMP1 reduced atherosclerotic lesions in apolipoprotein E knockout (*ApoE*$^{-/-}$) mice [190].

TIMP2 is constitutively expressed by SMCs and compared to other TIMPs is relatively unaffected by the addition of exogenous stimuli. Abundant TIMP2 was detected in macrophages at rupture-prone sites and in medial SMCs of atherosclerotic specimens from patients [7], and similarly, increased TIMP2 was also found in the aortic media subjacent to the lipid core of high-cholesterol fed rabbits, accompanied by excess MMP activity [6]. Overexpression of TIMP2 reduced the migration and apoptosis of macrophages/foam cells, as well as inhibited plaque development and destabilization [191]. Whereas *Timp2*-deficiency increased plaque vulnerability in *ApoE*$^{-/-}$ mice, in part by suppressing MMP14-dependent monocyte/macrophage accumulation into plaques [192]. In summary, TIMP2 exerts beneficial effects on the progression of atherosclerosis, possibly by regulating the behaviors of SMCs, monocytes/macrophages, and foam cells, processes that are involved with the MMP-dependent or independent functions.

TIMP3 is mostly expressed by vascular SMCs, fibroblasts, and macrophages. TIMP3 expression was reported to be significantly downregulated in microarray analysis of pericytes treated with glycosylated oxidized LDL [193]. Cardellini et al. have reported that TIMP3 expression was significantly reduced in carotid atherosclerotic plaques of type 2 diabetic patients [194]. Fabunmi et al. however, found a higher level of TIMP3 in the extracts of carotid atherosclerotic tissue [7]. Despite the divergent findings, these studies suggest the importance of TIMP3 in the development of atherosclerosis. Lack of TIMP3 exacerbated atherosclerosis in ApoE null mice possibly by increasing monocyte infiltration and polarizing macrophages towards a more inflammatory phenotype [195]. In contrast, macrophage-specific overexpression of TIMP3 reduced the inflammatory content and the amplitude of atherosclerotic plaques in *Ldlr*$^{-/-}$ mice [196]. Overexpression or deletion of TIMP3 in mice was also closely associated with the suppression and

occurrence of inflammatory metabolic disorders [197, 198]. These findings all point to an important role for TIMP3 in inflammatory-related vascular diseases, although the mechanisms are unclear. Unlike other TIMPs, TIMP4 is a special case and its role in the field of atherosclerosis is still unknown.

1.9.2. TIMPs in aortic aneurysm

Aortic aneurysm is characterized by dilatation of the vessel wall due to the degradation of ECM elements, primarily elastin and collagen in the media and adventitia layers, thereby weakening the aortic wall. The stoichiometric balance between these TIMPs and MMPs has a pivotal role in the homeostasis of aortic connective tissue. MMPs are instrumental in the development of aortic aneurysm disease [157, 199-204]. TIMPs on the other hand are the most important antagonists of post-translational regulation of MMPs activity and regulate inflammatory cell and VSMC behavior in aortic aneurysmal pathologies. Altered TIMP levels have been found in both patient aneurysm biopsies and animal aneurysm tissue [205-207], reflecting their response to MMP activities. Genetic manipulation of TIMPs in animal models further indicates that TIMP plays a critical role in the pathogenesis of aortic aneurysms.

TIMP1 expression is much higher in the whole aorta than in other TIMPs, suggesting that it may be the most important TIMP in the aorta. The studies found lower or higher levels of TIMP1 in AAA specimens compared to normal aortic samples, both accompanied by increased MMP activity [208-210]. *Timp1*-deficient mice developed larger aneurysms than wild-type (WT) mice after aortic elastase perfusion [211]. Moreover, loss of TIMP1 in hypercholesterolemic *apoE*$^{-/-}$ mice led to increased MMP activity and worsening aortic aneurysms [188]. Conversely, local overexpression of TIMP1 prevented aortic aneurysm degeneration and rupture in a rat model [9].

Overall, TIMP1 appears to show a protective effect on the development of aortic aneurysms and acts primarily as an inhibitor of MMPs. Studies have demonstrated increased, unchanged and decreased expression of TIMP2 in AAA biopsies [8, 208, 210]. Increased TIMP2 expression was also found in patients with TAA or TAAD [212]. In converse, *Timp2*-deficiency protected against CaCl2-induced AAA formation which was associated with decreased MMP2 activity [213]. However, TIMP2 gene expression increased in early but not in late stage of cerebral aneurysm progression in rats, accompanied by a dramatic increase in MMP2 and MMP9 in late stages, and *Timp2*-deficiency promoted the development of cerebral aneurysm in a mouse model [214]. Thus, the net effect (enhancement or inhibition) of TIMP2 on aneurysm formation is not clear, which may be related to the fact that TIMP2 is both a promoter and an inhibitor of MMP2 activity depending on the concentration [215].

Presently, studies investigating TIMP3 in aortic aneurysms are sparse and have not confirmed the role of TIMP4 in the development of aneurysms. Additionally, an increase in the MMP2/TIMP2 ratio has been observed in descending TAA specimens [216], while that of AAA samples has remained unchanged in comparison with control aortic tissue [210]. This represents a difference in proteolytic and inhibitory signatures between the thoracic and abdominal aorta, implying differences in the ECM remodeling during the development of aortic aneurysm.

Table 1. 7 TIMPs in atherosclerosis and aortic aneurysms

TIMPs	Mouse models	Phenotypes	Ref.
TIMPs in atherosclerosis			
TIMP1 knockout	*Timp1*$^{-/-}$/*Apoe*$^{-/-}$ + HFD	Reduced atherosclerotic plaque size but promoted aneurysm formation; pro-MMP2, MMP2 ↓	[188]
TIMP1 overexpression	*Apoe*$^{-/-}$ + HFD	Reduced atherosclerotic lesions; MMP2, MMP3, and MMP13 ↓	[190]
TIMP1 overexpression	APOE*3-Leiden mice + HFD + *Timp1* transgene	Prevented plaque rupture complications in atherosclerotic vein grafts with decreased MMP activity	[217]
TIMP2 knockout	*Timp2*$^{-/-}$/*Apoe*$^{-/-}$ + HFD	Heightened monocyte/macrophage invasion in plaques; MMP14 ↑	[192]
TIMP2 overexpression	*Apoe-/-* + *HFD*+ *Timp2* transgene	Reduced lesion area and increased plaque stability; MMP2 ↓	[191]

TIMP3 knockout	*Timp3*$^{-/-}$/*Apoe*$^{-/-}$ + HFD	Polarized macrophages towards a more inflammatory phenotype resulting in increased atherosclerosis	[195]
TIMP3 overexpression	*MacTim3 /LDLR*$^{-/-}$	Decreased the inflammatory content and the amplitude of atherosclerotic plaques	[196]
TIMPs in aortic aneurysms			
TIMP1 knockout	$CaCl_2$-induced TAA + *Timp1*$^{-/-}$	Increased progression of aneurysm formation; MMP9 ↑	[218]
TIMP1 knockout	Elastase perfusion-induced AAA + *Timp1*$^{-/-}$	Enhanced AAA formation; MMP2 and MMP9 ↑	[211]
TIMP1 knockout	*Timp1*$^{-/-}$/*Apoe*$^{-/-}$ + HFD	Promoted medial degradation and pseudo-microaneurysm formation	[219];
TIMP2 knockout	$CaCl_2$-induced AAA + *Timp2*$^{-/-}$	Attenuated AAA progression; MMP2 ↓	[213]
TIMP3 knockout	*Timp3*$^{-/-}$ + Ang II	AAA formation in response to Ang II; MMP2 ↑	[220]

Abbreviations: Ang II, angiotensin II; ApoE, Apolipoprotein E; MMP, matrix metalloproteinase; TIMP, tissue inhibitor of matrix metalloproteinase.

1.10. TIMPs in Therapeutics

The role of metalloproteinases in matrix degradation and molecule shedding has inspired the development of metalloproteinase inhibitor strategies. Synthetic molecular inhibitors against MMPs (e.g., hydroxamic acid derivatives) showed promise as therapeutic drugs for cancer in preclinical research, but all of them have so far failed to pass final phase III trials owing to many reasons, including metabolic instability, lack of efficacy and unwanted side effects [221]. A new generation of more specific MMP inhibitors targeting alternative binding sites, as well as antibody-based therapeutics are also currently in development [221]. Notably, generating effective and more specific MMP inhibitors will always be a challenge due to the high similarity of their active sites and extensive functional interconnectivity.

TIMPs, as endogenous inhibitors of metalloproteinases, could per se form a novel class of MMP inhibitors. Thus, the use of engineered TIMPs with super selectivity could be an alternative approach for the treatment of metalloproteinase-related diseases [49]. Several studies on variants in the TIMP structures that influence the affinity for different MMPs, including the residue 2 and AB loop, have represented the success of structure-based engineering of TIMP in specifically inhibiting MMP [49]. Likewise, gene-based therapies using TIMPs may have broad clinical

potential. Gene transfer to elevate local levels of TIMPs (TIMP1, TIMP2 and TIMP3) in a human vein graft model prevented MMP-induced neointima formation [222-224]. Overexpression of TIMP3 but not TIMP1 and TIMP2 promoted apoptosis of aortic SMCs implicating its potential application in gene therapy [225]. Furthermore, manipulation of TIMPs expression could be a new strategy to develop molecular inhibitors. For example, TIMP2 can be epigenetically silenced by promoter hypermethylation, while its expression can be re-established after demethylation by 5-aza-2'-deoxycytidine and trichostatin A in human cancer cell line [226]. The TIMP3 promoter is a frequent target of methylation and multiple microRNAs, so it is also possible to restore and reactivated the silenced TIMP3 by demethylation or by targeting short hairpin RNAs to inhibit microRNA-based silencing [227].

Even though TIMPs could theoretically be developed as a new therapeutic, they have only been used in model systems and *in vitro* experiments. Advances in therapy require a more comprehensive and in-depth understanding of the phenotypic effect and function of these multifunctional proteins in various diseases.

1.11. Characterization of TIMP4 and Its Role in Vascular Diseases

1.11.1. Structure, regulation, function

TIMP4 is the less-known member of the TIMP family. Originally cloned in human and later in mouse, it is a non-glycosylated 195 amino acid polypeptide with a molecular weight of 25 Da and is the largest of the four human TIMPs identified to date [228, 229]. TIMP4 exhibits 37% sequence identity with TIMP1 and 51% identity with TIMP2 and 3. Thus although the 3D structure of TIMP4

has not been determined, it can be expected to have a high structural similarity to these proteins due to its relatively high sequence identity with other TIMPs.

The expression pattern of TIMP4 is relatively limited compared to other TIMPs and is found mainly in adipose tissue, breast, cerebellum, heart, skeletal muscle, thyroid, kidney, colon, and lymph node (HGNC: 11823). Its expression is regulated by transcription factors, such as myogenin, GATA and Ets family members [230]. TIMP4 function can be regulated by posttranslational modifications, such as peroxynitrite-induced nitration and oligomerization of TIMP4 that impair its inhibitory activity against MMP2 contributing to cardiovascular disease and cancer [231].

TIMP4 inhibits almost all MMPs and some ADAMs (i.e MMP1, MMP2, MMP3, MMP7, MMP9, MMP26, MT1-MMP; ADAM28 and ADAM33), and relative to MMP9 is more specific for MMP2 in a manner similar to TIMP2 [232-236]. TIMP4 is also capable of forming a ternary MMP14-TIMP4-pro-MMP2 complex, but this does not lead to activation of pro-MMP2; instead, it inhibits MMP2 activation by suppressing MT1-MMP-mediated activation [237]. TIMP4 has been identified as the major MMP inhibitor in human platelets and may involve in regulation of platelet aggregation and recruitment [238].

In addition to its inhibitory effects, TIMP4 has been reported to have cell signaling functions. TIMP4, similar to TIMP1, may interact with putative cell surface receptor, CD63, thereby mediating cell survival pathways in breast epithelial cells [63]. Consistently, TIMP4 has been shown to inhibit apoptosis of human breast cancer cells and stimulate tumorigenesis [239].

1.11.2. Role in cancer progression and heart diseases

TIMP4 is found to be dysregulated during cancer progression of several organs, including breast, brain, colon, kidney, head and neck, bladder, prostate, endometrium and cervical. Due to the tissue-

specific differences and temporal expressional changes of carcinogenesis, current data do not allow conclusions to be made regarding the relevance of TIMP4 to cancer invasion and progression. However, the presence of TIMP4 may mark the invasive transition of some cancer. TIMP4 overexpression inhibited tumor growth by blocking vascularization of injected breast cancer cells [240]. TIMP4 was found to act as a potent inhibitor of MMP26, with increased expression in human ductal carcinoma in situ and associated with the initiation of tumor cell invasion [241]. A more comprehensive understanding of this section can be found in the reviews by Melendez-Zajgla et al. and Jackson et al. [227, 242].

TIMP4 is found to be highly expressed in the heart [229, 243]. Abnormal TIMP4 expression has been found in animal models of heart failure [244, 245], as well as in human cardiovascular disorders [246, 247]. Several studies have demonstrated that TIMP4 has a specific role in cardiovascular pathology. Plasma level of TIMP4 was significantly increased in patients after acute myocardial infarction (MI) indicating a role in the pathophysiology of postinfarction remodeling [248]. Similarly, *Timp4*$^{-/-}$ mice exhibited greater sensitivity to MI but not to pressure overload, suggesting that it may be a key regulator of MMP activity during healing following MI [249]. In addition, myocardial ischemia-reperfusion injury was caused by increased net myocardial MMP activity due to the loss of TIMP4 from the cardiac myocyte [250]. Takawale et al also demonstrated TIMP4 deficiency compromised myocardial reperfusion recovery after ischemia in mice [251]. In toto, TIMP4 appears to play a protective role in myocardial injury diseases.

1.11.3. Role in vascular diseases

Since being shown to be a unique cardio-specific MMP inhibitor, the role of TIMP4 in vascular disease seems to be overshadowed as a result. Arterial expression of TIMP4 was increased in

restenosis in response to rat vascular balloon injury [252]. TIMP4 was also visible in medial SMC layer in human non-atherosclerotic arteries and increased in areas of patient's atherosclerotic tissue populated by inflammatory cells [246]. Those together suggest a specific role of TIMP4 in vascular pathology. Firstly, TIMP4 can participate in vascular ECM remodeling after disease injuries by regulating proteolytic activities of MMP. TIMP4, but not TIMP1, 2, 3 protein level was significantly elevated in dilated BAV patient aortic tissue and was accompanied by increased expression of collagen type I [253]. Dollery et al. implicated that an increase in TIMP4 facilitated the laying down of collagen to form a mature lesion after vascular endothelial injury [252]. Additionally, TIMP4 was reported to be involved in regulating vascular SMC migration by controlling vascular matrix proteolytic balance. The addition of recombinant human TIMP4 protein reduced VSMC migration without affecting cell proliferation *in vitro* [252, 254], and the increase in TIMP4 prevented SMCs migration from the media into the neointima and thus prevent intimal hyperplasia. An inverse relationship between circulating TIMP4 levels and carotid artery intima-media thickness has been reported in an asymptomatic population [255]. Lastly, TIMP4 might also regulate cellular processes and function through MMP-dependent or independent mechanisms. Overexpression of TIMP4 was found to reduce total VSMC number without affecting DNA syntheses and cell cycle progress, and pro-apoptotic effects on SMCs in the vessel wall was observed after TIMP4 gene delivery [256]. Therefore, TIMP4 as one of the regulators of vessel cellular mechanism and ECM metabolism, implying its potential role in the process of vascular diseases.

However, the role of TIMP4 in atherosclerosis and aortic aneurysm has not been determined. Loss of TIMP4 suppressed the levels of circulating cholesterol and fatty acids in mice upon high fat diet feeding [257]. which may suggest a key role for TIMP4 in atherosclerosis represented by disorders of lipid metabolism. Also, lipid plays an important role in the etiology of AAA, and lipid-

lowing drugs can reduce risk of AAA [258, 259]. Downregulation of TIMP4 has been associated with moues AAA [260], and greater expression of TIMP4 in patient aneurysms has been shown [261], but the direct function of TIMP4 in aortic aneurysm has not been reported.

1.12. Characterization of TIMP3 and Its Role in Vascular Diseases

1.12.1. Structure, regulation, and targets

TIMP3 is unique among the four TIMPs due to its special structural features. The N-terminal five residues (Cys1-Thr-Cys-Ser-Pro5) in TIMP3 that interact with the active site of metalloproteinases determine their ability to inhibit the largest number of metalloproteases [262]. Furthermore, unlike other TIMPs that are soluble, TIMP3 is sequestered in the ECM after secretion [263]. This binding is believed to be due to the charge interaction of both N- and C-terminal domains with the sulfated glycosaminoglycan of the ECM [55]. The mature TIMP3 protein is about 24 kDa, contains an N-linked glycosylation site near the C-terminus, with a size of about 27 kDa after glycosylation [264]. Glycosylation of TIMP3 increased its affinity for glycan-binding metalloproteinases, while inhibiting its endocytosis and degradation inhibition [227].

Regulation of TIMP3 expression can occur at the transcriptional and post-transcriptional levels [262]. *Timp3* expression was highly induced by phorbol ester (PMA), epidermal growth factor (EGF), platelet-derived growth factor (PDGF) and TGFβ1 [7, 263]. TGFβ1 can induce *Timp3* expression through extracellular signal-regulated protein kinase (ERK)1/2-Sp1 signaling axis [265, 266]. TGFβ1 can also stimulate transcription of *Timp3* through activation of Smad signaling pathway [267]. MicroRNAs are shown to be involved in the post-transcriptional regulation of *Timp3*. MicroRNAs control the stability and translation of TIMP3 mRNA by base-pairing with the

3′ untranslated region (3′-UTR) in the exon 5 of TIMP3, thereby silencing *Timp3* gene expression [268]. MicroRNAs targeting TIMP3 have been widely reported in cardiovascular diseases [269-272]. Post-secreted TIMP3 proteins are confined in ECM, while overexpressed soluble TIMP3 is internalized by endocytosis of the cell surface LDL receptor-associated protein (LRP1) [273]. These contribute to the effective regulation of TIMP3 to inhibit cell surface protein shedding and pericellular protein hydrolysis.

TIMP3 targets the broadest spectrum of metalloproteinases, including all MMPs and a number of ADAMs [274]. MMPs mainly degrade ECM molecules, while ADAMs and MT-MMPs are considered to be canonical “sheddases”. TIMP3 has the unique ability to inhibit different metalloprotease families, renders it a master regulator of ectodomain shedding for various molecular other than ECM proteolysis, such as membrane-bound cytokines, growth factors and their receptors as well as adhesion molecules [262].

1.12.2. Function in ECM remodeling, inflammatory, angiogenesis and apoptosis

TIMP3 is known to inhibit MMP activity responsible for ECM turnover. TIMP3 loss resulted in elevated gelatinase and collagenase activities promoted maladaptive ECM remodeling and abnormal heart function in response to cardiac pressure overload, which was partially rescued by by MMPi (a broad-spectrum MMP-specific inhibitor) treatment [275]. Deletion of TIMP3 shifted the TIMP/MMP balance to favor MMP–mediated destruction of lung ECM, leading to loss of alveolar structure and lung efficiency [276].

In addition, TIMP3 exerts its anti-inflammatory effects by inhibiting ADAM17, a specific substrate of TIMP3 [277], also known as tumor necrosis factor-α converting enzyme (TACE), which is primarily responsible for the release of soluble TNFα from its membrane-bound

precursors [278]. Smookler et al have shown that TIMP3 regulated ADAM17-mediated shedding of TNFα and the TNFα receptor from macrophages in response to LPS [279]. The inflammatory involvement of TIMP3 is also reflected in its inhibitory effect on the shedding of adhesion molecules that control leukocyte migration. TIMP3 was found to block ADAM17-mediated cleavage of ICAM-1, an adhesion receptor that mediates inflammatory and immune responses. TIMP3 also mediated the proteolytic shedding of L-selectin [280], syndecan-1 and -4 [281] from the cell surface. Meanwhile, TIMP3 has been demonstrated to play a critical role in inflammatory diseases such as arthritis [282], hepatitis [283], colitis [284], and atherosclerosis [224].

TIMP3 is a potent inhibitor of the angiogenic effects of VEGF, blocking VEGF from binding to VEGF receptor-2 (VEGFR2) on endothelial cells and inhibiting downstream signaling and angiogenesis [285]. TIMP3 mutation causing human Sotheby's fundus dystrophy is a macular degenerative disease with sub-macular choroidal neovascularization [54, 286]. Meanwhile, TIMP3 was reported to also stabilize the capillary network during angiogenesis probably through inhibiting metalloproteinase and interacting with VEGFR2 [49].

Moreover, TIMP3 may inhibit angiogenesis by promoting EC apoptosis. TIMP3 was reported to induce apoptosis in many cancer cell lines [287, 288] and VSCM [225]. TIMP3 induces cell apoptosis in a different manner as detailed in reviews by Su et al and Spanò et al. [262, 268].

1.12.3. Multifaced role of TIMP3 in aortic aneurysm

TIMP3 mRNA expression was found to be greatly elevated in the aortic wall in patients with AAAs, which matched the increase in MMP3/Stromelysin-1 [289]. Genetic analysis of polymorphisms showed a strong association of TIMP3 with human AAA [290]. An increase in TIMP3 (but not TIMP1 or TIMP2) was also observed in ascending TAA accompanied by up-

regulation of more than one proteinase [291]. These suggest that TIMP3 is probably in an effort to counteract MMP activity in aneurysm development. Montezano et al has demonstrated that TIMP3 is the primary TIMP to preserve arterial ECM in response to Ang II, which can directly modulate vascular remodeling and function [292]. Subsequent deletion of TIMP3 was found to promote AAA in response to Ang II by blocking MMP activity [220]. However, the effect of TIMP3 alone in aortic aneurysm development is unknown, and apparently TIMP3 also has a role in the TAA but no relevant studies have been reported.

Furthermore, in addition to inhibiting MMP, TIMP3 prevents many molecules from being shed by ADAMs, and interacts directly with some molecules, such as VEGFR2 and Ang II type 2 receptor (AT2R), which have been found to be implicated in the pathology of aortic aneurysm. ADAM17 is exclusively inhibited by TIMP3. ADAM17 substrates including TNFα, epidermal growth factor receptor (EGFR), Notch1, and angiotensin-converting enzyme 2, have been reported to participate in AAA pathology [293-297]. And ADAM17 itself has been implicated in the pathology of AAA and TAA [298, 299]. Inhibition of ADAM10-mediated Notch1 signaling pathway was shown to reduce AAA formation in mice [300]. VEGFR2 expression was increased in experimental AAA [301]. Inhibition of VEGF-A or its receptor VEGFR2 activity suppressed elastase infusion-induced AAA by ameliorating mural inflammatory cell infiltration and neo-angiogenesis [302]. Additionally, endothelial adhesion molecules are common target substrates for metalloproteinases. Adhesion molecules contribute to EC survival and barrier integrity [303], whereas EC loss or disruption of endothelial lining is characteristic of human aortic aneurysms [304]. ADAM17 and ADAM10 have been demonstrated to regulate the release and functional modulation of junctional adhesion molecule A (JAM-A) in inflamed vascular endothelium [305]. The absence of ADAM17 in ECs preserved the endothelial barrier by preserving the structural integrity of cell-cell adhesions, thus exerted a protective effect against elastase-induced TAA [299].

Hence, TIMP3 has the potential to alter the activity of these substrate molecules affecting aortic aneurysm progression in different ways.

1.13. Rationale

Traditionally, TIMP4 was known as the 'heart TIMP', and has been reported to play a protective role in cardiac diseases [249-251]. Accordingly, its potential role in vascular disease could be obscured due to its unique performance in cardiac disease. TIMP1, TIMP2 and TIMP3 have been shown a role in atherosclerosis and aortic aneurysm by regulating MMP activities [188, 192, 195]. TIMP4 can also inhibit several MMPs (MMP2, 8, 9, and 13) involved in atherosclerosis and aortic aneurysm.

TIMP4 was significantly and inversely associated with carotid artery intima-media in asymptomatic young adults [255]. Increased TIMP4 was detected in patient atherosclerotic tissue populated by inflammatory cells [246]. Upregulations of TIMP4 have been found in injured vessels that were associated with ECM deposition, reduced VSMC migration and increased VSMC apoptosis [252, 254, 256]. Our lab reported that mice lacking TIMP4 had reduced plasm lipid and cholesterol concentration after following high fat feeding [257]. Therefore, TIMP4 could be involved in the pathological process of atherosclerosis and plaque deposition.

Additionally, downregulation of TIMP4 has been associated with mouse AAA development [260], but its direct function in AAA is unknown. A significant increase in TIMP4 expression was found in the patient's aneurysm tissue [261] suggesting a potential role of TIMP4 in aortic aneurysm. Hence, it is necessary to elucidate the exact role of TIMP4 in aortic aneurysm including TAA and AAA. Meanwhile, previous studies have found that the exclusively high expression of TIMP3 in human TAA or AAA tissues is positively correlated with the increase in MMP activity

[289, 291]. Our lab has shown *Timp3*-deficiency promotes AAA following Ang II infusion by blocking MMPs [220], but its role in TAA has not been reported. TIMP3 has been reported to be the primary TIMP to preserve ECM in response to Ang II [306]. TIMP3 has the widest range of inhibitory substrates that are related not only to matrix degeneration but also to pathological processes like inflammation, angiogenesis, and release of adhesion molecules that are relevant to the different pathological processes in TAA and AAA. Therefore, to fully understand the role of TIMP4 in aortic aneurysm, the effect of TIMP3 on aortic aneurysm can be further explored in parallel.

1.14. Hypotheses and Objectives

Since loss of TIMP4 led to reduced plasma cholesterol and lipid content, it would be anticipated that *Timp4*-deficiency would lead to reduced plaque deposition. Given the link between atherosclerosis and aortic aneurysm, this role of TIMP4 could impact aneurysm formation. However, I hypothesize that compared to TIMP4, TIMP3 will play a more important role in the progression of aortic aneurysms, because it has the broadest protease inhibition profile and is the primary TIMP to regulate vascular remodeling in diseases, and thereby *Timp3*-deletion will exaggerate the severity of both AAA and TAA in different ways. Specifically, the following objectives were set to test this hypothesis:

Objective 1: Determine the impact of *Timp4*-deficiency on plaque deposition in an atherogenic model mouse.

Objective 2: Determine the role of TIMP4 in atherosclerosis-related aortic aneurysm (using the Ang II-induced aneurysm model under a hypercholesterolemic condition).

Objective 3: Determine the impact of *Timp4* versus *Timp3*-deficiency on progression of TAA or AAA (using the peri-adventitial elastase-induced aneurysm model).

CHAPTER 2

MATERIALS AND METHODS

2.1. Antibodies

The antibodies used for immunohistochemistry (IHC), immunocytochemistry (ICC), and immunoblotting (IB) in this thesis are listed in **Table 2.1**. Dilution ratios were provided for each application. The corresponding isotype control for the primary antibody was used in the immunofluorescence staining.

Table 2. 1 Primary antibody dilution in different applications

Antibody	Catalogue NO.	Supplier	Dilution ratio /Application(s)
ABCA1	NB400-164	Novus	1:1000/IB
α-SMA	ab5649	Abcam	1:2000/IB; 1:500/ICC
β-Actin	4967S	Cell Signaling	1:2000/IB
Calponin	ab46794	Abcam	1/500 (IF); 1/1000 (IB)
Caspase 3	9665S	Abcam	1:1000/IB
CD31/PECAM-1	550274	BD Biosciences	1:100/IHC
CD45	550539	BD Biosciences	1:100/IHC
CD68 (human)	MCA5709	AbD Serotec	1/100 (IF)
CD68 (mouse)	MCA1957GA	EMD Millipore	1:100/IHC
Cleaved caspase3	9661S	Cell Signaling	1:500/IB
Galectin-3	ab118851	Abcam	1:100/IHC
Ly6B.2	MCA771GA	AbD Serotec	1:100/IHC
Ly6G	127602	BioLegend	1:500/IHC
OLR1	ab214427	Abcam	1:1000/IB
SM-MHC11	ab53219	Abcam	1:5000/IB; 1:100/ICC
SM22α	ab155272	Abcam	1:2000/IB; 1:100/ICC
TIMP3	ab93639	Abcam	1:200/IHC
TIMP4	ab58425	Abcam	1:200/IHC
VE-cadherin	ab205336	Abcam	1:200/IHC

Abbreviation: ABCA1, ATP-binding cassette transporter A1; α-SMA, smooth muscle alpha-actin; CD, cluster of differentiation; PECAM-1, platelet endothelial cell adhesion molecule; OLR, oxidized low-density lipoprotein receptor 1; SM-MHC11, smooth muscle myosin heavy chain 11; SM22α, smooth muscle protein 22-alpha; TIMP, tissue inhibitor of metalloproteinase; VE-cadherin, vascular endothelial cadherin.

2.2. Other Reagents

anti-mouse IgG, HRP-linked (7076S), anti-rat IgG, HRP-linked (7077S) and anti-rabbit IgG, HRP-linked (7074S) were purchased from Cell Signaling Technology. α-actin (sc-32251) was

obtained from Santa Cruz Biotechnology, Inc. Rat anti-CD68 (MCA1957GA) and Bio-Rad Protein Assay kit were purchased from Bio-Rad. Rabbit anti-CD36 (NB400-144) and rat anti-ABCA1 (NB400-164) were obtained from Novus Biologicals. Mouse anti-human CD68 (1/100, MCA 5709, AbD Serotec); Alexa Fluor 488 donkey anti-rabbit (A-21206), Alexa Fluor Plus 555 goat anti-rabbit secondary antibody (A32732), Alexa Fluor 594 goat-anti-rabbit (R37117), Alexa Fluor 594 donkey-anti-rabbit (A-21207) and Cyanine3 goat-anti-rat (A10522) were purchased from Thermo Fisher Scientific.

Total cholesterol assay kit (Fluorometric) (STA-390) was purchased from Cell Biolabs, Inc. LabAssay™ Triglyceride kit was purchased from FUJIFILM Wako. BODIPY™ 493/503 (D3922), DQ™ Gelatin from pig skin, fluorescein conjugate (D12054), TRIzol RNA Isolation Reagent (15596018), Prolong Gold Antifade Reagent with DAPI (P36935) and Prolong Gold Antifade Mountant (P10144) were purchased from Thermo Fisher Scientific. 10% buffered formalin (23-245684) was purchased from Fisher Scientific Inc. DMEM/F-12 (11330057), DMEM (11965092), HEPES (11330057), HBSS, no calcium, no magnesium, no phenol red (14175095), L-Glutamine (200 mM, 25030081), Fetal Bovine Serum (FBS, Canadian Origin, 12483020), Amphotericin B (Fungizone, 15290018), Penicillin-Streptomycin Solution (15140122) were purchased from Gibco. Falcon® cell scrapers (353085) were purchased from VWR international company. Paraformaldehyde (PFA, P6148), Oil red O, Elastic stain kit (HT25A), Evans blue (E2129), Celltyic M lysis buffer (C2978) and Filipin complex (F9765) were purchased from Sigma-Aldrich. *In Vitro* Vascular Permeability Assay kit (ECM 644) was purchased from Millipore Sigma. Collagenase type II (LS004174), elastase (LS002279), and soybean trypsin inhibitor (LS003570) were obtained from Worthington Biochemical for primary smooth muscle cell isolation. Bovine serum albumin (BSA, BAH66-1000) was purchased from Equitech-Bio, Inc. RIPA lysis and extraction buffer (89900), Pierce™ reversible protein stain kit for PVDF Membranes (24585) and

Restore™ PLUS Western Blot Stripping Buffer (46430) were purchased from Thermo Fisher Scientific.

2.3. Human Control (non-diseased) and Diseased Aortic Specimen Procurement

Human samples used in this dissertation was listed in **Table 2.2**. Abdominal aorta specimens were procured from male patients who underwent corrective surgery for abdominal aortic aneurysm at the Grey Nuns Hospital, Edmonton, AB. In the study in Chapter 3, specimens with atherosclerotic plaques and small aneurysms (<5cm) were used. In the study in Chapter 4, specimens without atherosclerotic plaques and aneurysms (>6cm) were used. Human thoracic aneurysmal specimens were procured from the proximal ascending aorta of patients (n=5 for each sex) undergoing prophylactic resection as a consequence of Marfan or bicuspid aortic valve (BAV) associated aortopathies. Patients with aortic dissection were excluded.

Control samples were non-atherosclerotic and non-aneurysmal healthy ascending or abdominal aortas obtained from donors through the Human Organ Procurement and Exchange (HOPE) program at the University of Alberta. The study protocols were approved by the Human Research Ethics Review Process (HERO) at the University of Alberta. This study was approved by Hearth Research Ethics Board and Covenant Health Research Center (HREB, Pro00089421).

All procurements were conducted following institutional approval. Aortic samples were either flash-frozen in liquid nitrogen and stored at −80°C for molecular studies or fixed in 10% formalin for histological analyses.

Table 2. 2 Clinical information for the human aorta specimens

	Human healthy abdominal aorta			Human abdominal atherosclerosis			Human abdominal aortic aneurysm			Human healthy thoracic aorta			Human thoracic aortic aneurysm		
SAMPLE#	#5	#6	#7	#28	#10	#23	#17	#34	#9	#1	#2	#3	#7	#3	#8

Age (years)	55	22	27	79	59	59	84	73	65	-	-	-	41	47	42
Sex	F	M	M	F	M	M	M	M	M	M	F	F	M	M	M
Aneurysm Size (Aortic diameter in cm)	NA	NA	NA	5	3.5	3	8.4	8.5	6.1	NA	NA	NA	BAV	BAV	Marfan
Comorbidities															
Smoking	NO	YES	YES	YES	NO	YES	NO	YES	NO	NO	NO	NO	-	-	-
Obesity	YES	NO	NO	NO	YES	NO	NO	YES	NO	NO	NO	NO	-	-	-
Family History	NO	NO	NO	NO	YES	NO	NO	NO	YES	NO	NO	NO	-	-	-
Diabetes	NO	NO	NO	YES	YES	NO	NO	NO	NO	NO	NO	NO	-	-	-
Atherosclerosis	NO	NO	NO	YES	YES	YES	NO	NO	NO	NO	NO	NO	-	-	-
Medications															
Statins	NO	NO	NO	YES	YES	YES	NO	YES	NO	NO	NO	NO	-	-	-
ACE Inhibitors	YES	NO	NO	NO	YES	YES	NO	NO	NO	NO	NO	NO	-	-	-
ARBs	NO	NO	NO	YES	NO	NO	NO	NO	NO	NO	NO	NO	-	-	-
Beta Blockers	NO	NO	NO	NO	YES	YES	YES	YES	NO	NO	NO	NO	-	-	-
Antiplatelets	YES	NO	NO	NO	YES	YES	NO	YES	NO	NO	NO	NO	-	-	-

Abbreviations: M=male, F=female, N/A, not applicable; ACE = Angiotensin converting enzyme; ARB = Angiotensin Receptor Blocker; BAV, bicuspid aortic valve.

2.4. Experimental Animal Care, Breeding and Genotyping

Low-density lipoprotein receptor-deficient mice (*Ldlr*$^{-/-}$), tissue inhibitor of metalloprotease-4 deficient mice (*Timp4*$^{-/-}$), *Ldlr*$^{-/-}$/*Timp4*$^{-/-}$ mice, *Ldlr*$^{-/-}$/*Timp3*$^{-/-}$ mice, *Timp3*$^{-/-}$ mice, and type (WT) mice were used in research presented in this dissertation, and their information is listed in **Table 2.3**. All mice are in C57BL/6J genetic background. *Ldlr*$^{-/-}$/*Timp4*$^{-/-}$ mice were generated by crossbreeding *Ldlr*$^{-/-}$ and *Timp4*$^{+/-}$ mice (see the **Figure 2.1**). *Timp4*$^{-/-}$ or *Timp3*$^{-/-}$ mice were generated after 3-5 generations of crossbreeding *Timp4*$^{+/-}$ or *Timp3*$^{+/-}$ mice. Colonies have been maintained at the Animal Facility in the specific pathogen-free (SPF), viral antibody-free (VAF) facility at University of Alberta. All experiments were performed according to the ARRIVE (Animal Research: Reporting of *in vivo* Experiments) guidelines, and in accordance with the guidelines of the University of Alberta Animal Care and Use Committee (ACUC) and the Canadian Council of Animal Care (CCAC).

Table 2. 3 Information of experimental mice

Species	Vendor or source	Background Strain	Persistent ID / URL
WT	The Jackson Laboratory	C57BL/6J	https://www.jax.org/strain/000664
***Ldlr*$^{-/-}$**	The Jackson Laboratory	C57BL/6J	https://www.jax.org/strain/002207
***Timp4*$^{+/-}$**	TIGM	C57BL/6J	https://www.tigm.org/
***Timp3*$^{+/-}$**	TIGM	C57BL/6J	https://www.tigm.org/

Abbreviations: C57BL/6J, C57 black 6; Ldlr, low-density lipoprotein; Timp, tissue inhibitor of metalloproteinases; TIGM: Texas A&M Institute for Genomic Medicine.

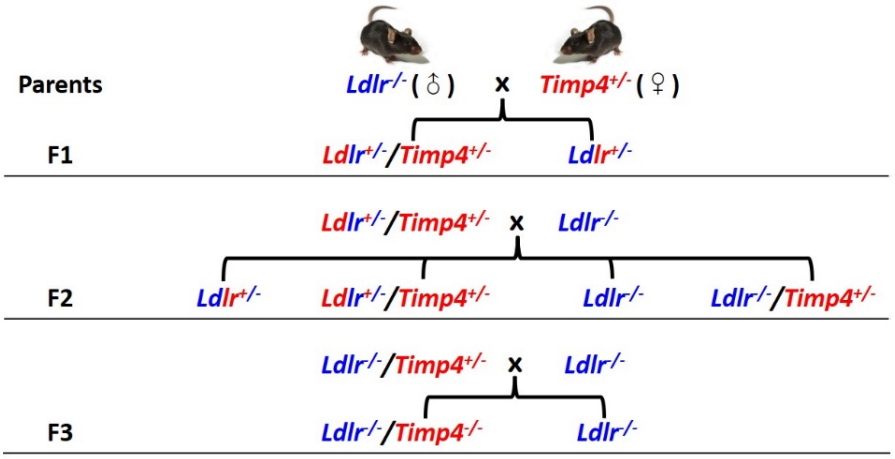

FIGURE 2. 1 FLOW CHART FOR BREEDING OF HETEROZYGOUS *LDLR*$^{-/-}$/ *TIMP4*$^{-/-}$ DOUBLE KNOCK OUT MICE IN 3 GENERATIONS.

Mice were genotyped by PCR performed on genomic DNA extracted from toe clip samples. PCR reactions and primers used for mouse genotyping are listed in **Tables 2.4** and **Table 2.5**.

Table 2. 4 PCR reactions for *Timp3, Timp4* and *Ldlr* mutations

***Timp4* reaction**			***Ldlr* reaction**			***Timp3* reaction**		
i	94°C	4 min	**i**	94°C	8 min	**i**	94°C	1 min
ii	94°C	15 sec	**ii**	94°C	20 sec	**ii**	94°C	30 sec
iii	65°C	30 sec	**iii**	65°C	30 sec	**iii**	60°C	30 sec
		-1°C /cycle			-0.5°C /cycle	**iv**	72°C	1 min
iv	72°C	40 sec	**iv**	68°C	15 sec	**v**	Go to ii, 34 times	
v	Go to ii, 10 times		**v**	Go to ii, 10 times		**vi**	72°C	10 min
vi	94°C	15 sec	**vi**	94°C	15 sec	**vii**	4°C	Forever
vii	55°C	30 sec	**vii**	60°C	30 sec	**viii**	End	
vii	72°C	40 sec	**viii**	72°C	40 sec			
ix	Go to vi, 30 times		**ix**	Go to vi, 28 times				
x	72°C	40 sec	**x**	72°C	2 min			

xi	4℃	Forever	**xi**	4℃	Forever
xii	End		**xii**	End	

Table 2. 5 Primers for *Timp4*, *Ldlr* and *Timp3* PCR reactions

Primer name	Sequence 5`→ 3`	Primer type	Targets
Timp4-F	TGCAGAGGGAGAGCCTGAA	Forward	Timp4
Timp4-R	GGTACATGGCACTGCATAGCA	Reverse	
19799 Common	TAT GCA TCC CCA GTC TTT GG	Forward	Ldlr
19800 Wild type R.	CTA CCC AAC CAG CCC CTT AC	Reverse	
oIMR7770 Mutant R.	ATA GAT TCG CCC TTG TGT CC	Reverse	
Timp3 Neo	TGA CCG CTT CCT CGT GCT TT	Forward	
Timp3-F	GGC TTG GGC TTG TCG TGC TC	Forward	Timp3
Timp3-R	CTC TCA CCC TCC TTC TCC AG	Reverse	

2.5. Experimental Mouse Model of Atherosclerosis

The mouse model of atherosclerosis was induced in *Ldlr*$^{-/-}$ mouse on the C57BL/6J background fed a high fat diet (HFD). HFD intervention started at 8 weeks of age and lasted for 3 months or 6 months to establish different degrees of plaque density in mice. HFD was purchased from Envigo (TD.88137) and consisted of 21.2% fat and 0.2% cholesterol. The composition of the diet is listed in **Table 2.6**. The diet was stored at 4°C and changed per week to avoid lipid perioxidation. Mice had ad libitum access to water and food. The body weights of mice were measured at the initial and endpoints to ensure that the mouse has taken sufficient HFD (**Figure 2.2**). Plasma and aorta were collected at the end points for the atherosclerosis assays.

Table 2. 6 Nutrient information of TD.88137 calories diet

Ingredient	% By weight	% Kcal from
Protein	17.3	15.2
Carbohydrate	48.5	42.7
Fat	21.2	42.0
kcal/g	4.5	
Cholesterol	0.2	

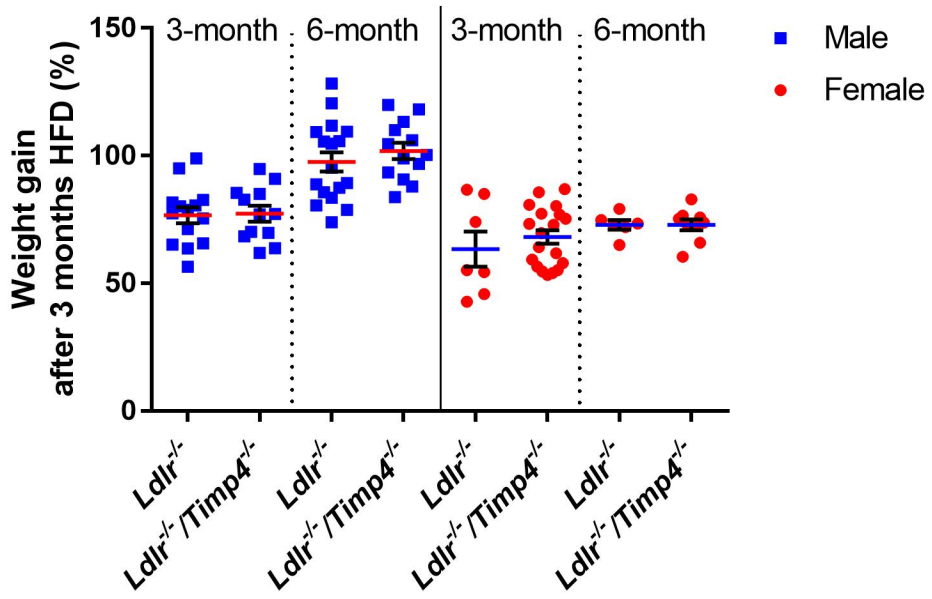

FIGURE 2. 2 THE PERCENTAGE WEIGHT GAIN OF *LDLR*$^{-/-}$ AND *LDLR*$^{-/-}$/*TIMP4*$^{-/-}$ MICE AFTER 3-MONTH OR 6-MONTH HFD. The percentage weight gain was calculated as [(the weight at endpoint - the initial weight) / the initial weight * 100].

2.6. Angiotensin II Pump Implantation

Alzet micro-osmotic pumps (Model 1004, Durect Co.) were implanted subcutaneously in mice to deliver 1.5 mg/kg/day of angiotensin II for four weeks.

Firstly, Alzet micro-osmotic pump was filled with Ang II solution according to the manufacturer's instructions. The weight of the empty pump and its flow moderator were recorded, then the prepared Ang II solution was drawn with a 1.0 ml syringe with 27-gauge filling tube, the air bubbles inside were expelled, and the Ang II solution was slowly filled into the empty pump with the syringe vertically, followed by fully inserting of the flow moderator. After that, the weight of the filled pump was recorded again, and the filling volume should be over 90% of the reservoir volume of the pump (100 µL). Then, the filled pump was incubated at 37 ºC for at least 12 hours to get it partially primed.

After anesthesia, the mouse was placed in prone position, and the skin was disinfected after removal of the hair. A ~1 cm incision perpendicular to the tail was made behind the ear above the shoulder blade of the front leg, and a subcutaneous tunnel under the skin was made using a hemostat, then a pocket for pump was created by advancing hemostat tip toward the tail. Next, the pump was fully inserted into the pocket with the moderator head positioned to the rear of the mouse, followed by the closure of the wound. Last, the mouse was placed on a heating pad until it regained consciousness.

2.7. Induction of Abdominal Aortic Aneurysm and Thoracic Aortic Aneurysm by Peri-adventitial Application of Elastase

AAA was induced in mice of each genotype by applying the infrarenal abdominal aorta with porcine pancreatic elastase Type I (20 U/mL) for 5 minutes as previously reported, with some modifications [143]. Briefly, 10-week-old male and female mice were first induced with isoflurane at 3% flow for less than 3 minutes followed by subcutaneous injection of meloxicam (2.5mg/kg BW, Metacam®) for analgesia. Then mice were placed in a supine position with a nose cone receiving isoflurane (1.5%) anesthesia. A 2.5 cm middle laparotomy was performed, and the intestines were gently removed out with damp cotton swabs and wrapped with moist gauze, and the infrarenal abdominal aortas from below the left renal vein to the iliac bifurcation were identified. The clean abdominal aortas were isolated by carefully dissection. After anatomic identification, the adventitia of exposed aortas was bathed in a small piece of sponge (5 mm × 1 mm× 1 mm) soaked with 10 μL of saline (control) or porcine pancreatic elastase (PPE; E1250, Sigma-Aldrich Co.) for 5 minutes. After elastase exposure, the sponge was removed, the peritoneal cavity was liberally irrigated with warm sterile saline, and the intestines were gently placed back into the belly. Then the fascial layers were closed with continuous suture, and skin with interrupted 6-0

polypropylene suture. The modification made in our procedure compared to the previously report is to use a diluted solution of porcine pancreatic elastase instead of applying the concentrated stock solution directly to the peri-adventitia of the mouse aorta. The dilution ratio of stock elastase used in the AAA induction was slightly increased from that used in previously reported TAA induction [299].

Experimental TAA was induced in mice by applying the descending thoracic aorta with porcine pancreatic elastase Type I (30 U/mL) for 5 minutes as described before [299]. Briefly, 10-week-old mice were first intraperitoneally injected with ketamine/xylazine cocktail (0.1mL/20g mouse weight) as a preanesthetic, then transferred to mechanical ventilation by connecting to a mouse ventilator (MiniVent Type 845, Harvard Apparatus) after endotracheal intubation. Mice were placed in the right lateral position, followed by a 1.0-cm posterolateral left thoracotomy at the 7th intercostal space (equivalent to the third-to-last false ribs space), thoracic cavities were then opened using rib retractors after careful incisions of the parietal pleura. After the chests were opened, the left lung lobes were slightly collapsed by covering them with moist gauze (6 mm x 4 mm), and then gently moved the lungs ventrally to expose the thoracic aortas. The pleura overlying the thoracic aorta was dissected for an approximately 5 mm section with a pair of blunt fine tip forceps, and the surrounding fluid was removed entirely using absorption triangles before a piece of saline- or elastase-soaked sponge (5 mm × 1 mm× 1 mm) were applied directly to the surface of the exposed aortas. After 5 minutes of elastase exposure, the sponge was removed. The chest cavities were irrigated liberally with warm saline and the lungs were re-inflated by occluding outflow on ventilator for two breaths. After all residual fluid in the chest cavity was removed, the ribs were closed with 6-0 sutures intercostal sutures, and the muscle layers were closed followed by the skin closure with wound clips.

After surgery, all incision sites were applied with Hibitane (Zoetis, 00053201) to prevent infection, all mice received 1 mL subcutaneous warmed sterile saline to reduce intraoperative fluid loss, and then were allowed to recover on a heating pad until they were fully recovered from anesthesia.

2.8. Tissue and Plasma Collection

Mice of each genotype were euthanized at indicated time points. Formalin-fixed aortas used for histological staining were first perfuse-fixed at 100 mmHg (calibrated using a 60 mL syringe without piston hung at the height of 136 cm) with 10% buffered formalin for 10 minutes. Optimal cutting temperature (OCT)-fixed aortas were perfused with 10mL pre-chilled phosphate-buffered saline (PBS) solution prior to collection, then quickly fixed using liquid nitrogen and stored at -80℃ for further processing. All the entire aortas from the heart to the iliac bifurcation were excised and cleaned by removing all perivascular fat in a home-made black silicon elastomer plate (SYLGARD™ 170, Dow Corning, 1696157). After the clean, aorta images were captured immediately by a digital camera (SONY, DSC-WX200), and a ruler was always aligned parallel to the aorta for scale reference, and spatial calibration when measuring aorta diameters. Aortic segments used for molecular analyses were snap-frozen with liquid nitrogen directly after dissection and stored at -80℃ for further cleaning and processing.

Plasma collection was performed at the indicated time points. Mice of each genotype were anesthetized, and blood was collected from right carotid vein, and then centrifuged at 2000 revolutions per minute (RPM) for 15 minutes. The supernatant plasma was then carefully collected from the blood cell pellet and stored at -80℃ for further analysis.

2.9. *En face* Oil Red-O (ORO) Staining, Lipid Deposition Visualization and Quantification

Atherosclerotic lesions were visualized and quantified by staining the aortas with ORO as described [307]. After aortas were dissected and cleaned, they were washed twice for 5 minutes in 78% methanol and stained for 60 minutes in fresh 0.2% (weight/volume) ORO staining solution. Aortas were then washed twice in 78% methanol (5 minutes per wash) to rinse out unbound or excess ORO solution. Next, aortas were placed on the black silicon dish and opened longitudinally from the aortic root to the iliac bifurcation. The whole aorta was secured with stainless steel minutien pins (Fine Science Tools, 26002-20), flattened with the lumen facing up. Images were captured by a digital camera. A ruler was aligned in parallel with the aortas for scale reference. Image-Pro Plus software (Media Cybernetics) was utilized for image analysis and plaque density quantification. Plaque density was quantified as the ORO-stained area (red) and expressed as a percentage of the total luminal surface area of the thoracic aorta (the aortic root to the diaphragm) or the abdominal aorta (the diaphragm to the iliac bifurcation).

For aortic valve analysis mice did not undergo whole body perfusion to avoid structural damage to the aortic valves that could result from this process. Freshly excised hearts were immediately placed in PBS to pump out residual blood, arrested in diastole in 1 M potassium chloride (KCl) solution, and fixed in 10% formalin. Hearts were carefully trimmed by removing the apical half of the heart at a plane parallel to the base of the aortic root, paraffin-embedded, and sectioned (5μm thick) serially until the three bipartite valve bases with attached leaflets were reached. Serial sections were obtained until the full valve structure was not visible (as examined under the microscope). Sections were processed for hemotoxylin and eosin (H&E) and Gomori Trichrome staining. The necrotic core was defined as the clear area that showed no staining with H&E or Trichrome. Fibrous cap was defined as the SMC- and collagen-rich area in Trichrome-stained

sections. Fibrous cap thickness was quantified at the site of the largest necrotic core, determined by measuring the area between the outer edge of the cap and the necrotic core boundary [308].

2.10. Cholesterol, Lipid and Lipoprotein Measurements in Plasma and Aortic tissue

Plasma: Total cholesterol assay kit (Fluorometric) (Cell Biolabs, STA-390) and LabAssayTM Triglyceride kit (FUJIFILM Wako) were used to detect cholesterol and triglyceride concentrations in plasma as per the manufacturer's instructions. Lipoprotein fractions from plasma were determined by fast-protein liquid chromatography (FPLC) in the Lipidomics Core Facility of University of Alberta.

Aortic tissue: Thoracic and abdominal aortas were separately homogenized and snap-frozen in 2 ml reinforced tubes containing 2.8 mm zirconium ceramic oxide beads (Thermo fisher scientific, 15-340-160), thoroughly homogenized using a TissueLyser II (QIAGEN), with freeze-thaw cycles in liquid nitrogen, 1–2 repeats of 2-minute cycles. The homogenates were suspended in Celltyic M lysis buffer (C2978) and left on ice for 30 minutes. The aortic lysates were transferred to 15 ml glass tubes (2 µL was saved for quantification of protein concentration). Lipids were extracted from the aortic homogenate using a modified procedure as described [309, 310]. Briefly, chloroform-methanol solution (2:1, volume/volume) was added to the aortic lysates, vigorously vortexed for 1 minute, and centrifuged at 15,000g for 10 minutes to induce phase separation. The bottom (organic) phase was collected and dried in a Gas Chamber (Benchtop Lab System) for 30 minutes. Extracted lipids were dissolved in appropriate amounts of assay buffer for further analysis. Total cholesterol assay kit (Fluorometric) (Cell Biolabs, STA-390) and LabAssay^{TM} Triglyceride kit (FUJIFILM Wako) were used to detect cholesterol and triglyceride concentrations in artic lysates as per the manufacturer's instructions. The individual cholesterol/triglyceride

concentrations were normalized to the corresponding total protein concentrations, and further expressed as microgram per gram aortic protein. Protein concentration was determined using a BCA kit (Bio-Rad). Cholesteryl ester levels were determined as the difference between total and free cholesterol levels.

2.11. Morphometric and Immunofluorescent Analyses of the Aorta

Formalin-fixed abdominal aortas were processed for H&E, Trichrome, and Verhoeff-Van Gieson (VVG) staining. The severity of elastin fiber deteriorations in the aortas were visualized by VVG staining using an elastic stain kit (Sigma-Aldrich, HT25A) as per the manufacturer's instructions. The internal aortic diameters were calculated from the internal perimeters of the VVG-stained aortic cross-sections, assuming that the cross-sections were full circles. The external aortic diameter was directly measured by the maximum diameter of the aneurysm or corresponding sham aorta in the photograph. The percentage of elastin degradation was quantified by taking the ratio of elastin-positive lengths to total aortic perimeter multiplied by one hundred. Collagen deposition and distribution in aneurysmal aortas were detected by picrosirius red (PSR) staining.

For immuno-staining, 5μm cryosections were used for staining with different antibodies. The cryosections were air-dried, fixed in fresh 4% paraformaldehyde (PFA) for 20 minutes at room temperature (RT), permeabilized in 0.1% Triton X-100 (in 1× PBS, pH 7.4; 10 minutes). Next, sections were blocked with 1% bovine serum albumin (BSA) (in 1× PBS, pH 7.4) for 1 hour, incubated with primary antibodies (diluted in 1% BSA in 1× PBS, pH 7.4) overnight at 4 °C, followed by incubation with fluorophore-conjugated secondary antibodies (diluted in 1% BSA/1×PBS, pH 7.4; 1 hr, RT). Primary antibodies targeting CD68 (macrophage), α-smooth

muscle actin (smooth muscle cell), and calponin (smooth muscle cells), Ly6B.2 (neutrophil), CD45 (lymphocyte) and CD31 (endothelial cell) were used.

The distributions and abundance of TIMP3 and TIMP4 in human healthy aortas versus aortic aneurysms or atherosclerotic aortas were determined on formalin-fixed paraffin embedded aortic sections. The sections were first deparaffinized and rehydrated, followed by heat-induced antigen retrieval in sodium citrate buffer (10 mM sodium citrate, 0.05% Tween 20, pH 6.0) at 100 °C for 20 minutes in a microwave at a 40% of power. Sections were then submitted BSA blocking, primary and secondary antibody incubation as described above. For all immunofluorescence staining, Prolong Gold Antifade Reagent with DAPI (Invitrogen, P36935) was used to visualize the nuclei. All fluorescent images were captured using an Olympus motorized inverted research microscope (Model IX81).

2.12. Filipin Staining and Visualization of Unesterified Cholesterol

Free cholesterol distribution in atherosclerotic abdominal aortas was visualized by filipin (F9765, Sigma) (excitation @ 360 nm and emission @ 480 nm) staining of cryopreserved 5μm sections, as before [311, 312]. Aorta cryosections were fixed in 4% PFA, washed 3 times in 1× PBS, and then incubated with 0.15 mg/ml filipin (dissolved in DMSO) in the dark (1 hour, RT). After washing 3 times with 1× PBS, slides were mounted with Prolong Gold Antifade Reagent, and Filipin blue fluorescence was visualized by fluorescent microscopy (Olympus IX81).

2.13. BODIPY Staining and Detection of Neutral Lipid Deposits in Tissue and SMCs

BODIPY™ 493/503 (D3922, Invitrogen) was used to visualize lipid droplets in the aortic wall (cryosections) and cultured primary SMCs as described before [88]. Aorta cryosection, or cultured

aortic SMCs were fixed in 4% fresh PFA for 20 minutes (for OCT-frozen aorta sections) or 10 minutes (for SMCs), washed with 1× PBS (3 times, 5 minutes), and incubated with 5μg/ml BODIPY (dissolved in DMSO) in the dark (30 minutes, RT). Following incubation, samples were washed in PBS, mounted with Prolong Gold Antifade Reagent with DAPI. BODIPY fluorophores (excitation @ 480nm, emission @ 515nm) were visualized and captured by fluorescent microscopy (Olympus IX81).

2.14. In Situ Gelatin Zymography

Total gelatinase activity was measured on OCT-frozen aortic section using fluorescein-conjugated gelatin (DQ gelatin, D-12054; Invitrogen) as the substrate, which emits fluorescence upon proteolytic cleavage by gelatinases in the aortic tissue. OCT-frozen slides were warmed at room temperature for 5 minutes and then incubated with reaction buffer (0.05M Tris, 0.15M sodium chloride, 5mM calcium dichloride and 0.2mM sodium azide; PH 7.6) for 30 minutes. DQ-gelatine was dissolved in water at 1 mg/mL, then diluted 1:10 in 1% (w/v) low-melting agarose (Sigma-Aldrich, A9414). The mixture was kept at 40℃ by gently heat to avoid gel formation, then quickly applied onto tissue sections and cover-slipped. After agarose mixture gelling by chill at 4 ºC for 5 minutes, slides were incubated for 1 hour in a dark chamber at 37ºC. FITC-fluorescence was visualized by fluorescent microscopy (Olympus IX81) and superimposed with elastin autofluorescence (using red filter) to show the elastin fibers. Gelatinase activity was detected as a green fluorescence in aortic media and adventitial layer, excluding elastin autofluorescence, and quantified using Image J software. The assessment of gelatinase activity was calculated by dividing the total integrated optical density (IOD_{sum}) value by all corresponding surface area ($Area_{sum}$, expressed as pixels).

2.15. Gelatin Zymography

MMP2 and MMP9 activity levels were assessed by in vitro gelatin zymography. Aorta lysate was extracted using RIPA buffer (Thermo Scientific™, 89900), and then adjust the concentration with a non-reducing loading dye. Aorta extracts were resolved on a specially formulated SDS-PAGE gel containing 1 mg/ml gelatin (Sigma-Aldrich, G8150). The "special" SDS-PAGE gel was composed of 9% contrast separating gel at the bottom, followed by 8% separating gel containing gelatin substrate and 5% stacking gel on top. Equal amounts (20 μg) of aortic extracts were separated by electrophoresis until the 50 KDa molecular weight marker reached the top of the 9% contrast separating gel. Then, contrast gel was separated from gelatin-incorporated gel and stained in 0.05% Coomassie Brilliant Blue R-250 (Bio-Rad, 161-0400). The gelatin-incorporated gel was washed 3 × 20 min in 2.5% Triton X-100 to renature the MMPs in gel, followed by incubating in zymography developing buffer (50mM Tris-Cl, pH 7.5, 5mM CaCl2, 150mM NaCl) at 37°C for 48 h. Gel was stained in 0.05% Coomassie Blue G-250 for 1 hour, then washed in de-staining buffer with 10% isopropanol and 10% acetic acid for 1 hour. Finally, gel was scanned as grayscale images and inverted for densitometric quantification. Bands of gelatinolytic activity were quantified using the inbuilt ImageQuant TL software (Version 7.0 GE Healthcare), and normalized to the loading control.

2.16. *In vivo* Evans Blue Permeability Assay

Evans blue dye can tightly bind to serum albumin *in vivo*, and thereby has been used in estimating vascular permeability. The highly extravasation of the intense bule dye within vessel indicates damage to the intimal layer and increased permeability of the endothelial cell barrier. The

Evans blue permeability assay was performed in mouse on day 3 post-TAA or AAA surgery as reported before [299]. Briefly, mice were injected with 100 μL of a 1% Evans blue (Sigma-Aldrich, E2129) solution in sterilize saline through sub-orbitally injection. 1 hour after dye injection, mice were euthanized, and perfused through the left ventricle with PBS to completely remove the Evans blue dye from the body. Then the whole aortas were dissected, the surrounding adipose tissues were removed, and images of the whole aorta were captured. The aortic segments that underwent elastase incubation were submitted OCT embedding. Aortic cross-sections were obtained and fixed with 4% PFA for 15 minutes. After 3 times wash with 1 X PBS, the sections were mounted by Prolong Gold Antifade Reagent with DAPI and used for imaging. Due to the autofluorescence characteristic of Evans blue (excitation at 620 nm, emission at 680 nm), the amount of Evans blue that permeated into the aortic wall was visualized (red) using the fluorescent microscope as mentioned above.

2.17. *En Face* Immunostaining for VE-cadherin

Mice are euthanized at the designated end point time. The abdominal and thoracic cavity was exposed by sequentially incising the skin and ribs on both sides. Then, an incision in the vena cava was made for draining blood, and the circulatory system was submitted a gravity perfusion setup at 100 mmHg (created by using a saline bag hung at the height of 136 cm) with pre-cooled saline solution containing heparin (40 U/mL, C504710, Fresenius-Kabi, Inc.) for about 5 minutes, until the saline flowing out from the cut becomes clear, followed by fixation with fresh 4% paraformaldehyde solution for 10 more minutes. The aortic segment incubated with elastin or saline was dissected and carefully remove the fat and connective tissues attached to the aorta, open the aorta longitudinally to expose the endothelium layer. Aorta segment was incubated in a

permeabilizing solution (0.2 % Triton X-100 in PBS) for 10 min with rotation, then blocked in 3% BSA containing 10% normal serum from the animal species in which the secondary antibodies have been made in PBS for 30 minutes, and then incubated with primary antibodies (diluted in 1% BSA 10% normal serum as described above) overnight at 4 °C followed by incubation with fluorophore-conjugated secondary antibodies (diluted in 1% BSA/1× TBST, pH 7.4) for 1 hour at room temperature. Primary antibodies targeting VE-cadherin (endothelial cell adherent marker) was used.

2.18. Macrophage Isolation and Culture

Primary bone marrow macrophages (BMM) were isolated from male *Ldlr*$^{-/-}$ and *Ldlr*$^{-/-}$*/Timp4*$^{-/-}$ mice as described [313]. L929-conditioned medium, which contains the macrophage colony-stimulating factor, was prepared by growing L929 cells (ATCC, C3H/An) in DMEM medium for 7 days. Mice were euthanized by cervical dislocation. The entire body was disinfected with 70% ethanol, the skin was removed, and the legs were transferred to a 100mm plate containing sterile DMEM. After removing the muscles, bones were washed twice with sterile 1× PBS. The tibia was removed, bone marrow was flushed out with Dulbecco's modified eagle medium (DMEM), using a 10 ml syringe and a 25-gauge needle, collected, and filtered through a cell strainer. The bone marrow cells were counted using a hemocytometer, and cell density was adjusted to 2×10^6 cells/ml in DMEM medium supplemented with 10% FBS, penicillin/streptomycin (100U/100µg per mL) and 10% L929-conditioned medium. Cells were grown in a humidified incubator with 5% CO_2 at 37 °C for 5-7 days. For all experiments, cells were used at passages 1-2 and serum-deprived overnight prior to the start of indicated experimental protocols. Oxidized LDL (oxLDL, 10 µg/mL; 48 hours) was used as the atherogenic stimulus.

2.19. Smooth Muscle Cell Isolation and Culture

Primary mouse descending aortic smooth muscle cells were isolated from 4-week-old male *Ldlr*$^{-/-}$ and *Ldlr*$^{-/-}$*/Timp4*$^{-/-}$ mice as described [299]. Briefly, the entire body of mouse was sprayed with 70% ethanol, the abdominal cavity was rapidly opened, and the descending aorta was dissected after perfusion with sterile PBS (containing 100 U/mL penicillin, 100 μg/mL streptomycin and 250 ng/ml Fungizone). The excised aorta was stripped off the surrounding adipose and connective tissue in ice-cold sterile PBS. The cleaned aorta was incubated in digestion buffer [1× Hanks' balanced salt solution (HBSS), 2 mg/ml BSA, 1 mg/ml collagenase type II, 0.774 U/mL elastase, and 1 mg/mL soybean trypsin inhibitor] at 37 °C for 10 minutes to detach the adventitial layer from the medial layer. Following strip off the adventitial layer, aorta was minced into small pieces (2 mm × 2 mm) and further incubated in the digestion buffer at 37°C for up to 1.5 hours. The enzymes (collagenase and elastase) were inactivated by adding an equal volume of DMEM/F12 culture medium supplemented with 20% FBS (DF20). The cell pellet was collected by centrifugation (300g for 5 min) and resuspended in DF20 media (+100 U/mL penicillin/100 μg/mL streptomycin) and plated on a 0.1% gelatin-coated dish at a density of depending on cell cluster yield. Cells were left undisturbed in a humidified incubator (37 °C/5% CO_2 in air) for at least 48 hours to allow attaching and spreading. For all experiments, cells were used at passages 3-5 and serum-deprived for 24 hours prior to the start of indicated experimental protocols. Oxidized LDL (oxLDL, 20 μg/mL; 72 hours) was used as the atherogenic stimulus.

2.20. Immunofluorescent Staining for Trans-differentiation of SMCs to Macrophage-Like Cells, and Macrophages to Foam Cells

SMCs were co-immunostained for SMC proteins (Calponin) and macrophage marker (CD68). Briefly, SMCs (1×10^4/mL) were seeded on Lab-Tek™ II chamber coverslips (Thermo Fisher Scientific), after 24 hours of serum starvation, the medium was replaced with DMEM supplemented with 20 µg/mL oxLDL and cultured for 72 hours. Next, cells were washed once with 1×PBS (pH 7.4), and then fixed in 4% PFA (prepared in 1×PBS, pH 7.4) at room temperature for 10 minutes, and permeabilized with 0.1% Triton-X100 (prepared in 1× PBS, pH 7.4) for 10 minutes at room temperature. SMCs were blocked with 1% BSA (prepared in 1× PBS, pH 7.4) for 30 minutes, and co-incubated with anti-Calponin (1:500 dilution) and anti-CD68 (1:50 dilution) overnight at 4 °C followed by incubation with Alexa Fluor 488 goat-anti-rabbit (A27034) and Alexa Fluor 594 goat-anti-rat (A-11007) secondary antibody (1:1,000 dilution) for 1 hour at room temperature, and then cell nuclei were stained with Prolong Gold Antifade Reagent with DAPI. Images were captured by an Olympus motorized inverted research microscope (Model IX81).

BMMs were co-stained for macrophage marker (CD68) and lipid droplets (Bodipy 493/503). Briefly, BMMs (2×10^6/mL) were seeded on Lab-Tek™ II chamber coverslips (Thermo Fisher Scientific), after 12 hours of serum starvation, the medium was replaced with DMEM supplemented with 10 µg/ml oxLDL and cultured for 48 hours. BMMs were fixed and treated as described above, incubated with anti-CD68 (1:50 dilution) overnight at 4°C followed by incubation with Cyanine3 goat-anti-rat (A10522) secondary antibody (1:1,000 dilution) and Bodipy 493/503 dye (5 µg/mL) for 1 hour at room temperature. Cell nuclei were stained with Prolong Gold Antifade Reagent with DAPI. Finally, foam cells were visualized by an Olympus motorized inverted research microscope (Model IX81).

2.21. Primary Human Aortic Endothelial Cell Culture and siRNA Transfection

Primary human aortic endothelial cells (HAoECs) (ATCC, PCS-100-011™) were cultured as per the manufacturer's instruction. Briefly, HAoECs were cultured in vascular cell basal medium (ATCC PCS-100-030) supplemented EC growth kit-BBE (ATCC PCS-100-040), 2% FBS, 100 U/mL penicillin and 100 μg/mL streptomycin (EC growth medium), at 37°C in an atmosphere of 5% CO_2. Purity of cells was confirmed by morphology (cobblestone appearance with large dark nuclei). Cells at passages 3-6 were used for experiments.

siRNA transfections were conducted as before [314]. Briefly, HAoECs were seeded at subconfluence (0.5×10^5 cells/mL) in EC growth medium with no antibiotics (which could interfere with siRNA transfection efficiency) for 12 hours before processing the cells further. Cells then were transfected with Lipofectamine® RNAiMAX transfection reagent (Invitrogen, 13778-150) as per the manufacturer's protocol. We transfected HAoECs with *Timp3* siRNA (Thermo Fisher, 118555) or *Timp4* siRNA (Thermo Fisher, 118690) at final concentration 15 nM for 12 hours. Scrambled siRNA (Ambion, 4390844) was used as control. TIMP3 and TIMP4 knockdown were confirmed by TaqMan PCR 72 hours post-transfections. After siRNA transfection, HAoECs were serum starved in vascular cell growth medium supplemented with 1% FBS for at least 24 hours prior to the start of indicated molecular experiments. All assays were conducted 48 hours after siRNA transfection.

2.22. *In vitro* Endothelial Cell Permeability Assay

Changes in endothelial cell permeability after elastase incubation were measured with an *in vitro* vascular permeability assay kit according to the manufacturer's instructions (ECM 644, EMD Millipore). Briefly, HAoECs were transfected with scrambled or *Timp3* siRNA or *Timp4* siRNA for 12 hours. After trypsinization, a total number of 0.5×10^6/mL HAoECs at passage 3 were

seeded into porous the collagen-coated inserts (24-well format). The cells were incubated for 72 hours to allow for a monolayer formation. Following endothelial monolayer formation, the insert was lifted out and the growth medium in the receiver plate was replaced with the new growth medium containing vehicle or porcine pancreatic elastase type I (0.4 U/mL) for 5 minutes. Then, transfer each insert to the fresh receiver tray, 150 µl of culture medium containing fluorescein isothiocyanate (FITC)-dextran was added to each insert, and 500 µl of growth medium without FITC-dextran was added to each receiver plate well. The FITC-dextran was allowed to permeate through the monolayer, and levels of FITC-dextran was measured in the receiver chamber for 5 hours. Every 30 minutes, 100 µl of media was removed from the receiver well and transfer to wells of the black 96-well opaque plate provided for fluorescence measurement. Permeability was quantified by fluorescent intensity (of FITC-dextran) on a plate reader (SpectraMax M5, Molecular Devices) via fluorescence at 485 nm excitation/535 nm emission wavelengths in a time-dependent fashion. The fluorescent intensity signal for each group was normalized to the intensity at each initial 0 time point. The experiment was run in triplicates.

2.23. RNA Extraction and Quantitative Real-time PCR

For aortic samples, fresh tissues (50-100 mg) were flash-frozen in liquid nitrogen, then were quickly pulverized while still frozen using a clean mortar and pestle. The grounded powders were transferred into the RNase-free microcentrifuge tube followed by the addition of 1 mL of TRIzol reagent. For cultured cells, 0.5 ml of TRIzol reagent was added into 35mm culture dish containing aortic SMCs or BMMs (5×10^5 -1×10^6) after complete washing off the culture media with 1× PBS. Cells were collected using sterile cell scrapers and homogenized by pipet lysate up and down. Total RNA was then extracted from these lysates according to the manufacturer's protocol for TRIzol

reagent (15596018, Invitrogen). Specifically, 0.2 mL of chloroform per 1 mL of TRIzolTM was added to lysates, and then mix thoroughly by shaking. Subsequently, samples were centrifuged at 12,000 × g for 15 minutes, followed by carefully transferring the upper aqueous phase containing the RNA to a new tube, and adding 0.5 mL of isopropanol to the aqueous phase. Aortic RNA was precipitated at 4°C for 7 days and cellular RNA was precipitated for 3 days, then the RNA pellets were obtained by centrifugation at 12,000 × g for 10 min at 4°C, followed by washing with 75% ethanol, then air-drying the RNA pellets, and finally resuspending the RNA pellets with RNase-free water.

The total RNA concentration was quantified using the NanoDrop™ 2000/2000c spectrophotometer. 1 μg of the total RNA from each sample was reverse transcribed to form complementary deoxyribonucleic acid (cDNA) using a cycle kit (Invitrogen). Quantitative real time-PCR was carried out on a LightCycler 480 II system (Roche) using the LightCycler 480 Probes Master kit (Roche, 04887301001) and TaqMan primer-probe mix (Invitrogen) for each gene is listed in **Table 2.6**. *18S* or hypoxanthine-guanine phosphoribosyltransferase (*Hprt*) was used as an internal control. The relative gene expression raw data were normalized to *18S* or *Hprt* and presented as relative gene expression for each gene.

Table 2. 7 Mouse assay IDs for the genes that were measured by TaqMan real-time PCR

Gene symbol	Protein name	Assay ID
Abc-A1	ATP-binding cassette transporter A1	Mm00442646_m1
Abc-G1	ATP-binding cassette transporter G1	Mm00437390_m1
Ccl2	CC motif chemokine ligand 2	Mm00441242_m1
Ccl3	CC motif chemokine ligand 3	Mm00441259_m1
Cd163	Cluster of Differentiation 163	Mm00474091_m1
Cd206	Cluster of Differentiation 206	Mm01329362_m1
Cd36	Cluster of Differentiation 36	Mm00450236_m1
Cd38	Cluster of Differentiation 38	Mm01220906_m1
Il1β	Interleukin 1 beta	Mm00434228_m1
Il6	Interleukin 6	Mm00446190_m1
Mmp2	Matrix metalloproteinase 2	Mm00439498_m1

Mmp3	Matrix metalloproteinase 3	Mm00440295_m1
Mmp7	Matrix metalloproteinase 7	Mm00487724_m1
Mmp8	Matrix metalloproteinase 8	Mm00439509_m1
Mmp9	Matrix metalloproteinase 9	Mm00442991_m1
Mmp12	Matrix metalloproteinase 12	Mm00500554_m1
Mmp13	Matrix metalloproteinase 13	Mm00439491_m1
Mmp14/Mt1-mmp	Matrix metalloproteinase 14/ Membrane type 1 matrix metalloproteinase	Mm00485054_m1
Olr1	Oxidized low-density lipoprotein receptor 1	Mm00454582_m1
Sra1/Msr1	Macrophage scavenger receptor 1	Mm00446214_m1
Srb1/ Scarb1	Scavenger receptor class B type 1	Mm00450236_m1
Timp1	Tissue inhibitor of metalloproteinases 1	Mm01341361_m1
Timp2	Tissue inhibitor of metalloproteinases 2	Mm00441825_m1
Timp3	Tissue inhibitor of metalloproteinases 3	Mm00441826_m1
Timp4	Tissue inhibitor of metalloproteinases 4	Mm01184417_m1
Tnfα	Tumor necrosis factor alpha	Mm00443258_m1

2.24. Protein Extraction and Immunoblotting Analysis

Total protein was extracted from aortas or cells using Celltyic M lysis buffer (C2978, Sigma-Aldrich) containing a protease and phosphatase inhibitor cocktail (Calbiochem). Total protein concentration was determined with a BCA kit (DC™ Protein Assay Kit, 5000112, Bio-Rad) according to the manufacturer's instruction.

For immunoblotting analyses, equal amounts (20-35 μg) of total protein were fractionated by electrophoresis under denaturing conditions on an 8-20% SDS-polyacrylamide gel, and transferred onto a PVDF membrane (EMD Millipore, IPV00010). The PVDF membranes were pre-stained by Pierce™ reversible protein stain kit (24585, thermo Fisher) and cut into multiple strips (2-3) based on the predicted molecular weights of target proteins, using a Plus Pre-stained Protein Ladder (Thermo Fisher Scientific, 26619) as a reference. Then PVDF membranes were blocked in 3% BSA (prepared in 1× TBST, pH 7.4) for 1 hour at RT, and incubated with primary antibodies with desired dilution ratio in 3% BSA/TBST overnight at 4 °C. The next day, the membranes were washed 3 times for 5 minutes with 1× TBST, and incubated with species-relevant HRP-linked secondary antibodies (1:5,000) for 1 hour at RT. After TBST wash, membranes were incubated in

Clarity Max™ Western ECL Substrate (Bio-Rad, 1705062) as per the manufacturer's protocols, and target bands were detected by ImageQuant LAS 400 system (GE Healthcare). The intensity of bands was quantified using the Image-Pro Plus software (Media Cybernetics) and normalized to a loading control.

2.25. Beads-based Multiplex Cytokine Protein Array

Cytokine and chemokine profiles in mouse plasma samples were quantified using Mouse Cytokine Array / Chemokine Array 31-Plex Panel (Eve Technologies, MD31). The 31-plex Discovery assay is based on the Luminex technology and utilizes the MILLIPLEX® MAP Mouse Cytokine/ Chemokine Magnetic Bead Panel Assay (EMD Millipore, MCYTMAG70PMX32BK) that comprises of fluorescent color-coded beads pre-coated with capture antibodies targeting 31 specific cytokines. In brief, plasma was obtained from blood samples of each genotype and each treatment mouse. Plasma samples were incubated with the beads before the addition of biotinylated detection antibodies followed by phycoerythrin-conjugated streptavidin. Bound cytokines and chemokines were identified and quantitated using the BioPlex 200 bead analyzer consisting of a dual-laser system which activates the fluorescent beads to identify the specific cytokines; and excites the PE conjugate to determine the magnitude of fluorescence, which is in direct proportion to reflect the amount of bound cytokine/chemokine. Fluorescence intensity values were recorded as relative fluorescent units (RFU) and converted to protein concentration (pg/mL) based on a protein standard linear curve consisting of purified cytokines at known concentrations included in each batch run. The individual cytokine/chemokine concentrations were further converted to pg per mg plasma protein.

2.26. Statistics

All values are reported as Mean ± SEM. Statistical analyses were performed by using IBM SPSS software (Version 21). Normality of data distribution was determined via the Shapiro-Wilk W test, and all data showed normal distribution. Comparison between any two groups was performed using unpaired student's t-test. Comparison among multiple groups involving one main factor was performed by 1-way analysis of variance (ANOVA) followed by Bonferroni post hoc test. Comparison among multiple groups (e.g., genotype × treatment) was performed by two-way ANOVA followed by Bonferroni post-hoc test. For *in vivo* data, the sample size (n-value) refers to the number of mice; for *in vitro* experiments the n-value refers to the number of independent experiments. Statistical significance was recognized at $p<0.05$.

CHAPTER 3

ROLE OF TIMP4 IN ATHEROSCLEROSIS

LOSS OF TIMP4 PROMOTES ATHEROSCLEROTIC PLAQUE DEPOSITION IN THE ABDOMINAL AORTA DESPITE SUPPRESSED PLASMA CHOLESTEROL LEVELS

Mei Hu, MD[1], Sayantan Jana, PhD[1], Tolga Kilic, BSc[1], Faqi Wang, PhD[1], Mengcheng Shen, PhD[1], Gerrit Winkelaar[2], Gavin Y. Oudit, MD/PhD[1,3], Katey Rayner, PhD[4], Da-wei Zhang, PhD[5], Zamaneh Kassiri, PhD[1]

[1] Department of Physiology, Cardiovascular Research Center, University of Alberta, Edmonton, Alberta.

[2] Division of Vascular Surgery, University of Alberta and The Northern Alberta Vascular Center, Grey Nuns Hospital, Edmonton, Alberta, Canada

[3]Department of Medicine/Division of Cardiology, Mazankowski Alberta Heart Institute, Cardiovascular Research Center, University of Alberta, Edmonton, Alberta, Canada

[4] University of Ottawa Heart Institute; Department of Biochemistry, Microbiology and Immunology, University of Ottawa, Ottawa, Ontario, Canada

[5] Department of Pediatrics, Lipid Group, University of Alberta, Edmonton, AB, Canada.

Contributions:

MH: Conceived and designed experiments, performed all experiments on human specimens, performed all the *in vivo* and *in vitro* murine experiments, collected and analyzed the data, prepared figures, interpreted the results, and wrote the manuscript.

SY: Contributed to immunoblotting experiments.

TK: Contributed to TaqMan experiments.

FQW: Contributed to macrophage cell culture.

MCS: Helped for collecting and cleaning aorta.

GW: Provided human diseased aortic specimens and edited the manuscript.

GYO: Provided human non-diseased aortas and edited the manuscript.

KR: Contributed to data interpretation and edited the manuscript.

DWZ: Contributed to data interpretation and edited the manuscript.

ZK: Corresponding author. Conceived hypothesis, analyzed data, wrote, and revised the manuscript.

***** A version of this chapter has been published. *Hu M, Jana S, Kilic T, Wang F, Shen M, Winkelaar G, Oudit GY, Rayner K, Zhang DW, Kassiri Z. Loss of TIMP4 (Tissue Inhibitor of Metalloproteinase 4) Promotes Atherosclerotic Plaque Deposition in the Abdominal Aorta Despite Suppressed Plasma Cholesterol Levels. Arterioscler Thromb Vasc Biol. 2021 Jun;41(6):1874-1889. doi: 10.1161/ATVBAHA.120.315522. Epub 2021 Apr 1. PMID: 33792349.* This chapter has been modified from this article.

3.2. Introduction

Atherosclerosis and its complications continue to be a leading cause of morbidity and mortality [315]. Although significant improvements have been made in reducing the mortality associated with atherosclerosis in high-income countries [316], the burden of recurrent events remains high which has left atherosclerosis high on the list of global health challenges [317]. Plaque formation is the result of a series of interactions between different cell types in the arterial wall. Tissue inhibitor of metalloproteinases (TIMPs) are best known as the physiological inhibitors of matrix metalloproteinases (MMPs) that mediate the turnover of the extracellular matrix (ECM), and are important in plaque stability by regulating fibrous cap formation [318], although their role in other aspects of plaque deposition and growth has been less explored.

Among the key features of atherosclerosis is inflammation, while macrophages as well as smooth muscles cells have been reported to contribute to plaque formation [19, 319-321]. TIMP4 has been detected in the medial smooth muscle cells (SMCs) and the adventitia in human arteries [246], and found to be upregulated in the intima, media and adventitia of large arteries after balloon injury in rats [322]. In human aortic SMC *in vitro*, TIMP4 overexpression suppressed migration and promoted apoptosis [254, 323]. In advanced atherosclerotic lesions in human arteries, TIMP4 has been detected around necrotic lipid cores [246]. While lipid lowering therapies are effective, therapeutic approaches to directly curtail the atherosclerotic process in the vasculature are non-existent [316].

We recently reported that in a model of metabolic syndrome, *Timp4*-deficiency results in lower plasma cholesterol levels and less adipose tissue deposition in mice [257]. Since plasma cholesterol is strongly linked to the severity of atherosclerosis [324]. we predicated that *Timp4*-deficiency in hyperlipidemic conditions would protect against plaque deposition. However, contrary to our

prediction, we found that despite the lower plasma cholesterol, *Timp4*-deficiency increased plaque deposition in the abdominal aorta of *Ldlr*$^{-/-}$ mice, a localized effect that was not detected in the thoracic aorta nor the aortic valves. We and others have reported that thoracic and abdominal aorta possess distinct regional heterogeneity in response to different stimuli or injuries [44, 133, 220, 325]. Our study reveals a novel function of TIMP4 in regional heterogeneity of the aorta, and its anti-atherogenic function by regulating trans-differentiation of aortic SMC into macrophage-like cells and subsequently foam cells.

3.3. Methods

The detailed Materials and methods information is available in **Chapter 2 Materials and Methods**.

3.3.1. Human Abdominal Aorta Specimens

Abdominal aorta specimens were procured from male patients who underwent corrective surgery for abdominal aortic aneurysm at the Grey Nuns Hospital, Edmonton, AB. In this study, specimens with atherosclerotic plaques and small aneurysm (<4cm) were used. Non-atherosclerotic abdominal aortas were obtained through the Human Organ Procurement and Exchange (HOPE) program (Alberta, Canada) from male donors. This study was approved by Hearth Research Ethics Board and Covenant Health Research Center (HREB, Pro00089421).

3.3.2. Animals

Low-density lipoprotein receptor-deficient mice (*Ldlr*$^{-/-}$) were purchased from The Jackson Laboratory (Stock No: 002207). Heterozygous tissue inhibitor of metalloprotease-4 deficient mice (*Timp4*$^{+/-}$, C57BL/6J background; Texas A&M Institute for Genomic Medicine) were bred to generate *Timp4*$^{-/-}$ and WT mice. *Ldlr*$^{-/-}$/*Timp4*$^{-/-}$ mice were generated by cross-breeding *Ldlr*$^{-/-}$ and *Timp4*$^{-/-}$ mice. All mice were in the same C57BL/6J genetic background, and colonies have been maintained at the Animal Facility in the viral antibody-free (VAF) facility at University of Alberta. At 8 weeks of age, mice received a high-fat diet (HFD) (22% fat by weight, 42% kcal from fat; # TD.88137 from Envigo) or continued to receive regular laboratory chow diet (4% fat by weight, 10% calories from fat, Teklad, 7001) for 3 or 6 months. All experiments were performed according to the ARRIVE (Animal Research: Reporting of *in vivo* Experiments) guidelines, and in accordance with the guidelines of the University of Alberta Animal Care and Use Committee (ACUC) and the Canadian Council of Animal Care (CCAC). Male and female mice were used in this study.

3.3.3. Tissue and plasma collection

At indicated time points, mice of each genotype were anesthetized. Formalin-fixed aortas used for histological staining were first perfuse-fixed at 100 mmHg (calibrated using a 60 mL syringe without piston hung at the height of 136 cm) with 10% buffered formalin (Fisher Scientific Inc., 23-245684) for 10 minutes.

perfused-fixed (through the apex of the left ventricle) with 10% buffered neutral formalin at 100 mmHg to fix the blood vessels in their native state. The entire aorta was dissected, cleaned and fixed or frozen for various analyses as described below. Plasma collection was performed at indicated time points after a 6-hour fasting period.

3.3.4. *En face* Oil Red-O (ORO) staining, lipid deposition visualization and quantification

Atherosclerotic lesions were visualized and quantified by staining the aortas with ORO as described [307]. Image-Pro Plus software (Media Cybernetics) was used for image analysis and plaque density quantification, the ORO-stained area (red) as a percentage of the total luminal surface area of the thoracic aorta (the aortic root to the diaphragm) or the abdominal aorta (the diaphragm to the iliac bifurcation).

For aortic valve analyses, mice did not undergo whole body perfusion to avoid structural damage to the aortic valves that could result from this process. Freshly excised hearts were fixed in 10% formalin and paraffin-embedded after the apex was trimmed, and sectioned (5µm thick) serially until the three bipartite valve bases with attached leaflets were reached; then serial sections were obtained and processed for staining. The necrotic core was defined as the clear area that showed no staining with H&E or Trichrome. Fibrous cap was defined as the SMC- and collagen-rich area in Trichrome-stained sections. Fibrous cap thickness was quantified at the site of the largest necrotic core, determined by measuring the area between the outer edge of the cap and the necrotic core boundary [308].

3.3.5. Cholesterol, lipid and lipoprotein measurements in plasma and aortic tissue

Plasma: Total cholesterol assay kit (Fluorometric) (Cell Biolabs, STA-390) and LabAssayTM Triglyceride kit (FUJIFILM Wako) were used to measure cholesterol and triglyceride concentrations in plasma as per the manufacturer's instructions. Lipoprotein fractions from plasma

were determined by fast-protein liquid chromatography (FPLC) at the Lipidomics Core Facility of University of Alberta.

Aortic tissue: Thoracic and abdominal aortas were separately homogenized and snap-frozen in 2 ml reinforced tubes using a TissueLyser II (QIAGEN). The homogenates were suspended in Celltyic M lysis buffer (C2978) and left on ice for 30 minutes, transferred to 15 mL glass tubes and lipids were extracted using a modified procedure described previously. The individual cholesterol/triglyceride concentrations were normalized to the total protein concentration and expressed as microgram per gram aortic protein. Protein concentration was determined using a BCA kit (Bio-Rad). Cholesteryl ester levels were calculated as the difference between total and free cholesterol levels.

3.3.6. Morphometric and immunofluorescent analyses of the aorta

Formalin-fixed abdominal aortas were paraffin-embedded and processed for Trichrome and Verhoeff-Van Gieson (VVG) staining as before [133]. For immuno-staining, freshly excised abdominal aortas were embedded in OCT medium, freeze-fixed in liquid nitrogen; 5µm cryosections were used for staining with different antibodies as described [299]. All fluorescent images were captured using an Olympus motorized inverted research microscope (Model IX81).

3.3.7. Filipin staining and visualization of unesterified cholesterol for aorta

Free cholesterol distribution in atherosclerotic abdominal aortas were visualized by filipin (F9765, Sigma) (excitation @ 360 nm and emission @ 480 nm) staining of cryopreserved 5µm

sections, as before [311, 312]. Filipin blue fluorescence was visualized by fluorescent microscopy (Olympus IX81).

3.3.8. BODIPY staining and detection of neutral lipid deposits in aortic tissue and primary SMCs

BODIPY™ 493/503 (D3922, Invitrogen) was used to visualize lipid droplets in the aortic wall (cryosections) and in cultured primary SMCs as described before [88]. Bodipy fluorophores (Ex. @ 480nm, Em. @ 515nm) were visualized and captured by fluorescent microscopy (Olympus IX81).

3.3.9. In situ gelatin zymography

Total gelatinase activity was measured on OCT-frozen abdominal aorta section (5 μm sections) using fluorescein-conjugated gelatin (DQ gelatin, D-12054; Invitrogen) as the substrate, which emits fluorescence upon proteolytic cleavage by gelatinases in the aortic tissue [326]. Fluorescence was visualized by fluorescent microscopy (Olympus IX81). The images were superimposed with elastin autofluorescence (using red filter) to show the elastin fibers. The fluorescent intensity of gelatinase was quantified using the Image-Pro Plus software. The average fluorescent intensity of gelatinase activity for each cross-section, excluding elastin autofluorescence, was calculated by dividing the total integrated optical density (IOD_{sum}) value by the total corresponding aorta surface area ($Area_{sum}$, expressed as pixels).

3.3.10. Macrophage isolation and culture

Primary bone marrow macrophages (BMM) were isolated from male *Ldlr*$^{-/-}$ and *Ldlr*$^{-/-}$*/Timp4*$^{-/-}$ mice as described [313]. For all experiments, cells were used at passages 1-2 and serum-deprived overnight prior to the start of indicated experimental protocols. Oxidized LDL (oxLDL, 10 μg/mL; 48 hours) was used as the atherogenic stimulus.

3.3.11. Smooth muscle cell isolation and culture

Primary mouse aortic smooth muscle cells were isolated from thoracic (above the diaphragm) and abdominal (diaphragm to iliac arteries) from 4-week-old male *Ldlr*$^{-/-}$ and *Ldlr*$^{-/-}$*/Timp4*$^{-/-}$ mice as described [299]. For all experiments, cells were used at passages 3-5 and serum-deprived for 24 hours prior to the start of indicated experimental protocols. Oxidized LDL (oxLDL, 20 μg/mL; 72 hours) was used as the atherogenic stimulus.

3.3.12. Immunofluorescent staining for trans-differentiation of SMCs to macrophage-like cells, and macrophages to foam cells

Cultured primary SMCs were stained with Bodipy 493/503 to visualize lipid droplets, or co-immunostained for SMC proteins (Calponin) and macrophage marker (CD68) following treatment with vehicle or oxLDL. Cell nuclei were stained with Prolong Gold Antifade Reagent with DAPI. Images were captured by an Olympus motorized inverted research microscope (Model IX81).

BMMs were co-stained for macrophage marker (CD68) and lipid droplets (Bodipy 493/503). Cell nuclei were stained with Prolong Gold Antifade Reagent with DAPI. Foam cells were visualized by an Olympus motorized inverted research microscope (Model IX81).

3.3.13. RNA extraction and quantitative real-time PCR

Flash-frozen thoracic or abdominal aortas were pulverized by mortar and pestle in liquid nitrogen. The total RNA was extracted from the aortas, aortic SMCs, or BMMs using TRIzol reagent according to the manufacturer's protocol. Quantitative real time-PCR was carried out on a LightCycler 480 II system (Roche) using the LightCycler 480 Probes Master kit (Roche, 04887301001) and TaqMan primer-probe mix for each gene **(see in Table 2.6)**. HPRT was used as the internal control.

3.3.14. Protein extraction and immunoblotting analysis

Total protein was extracted from abdominal or thoracic aorta, primary aortic SMCs, or BMMs using CelLytic M lysis buffer containing EDTA-free protease inhibitor cocktails. Total protein concentration was determined with a BCA kit (Bio-Rad). Western blotting was performed or aortic tissue, SMC or macrophage protein extracts as before [220, 299]. The intensity of bands was quantified using the Image-Pro Plus software (Media Cybernetics), and normalized to a β-actin control.

3.3.15. Beads-based multiplex cytokine protein array

Cytokine and chemokine profiles in mouse plasma samples were quantified using Mouse Cytokine Array/Chemokine Array 31-Plex Panel (Eve Technologies, MD31). The individual concentration of cytokines and chemokines were further normalized by plasma protein levels and expressed as pg per mg plasma protein.

3.3.16. Statistics

All values are reported as Mean ± SEM. Statistical analyses were performed by using IBM SPSS software (Version 21). Normality of data distribution was determined by the Shapiro-Wilk W test, and all data showed normal distribution. Comparison between any two groups was performed using unpaired student's t-test (Figures 3A and 6A). Comparison among multiple groups (genotype × treatment) was performed by two-way ANOVA followed by Bonferroni post-hoc test. Statistical significance was recognized at $p<0.05$.

3.4. Results

3.4.1. *Timp4*-deficiency increases plaque deposition in the abdominal but not in the thoracic aorta

We previously reported that loss of TIMP4 reduces HFD-mediated dyslipidemia and obesity [257]. To investigate if this function of TIMP4 suppresses severity of atherosclerosis, male and female *Ldlr*$^{-/-}$, *Ldlr*$^{-/-}$/*Timp4*$^{-/-}$, and *Timp4*$^{-/-}$ mice were fed regular laboratory chow diet, or high fat diet (HFD) for periods of 3 or 6 months to induce atherosclerosis [327]. Plaque deposition in the aortic arch of male *Ldlr*$^{-/-}$/*Timp4*$^{-/-}$ mice was significantly lower than that in *Ldlr*$^{-/-}$ mice, and comparable in the descending thoracic aorta between the genotypes after 3 months **(Figure 3.1 A)** or 6 months of HFD **(Figure 3.1 B)**. In contrast, a significantly higher plaque deposition in the abdominal aorta was detected in *Ldlr*$^{-/-}$/*Timp4*$^{-/-}$ compared to *Ldlr*$^{-/-}$ mice after 3 months **(Figure 3.1 A)** or 6 months of HFD **(Figure 3.1 B)**. Female *Ldlr*$^{-/-}$/*Timp4*$^{-/-}$ mice similarly exhibited lower plaque density in the aortic arch, similar plaque density in descending thoracic aorta, but greater

plaque density in the abdominal aorta compared to *Ldlr*$^{-/-}$ mice after 3 or 6 months of HFD **(Figure 3.2)**. Wildtype and *Timp4*$^{-/-}$ mice (with intact LDLR expression) did not develop plaques after 6 months of HFD feeding **(Figure 3.3)**. Plaque lesion size and characteristics were also examined in the aortic valve, which similar to the aortic arch, exhibited reduced lesion size in *Ldlr*$^{-/-}$/*Timp4*$^{-/-}$ mice, while *Timp4*-deficiency did not alter cap thickness, cap area-to-lesion area, nor the size of necrotic core **(Figure 3.4 A-B)**. Overall, these data indicate that *Timp4*-deficiency increases plaque deposition in the abdominal aorta, but not in the aortic valve, arch or the thoracic aorta.

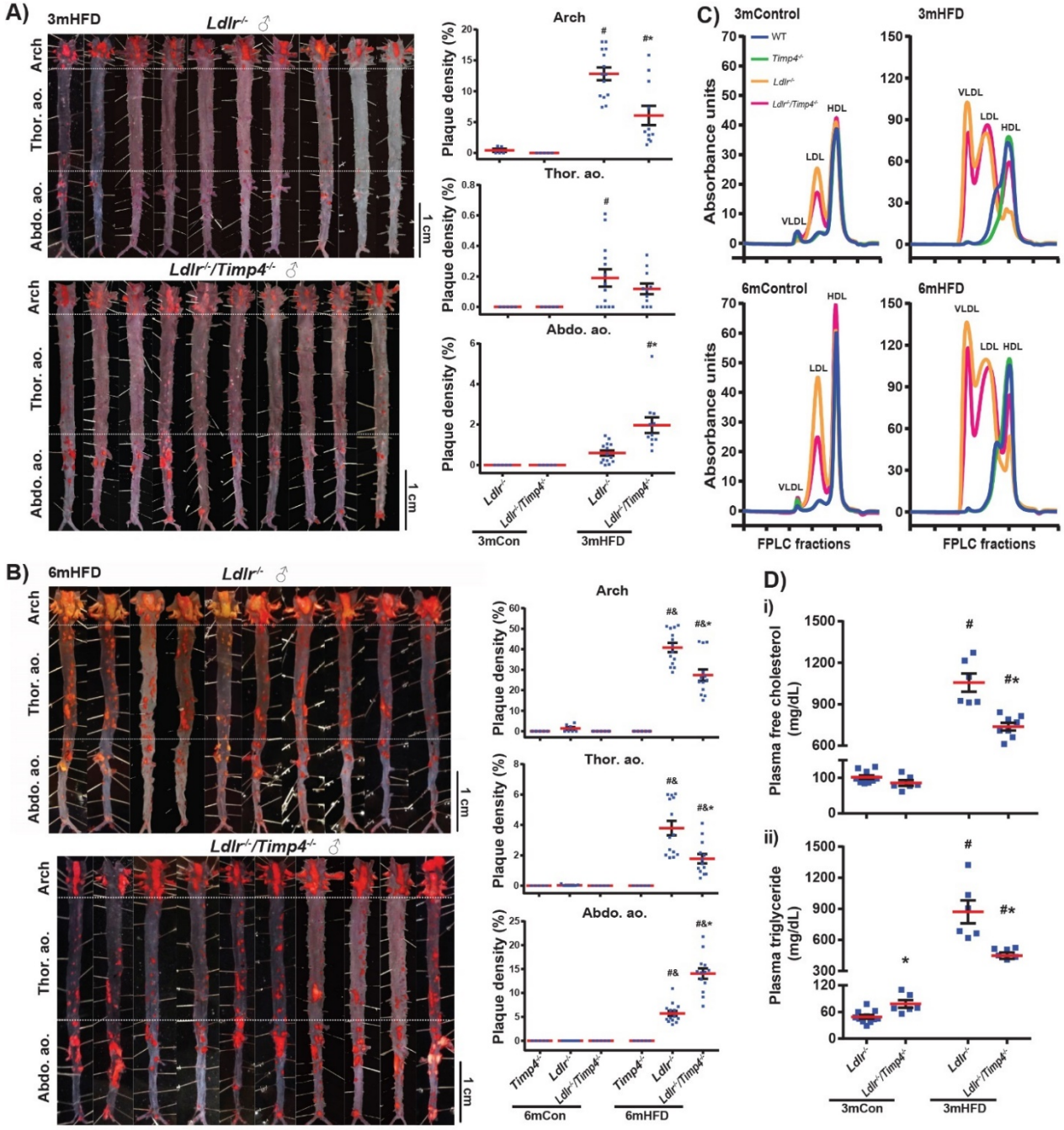

FIGURE 3. 1 *TIMP4* (TISSUE INHIBITOR OF METALLOPROTEINASE 4)-DEFICIENCY LEADS TO INCREASED PLAQUE DEPOSITION IN THE ABDOMINAL BUT NOT THE THORACIC AORTA DESPITE LOWER PLASMA CHOLESTEROL AND TRIGLYCERIDE IN MALE MICE.

Representative images of Oil Red-O–stained aortas (e*n face* staining) and quantification of *en face* lesion area at the aortic arch, thoracic, and abdominal aorta in male mice of each genotype after 3m (A) or 6m (B) of regular diet (control, Con) or high-fat diet (HFD). White dotted line divides the aorta into 3 different regions of the aortic arch, thoracic aorta, and abdominal aorta. n=5–15/group. Scale bar, 1 cm. C, Plasma cholesterol fast-protein liquid chromatography (FPLC) profiles showing redistribution of cholesterol out of HDL (high-density lipoprotein) and into LDL (low-density lipoprotein) and VLDL (very low-density lipoprotein) in male mice with 3m and 6m of regular diet or HFD feeding. n=5-8/group/genotype. D, Fluorometric analysis for fasting plasma showing lower cholesterol and triglyceride levels in *Ldlr*$^{-/-}$*/Timp4*$^{-/-}$ mice compared with *Ldlr*$^{-/-}$ mice following 3m of Con or HFD. n=6–10/group. 3m indicates 3 months;

6m, 6 months; Arch, aortic arch; and Thor. /Abdo. Ao., thoracic/abdominal aorta. #*P*<0.05 vs corresponding Con group; &*P*<0.05 vs corresponding *Timp4*$^{-/-}$ group; **P*<0.05 vs corresponding *Ldlr*$^{-/-}$ group.

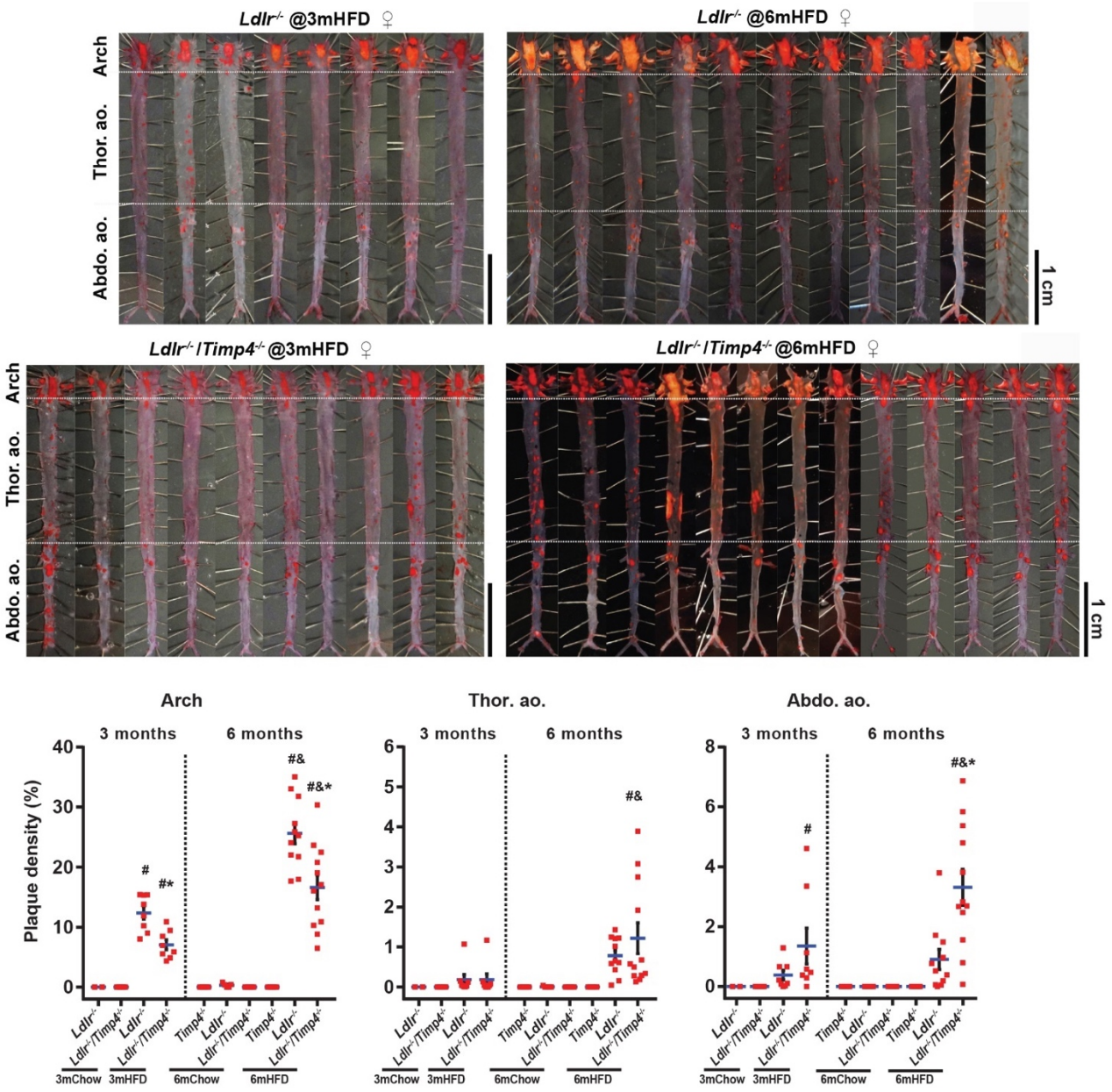

FIGURE 3. 2 *TIMP4*-DEFICIENCY IN FEMALE MICE LEADS TO MORE PLAQUE DEPOSITION IN THE ABDOMINAL BUT NOT THE THORACIC AORTA.

Images of Oil Red O-stained aorta (*en face* assay) and its quantification of *en face* plaque area in the aortic arch, thoracic and abdominal aorta in female mice after 3 months or 6 months of HFD. Dotted line divides the aorta into the aortic arch, thoracic aorta and abdominal aorta. n=5-13/group. Scale bar, 1 cm. Thor. /Abdo. ao., thoracic/abdominal aorta; HFD high fat diet. #*P*<0.05 vs corresponding control (Con) group; & *P*<0.05 vs corresponding *Timp4*$^{-/-}$ group; * *P*<0.05 vs corresponding *Ldlr*$^{-/-}$ group.

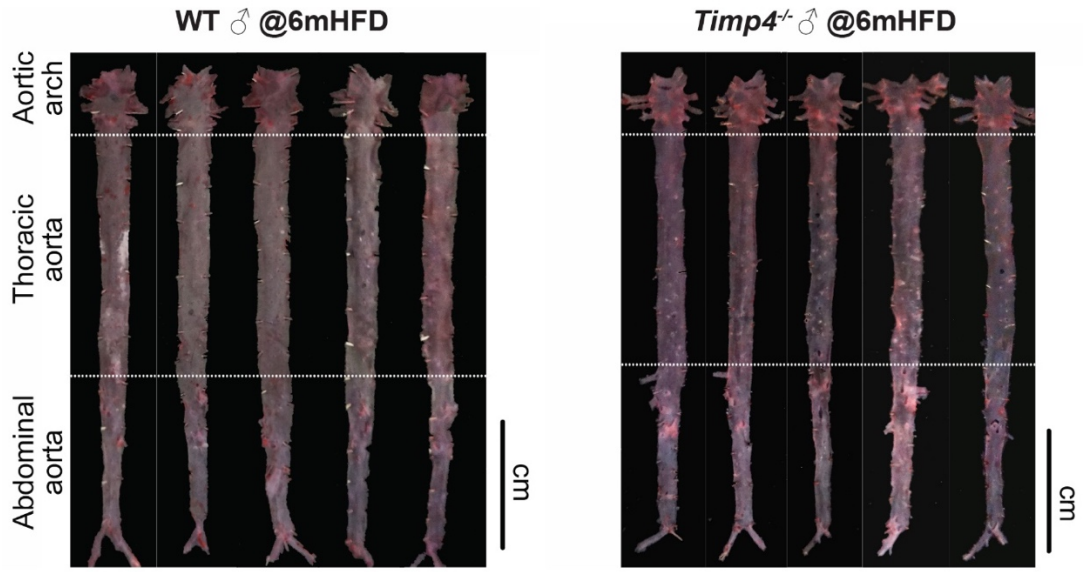

FIGURE 3. 3 WILDTYPE (WT) AND *TIMP4*-DEFICIENT (*TIMP4*$^{-/-}$) MICE DO NOT DEVELOP ATHEROSCLEROTIC PLAQUES AFTER 6 MONTHS OF HFD FEEDING.

Images of Oil Red O-stained aortas (*en face* staining) in male mice of WT and *Timp4*$^{-/-}$ after 6 months of high fat diet (HFD) feeding. White dotted line divides the aorta into three regions of the aortic arch, thoracic aorta and abdominal aorta. n=5/group. Scale bar, 1 cm.

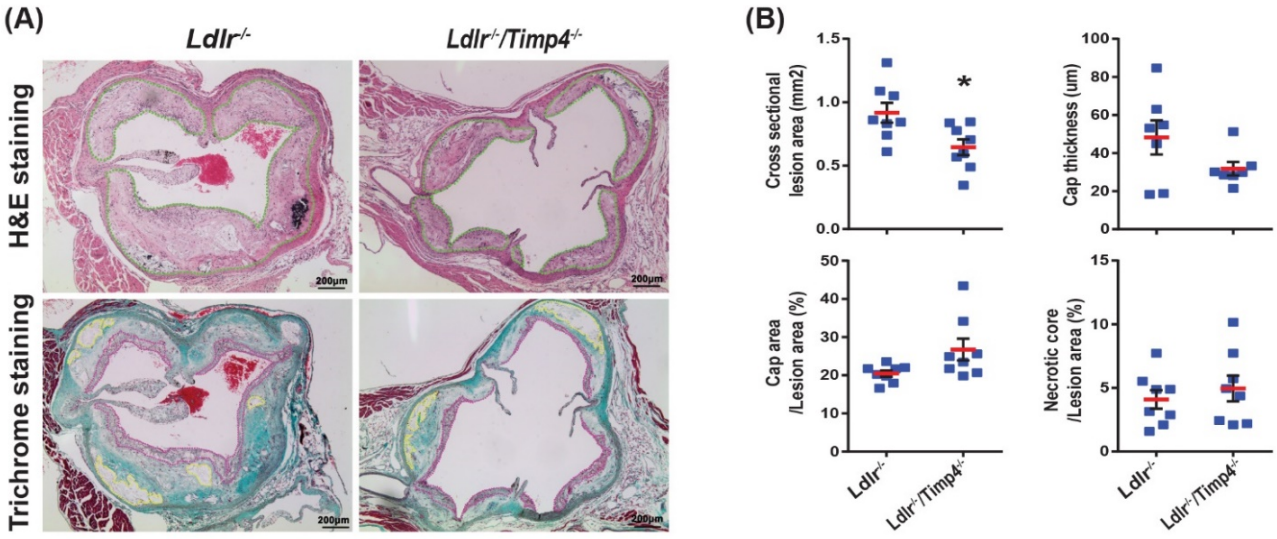

FIGURE 3. 4 *LDLR*$^{-/-}$/*TIMP4*$^{-/-}$ MICE HAVE LESS PLAQUE DEPOSITION IN THE AORTIC SINUS.

Representative cross-section images of aortic valve (stained with H&E or trichrome) **(A)** and its quantification **(B)** from male mice after 6-month high fat food. Lesion area is defined as the area of plaque built up in the aortic sinus (green line); Necrotic core is defined as a clear area that is Trichrome free (yellow line); Fibrous cap is defined as the smooth muscle cell- and collagen-rich area (magenta line); Cap thickness is measured from the thinnest part of the cap; n=8-9/group. **P*<0.05 vs corresponding *Ldlr*$^{-/-}$ group.

3.4.2. High fat-induced rise in plasma cholesterol and TG is suppressed in mice lacking TIMP4

We first investigated if the observed regional differences in plaque deposition are linked to the impact of TIMP4 on lipid metabolism. Free cholesterol and triglyceride levels were markedly elevated in *Ldlr*$^{-/-}$ mice following HFD, but this increase was significantly lower in HFD-fed *Ldlr*$^{-/-}$/*Timp4*$^{-/-}$ mice (**Figure 3.1 D**). Further analysis of plasma cholesterol profile (by FPLC, Fast Protein Liquid Chromatography) revealed that in all genotypes (WT, *Timp4*$^{-/-}$, *Ldlr*$^{-/-}$, *Ldlr*$^{-/-}$/*Timp4*$^{-/-}$) receiving the regular laboratory chow diet, plasma cholesterol is predominantly comprised of high-density lipoprotein (HDL), followed by much smaller fractions of low-density lipoprotein (LDL) and very low-density lipoprotein (VLDL); while predictably, LDL levels are elevated in mice lacking LDLR after 3 or 6 months of regular laboratory chow diet (**Figure 3.1 C, top panel,** yellow line). Three or six months of HFD resulted in redistribution of plasma cholesterols with VLDL and LDL cholesterols comprising the majority of the plasma cholesterol in *Ldlr*$^{-/-}$ mice (**Figure 3.1 C, bottom panel,** yellow line). In *Ldlr*$^{-/-}$/*Timp4*$^{-/-}$-HFD mice, however, HDL levels remained markedly higher and VLDL lower than in *Ldlr*$^{-/-}$-HFD mice (**Figure 3.1 C, bottom panel,** red line). In WT and *Timp4*$^{-/-}$ mice, the higher HDL to LDL/VLDL ratio was sustained following HFD (**Figure 3.1 C,** blue and green lines, respectively). These data demonstrate that consistent with our previous report on *Timp4*-deficient mice [257], loss of TIMP4 improves lipid and cholesterol metabolism under hyperlipidemic conditions resulting in reduced levels of TG and VLDL, and sustained HDL. These data further reveal that the higher plaque density in the abdominal aorta of *Ldlr*$^{-/-}$/*Timp4*$^{-/-}$-HFD mice is not due to a higher plasma cholesterol level in these mice.

3.4.3. Adverse aortic remodeling and higher cholesterol content in the abdominal aorta of *Ldlr*$^{-/-}$*/Timp4*$^{-/-}$-HFD mice

Next, we examined whether the increased plaque deposition in the abdominal aorta of *Ldlr*$^{-/-}$*/Timp4*$^{-/-}$-HFD mice is associated with exacerbated structural disruption in the aortic wall. Gomori Trichrome, H&E and VVG show larger plaques, associated with greater loss and disruption of the elastin fibers in the medial layer in *Ldlr*$^{-/-}$*/Timp4*$^{-/-}$ **(Figure 3.5 A)**. In addition, immunofluorescence imaging revealed a more severe loss of smooth muscle cells (calponin staining, red) and elastin fiber disruption (green, autofluorescence) at the site of plaque deposition in these aortas **(Figure 3.5 A, far right panels)**. Bodipy 493/503 and Filipin staining were used to visualize lipid and cholesterol content in the aortic wall, respectively **(Figure 3.5 B)**, and biochemical measurement of total cholesterol and cholesterol ester levels in the aortic wall showed lower levels in the thoracic aorta but higher levels in the abdominal aorta of HFD-fed *Ldlr*$^{-/-}$*/Timp4*$^{-/-}$ compared to *Ldlr*$^{-/-}$ mice **(Figure 3.5 C)**. Triglyceride content in the aortic wall was comparable between *Ldlr*$^{-/-}$*/Timp4*$^{-/-}$ and *Ldlr*$^{-/-}$ mice (data not shown). Therefore, the increased plaque size in the abdominal aorta is associated with adverse structural remodeling and increased cholesterol content in the aortic wall.

The higher cholesterol content in the abdominal aortic wall could result from increased lipid uptake or reduced cholesterol efflux by the cells in this region, or both. mRNA expression levels of candidate molecules responsible for modified lipoprotein uptake, CD36, oxidized low-density lipoprotein receptor 1 (OLR1) and scavenger receptor class (SR)-A1, were increased in the abdominal but reduced in the thoracic aorta of *Ldlr*$^{-/-}$*/Timp4*$^{-/-}$-HFD compared to *Ldlr*$^{-/-}$-HFD mice. Meanwhile, expression of SR-B1, ATP-binding cassette transporter A1 and G1 (ABCA1/ABCG1), which mediate cholesterol efflux from the cell were comparable in the abdominal aorta between *Ldlr*$^{-/-}$*/Timp4*$^{-/-}$ and *Ldlr*$^{-/-}$ mice **(Figure 3.5 D)**.

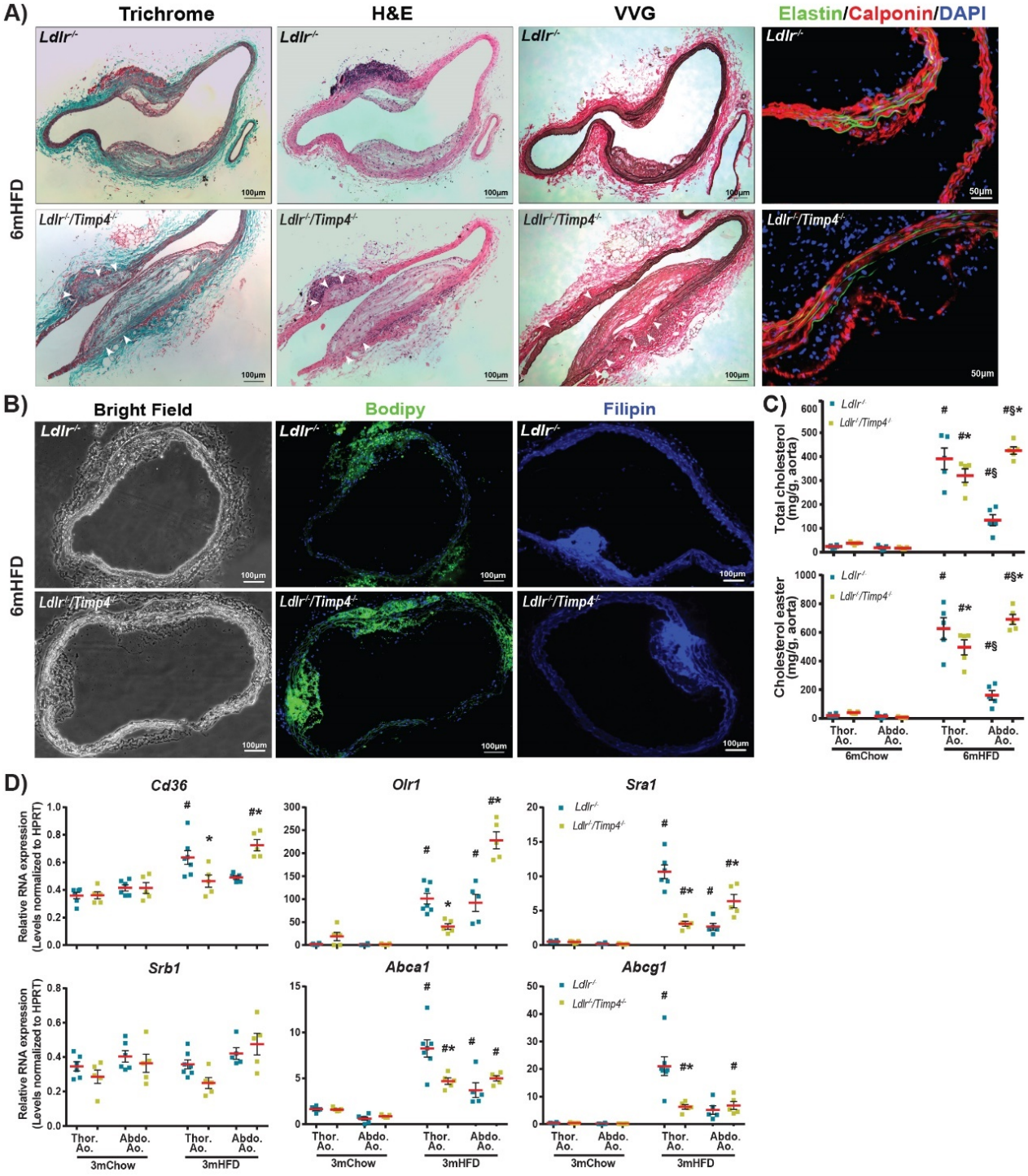

FIGURE 3. 5 ABDOMINAL AORTA IN *LDLR*$^{-/-}$/*TIMP4*$^{-/-}$ MICE SHOW ADVERSE REMODELING ASSOCIATED WITH PLAQUE BUILD-UP AND HIGHER CHOLESTEROL CONTENT.

A. Representative images of trichrome, hematoxylin and eosin stain (H&E), Verhoeff-Van Gieson (VVG), and immunofluorescent staining (elastin fibers, green autofluorescence; smooth muscle cells, calponin, red) of abdominal aortic cross-section from male mice after 6-mo high-fat diet (HFD). Nuclei were stained by DAPI (4′,6-diamidino-2-phenylindole dihydrochloride; blue). B. Representative images of abdominal aortic cross-section showing and plaque deposition (bright field; neutral lipid, Bodipy 493/503, green; free cholesterol, filipin, blue) from male mice after 3-mo HFD. C, Fluorometric analysis for aortic tissue showing higher total cholesterol and cholesterol ester levels

in *Ldlr*$^{-/-}$/*Timp4*$^{-/-}$ mice compared with *Ldlr*$^{-/-}$ mice following 6-mo HFD. n=5–6/group. D, mRNA expression levels of lipid uptake mediated-receptors and lipid transporters associated with the ability of lipid uptake in abdominal aorta from male mice following 3-month HFD. n=5–7/group. White arrows show the elastin breaks in the medial layers. 3m indicates 3 months; 6m, 6 months; HPRT, hypoxanthine phosphoribosyltransferase; and Thor. /Abdo. Ao., thoracic/abdominal aorta. #P<0.05 vs corresponding control (Con) group; §P<0.05 vs corresponding thoracic aorta group; *P<0.05 vs corresponding *Ldlr*$^{-/-}$ group.

3.4.4. Increased inflammation detected in the abdominal aorta of *Ldlr*$^{-/-}$/*Timp4*$^{-/-}$-HFD mice

Inflammation is a central characteristic of atherosclerotic lesions, promoting plaque growth and instability. We assessed the extent of inflammation in the abdominal aorta by co-immunostaining for CD68, a marker for macrophages and macrophage-like cells, and α-smooth muscle actin, a marker for SMCs. We found a significantly greater density of CD68$^+$ cells in the abdominal aorta lesion in HFD-fed *Ldlr*$^{-/-}$/*Timp4*$^{-/-}$ compared to *Ldlr*$^{-/-}$ mice **(Figure 3.6 A)**. Consistent with the less severe lesions in the aortic valves, less CD68$^+$ cells were detected in this region of *Ldlr*$^{-/-}$/*Timp4*$^{-/-}$-HFD compared to *Ldlr*$^{-/-}$ mice **(Figure 3.7)**. The extent of inflammation in the abdominal aorta was further confirmed by mRNA expression of cytokines and macrophage markers in the thoracic and abdominal aorta in all genotypes. While all cytokines were elevated in both HFD-fed groups, pro-inflammatory cytokines, interleukin-6 (*Il6*) and *Il1β*, chemokine *Ccl2* (C-C motif chemokine ligand-2), and M1-macrophage markers, *Cd38* and *Cd163,* were significantly higher in the abdominal aorta (but not thoracic aorta) of *Ldlr*$^{-/-}$/*Timp4*$^{-/-}$ compared to *Ldlr*$^{-/-}$ mice **(Figure 3.6 B)**. Tumor necrosis factor-α (*Tnfα*) and *Cd206* (an M2-macrophage marker) were comparable between genotypes **(Figure 3.6 B)**. We also examined if loss of TIMP4 is associated with systemic inflammation in these mice by measuring the protein levels of inflammatory mediators (IL1α, IL6, IL12(70), IL5, IL9, IL13, CCL3, CCL11, C-X-C motif chemokine ligand [CXCL]-9 and CXCL10) in the plasma of these animals using a plasma cytokine array, but found no difference among the

genotypes **(Figure 3.8)**. Therefore, *Timp4*-deficiency was associated with increased inflammation in the abdominal aorta.

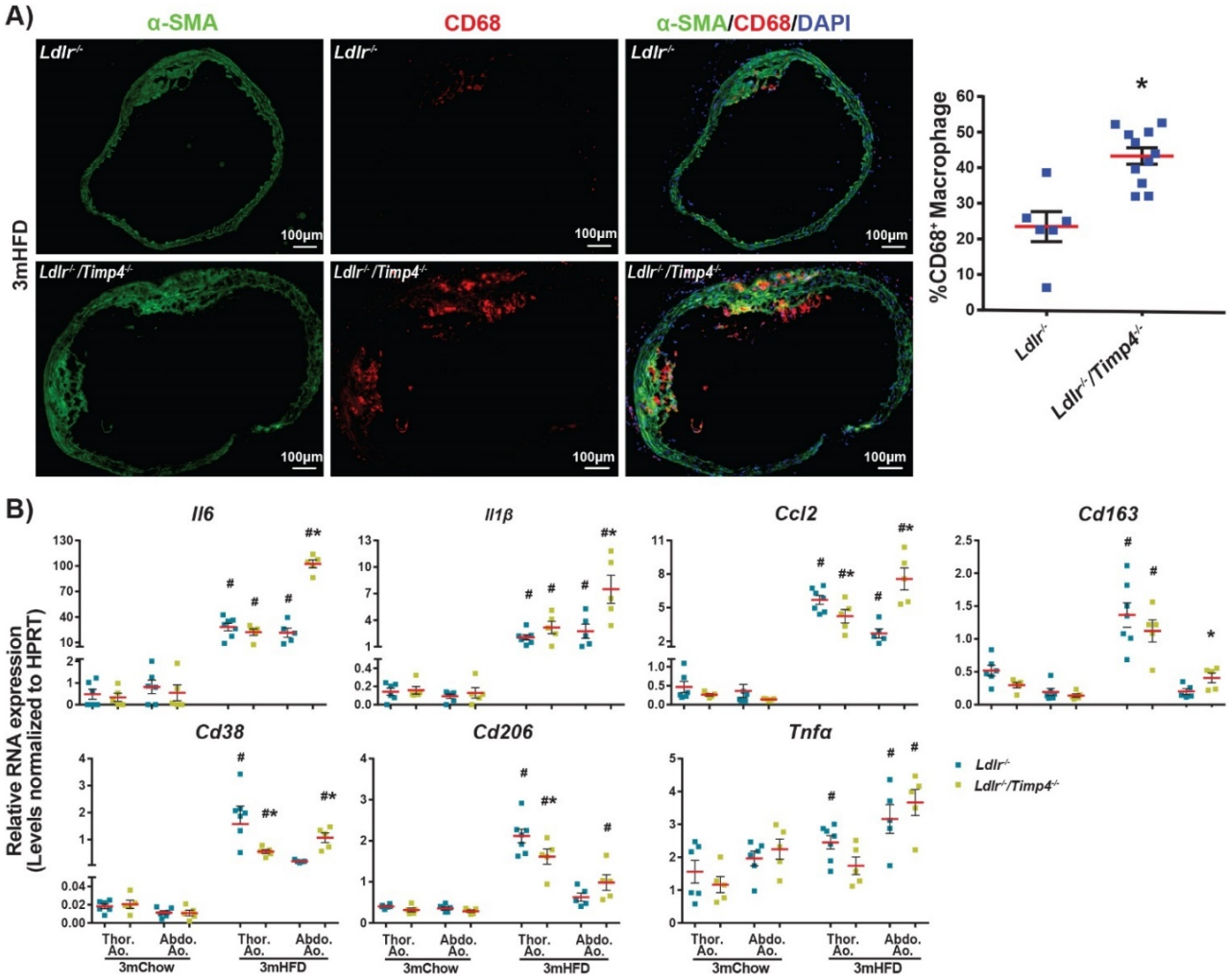

FIGURE 3. 6 HIGHER PLAQUE DENSITY IN *LDLR*$^{-/-}$/*TIMP4*$^{-/-}$ MICE IS ASSOCIATED WITH GREATER INFLAMMATION IN THE ABDOMINAL AORTA AFTER 3-MO HIGH-FAT DIET (HFD).

Representative immunofluorescent staining and quantification showing increased macrophage infiltration (macrophage, CD68, red; smooth muscle cells, α-SMA [alpha-smooth muscle actin], green) in *Ldlr*$^{-/-}$/*Timp4*$^{-/-}$ male mice after 3 mo of HFD. n=6–11 sections from 4-6 individual mice/group. Nuclei were stained with DAPI (4′,6-diamidino-2-phenylindole dihydrochloride; blue). B. mRNA expression levels of inflammatory cytokines, chemokines, macrophage markers, and macrophage polarization-controlling receptor associated with vascular inflammation in thoracic and abdominal aorta from male mice following 3-mo HFD. n=5–7/group. 3m indicates 3 months; HPRT, hypoxanthine phosphoribosyltransferase; and Thor. /Abdo. Ao., thoracic/abdominal aorta. #P<0.05 vs corresponding control (Con) group; *P<0.05 vs corresponding *Ldlr*$^{-/-}$ group.

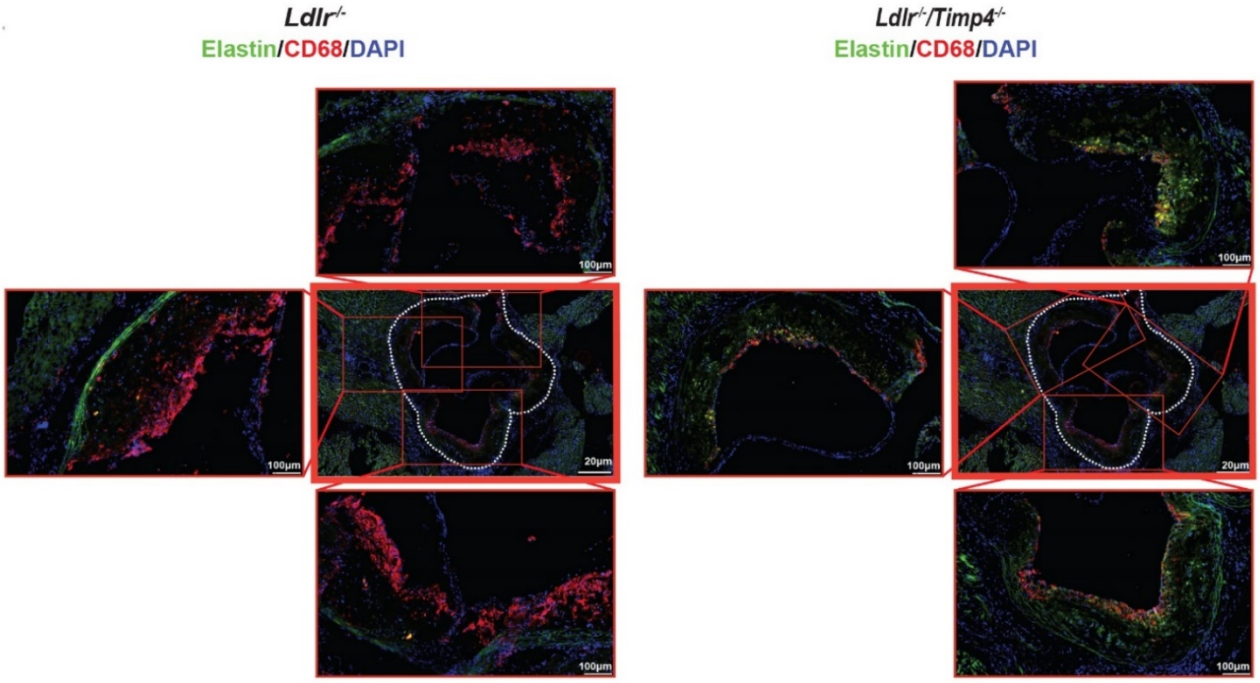

FIGURE 3. 7 *LDLR*$^{-/-}$*/TIMP4*$^{-/-}$ MICE HAVE LESS INFLAMMATION IN THE AORTIC SINUS.

Representative immunofluorescent staining showing reduced macrophage infiltration (CD68, red) in aortic sinus from *Ldlr*$^{-/-}$*/Timp4*$^{-/-}$ male mice after 6 months of HFD. White dotted line indicated the aortic valve. **P*<0.05 vs corresponding *Ldlr*$^{-/-}$ group.

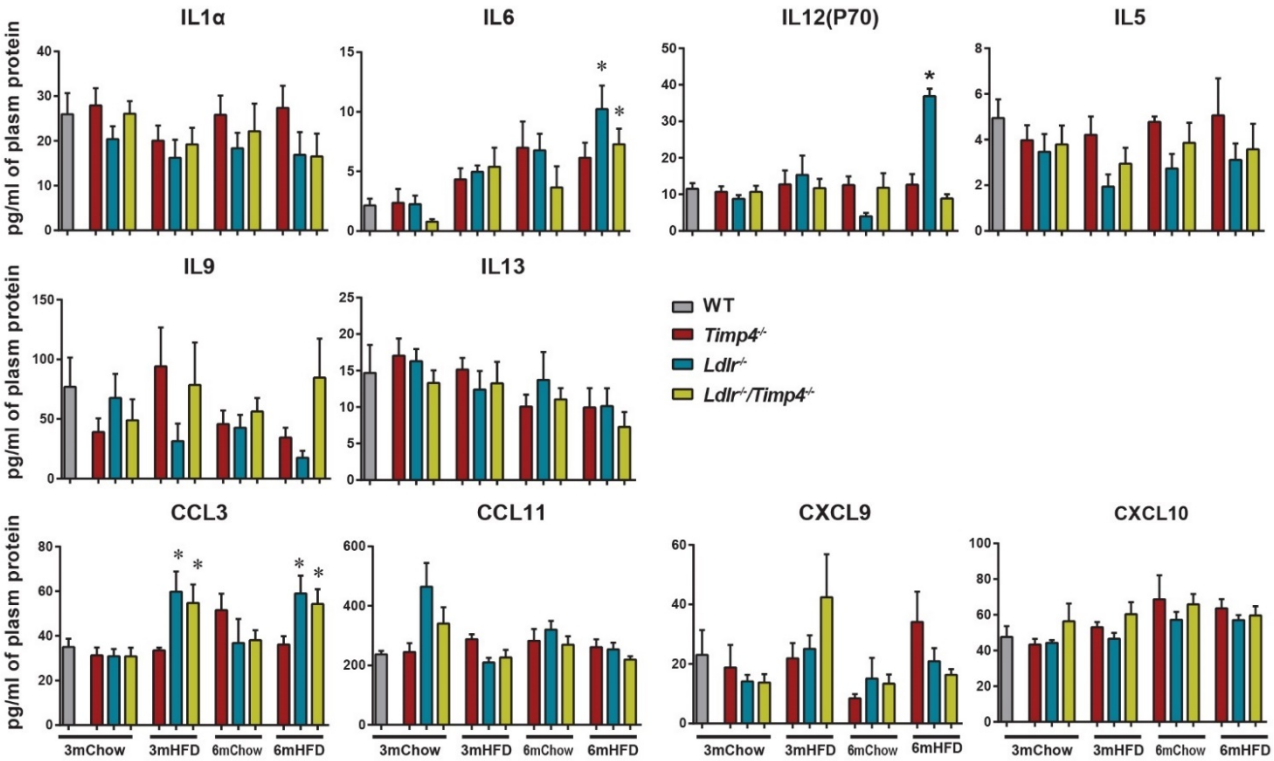

FIGURE 3. 8 SYSTEMIC INFLAMMATORY PROFILE IN PLASMA.

Average protein levels of inflammatory and anti-inflammatory cytokines and chemokines in plasma from WT (grey), *Timp4*$^{-/-}$ (red), *Ldlr*$^{-/-}$ (blue) and *Ldlr*$^{-/-}$*/Timp4*$^{-/-}$ (yellow) male mice fed 3- or 6- month of control (con) or high fat food. n=5/group. **P* <0.05 vs corresponding Control diet group. IL, interleukin; CCL, C-C motif chemokine ligand; CXCL, C-X-C motif chemokine ligand.

3.4.5. Loss of TIMP4 increases protease activity in the abdominal aorta

TIMPs are best known for their function as an inhibitor of matrix metalloproteinases (MMPs). To investigate if loss of TIMP4 in a pro-atherogenic condition leads to increased proteolytic activity, we performed *in situ* gelatinase activity which revealed a comparable protease activity in the thoracic aortas of the two genotypes, but a greater increase in protease activities in the abdominal aorta of *Ldlr*$^{-/-}$*/Timp4*$^{-/-}$-HFD compared to *Ldlr*$^{-/-}$-HFD mice **(Figure 3.9 A)**. Consistent with this observation, mRNA expression of MMPs that have been shown to contribute to atherosclerosis or vascular remodeling, *Mmp2*, *Mmp3, Mmp8*, *Mmp12*, and *Mmp13,* were higher in the abdominal aorta from *Ldlr*$^{-/-}$*/Timp4*$^{-/-}$-HFD mice, while *Mmp9* and *Mt1-mmp* were increased similarly in both HFD-fed genotypes **(Figure 3.9 B)**. The thoracic aorta, however, showed the opposite pattern with levels of most MMPs (*Mmp2*, *Mmp3*, *Mmp8*, *Mmp12*, *Mmp13* and *Mt1-MMP*) being lower in *Ldlr*$^{-/-}$*/Timp4*$^{-/-}$-HFD compared to *Ldlr*$^{-/-}$-HFD group **(Figure 3.9)**. These data collectively support that loss of TIMP4 increases the proteolytic activities in the abdominal, but not in the thoracic aorta, consistent with the higher plaque density in the abdominal aorta in these mice.

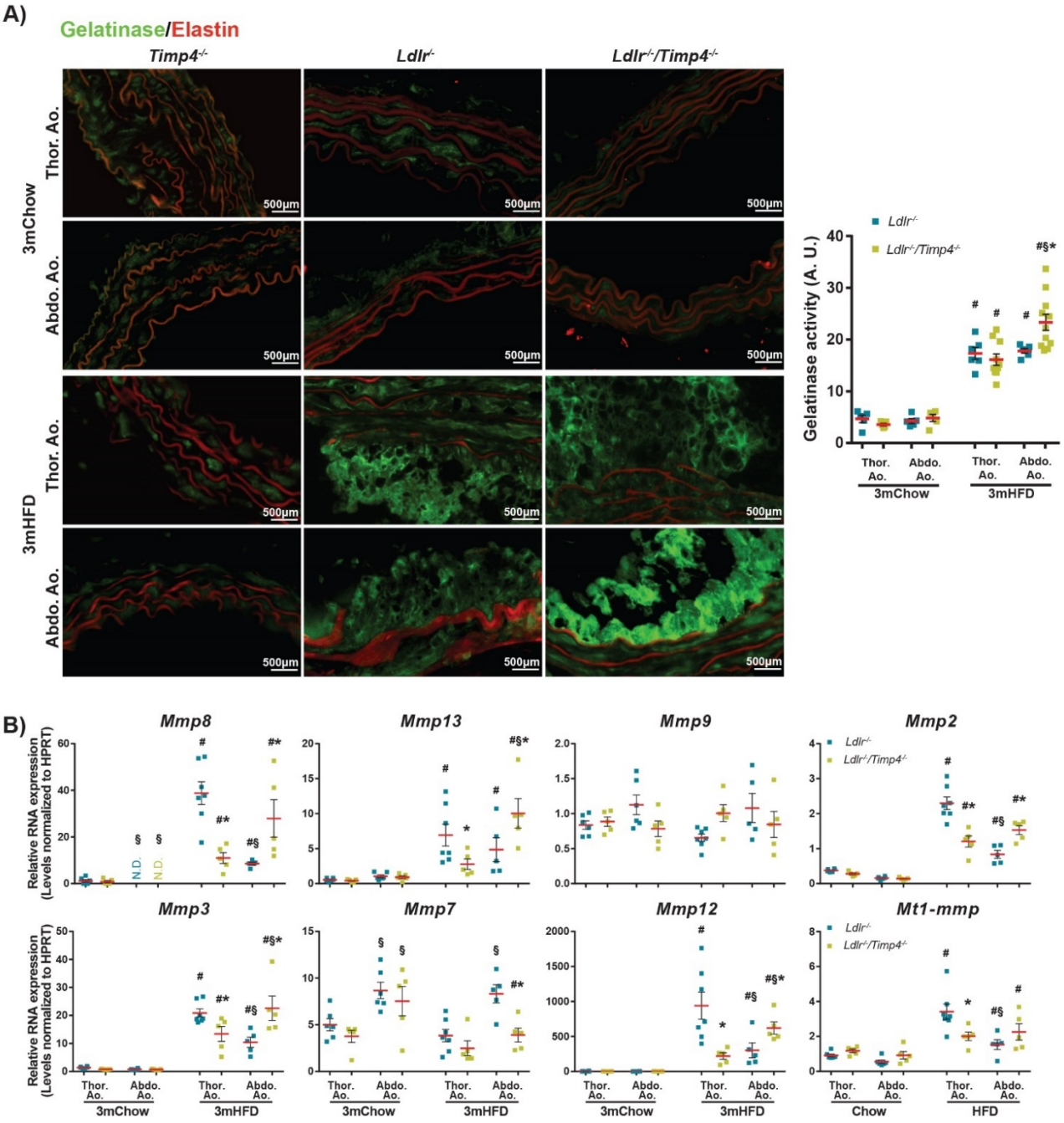

FIGURE 3. 9 PROTEASE ACTIVITY IS INCREASED IN THE ABDOMINAL AORTA OF HIGH-FAT DIET (HFD)-FED *LDLR*$^{-/-}$/*TIMP4*$^{-/-}$ MICE.

A. Representative images of in situ zymography and quantification of gelatinase activity in cryosections of thoracic aorta and abdominal aorta from mice of indicated groups (elastin exhibited fiber-like autofluorescence; gelatinase activity detected by the fluorescence between elastin fibers). n=5–10 sections from 3-5 individual mice/group. B. mRNA expression levels of matrix metalloproteinases in thoracic and abdominal aorta from male mice following 3-mo HFD. n=5–7/group. 3m indicates 3 months; A.U., arbitrary unit; HPRT, hypoxanthine phosphoribosyltransferase; N.D., not detected; and Thor. /Abdo. Ao., thoracic/abdominal aorta. #P<0.05 vs corresponding control (Con) group; §P<0.05 vs corresponding thoracic aorta group; *P<0.05 vs corresponding *Ldlr*$^{-/-}$ group.

3.4.6. Regional expression profile of TIMPs in the aorta and aortic SMCs

To decipher why the negative impact of TIMP4 loss is confined to the abdominal aorta, and does not encompass the thoracic aorta, we asked if there is a regional heterogeneity in TIMP4 expression in the aorta. Expression of the four *Timp*s was measured in the thoracic aorta, the abdominal aorta, and in SMCs isolated from the corresponding regions in wildtype and *Timp4*-deficient mice **(Figure 3.10 A)**. Expression of *Timp1*, *Timp2* and *Timp3* were comparable between the thoracic and the abdominal aorta, and between WT and *Timp4*$^{-/-}$ mice **(Figure 3.10 A).** *Timp4* was only detected in the WT group, and interestingly, its expression in the abdominal aorta was ~ 2.5-fold higher than in the thoracic aorta **(Figure 3.10 A, left panel)**; and ~2-fold higher in the abdominal SMCs compared to the thoracic aortic SMCs **(Figure 3.10 A, right panel)**. In the abdominal aortic SMCs, expression of *Timp1* and *Timp3* were also higher in *Timp4*$^{-/-}$ compared to WT group, which could be a compensatory mechanism to overcome *Timp4* loss **(Figure 3.10 A, right panel)**.

Next, we examined if this regional heterogeneity of *Timp4* expression is affected by *Ldlr*-deficiency and HFD-induced hyperlipidemia. mRNA expression analyses revealed that in the thoracic aorta, *Timp1* and *Timp2* increased to a greater extent in *Ldlr*$^{-/-}$ compared to *Ldlr*$^{-/-}$*/Timp4*$^{-/-}$ mice following HFD **(Figure 3.10 B)**. In the abdominal aorta, expression of *Timp1* increased to a greater level in *Ldlr*$^{-/-}$*/Timp4*$^{-/-}$-HFD, *Timp2* and *Timp3* remained comparable between genotypes **(Figure 3.10 B).** *Timp4* expression decreased following HFD, however it remained significantly higher in the abdominal than in the thoracic aorta following regular laboratory diet or HFD diet **(Figure 3.10 B)**. These data indicate that TIMP4 exhibits higher baseline expression in the abdominal aorta which decreased significantly following HFD. The fact that these changes did not

occur in the thoracic aorta suggests that TIMP4 plays a critical protective role in the abdominal aorta.

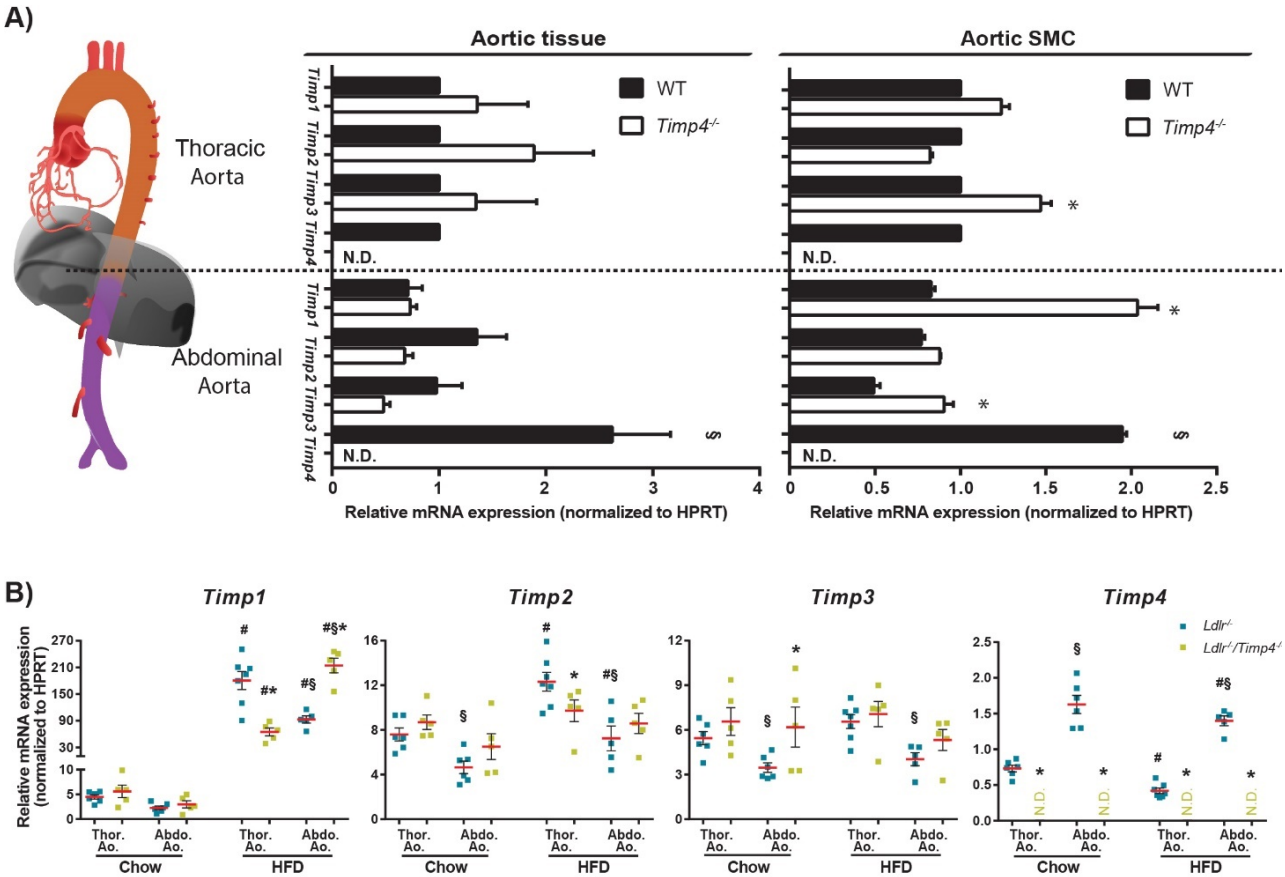

FIGURE 3. 10 REGINAL EXPRESSION PROFILE OF THE 4 TIMPS (TISSUE INHIBITOR OF METALLOPROTEINASES) IN THE AORTA AND AORTIC SMOOTH MUSCLE CELLS.

A. mRNA expression of *Timp1*, *Timp2*, *Timp3*, and *Timp4* in the thoracic and abdominal aorta and the corresponding smooth muscle cells (SMCs) from wild-type (WT) and *Timp4*$^{-/-}$ male mice (all normalized to WT-thoracic group for each gene), n=3–5/group. B. TaqMan mRNA expression of *Timp1*, *Timp2*, *Timp3*, and *Timp4* in the thoracic and abdominal aorta from *Ldlr*$^{-/-}$ and *Ldlr*$^{-/-}$/*Timp4*$^{-/-}$ male mice after 3 mo of control (Con) or high-fat diet (n=5–7). HPRT indicates hypoxanthine phosphoribosyltransferase; N.D., not detected; and Thor. /Abdo. Ao., thoracic/abdominal aorta. #P<0.05 vs corresponding Con group; §P<0.05 vs thoracic aorta; *P<0.05 vs corresponding WT (A) or *Ldlr*$^{-/-}$ group (B).

3.4.7. Loss of TIMP4 does not increase transformation of macrophages to foam cells

Since macrophages are considered the main precursor cells for foam cells, we investigated if *Timp4*-deficiency enhances macrophage-to-foam cell transformation. We used primary bone

marrow-derived macrophage culture from *Ldlr*$^{-/-}$/*Timp4*$^{-/-}$ and *Ldlr*$^{-/-}$ mice to test the direct impact of *Timp4* loss on macrophage function. *Ldlr*$^{-/-}$/*Timp4*$^{-/-}$ macrophages exhibited reduced lipid uptake ability when treated with oxidized low-density lipoprotein (oxLDL), as assessed by Bodipy and CD68 co-staining **(Figure 3.11 A)**. mRNA expression of macrophage markers and cytokines (*Cd68*, *Cd38*, *Cd206*, *Il1β*), *Timp*s (*Timp1-4*), lipid uptake proteins (*Cd36*, *Olr1*, *Sra1*, *Srb1*) and lipid efflux proteins (*Abca1*, *Abca1*) were altered similarly in both genotypes following oxLDL treatment **(Figure 3.11 B)**. Protein analyses showed that macrophage protein, Mac2, was comparable between genotypes; lipid transporter, CD36, was lower in *Ldlr*$^{-/-}$/*Timp4*$^{-/-}$ macrophages, whereas cholesterol efflux protein, ABCA1, increased similarly in both genotypes following oxLDL treatment **(Figure 3.11 C)**. Therefore, *Timp4*-deficiency in macrophages does not increase their lipid uptake nor foam cell-forming properties.

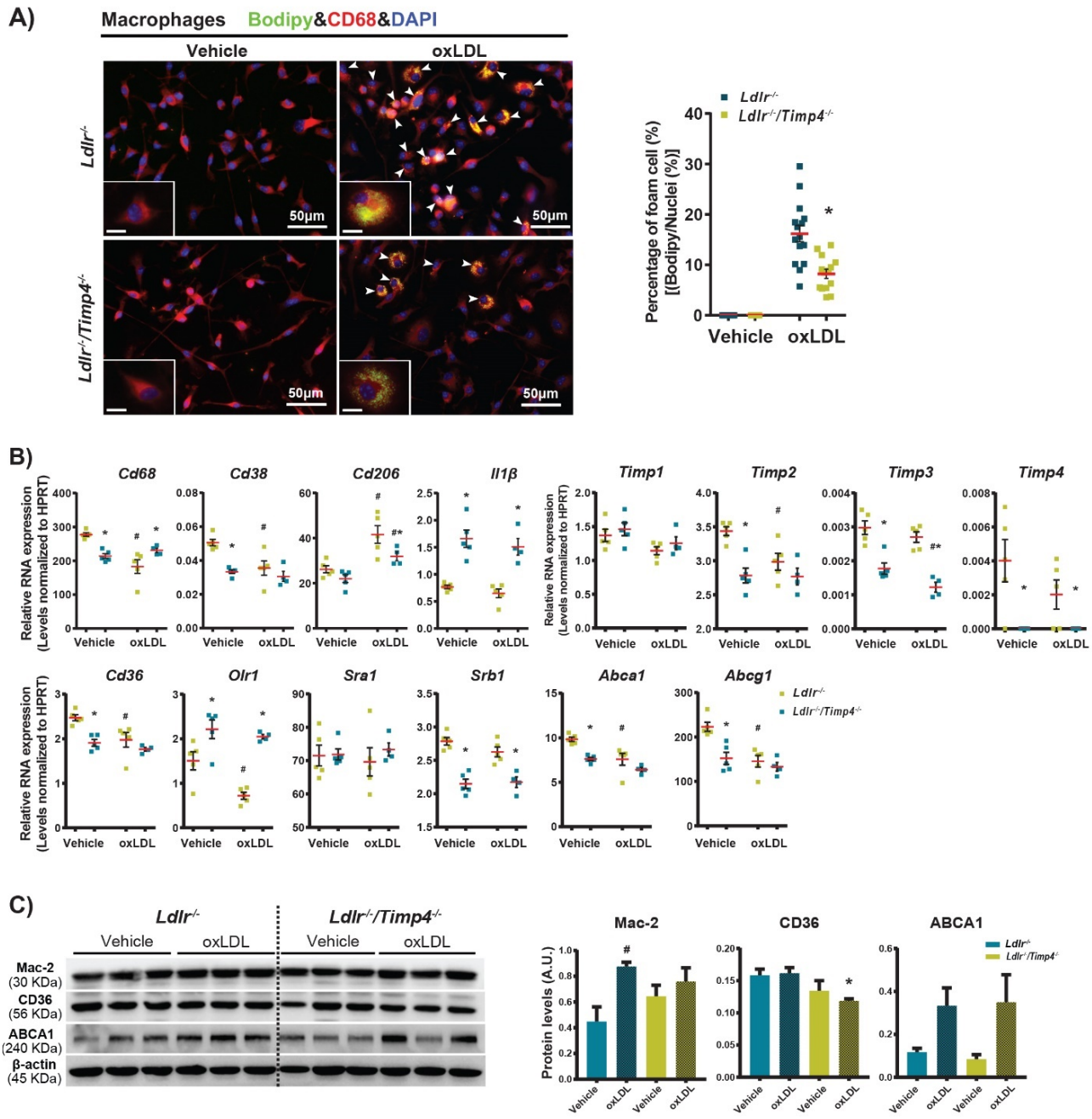

FIGURE 3. 11 *TIMP4*-DEFICIENCY DOES NOT ENHANCE THE FORMATION OF MACROPHAGE-DERIVED FOAM CELLS.

A. Representative fluorescence microscopy and quantitative analysis showing more lipid-laden foam cells (arrow; Bodipy staining indicates lipid drops; CD68 represents macrophage) in *Ldlr*$^{-/-}$ macrophages compared with *Ldlr*$^{-/-}$/*Timp4*$^{-/-}$ macrophages after oxLDL (oxidized low-density lipoprotein) treatment. Scale bars in small boxes indicate 10μm. n=11-13/group. Nuclei were stained with DAP (4′,6-diamidino-2-phenylindole dihydrochloride; blue). **B.** Expression level of macrophage maker (Cd68, Cd38, and Cd206), Il1β, lipid uptake mediated-receptors (*Cd36*, *Olr1*, *Sra1*, and *Srb1*), lipid transporters (*Abca1* and *Abcg1*), and *Timp*s in macrophages in indicated groups. n=5/group. **C**, Representative immunoblots and quantification for Mac-2 (macrophage-2) staining, ABCA1 (ATP-binding cassette transporter A1), and CD36 in macrophages in indicated groups (values normalized to β-actin). A.U.

indicates arbitrary unit; and HPRT, hypoxanthine phosphoribosyltransferase. #P<0.05 vs corresponding vehicle group; *P<0.05 vs corresponding *Ldlr*$^{-/-}$ group.

3.4.8. Timp4-deficiency renders SMCs more prone to transformation to macrophage-like cells

Accumulating evidence has indicated that SMCs can contribute to plaque deposition by transforming to macrophage-like cells, acquiring the lipid uptake ability, and subsequently becoming foam cells [19, 88, 319, 320]. We investigated if TIMP4 is involved in transformation of SMCs to macrophage-like cells in hyperlipidemic conditions. Treatment of primary aortic SMCs from *Ldlr*$^{-/-}$ and *Ldlr*$^{-/-}$*/Timp4*$^{-/-}$ mice with oxLDL resulted in a markedly higher lipid accumulation in *Ldlr*$^{-/-}$*/Timp4*$^{-/-}$ SMCs **(Figure 3.12 A,** Bodipy staining, green**)**, concomitant with a significant reduction in the expression of smooth muscle contractile proteins, calponin, SM22, and alpha-smooth muscle actin (αSMA) in these cells, compared to *Ldlr*$^{-/-}$ SMCs **(Figure 3.12 B)**. Consistent with these *in vitro* data, a greater degree of SMC transdifferentiation, detected by higher CD68^{+}-to-αSMA^{+} staining ratio was detected in the abdominal aorta of *Ldlr*$^{-/-}$*/Timp4*$^{-/-}$ compared to *Ldlr*$^{-/-}$ mice *in vivo* **(Figure 3.13 A).** *In vitro*, oxLDL induced an increase in expression of CD68, a macrophage protein, in *Ldlr*$^{-/-}$*/Timp4*$^{-/-}$ SMCs **(Figure 3.12 C, Figure 3.13 B)**. These data indicate that in the absence of TIMP4, SMCs acquire characteristics of macrophages such as CD68 expression and lipid uptake.

Examining the molecules responsible for lipid uptake (CD36, OLR1 and SR-A), and the rate-limiting proteins responsible for cholesterol efflux (ABCA1 and ABCG1) showed that oxLDL did not increase the mRNA expression of lipid transporters, *Cd36*, *Olr1* and *SrA1* in either genotype **(Figure 3.13 C)**. However, the protein levels of ABCA1, the primary cholesterol efflux proteins, was markedly decreased in oxLDL-treated *Ldlr*$^{-/-}$*/Timp4*$^{-/-}$ compared to *Ldlr*$^{-/-}$ SMCs, despite a

similar rise in its mRNA levels in both genotypes **(Figure 3.13 D)**. Protein levels for CD36 and OLR1 remained comparable between genotypes **(Figure 3.12 D)**. OxLDL significantly increased *Timp4* expression in *Ldlr*$^{-/-}$ SMCs, but decreased *Timp1* and *Timp3* expression similarly in both genotypes, and did not alter *Timp2* **(Figure 3.13 E)**. Therefore, this increase in TIMP4 could be a protective mechanism by SMCs to control the excess proteolytic activities triggered in the hyperlipidemic environment. In the absence of TIMP4, the increased proteolytic degradation of ABCA1 protein (without altered mRNA levels) would reduce the ability of the SMCs to export the excess lipid, therefore transforming to foam cells.

In contrast to the abdominal aortic SMCs, SMCs isolated from the thoracic aorta of *Ldlr*$^{-/-}$ */Timp4*$^{-/-}$ and *Ldlr*$^{-/-}$ mice exhibited a similar capacity in lipid uptake and transformation to macrophage-like cells in response to oxLDL **(Figure 3.14 A-B)**. In addition, expression of SMC proteins, calponin, SM22α and αSMA were comparable between the genotypes, while oxLDL triggered a similar increase in ABCA1 protein levels in both genotypes **(Figure 3.14 C-D)**. These data collectively demonstrate that loss of TIMP4 differentially impacts the SMCs in the abdominal compared to the thoracic aorta.

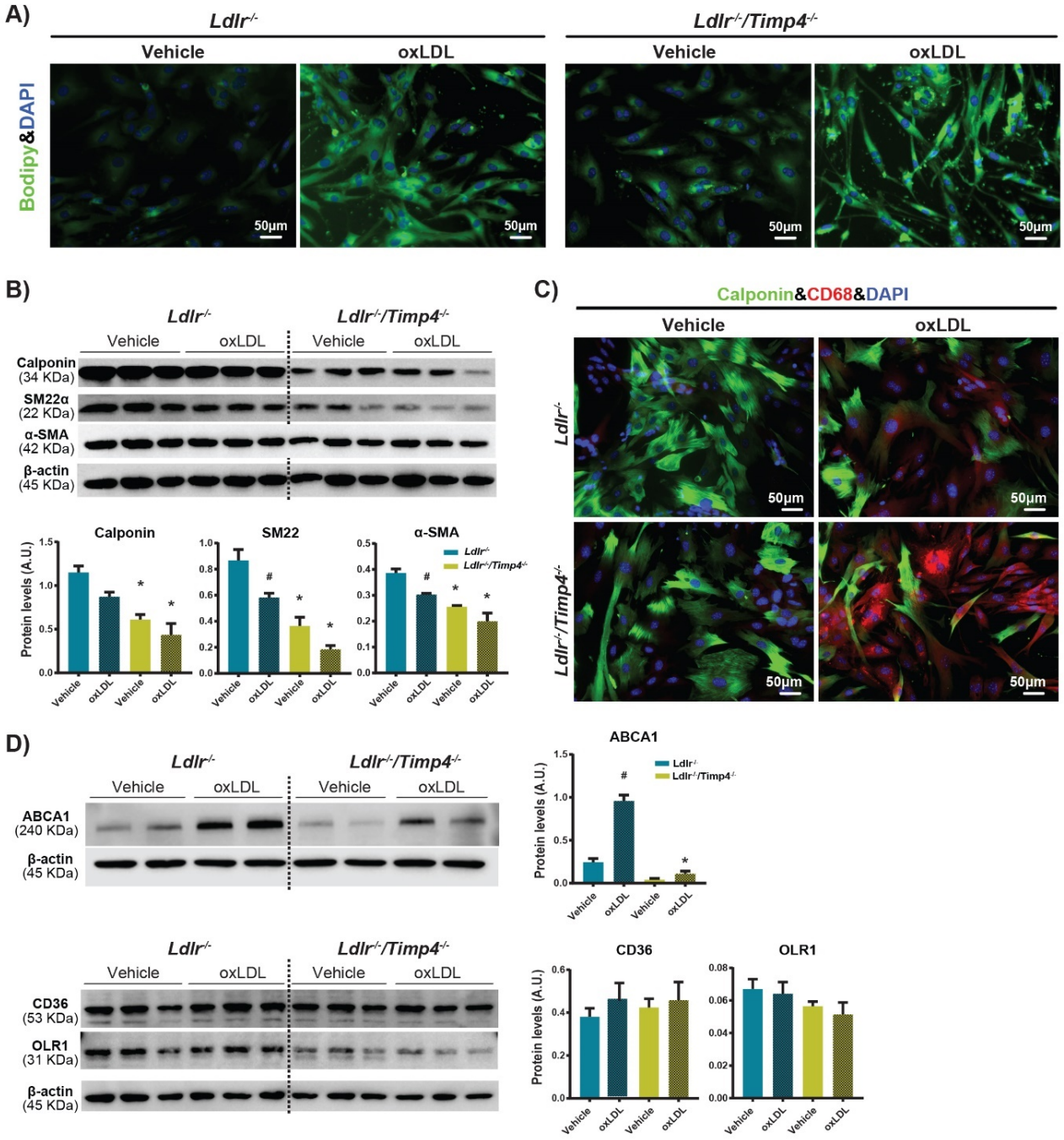

FIGURE 3. 12 PRIMARY ABDOMINAL *LDLR*$^{-/-}$/*TIMP4*$^{-/-}$ AORTIC SMOOTH MUSCLE CELLS HAVE A HIGHER POTENCY IN TAKING UP LIPIDS AND ACQUIRE A "MACROPHAGE-LIKE" PHENOTYPE.

A. Representative fluorescence microscopy of lipid droplets stained by Bodipy (green) in primary aortic smooth muscle cells (SMCs) treated with or without oxLDL (oxidized low-density lipoprotein). B. Representative immunoblots and quantification for SMC markers (calponin, SM22α [smooth muscle protein 22-alpha] and α-SMA [alpha-smooth muscle actin]) in primary aortic SMCs from indicated groups (values normalized to β-actin). C. Representative immunofluorescent images of SMCs stained by calponin (green) and macrophage-like SMCs stained by CD68 (red) in primary aortic SMCs treated with or without oxLDL. Nuclei were stained by DAPI (4′,6-diamidino-2-phenylindole dihydrochloride; blue). D. Representative immunoblots and quantification for ABCA1 (ATP-binding cassette transporter A1), CD36, and OLR1 (oxLDL receptor 1) in primary aortic SMCs in the indicated groups (values

normalized to β-actin). A.U. indicates arbitrary unit. #P<0.05 vs corresponding vehicle group; *P<0.05 vs corresponding *Ldlr*$^{-/-}$ group.

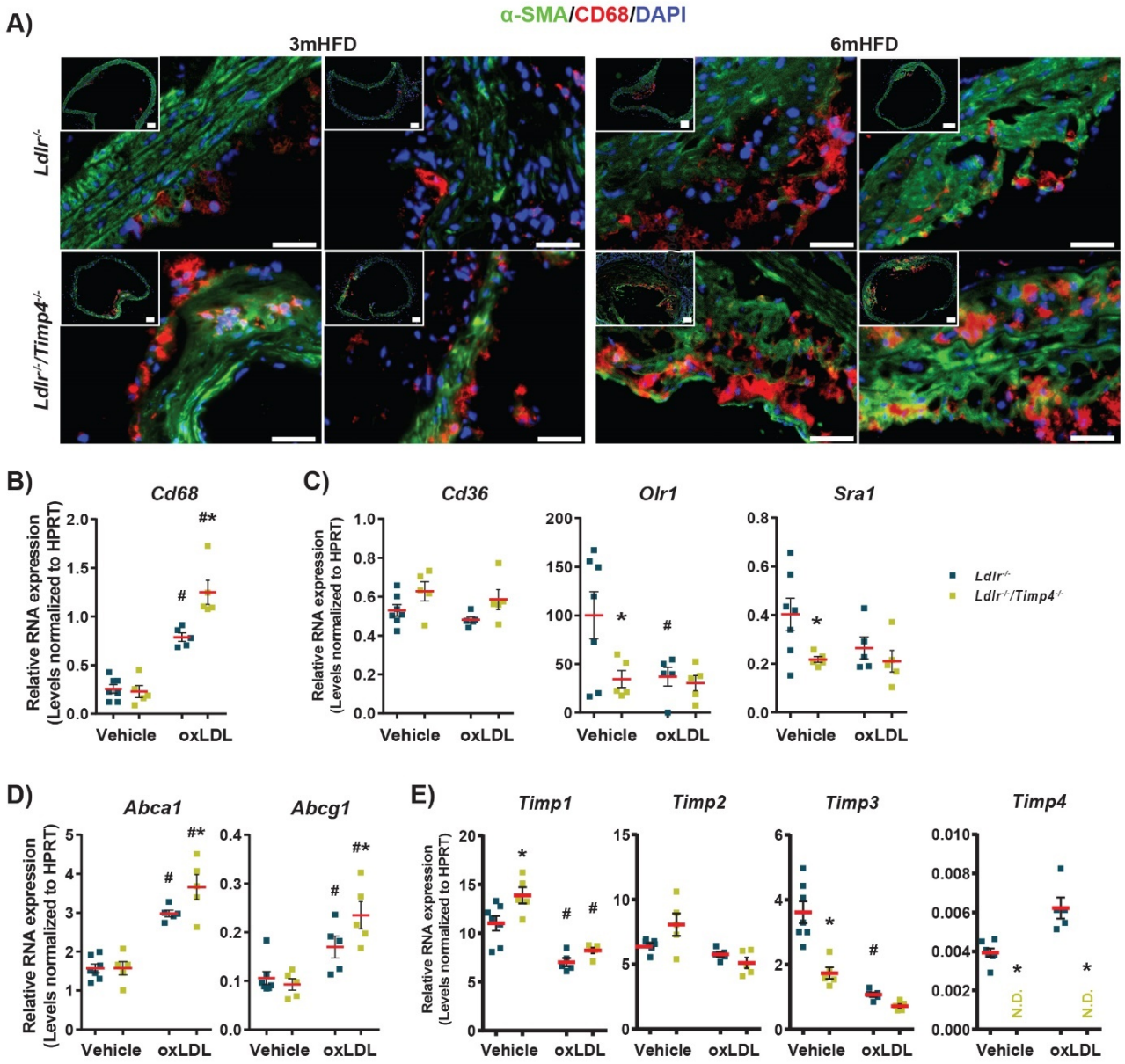

FIGURE 3. 13 EXPRESSION LEVEL OF MACROPHAGES, LIPID UPTAKE RECEPTORS AND TRANSPORTERS AND TIMPS IN IN ABDOMINAL AORTIC SMCS AFTER OXLDL TREATMENT.

A) Co-immunostaining for α-SMA and CD68 in abdominal aorta after 3 or 6 months of HFD; B-E) mRNA expression levels of macrophage marker, lipid uptake receptors and transporters and TIMPs in abdominal aortic SMCs after oxLDL treatment. (A) Representative immunofluorescent staining showing higher number of α-SMA/CD68 positive cells in the abdominal aorta cross-section of *Ldlr*$^{-/-}$/*Timp4*$^{-/-}$, compared to *Ldlr*$^{-/-}$ mice after 3 or 6 month-HFD. Scale bar =100 μm. (B) Expression level of macrophage maker (Cd68) in primary aortic SMCs in the indicated groups. n=5-7/group. (C) Expression levels of lipid uptake mediated-receptors (Cd36, Olr1 and Sra1) in primary aortic SMCs in the indicated groups. n=5-7/group. (D) Expression levels of lipid transporters (Abc-A1 and Abc-G1) in primary aortic SMCs in the indicated groups. n=5-7/group. (E) mRNA expression of Timp1, Timp2, Timp3 and Timp4 in primary

aortic SMCs in the indicated groups. n=5-7/group. #*P*< 0.05 vs corresponding control group; * *P*<0.05 vs corresponding *Ldlr*$^{-/-}$ group. SMCs, smooth muscle cells; oxLDL, oxidized low-density lipoprotein; Olr1, oxidized low-density lipoprotein receptor 1; Sra1, scavenger receptor class a1; Abca1/g1, ATP-binding cassette transporter a1/g1. N.D.= not detected.

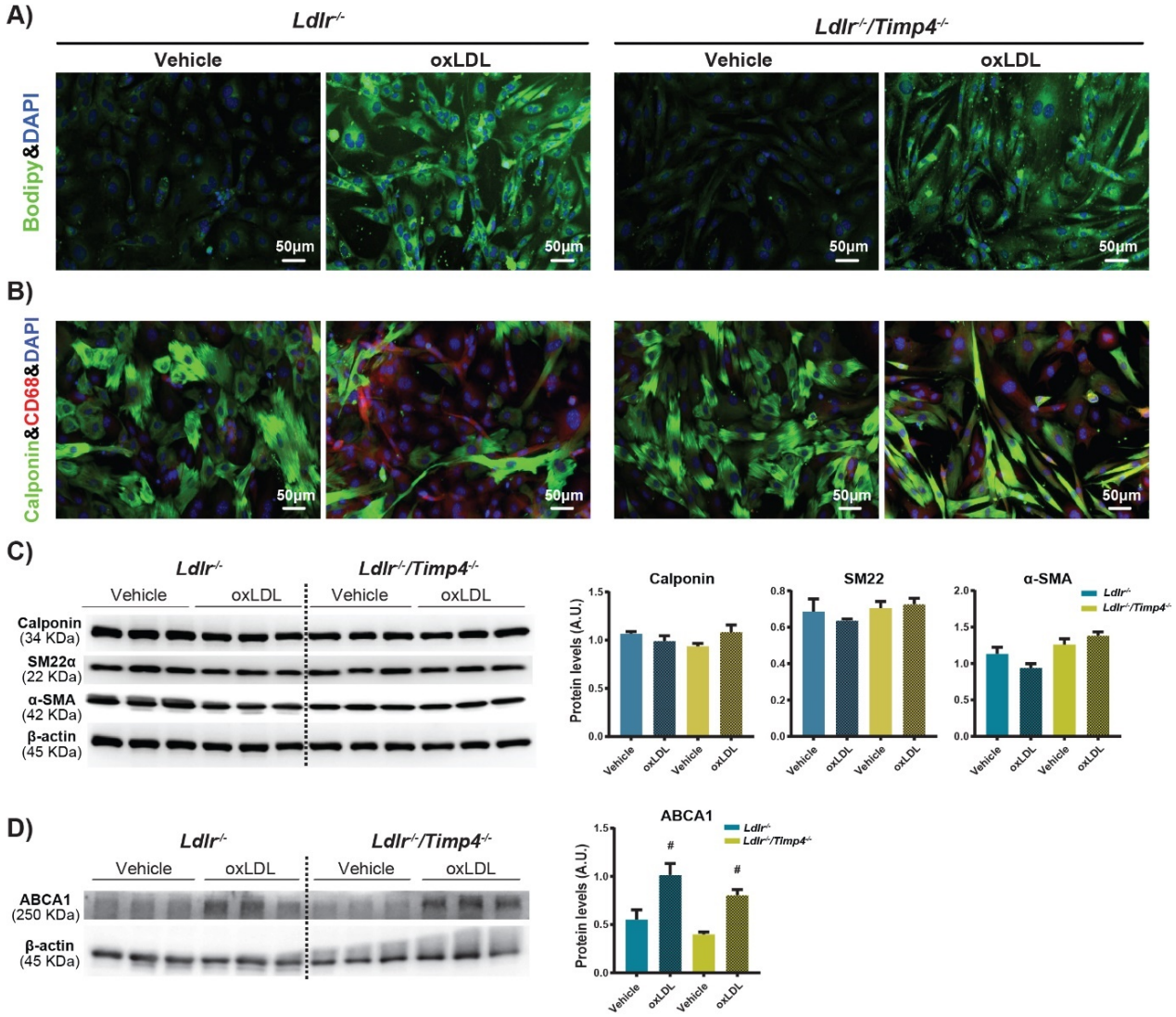

FIGURE 3. 14 THORACIC AORTA SMOOTH MUSCLE CELLS FROM *LDLR*$^{-/-}$*/TIMP4*$^{-/-}$ MICE DO NOT SHOW ENHANCED POTENCY IN LIPID UPTAKE COMPARED TO *LDLR*$^{-/-}$ MICE.

(A) Representative fluorescence microscopy of lipid droplets stained by Bodipy (green) in thoracic aortia SMCs treated with vehicle or without oxLDL. (B) Representative co-immunofluorescent staining images of thoracic aorta SMCs stained for calponin (green) and macrophage marker (red) showing less macrophage-like transformation of *Ldlr*$^{-/-}$*/Timp4*$^{-/-}$ compared to *Ldlr*$^{-/-}$ thoracic SMCs in the presence of oxLDL. Nuclei were stained by DAPI (blue). (C) Representative immunoblots and quantification for SMC markers (calponin, SM22α and α-SMA) in thoracic aortia SMCs from indicated groups (values normalized to β-actin). (D) Representative immunoblots and protein quantification for ABCA1 in thoracic aortic SMCs in the indicated groups (values normalized to β-actin). #*P*<0.05 vs

corresponding vehicle group. SMCs, smooth muscle cells; oxLDL, oxidized low-density lipoprotein; α-SMA, alpha-smooth muscle actin; ABCA1, ATP-binding cassette transporter A1.

3.4.9. Atherosclerotic abdominal aortas from patients show reduced TIMP4 with increased lipid deposition

To validate our findings in the mouse model, we investigated the correlation between TIMP4 levels and plaque deposition in atherosclerotic abdominal aorta from patients compared to non-diseased aortas. We detected high expression of TIMP4 in the medial layer of the non-diseased aortas which exhibited no lipid deposition (negative Bodipy staining) and no CD68-positive cells **(Figure 3.15 A)**. In contrast, in atherosclerotic aortas TIMP4 expression was markedly reduced particularly at the site of lipid deposits as evident by positive Bodipy staining and presence of CD68-expressing cells **(Figure 3.15 B, Figure 3.16)**. These data support our findings that a reduction in TIMP4 is a contributing factor to increased lipid deposition and atherosclerotic plaque formation.

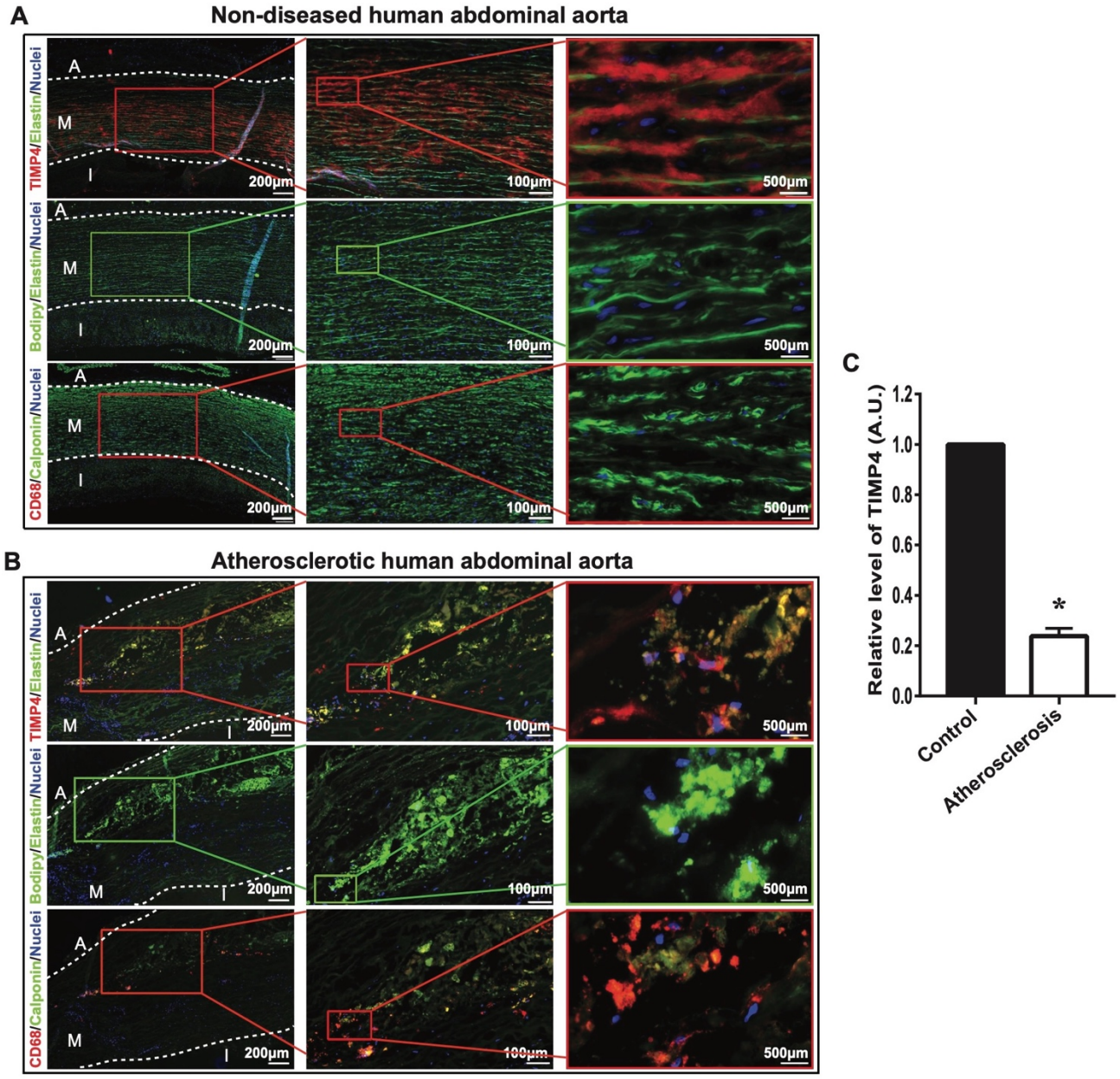

FIGURE 3. 15 EXPRESSION OF TIMP4 (TISSUE INHIBITOR OF METALLOPROTEINASE 4) IS DECREASED IN ATHEROSCLEROTIC ABDOMINAL AORTA FROM PATIENTS.

Representative immunofluorescent staining for TIMP4 (red), Bodipy staining (lipid deposits, green), CD68 (macrophage marker, red), and calponin (smooth muscle cell marker, green) in nondiseased abdominal aorta (A) and atherosclerotic abdominal aorta (B) from patients. Elastin autofluorescence appears green. White dotted line divides the aortic tunica into 3 different layers of the intima (I), media (M), and adventitia (A). C. The quantification of TIMP4 in control (nonatherosclerosis, n=3) and abdominal atherosclerotic aortas from patients (n=5). A.U. indicates arbitrary unit. *P<0.05 vs control.

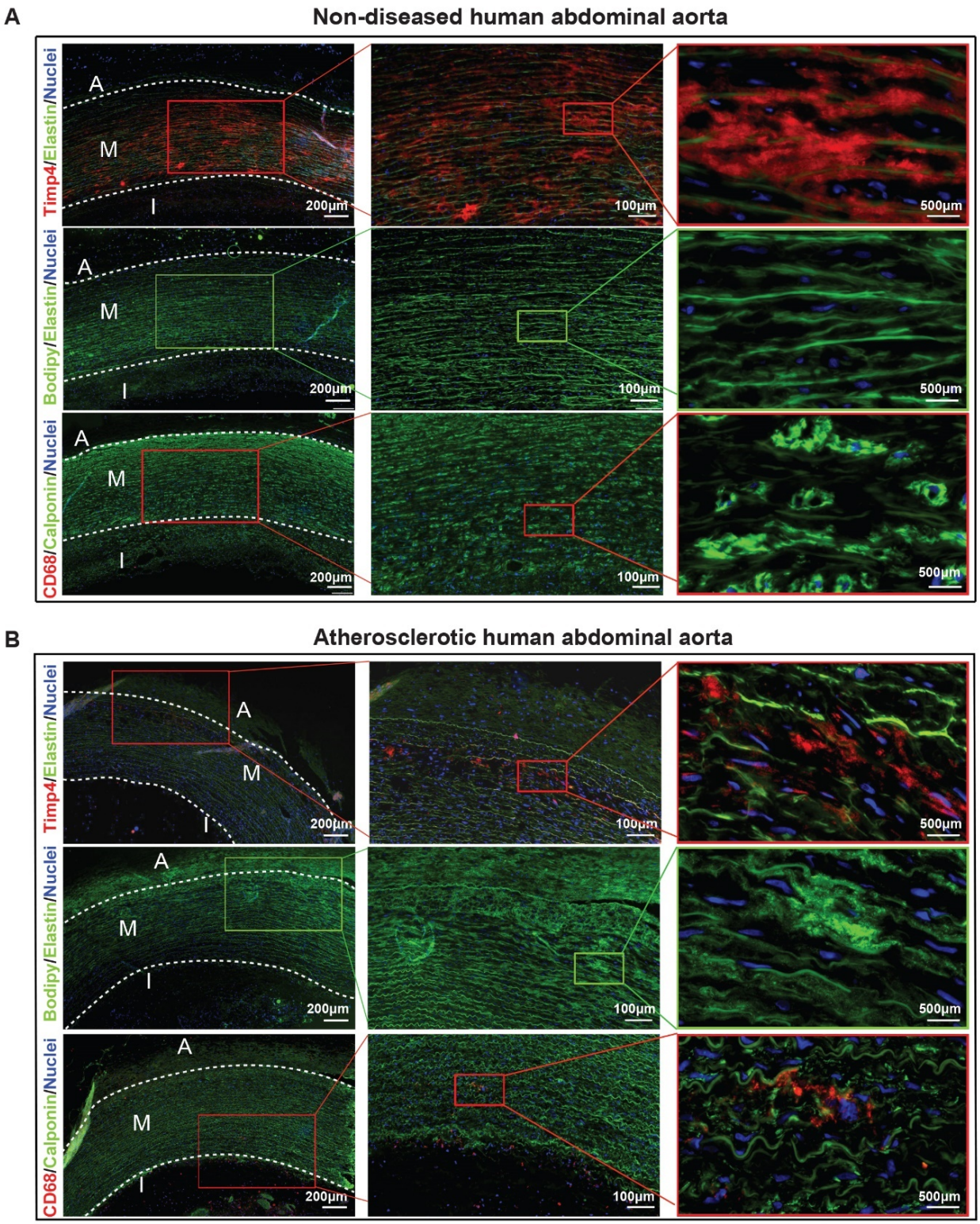

FIGURE 3. 16 EXPRESSION OF TIMP4, LIPIDS AND MACROPHAGES IN ATHEROSCLEROTIC HUMAN ABDOMINAL AORTA.

Immunofluorescent staining for TIMP4 (red), Bodipy staining (lipid deposits, green) CD68 (macrophage marker, red) and calponin (smooth muscle cell marker, green) in non-diseased abdominal aorta **(A)** and atherosclerotic abdominal

aorta **(B)** from patients. Elastin autofluorescence appears green. White dotted lines separate the three different layers of the aortic wall into intima (I), media (M), and adventitia (A).

3.5. Discussion

Atherosclerosis, fatty lesions in the arterial wall, continues to be a major cause of morbidity and mortality worldwide [324]. TIMPs are best known for their role in regulating ECM remodeling, and as such their contribution to atherosclerosis has primarily focused on their role in plaque stability [328]. Overexpression of TIMP1 reduced atherosclerotic lesions in *Apoe*$^{-/-}$ mice [190], whereas, loss of *Timp1* or *Timp2* did not alter the lesion size in *Apoe*$^{-/-}$ mice [192]. *Timp3*-deficiency exacerbated atherosclerosis in *Apoe*$^{-/-}$ mice [195], while its overexpression in macrophages reduced lesion size, and increased plaque stability in *Ldlr*$^{-/-}$ mice [196]. In advanced atherosclerotic lesions from patients, TIMP4 is detected around necrotic lipid cores but not inside the necrotic core [246], however, the direct contribution of TIMP4 in atherosclerosis has remained unknown. In a study of 499 Chinese patients, polymorphism of TIMP4 (allele T at 3' UTR) but not the other TIMPs, was found to be an independent predictor of coronary plaque progression in non-diabetic and type 2 diabetic patients [329]. We previously reported that loss of TIMP4 suppresses HFD-induced obesity by reducing lipid uptake and reducing plasma lipid and cholesterol levels [257]. Based on this observation we hypothesized that absence of TIMP4 should offer protection against atherosclerosis which has been strongly linked to plasma cholesterol levels [330, 331]. In contrast to our initial hypothesis, mice lacking TIMP4 exhibited worsened atherosclerosis in the abdominal aorta despite the lower plasma lipid and cholesterol levels. Further mechanistic analyses revealed that loss of TIMP4 does not impact macrophage-to-foam cell conversion, but increases the potency of SMCs to transform to macrophage-like cells and ultimately foam cells in hyperlipidemic conditions.

The novelty of the findings in our study is three-fold. First, plasma cholesterol levels are not the sole indicator of atherosclerosis risk. This is consistent with reports from human biopsies published in 1960s showing that serum cholesterol levels did not always correlate with the degree of atherosclerosis in humans [332-334], a concept that has not received sufficient attention since then [334, 335]. Second, TIMP4 protects SMCs from transforming to macrophage-like cells in hyperlipidemic conditions. This reveals a novel function for TIMP4, particularly critical in atherosclerosis progression. Third, TIMP4 is one of the factors underlying the regional heterogeneity of the aorta, as we and others have reported to underlie the differential regional susceptibility of the aorta to disease [5, 44, 336]. TIMP4 expression is higher in the abdominal compared to the thoracic aorta, which could indicate that presence of this TIMP in the abdominal aorta is more critical (than in other aortic regions) such that its loss selectively increases the susceptibility of the abdominal aorta to excess plaque deposition. Interestingly, this unique function of TIMP4 (compared to the other three TIMPs) is despite its much lower expression in the aorta, which suggests that the expression levels of TIMP4 may not be a direct indicator of its physiological significance. We further demonstrate that absence of TIMP4 increases the susceptibility of the SMCs (but not macrophages) to transdifferentiation to macrophage-like cells and foam cells in hyperlipidemic conditions.

The higher plaque size in the abdominal aorta of *Ldlr*$^{-/-}$/*Timp4*$^{-/-}$-HFD mice was associated with increased MMP expression and MMP-mediated proteolysis. This could be the cumulative outcome of absence of TIMP4 to inhibit the active MMPs, and increased MMP production by inflammatory cell [5]. Although the greater proteolysis and inflammation could also be partly the consequence of higher plaque size. Increased MMP activities adversely alters the extracellular matrix (ECM) structure and integrity in the aortic wall, thereby increasing susceptibility to cholesterol deposition and atherosclerosis [5]. In addition, increased MMP activity in *Ldlr*$^{-/-}$/*Timp4*$^{-/-}$-HFD mice could

explain the decreased ABCA1 protein but not mRNA levels in aortic SMCs from these mice. Role of SMCs in atherosclerotic plaques is widely recognized [337], as transdifferentiation of SMCs to macrophage-like foam cells has been reported in *Apoe*$^{-/-}$ mice [88] and in coronary plaques in humans [19], and confirmed by cell lineage tracing [338]. However, the mechanism underlying SMC transdifferentiation is not fully understood yet. Cholesterol transporters responsible for this action are critical for cholesterol uptake and release from macrophages and smooth muscle cells. We found that while oxLDL increases ABCA1 mRNA, its protein levels are decreased in *Timp4*$^{-/-}$ SMCs, a post-translational regulation likely mediated by the increased proteolytic activities in the *Ldlr*$^{-/-}$/*Timp4*$^{-/-}$ SMCs. The reduced ABCA1 protein levels compromise cholesterol efflux from SMCs leading to excess lipid accumulation and transformation of the SMCs to foam cells. This is consistent with data from SMCs in human coronary intima that showed reduced ABC-A1, compared to intimal leukocytes [19]. Reduced ABCA1 in SMCs has also been shown in the *Apoe*$^{-/-}$ model of atherosclerosis, where SMCs were found to comprise majority of the foam cells [88]. Interestingly, ABCA1 protein levels in macrophages were not affected by *Timp4*-deficiency, highlighting a cell-type specific function of TIMP4 in hyperlipidemic conditions.

3.6. Conclusion

In summary, our study demonstrates that atherosclerotic plaque deposition can occur independently from plasma cholesterol levels but is rather more directly related to the regional susceptibility of the aorta. We have identified TIMP4 as a key player in regional heterogeneity of the aorta in plaque deposition through regulating SMC susceptibility to acquiring macrophage-like properties in hyperlipidemic conditions such that its loss renders the abdominal aorta more susceptible to plaque deposition despite lower circulating plasma cholesterol levels. Hence,

targeting TIMP4 can lead to novel approaches to limit the atherosclerotic injury process in the vascular wall, the primary driver of adverse vascular ischemic events.

CHAPTER 4

ROLE OF TIMP4 IN ATHEROSCLEROSIS-RELATED AORTIC ANEURYSM

4.1. Introduction

Aortic aneurysm is a permanent focal dilation of the artery that grows irreversibly and is usually asymptomatic, therefore carries a high risk of fatal rupture. Currently, no therapeutic drugs are proven to limit aneurysm progression and rupture, and endovascular or open surgical repair is the only available approach [3]. Abdominal aortic aneurysms (AAAs) are the most common aneurysms of the aorta. The histopathologic features of the end-stage disease include thinning of the aortic wall, degeneration of the medial elastin lamellar, adventitia inflammation, atherosclerosis, and intramural thrombosis [339]. AAA can occur in association with atherosclerosis, but the two aortic conditions can occur independently of each other [340].

TIMP4, as one of the physiological inhibitors of MMPs, can inhibit a number of MMPs (MMP2, 8, 9 and 13) which are involved in aortic aneurysms. TIMP4 overexpression inhibits aortic SMC migration and promotes *in vitro* and *in vivo* [254, 256]. Upregulation of TIMP4 in response to aortic injury has been linked to VSMC migration [252]. Downregulation of TIMP4 has been associated with AAA [341], however, the direct function of TIMP4 in aortic aneurysm has not been reported.

Our previous study has revealed that *Ldlr*$^{-/-}$*/Timp4*$^{-/-}$ mice on HFD exhibit greater plaque density in the abdominal aorta but not in thoracic aorta. *Timp4*-deficiency increases susceptibility of the abdominal aorta to atherosclerosis, suggesting that *Timp4*-deficiency specifically increases the susceptibility of abdominal aorta to atherosclerosis. Therefore, in this study I utilized Ang II-induced high-fat fed *Ldlr*$^{-/-}$ mice to establish a hypercholesterolemic aneurysm model and investigated the susceptibility of *Timp4*-deficient abdominal aorta to AAA and the role of atherosclerosis in this susceptibility.

4.2. Methods

The detailed Materials and methods information is available in **Chapter 2** Materials and Methods.

4.2.1. Experimental animals and procedures

Ldlr$^{-/-}$ mice were crossed with *Timp4*$^{+/-}$ mice to generate *Ldlr*$^{-/-}$*/Timp4*$^{-/-}$ mice. *Ldlr*$^{-/-}$ and *Ldlr*$^{-/-}$*/Timp4*$^{-/-}$ mice received 6 weeks of HFD to initiate hypercholesterolemia, followed by 4 weeks of Angiotensin II infusion (1.5mg/Kg/d, Alzet pumps, Model 1004) as they continue to receive HFD.

4.2.2. Angiotensin II pump implantation

Alzet micro-osmotic pumps (Model 1004, Durect Co.) were implanted subcutaneously in male mice to deliver 1.5 mg/kg/day of angiotensin II or vehicle (saline) for four weeks.

4.2.3. *En face* Oil Red-O (ORO) staining

At indicated time points, mice of each genotype were anesthetized, perfused-fixed (through the left ventricle) with 10% buffered neutral formalin at 100 mmHg to fix the blood vessels in their native state. The entire aorta was dissected, cleaned, and fixed in 10% neutral formalin.

After dissection from the mouse, the entire aorta was cleaned by removal of connective tissue and stained with ORO solution. Atherosclerotic lesions can be visualized after the aorta was cut open and the lumen was placed face up. Images were then taken with a digital camera.

4.2.4. Histological staining

Formalin-fixed abdominal aortas were paraffin-embedded and processed for Trichrome and VVG staining. The changes in collagen content and SMC density were represented by Trichrome staining. The severity of elastin fiber deterioration in aorta was visualized by VVG staining.

4.3. Results

4.3.1. Less severe aortic aneurysm developed in *Ldlr*$^{-/-}$*/Timp4*$^{-/-}$ mice after Ang II infusion

To determine the role of TIMP4 in aortic aneurysm formation, we generated *Ldlr*$^{-/-}$*/Timp4*$^{-/-}$ mice and subjected *Ldlr*$^{-/-}$ and *Ldlr*$^{-/-}$*/Timp4*$^{-/-}$ mice to Ang II-induced aortic aneurysm model. After 4 weeks of Ang II infusion, large AAAs were evident in *Ldlr*$^{-/-}$ mice; in comparison, AAAs were absent or smaller in *Ldlr*$^{-/-}$*/Timp4*$^{-/-}$ mice (**Figure 4.1 A-i**). AAA occurred in 56.3% of *Ldlr*$^{-/-}$ mice (9 of 16) including 12.5% mortality (due to rupture), whereas the incidence of AAA in *Ldlr*$^{-/-}$*/Timp4*$^{-/-}$ mice was only 14.2%, all of which were found in the abdominal aorta. (**Figure 4.1 A-ii**). Figure 4.1 A-iii showed a ruptured AAA in *Ldlr*$^{-/-}$ mice featured with diffuse perivascular hemorrhage. Mortality from ruptured AAA is defined as diffuse retroperitoneal hemorrhage around the abdominal aorta found at autopsy (**Figure 4.1 A-iii**).

4.3.2. More atherosclerotic plaque deposited in *Ldlr*$^{-/-}$*/Timp4*$^{-/-}$ abdominal aorta

We previously found that loss of *Timp4*-deficiency increased plaque deposition in the abdominal aorta but not in the aortic valve, arch, or the thoracic aorta. The contributions of Ang II to the initiation and progression of atherosclerosis have been widely evidenced by clinical and animal

research. Hence, plaque deposition in the aortic arch, thoracic aorta and abdominal aorta was examined in mice after HFD feeding followed Ang II perfusion. Likewise, we also found plaque formation in the abdominal aorta of *Ldlr*$^{-/-}$/*Timp4*$^{-/-}$ mice was significantly higher than that of *Ldlr*$^{-/-}$ mice after HFD and treatment with Ang II (**Figure 4.1 B**). Together, these data indicate that atherosclerosis is not a requirement for the Ang II induced-AAA formation in *Ldlr*$^{-/-}$/*Timp4*$^{-/-}$ mice.

4.3.3. *Timp4*-deficiency ameliorated adverse ECM remodeling and the development of Ang II-mediated aneurysm

Histological assessment of the abdominal aorta in *Ldlr*$^{-/-}$ and *Ldlr*$^{-/-}$/*Timp4*$^{-/-}$ mice showed that consistent with the aneurysmal dilation, adverse remodeling of the aortic wall and aortic dissection were detected in *Ldlr*$^{-/-}$ mice, which were not or rarely found in *Ldlr*$^{-/-}$/*Timp4*$^{-/-}$ mice. Adverse ECM remodeling in *Ldlr*$^{-/-}$ aortic wall was demonstrated by degradation of elastin lamella [visualized by Verhoeff-Van Gieson (VVG) staining], loss of medial VSMC and excess adventitial collagen accumulation (trichrome staining) (**Figure 4.1 C**). Moreover, frequent medial disruption, intramural hemorrhage and thrombosed false lumen were observed in *Ldlr*$^{-/-}$ mice but not *Ldlr*$^{-/-}$/*Timp4*$^{-/-}$ mice (**Figure 4.1 C**). Therefore, these data suggest that *Timp4*-deficiency confers protection from Ang II-induced AAA formation in *Ldlr*$^{-/-}$ mice.

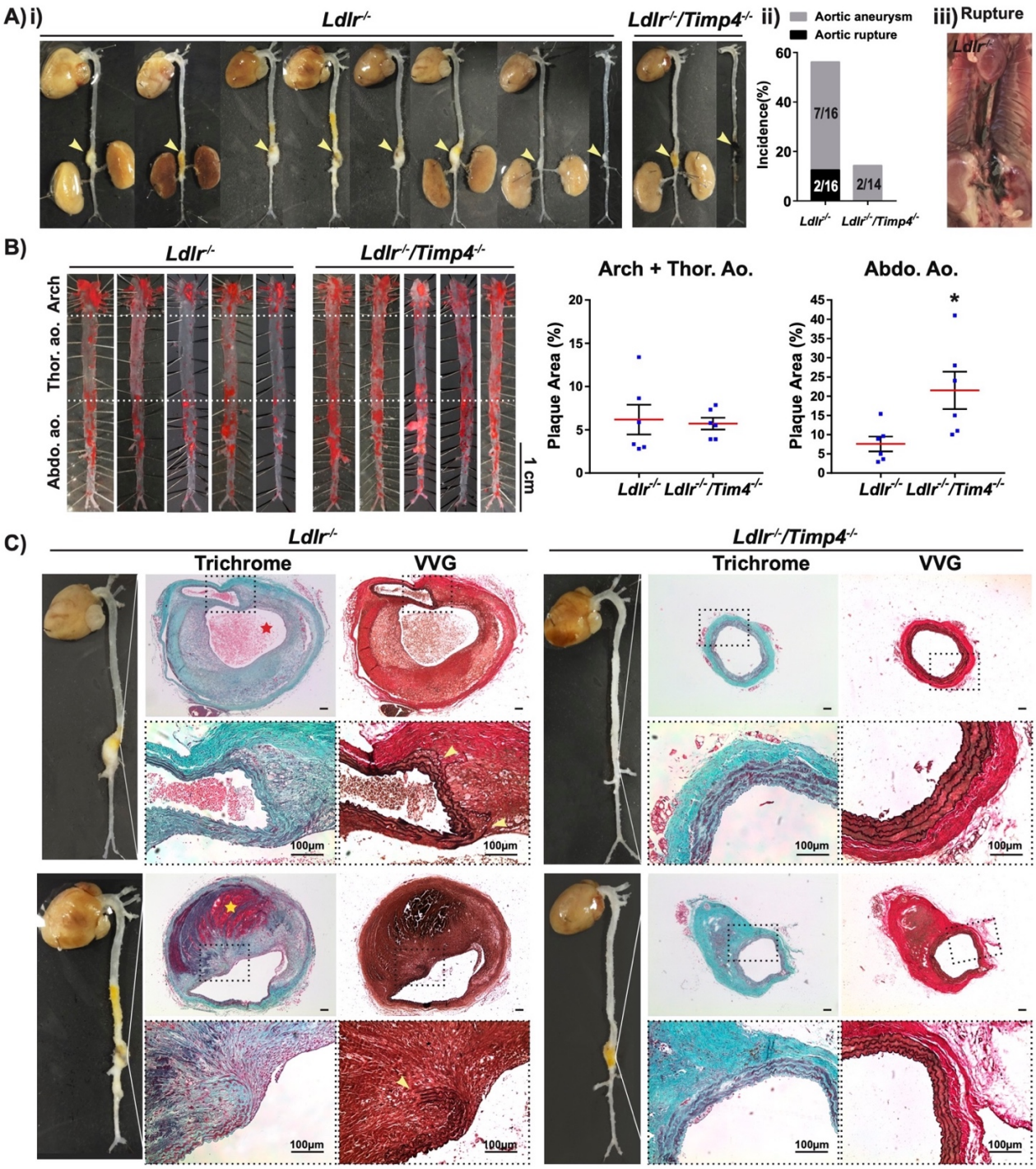

FIGURE 4.1 *TIMP4*-DEFICIENCY ALLEVIATED THE AAA FORMATION IN RESPONSE TO ANG II IN HYPERCHOLESTEROLEMIC MICE.

(A) i) Photographs of entire aorta showing the AAA formation (arrowheads) in *Ldlr*$^{-/-}$ and *Ldlr*$^{-/-}$*/Timp4*$^{-/-}$ mice after HFD feeding followed by 4-weeks of AngII infusion. **ii)** Demography showing the frequency of AAA formation and rupture in *Ldlr*$^{-/-}$ and *Ldlr*$^{-/-}$*/Timp4*$^{-/-}$ *mice*. **iii)** Representative picture of aortic rupture. **(B)** Representative images of Oil Red O-stained aortas showing plaque distribution, and quantification of *en face* lesion area at the aortic arch, thoracic, and abdominal aorta in mice of each genotype after HFD feeding and AngII infusion. **(C)** Representative images of trichrome and VVG staining of abdominal aortic cross-sections showing smooth muscle cells (red/magenta; trichrome), collagen (blue; trichrome) and elastin (black; VVG). Yellow star indicates an intramural thrombus and red

star points a false lumen and partial thrombosis. Arrowheads point to elastin breakage. Thor.: Thoracic; Abdo.: Abdominal; HFD: High fat food; VVG: Verhoeff-Van Gieson. *P<0.05 vs *Ldlr*$^{-/-}$ group (Student *t* test).

4.4. Discussion

AAA remains a significant health risk as its irreversible growth pattern and asymptomatic nature. More importantly, there is currently no effective drug for the treatment of AAA except surgery. The pathological process AAA is involved by evident medial destruction, ECM remodeling, SMC disappearance and chronic inflammation [100]. Given the featured structure degradation of aortic wall, the role of proteinases such as MMPs has been validated in different AAA models [342], however, as the specific inhibitor of MMPs, the role of TIMP in AAA has been less studied, where the role of TIMP4 in this disease is still unknown.

Our previous study demonstrated that deficiency of TIMP4 increased HFD-mediated plaque deposition in abdominal aorta (but not thoracic aorta) despite lower plasma cholesterol levels [343]. Based on this observation, we hypothesized that absence of TIMP4 could increase the susceptibility of abdominal aorta to aneurysm dependent or independent on abdominal atherosclerosis. Contrary to our initial hypothesis, despite the same increase in abdominal plaque accumulation, TIMP4 deficiency prevented the formation and development of AAA in response to Ang II. This suggests that atherosclerosis is not a necessary condition for AAA formation, which is consistent with previous studies [165]. It also implies a negative regulatory role of TIMP4 in Ang II-induced AAA.

The Ang II model is a commonly used model for aortic aneurysms [344, 345]. Ang II model is usually dependent on elevated plasma lipid levels and traditionally achieved by utilizing apolipoprotein E (*apoE*) or *Ldlr* knockout mice [138, 346]. However, our previous study showed that loss of TIMP4 in *Ldlr*$^{-/-}$ mice receiving an HFD decreased circulating blood lipid levels [343], and this effect of TIMP4 on lipids may interfere with the formation of Ang II-mediated AAA in

atherosclerosis-susceptible mice. The porcine pancreatic elastase model is another common model of aortic aneurysm but is not dependent on hyperlipidemia [347], so this model may be able to explore the role of TIMP4 more directly in aortic aneurysm development compared with the Ang II model.

CHAPTER 5

ROLE OF TIMP4 VERSUS TIMP3 IN AAA AND TAA

LOSS OF TIMP3, BUT NOT TIMP4, EXACERBATES THORACIC AND ABDOMINAL AORTIC ANEURYSM

Mei Hu[1], Ilamaran Meganathan[1] Zamaneh Kassiri[1]

[1]Department of Physiology, Faculty of Medicine and Dentistry, University of Alberta, Edmonton, AB, Canada

Contributions:

MH: Conceived and designed experiments, performed all experiments on human specimens, performed all the *in vivo* murine experiments, collected, and analyzed the data, prepared figures, interpreted the results, and wrote the manuscript.

IM: Contributed to endothelial cell culture and permeability assay.

ZK: Corresponding author. Conceived hypothesis, analyzed data, wrote, and revised the manuscript.

* A version of this chapter has been submitted to a peer-reviewed journal (Arteriosclerosis, Thrombosis, and Vascular Biology) as *Hu M, Meganathan I, Kassiri Z. Loss of TIMP3, but not TIMP4, exacerbates thoracic and abdominal aortic aneurysm.*

5.1. Introduction

Aortic aneurysm is focal dilation of the aorta and is associated with a significant risk of morbidity and mortality but remains a disease without a pharmacological treatment. Aortic aneurysm can form in different regions of the aorta owing to the regional heterogeneity of the aorta. Thoracic and abdominal aortic aneurysms (TAA, AAA) are distinct entities that are associated with different initiating factors and molecular mechanisms, but also share similar characteristics [5, 348].

Tissue inhibitor of metalloproteinases (TIMPs) are best known for their function as inhibitors of matrix metalloproteinases (MMPs) that mediate structural remodeling of the vascular extracellular matrix (ECM), TIMPs can also contribute to other cellular functions such as angiogenesis, cell survival, proliferation, and migration [62, 251, 343, 349, 350]. TIMP3 and TIMP4 have been shown to exhibit region-specific functions in aortic pathologies. Loss of TIMP3 impairs vascular remodeling following Angiotensin II infusion leading to suppressed hypertension [306] and AAA [220]. Loss of TIMP4 promotes aortic smooth muscle cells activation and transition to macrophage-like-foam cells in hyperlipidemic conditions leading to increased atherosclerotic plaque deposition in the abdominal aorta despite lower plasma cholesterol levels [343]. TIMP4 suppressed smooth muscle cell migration *in vitro*, and its increased expression following balloon injury in carotid artery was linked to worse outcome [252].

We investigated if TIMP3 and TIMP4 differentially impact thoracic aortic aneurysm (TAA) or abdominal aortic aneurysm (AAA). We used the peri-adventitial elastase model [351] to induce aortic aneurysm in the thoracic or the abdominal aorta in mice lacking TIMP3 (*Timp3*$^{-/-}$) or TIMP4 (*Timp4*$^{-/-}$) compared to parallel wildtype (WT). We found that loss of TIMP3, but not TIMP4, exacerbated both TAA and AAA compared to WT mice, in males and females. The worsened AAA and TAA in *Timp3*$^{-/-}$ mice were associated with common features (e.g., increased MMP activity

and smooth muscle cell transformation), however in AAA, *Timp3*-deficiency compromised luminal endothelial barrier and worsened inflammation in the medial layer of the abdominal aorta, whereas in TAA, the expanded vasa-vasorum in *Timp3*$^{-/-}$ mice appeared to be the source of increased inflammation. This study highlights the critical role of TIMP3 in aortic remodeling following injury and is unique region-dependent function whereby it can regulate different cellular events in the thoracic versus the abdominal aorta.

5.2. Methods

The detailed Materials and Methods information is available in Chapter 2 Materials and Methods.

5.2.1. Human control (non-diseased) and aneurysmal thoracic and abdominal aorta specimen procurement

Human abdominal aneurysmal aorta (AAA) specimens were procured from patients with non-atherosclerotic AAA undergoing corrective surgery, and thoracic aneurysmal specimens (TAA) were procured from the ascending aorta of patients undergoing prophylactic resection as a consequence of bicuspid aortic valve-associated aortopathies. Patients with aortic dissection and atherosclerosis were excluded. Control samples were non-aneurysmal healthy ascending aortas obtained from donors through the HOPE (Human Organ Procurement and Exchange) Program at the University of Alberta. The study protocols were approved by the Human Research Ethics Review Process at the University of Alberta. All procurements were conducted following institutional approval. Aortic samples were either flash-frozen in liquid nitrogen and stored at -

80°C for molecular studies or fixed in 10% formalin for histological analyses. Clinical information regarding the human specimens is provided in **Table 2.2**.

5.2.2. Animals

Tissue inhibitor of metalloprotease-3 (*Timp3*$^{-/-}$), *Timp4*$^{-/-}$ and WT mice were used in this study. All mice were in C57BL/6J genetic background, and colonies maintained at the Animal Facility in the viral antibody-free (VAF) facility at University of Alberta. All experiments were performed according to the ARRIVE (Animal Research: Reporting of *in vivo* Experiments) guidelines, and in accordance with the guidelines of the University of Alberta Animal Care and Use Committee (ACUC) and the Canadian Council of Animal Care (CCAC). Male and female mice were used in this study.

5.2.3. Induction of abdominal aortic aneurysm and thoracic aortic aneurysm by peri-adventitial application of elastase

Experimental AAA was induced in mice of each genotype by applying the infrarenal abdominal aorta with porcine pancreatic elastase Type I (20 U/ml) for 5 minutes as previously reported, with some modifications [143]. Briefly, 10-week-old male and female mice (WT, *Timp3*$^{-/-}$ and *Timp4*$^{-/-}$) were placed in a supine position receiving isoflurane (1.5%) anesthesia. A laparotomy was performed, and the intestines were gently removed out and the infrarenal abdominal aortas were identified and carefully isolated. Next, the adventitia of exposed aortas was bathed in a small piece of sponge soaked with 10 µL of saline (control) or porcine pancreatic elastase (PPE; E1250, Sigma-

Aldrich Co.) for 5 minutes. After elastase exposure, the sponge was removed, the intestines were gently placed back into the belly, the fascial layers and skin were closed in turn.

Experimental TAA was induced in mice by applying the descending thoracic aorta with porcine pancreatic elastase Type I (30 U/ml) for 5 minutes as described before [299]. Briefly, 10-week-old mice were first anesthetized intraperitoneally and then transferred to mechanical ventilation after tracheal intubation by connecting a mouse ventilator. Mice were subjected to thoracotomy in the left lateral recumbent position. After the chests were opened, the left lung was collapsed with moist gauze to expose the thoracic aorta. The pleura overlying the thoracic aorta was dissected carefully，and a piece of saline- or elastase-soaked sponge were applied to the surface of the exposed aortas.

After 5 minutes of elastase exposure, the sponge was removed, the lungs were re-inflated, the ribs, muscle layers and skin were closed in turn.

5.2.4. Aorta collection and imaging

Mice of each genotype were euthanized on day 3 or 14 after surgery. Aortic segments incubated with elastase or saline were collected. All the entire aortas were excised and cleaned by removing all perivascular fat. After the clean, aorta images were captured to quantify the outer diameter. Maximal external aortic diameters were measured directly from photographs of the abdominal and thoracic aortas.

5.2.5. Morphometric and immunofluorescent analyses of human and mouse aorta

The severity of elastin fiber deteriorations in the abdominal and thoracic aortas were visualized by VVG staining. The internal aortic diameters were calculated from the internal perimeters of the

VVG-stained aortic cross-sections, assuming that the cross-sections were full circles. Collagen deposition and distribution in aneurysmal aortas were detected by picrosirius red (PSR) staining. For immuno-staining, freshly excised abdominal aortas were embedded in OCT medium, freeze-fixed in liquid nitrogen; 5μm cryosections were used for staining with different antibodies as described [343]. All fluorescent images were captured using an Olympus motorized inverted research microscope (Model IX81).

5.2.6. In situ zymography

Total gelatinase activity was measured on OCT-frozen aortic section using fluorescein-conjugated gelatin (DQ gelatin, D-12054; Invitrogen) as the substrate, which emits fluorescence upon proteolytic cleavage by gelatinases in the aortic tissue [289]. Fluorescence was visualized by fluorescent microscopy (Olympus IX81). The images were superimposed with elastin autofluorescence (using red filter) to show the elastin fibers. The fluorescent intensity of gelatinase was quantified using the Image-Pro Plus software. The average fluorescent intensity of gelatinase activity for each cross-section, excluding elastin autofluorescence, was calculated by dividing the total integrated optical density (IODsum) value by the total corresponding aorta surface area (Areasum, expressed as pixels).

5.2.7. Gelatin zymography

MMP2 and MMP9 activity levels were assessed by *in vitro* gelatin zymography as described before [343]. Equal amounts (20 μg) of aortic extracts were separated by SDS-PAGE gel containing 1 mg/ml gelatin. The gelatin-incorporated gel was incubated in zymography developing buffer

(50mM Tris-Cl, pH 7.5, 5mM CaCl2, 150mM NaCl) at 37°C for 48 h. The gel was stained in 0.05% Coomassie Blue G-250, and grayscale images were scanned and inverted for densitometric quantification. Bands of gelatinolytic activity were quantified and normalized to the loading control.

5.2.8. *In vivo* Evans blue permeability assay

The Evans blue permeability assay was performed in mouse on day 3 post-TAA or AAA surgery as reported before [299]. The aortic segments that underwent elastase incubation were submitted OCT embedding. Aortic cross-sections were obtained and fixed with 4% PFA for 15 minutes. After 3 times wash with 1 X PBS, the sections were mounted by Prolong Gold Antifade Reagent with DAPI and used for imaging.

5.2.9. *En face* immunostaining for VE-cadherin

Mouse was euthanized on day 3 after TAA or AAA. Aortic segments from aneurysms or controls were removed after perfusion fixation of the circulatory system with 4% paraformaldehyde solution. Aortic segments were unfolded and immunofluorescence staining for VE-cadherin was performed, followed by flattening on a glass slide and sealing with coverslips. The endothelial lining was visible under an Olympus motorized inverted research microscope (Model IX81).

5.2.10. Primary human aortic endothelial cell culture, siRNA transfection and *in vitro* permeability Assay

HAoECs were used at passages 3 to 5 for the experiments described in this study. *Timp3* siRNA (Thermo Fisher, 118555) or *Timp4* siRNA (Thermo Fisher, 118690) was used to knock down

Timp3 or *Timp4* in HAoECs, and scrambled siRNA (Ambion; 4390844) was used as control. In vitro EC permeability assay was performed using a vascular permeability assay kit according to the manufacturer's instruction (EMD Millipore) as before [314].

5.2.11. RNA and protein extraction and analyses

Total RNA was extracted from the aortic segments incubated with elastase or saline from mice on day 14 post-TAA or AAA surgery using TRIzol reagent (Invitrogen; 15596-018) according to the manufacturer's protocol. Quantitative Taqman real-time polymerase chain reaction was performed using TaqMan primer-probe mix for each gene (**Table 2.6**) and a LightCycler 480 II system (Roche) using the LightCycler 480 Probes Master kit (Roche; 04887301001). The reference gene *18S* or *Hprt* was used as an internal control.

Total protein was extracted from the thoracic or abdominal aorta segments, incubated with elastase or saline, from mice on day 3 or 14 post-TAA or AAA surgery using CelLytic M lysis buffer as before [299, 343]. Bands were detected using the ImageQuant LAS 400 system (GE Healthcare), and band intensity was quantified using ImageQuant TL software (Version 7.0 GE Healthcare) and were normalized to the corresponding β-actin band intensity.

5.2.12. Statistics

Statistical analyses were performed by using IBM SPSS software. Normality of data distribution was determined by the Shapiro-Wilk W test. Comparison among multiple groups involving one main factor was performed by 1-way ANOVA followed by Bonferroni post hoc test. Comparison

among multiple groups involving 2 factor was performed by 2-way ANOVA followed by Bonferroni post hoc test. Statistical significance was recognized at $p<0.05$.

5.3. Results

5.3.1. Loss of TIMP3, but not TIMP4, Exacerbates AAA and TAA

To investigate the role of TIMP3 and TIMP4 in AAA versus TAA, male and female *Timp3*$^{-/-}$, *Timp4*$^{-/-}$ and WT mice were subjected to peri-adventitial elastase application. After 14 days, mice lacking TIMP3, developed a more severe aortic aneurysm, whereas in *Timp4*$^{-/-}$ mice aortic aneurysm was comparable to the parallel WT mice in male **(Figure 5.1 A, C)** and in female mice **(Figure 5.2)**. The increase in the diameter of the aneurysmal aorta was significantly greater in *Timp3*$^{-/-}$ compared to WT and *Timp4*$^{-/-}$ mice in both aneurysm models **(Figure 5.1 Ci-ii, Di-ii)**. Consistent with aneurysm formation, elastin fiber degradation and disarray were observed in the aneurysmal aorta from all genotypes but were markedly more severe in *Timp3*$^{-/-}$ mice **(Figure 5.1 A, B, Ciii, Diii)**. Similar patterns were observed in female *Timp3*$^{-/-}$ mice following AAA or TAA compared to WT and *Timp4*$^{-/-}$ females **(Figure 5.2)**. Histological analyses showed a more excessive peri-adventitial fibrosis in *Timp3*$^{-/-}$-AAA compared to all other groups, although peri-adventitial elastase application did increased fibrosis in AAA and TAA samples from all genotypes **(Figure 5.3 A, B).**

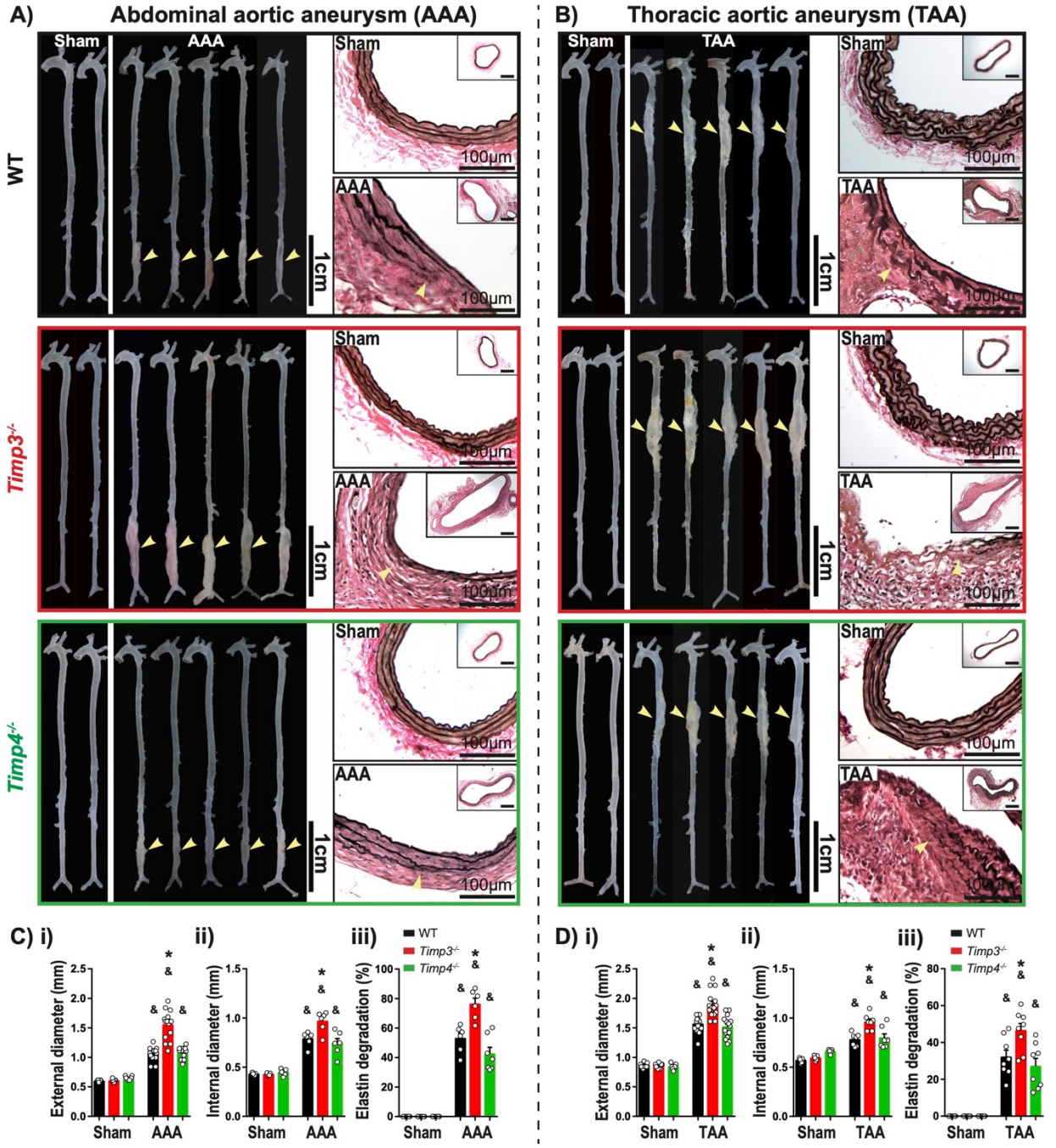

FIGURE 5. 1 LOSS OF TIMP3 (TISSUE INHIBITOR OF METALLOPROTEINASE 3) BUT NOT TIMP4 GREATLY EXACERBATES ELASTASE-INDUCED AAA AND TAA.

Representative pictures of whole aorta (left) and verhoeff–van gieson (VVG) staining (right) of WT, *Timp3*$^{-/-}$ and *Timp4*$^{-/-}$ male mice 14 days after application with or without elastase on the abdominal aorta **(A)** and the thoracic aorta **(B)**. Quantification of the maximum external diameter **i)** internal diameter **ii)** and elastin degradation **iii)** of abdominal aorta **(C)** and thoracic aorta **(D)**, n=7-15 mice per group. Arrows show the breakage or loss of elastin fibers. Averaged values are presented as Mean ± SEM. AAA, abdominal aortic aneurysm. TAA, thoracic aortic aneurysm. Timp3/4,

tissue inhibitor of metalloproteinase -3/4. &P<0.05 vs corresponding sham group; *P<0.05 vs corresponding WT group (2-way ANOVA followed by the Tukey post hoc test).

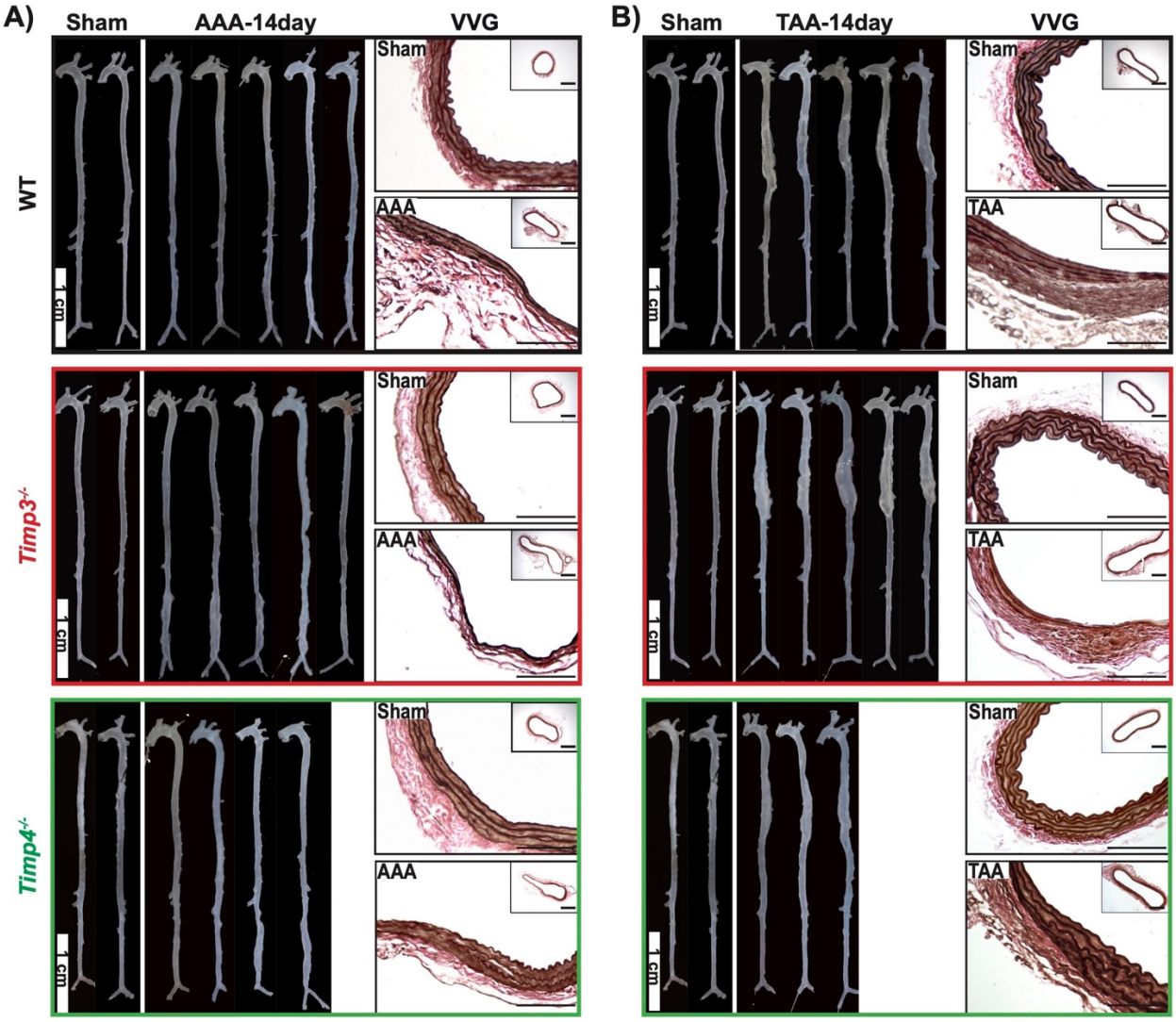

FIGURE 5. 2 TIMP3-DEFICIENCY GREATLY EXACERBATES ELASTASE-INDUCED EXPANSION OF AORTIC ANEURYSMS IN FEMALE MICE.

Pictures of whole aorta in female mice 14 days post-elastase or saline application of abdominal aorta (A) and thoracic aorta (B), and representative images of aortic cross-sections stained for VVG (Verhoeff-van Gieson) in indicated groups showing elastin fiber structure in AAA (A) and TAA (B). Scale bars: 100 μm. AAA, abdominal aortic aneurysm. TAA, thoracic aortic aneurysm. Timp3/4, tissue inhibitor of metalloproteinase -3/4.

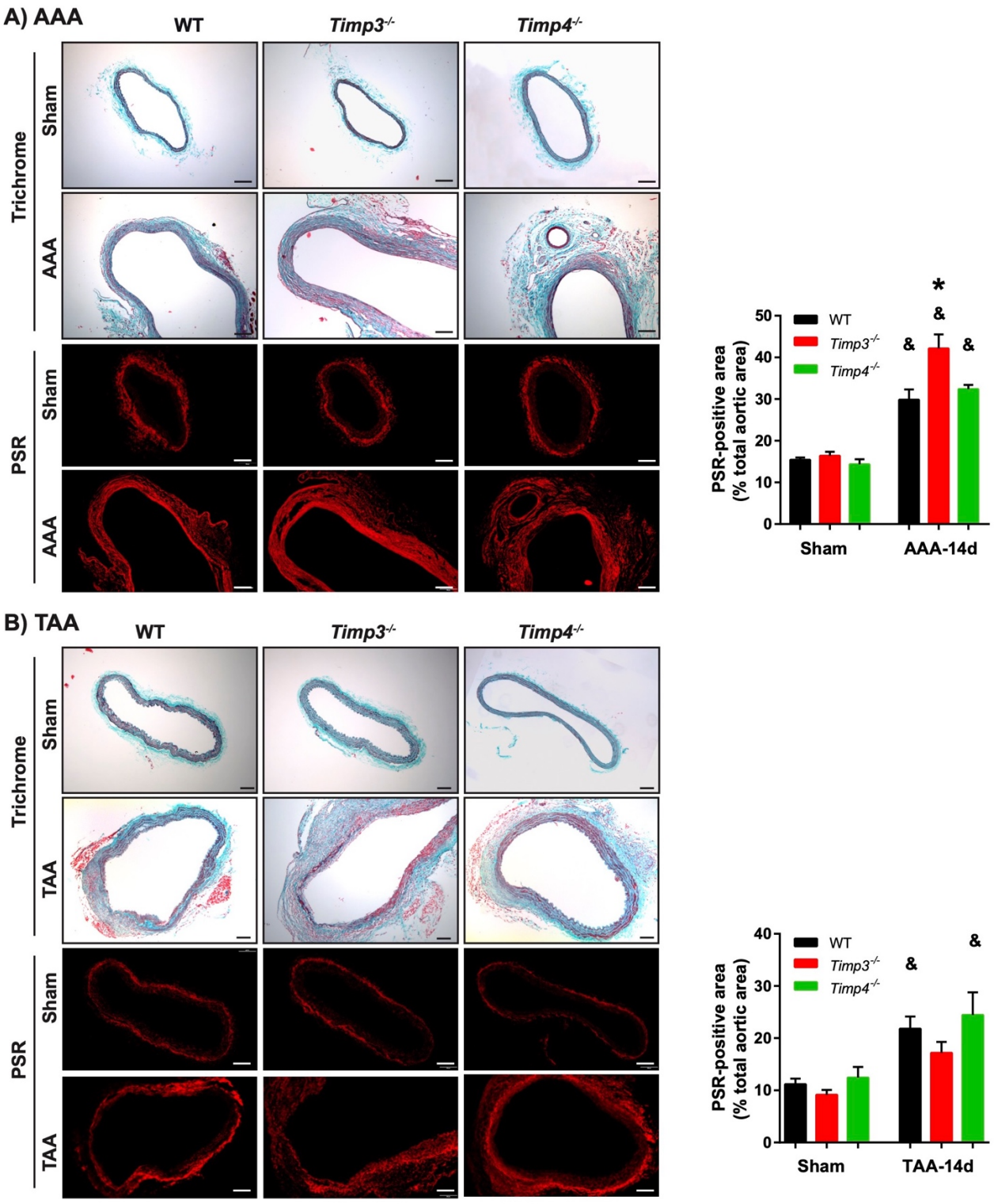

FIGURE 5. 3 *TIMP3*$^{-/-}$ MICE EXHIBIT A GREATER PERIADVENTITIAL FIBROSIS FOLLOWING AAA BUT NOT TAA.

Representative images of aortic cross-sections of trichrome staining and picrosirius red staining (PSR) of male mice following sham or 14 days post-AAA (A) or TAA (B) showing fibrillar collagen deposition, and the quantification of PSR positive staining. Scale bar indicates 100µm. Aver- aged values are presented as Mean ± SEM. &P<0.05 vs corresponding sham group; *P<0.05 vs corresponding WT group (2-way ANOVA followed by the Tukey post hoc

test). AAA, abdominal aortic aneurysm. TAA, thoracic aortic aneurysm. Timp3/4, tissue inhibitor of metalloproteinase -3/4.

5.3.2. SMC Transformation and Increased Proteinase Activity in *Timp3*$^{-/-}$ Aneurysmal Aorta

Smooth muscle cells (SMCs) are responsible for vascular contractility and are a major cell source for production of ECM proteins and the MMPs that mediate ECM turnover in the vessels. In disease, SMCs can transform from a contractile state to a synthetic state with increased production of various proteins. Loss of SMC contractile properties is a critical factor in the pathophysiology of aortic aneurysm [352]. Immunofluorescent staining **(Figure 5.4 A, B)** and immunoblotting **(Figure 5.4 C, D)** for αSMA (alpha-smooth muscle actin) showed decreased population of SMCs in the aneurysmal aortas which was more pronounced in *Timp3*$^{-/-}$ mice post-AAA **(Figure 5.4 A, C)** and -TAA **(Figure 5.4 B, D)** compared to parallel WT and *Timp4*$^{-/-}$ mice. Consistently, immunoblotting for other SMC contractile markers, SM22 (smooth muscle 22) and calponin showed marked reductions in the aneurysmal *Timp3*$^{-/-}$ aortas compared to parallel *Timp4*$^{-/-}$ and WT groups **(Figure 5.4 C, D)**. In addition, increased apoptosis was detected in aneurysmal *Timp3*$^{-/-}$ aortas evident by a higher level of cleaved caspase 3 **(Figure 5.4 E, F)** which could partly explain the reduced SMC density in *Timp3*$^{-/-}$-TAA and -AAA groups.

MMPs can degrade ECM proteins, while their activity is kept in check by TIMPs [349]. The aberrant ECM remodeling in *Timp3*$^{-/-}$-TAA and -AAA mice was associated with a significantly greater increase in proteinase activity in these mice compared to parallel WT and *Timp4*$^{-/-}$ groups as detected by *in situ* gelatin zymography **(Figure 5.5 A, C)**. *In vitro* gelatin zymography showed an increase in MMP9 and MMP2 levels in the aneurysmal aortas of all genotypes compared to their corresponding control groups, and while the increase in MMP9 was similar in all groups, the increase in MMP2 (pro and cleaved) was significantly greater in *Timp3*$^{-/-}$-AAA and TAA group

(Figure 5.5 B, D). TaqMan RT-PCR showed that mRNA expression *Mmp2*, *-9*, *-12*, *-13* and *-14* (*Mt1-mmp*) increased in all genotypes following AAA or TAA, while expression of *Mmp2*, *Mmp13* and *Mmp14* in AAA, and only *Mmp14* in TAA samples were significantly higher in *Timp3*$^{-/-}$ compared to the corresponding WT and *Timp4*$^{-/-}$ groups **(Figure 5.6 A)**. To assess if there is a potential compensatory increase of other *Timp*s in the absence of *Timp3* or *Timp4*, we found that *Timp1* increased similarly in all genotypes post-AAA, but only in WT and *Timp3*$^{-/-}$ post-TAA. In WT and *Timp4*$^{-/-}$ mice, *Timp3* decreased post-AAA but not TAA; and *Timp4* only decreased in the WT-AAA but not in other groups. TIMP2 remained unaltered in both aneurysm groups **(Figure 5.6 B)**. Overall, these data suggest that absence of TIMP3 results in a more pronounced SMC loss and transformation, and a greater increase in proteolytic activities following AAA and TAA compared to *Timp4*$^{-/-}$ or WT mice.

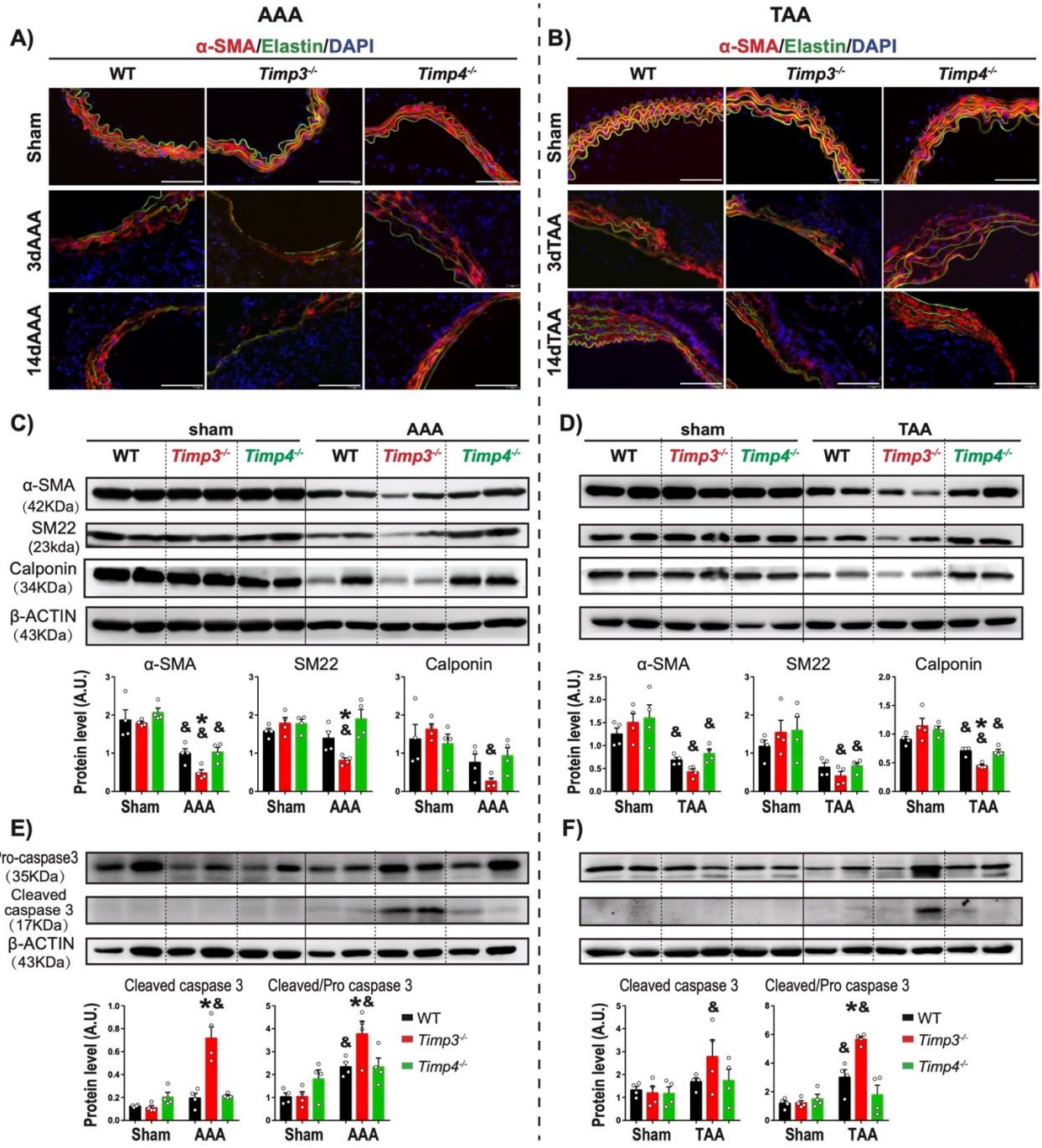

FIGURE 5. 4 AORTIC ANEURYSM IN TIMP3-DEFICIENT MICE IS ASSOCIATED WITH GREATER SMOOTH MUSCLE CELL LOSS COMPARED TO *TIMP4*$^{-/-}$ OR WT.

Representative immunofluorescent staining for alpha-smooth muscle actin (α-SMA, red; elastin, elastin autofluorescence, green) of aortic cross-sections from **abdominal (A)** or **thoracic aorta (B)** 3 days or 14 days after incubation with elastase or saline. Scale bars=100 μm. Representative immunoblot and average protein levels for vascular smooth muscle makers from **abdominal (C)** or **thoracic aorta (D)**. Representatives immunoblot and average protein levels for molecular markers of apoptosis (pro- and cleaved caspase 3) from **abdominal (E)** or **thoracic aorta (F)**. Averaged values are presented as Mean ± SEM. AAA, abdominal aortic aneurysm. TAA, thoracic aortic aneurysm.

Timp3/4, tissue inhibitor of metalloproteinase -3/4. &P<0.05 vs corresponding sham group; *P<0.05 vs corresponding WT group (2-way ANOVA followed by the Tukey post hoc test).

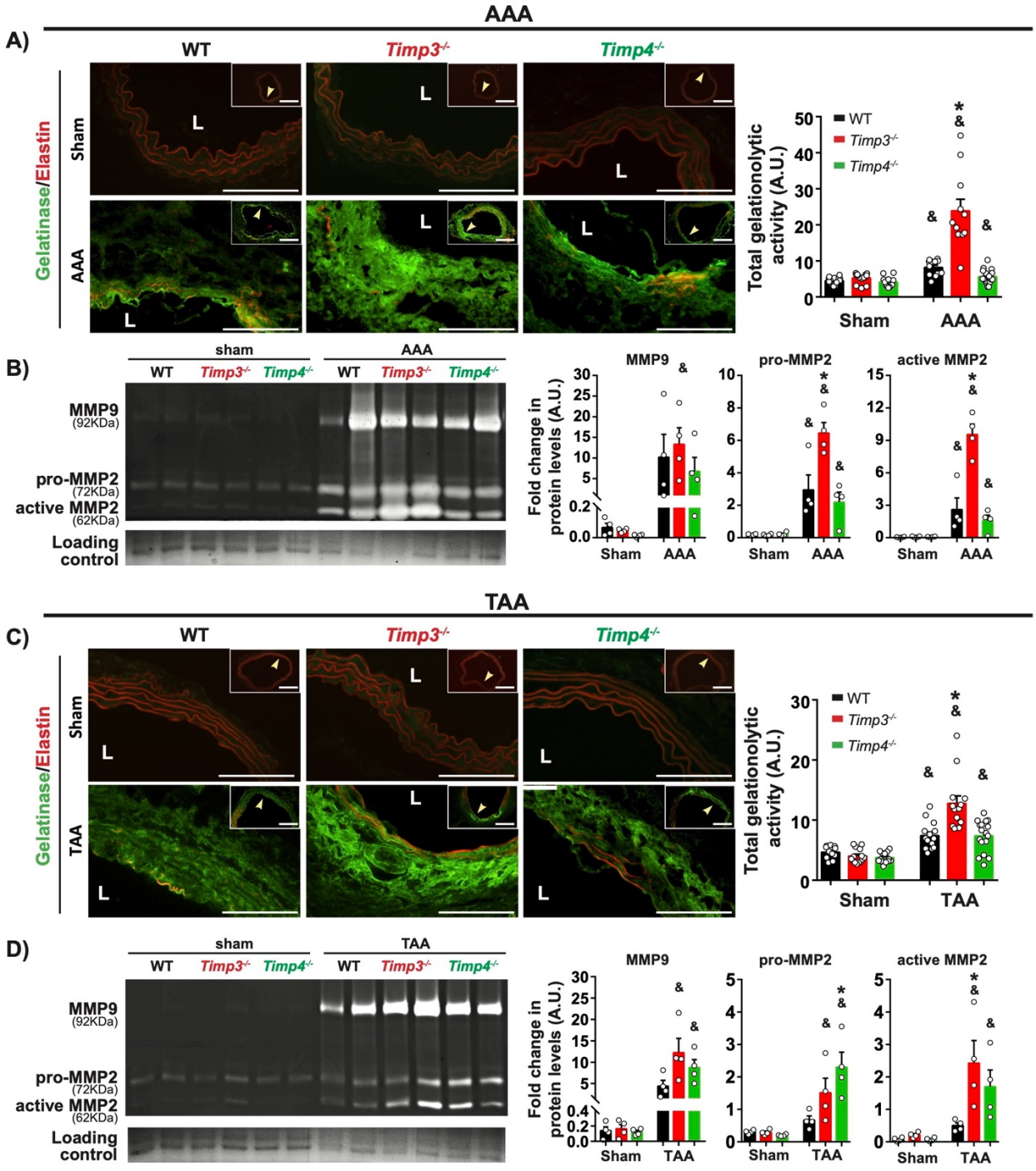

FIGURE 5. 5 TIMP3 DEFICIENCY RESULTS IN A GREATER INCREASE IN PROTEASE ACTIVITIES IN AAA AND TAA.

Representative images of in situ zymography and quantification of protease activity in aorta sections post-AAA **(A)** or -TAA **(C)** from male mice in indicated groups (elastin autofluorescence, red; gelatinase activity, green). Arrows in the inserts indicate the area of the aorta that are magnified. L indicates lumen; n=10-15 sections/aorta, 3-4 mice/genotype/group. Representative in gel gelatin zymography and averaged levels of MMP9, pro-MMP2, and

cleaved MMP2 levels in AAA **(B)** and TAA **(D)** from male mice in indicated groups. Coomassie blue–stained gel was used as the protein loading control. n=4/group. Scale bars=100 μm. Averaged values are presented as Mean ± SEM. &P<0.05 vs corresponding sham group; MMP, matrix metallopeptidase; AAA, abdominal aortic aneurysm. TAA, thoracic aortic aneurysm. Timp3/4, tissue inhibitor of metalloproteinase -3/4. &P<0.05 vs corresponding sham group, *P<0.05 vs corresponding WT group (2-way ANOVA followed by the Tukey post hoc test).

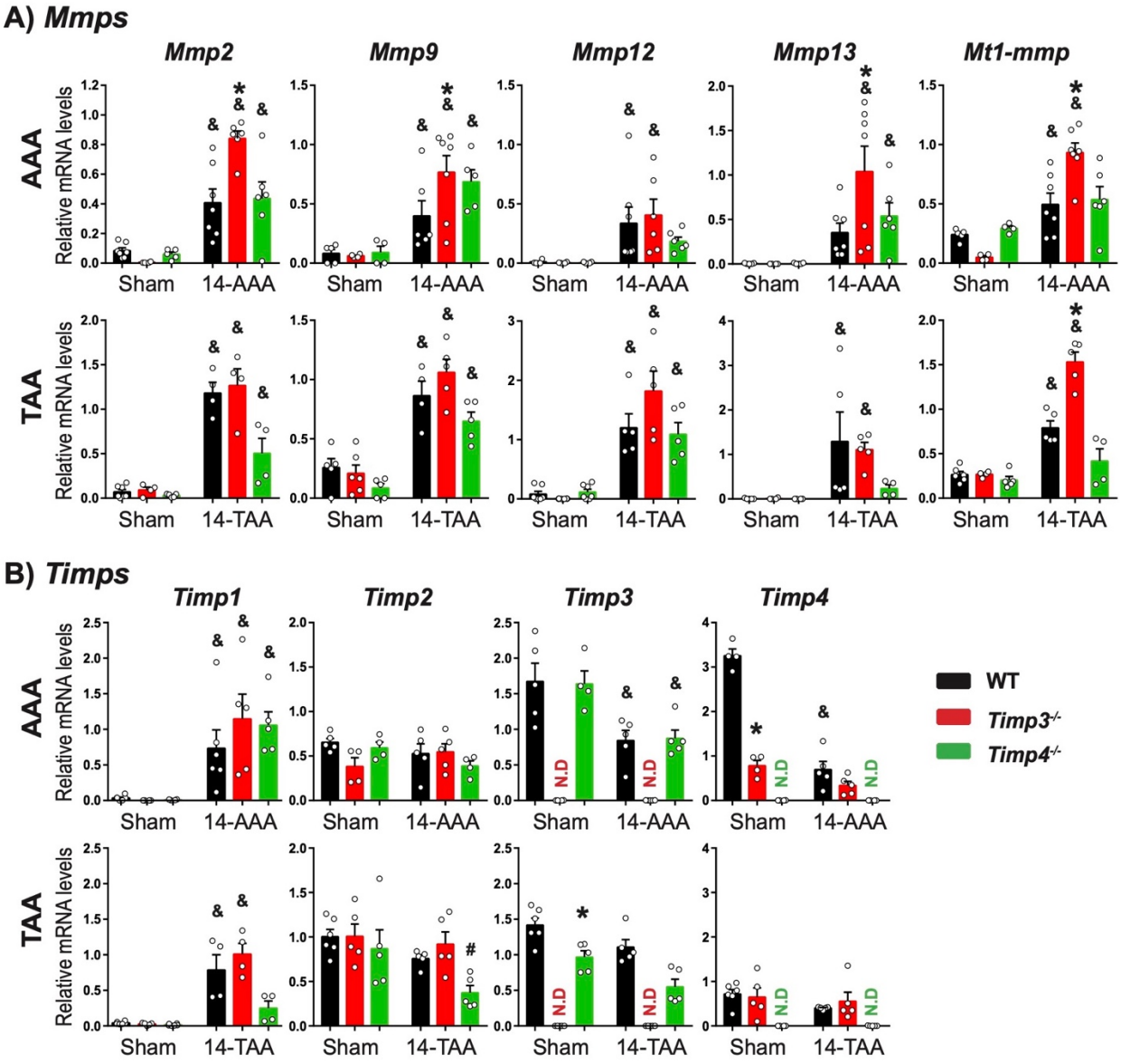

FIGURE 5. 6 TAQMAN MRNA EXPRESSION OF MMPS AND TIMPS IN THE THORACIC AORTA AND ABDOMINAL AORTA WITH OR WITHOUT ANEURYSMS IN THE MALE MICE.

A) mRNA expression of *Mmp* (matrix metalloproteinase) 2, 9, 12, 13 and *MT1-mmp* (membrane type 1 matrix metalloproteinase) in indicated groups. **B)** TaqMan mRNA expression of *Timp* (tissue inhibitor of metalloproteinase) 1, 2, 3 and 4 in indicated groups. Averaged values are presented as Mean ± SEM. N.D. indicates not detected.

AAA/TAA, abdominal/thoracic aortic aneurysm. *P<0.05 vs corresponding WT group; &P<0.05 vs corresponding Sham group (2-way ANOVA followed by the Tukey post hoc test).

5.3.3. Different Pattern of Inflammation in *Timp3*$^{-/-}$ Aortic Wall following AAA vs TAA

Inflammation is an important factor in the development of aortic aneurysm [353, 354]. Immunofluorescent staining showed an accumulation of macrophages (CD68), leukocytes (CD45) and neutrophils (Ly6B.2) in the aortic wall at 3 days after AAA or TAA in all genotypes, consistent with the higher mRNA expression of inflammatory cytokines, Interleukin (*Il*)-*1β*, *Il6*, Interferon gamma *(Ifn-γ)*, Tumor necrosis factor-alpha (*Tnfα*), monocyte chemoattractant protein-1 (*Ccl2/Mcp-1*), and macrophage inflammatory protein 1-alpha (*Ccl3/Mip-1α*) **(Figure 5.7 A-D)**. The *Timp3*$^{-/-}$ aneurysmal aorta exhibited significantly greater inflammation, but interestingly, the location of inflammatory cells in AAA differed from that in TAA in these mice. Following AAA, CD45^{+} leukocytes and neutrophils were detected primarily in the medial layer and macrophages in the medial and adventitial layer, whereas post-TAA, the inflammatory cells were almost exclusively present in the adventitial layer in *Timp3*$^{-/-}$ mice **(Figure 5.7 A, C)**, as well as a significant increase in mRNA expression of *Il6* in AAA, and *Il6*, *Tnfα* and *Ccl2* in TAA **(Figure 5.7 B, D)**. *Timp4*$^{-/-}$ mice showed comparable inflammation compared to WT mice post-AAA or TAA **(Figure 5.7 A-D)**. Therefore, TIMP3 deficiency increased susceptibility to inflammation in aortic aneurysm, but in the medial region following AAA, compared to the adventitia following TAA.

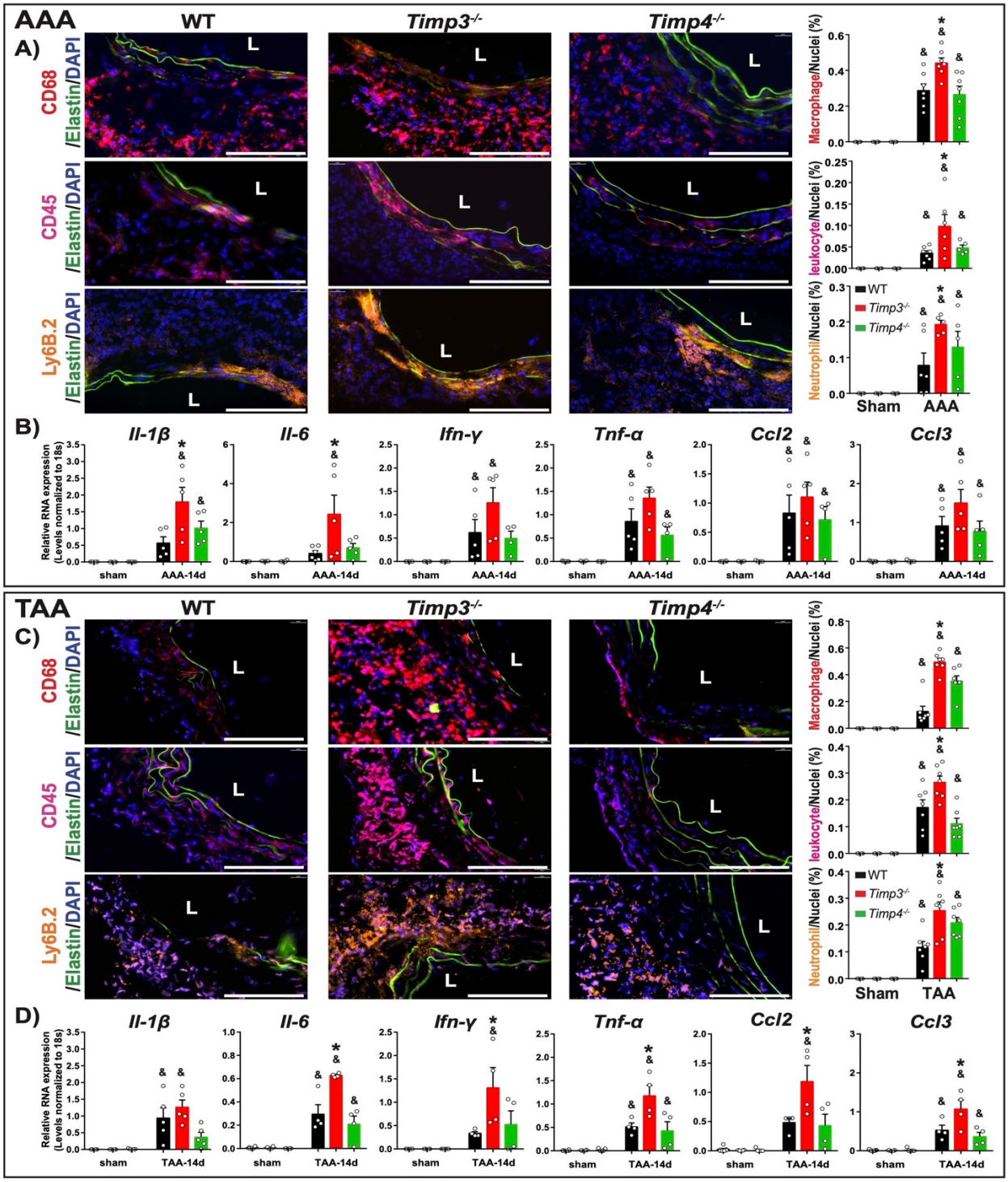

FIGURE 5. 7 DEFICIENCY OF TIMP3 RESULTED IN MARKEDLY INCREASED ACCUMULATION OF INFLAMMATORY CELLS IN THE MEDIA OF AAA, AND ADVENTITIA OF TAA.

Representative immunofluorescent staining and quantification showing macrophage (CD68, red), leukocyte (CD45, pink) and neutrophil (Ly6B.2, orange) infiltration into aortic wall of male mice at day 3 post-aneurysm induction，predominantly in the media layer of AAA **(A)** and in the adventitial layer of TAA **(C)**. Scale bars=100 μm. n=4-6 sections/aorta,3 mice/genotype/group. mRNA levels of inflammatory cytokines and chemokines in abdominal aortas **(B)** and thoracic aortas **(D)** at day 3 post-AAA or TAA induction. n=5/group. Averaged values are presented as Mean

± SEM. *Il*, interleukin; *Ifn*, interferon; *Tnf*, tumor necrosis factor. *Ccl* indicates C-C motif chemokine ligand. &P<0.05 vs corresponding sham group; *P<0.05 vs corresponding WT group (2-way ANOVA followed by the Tukey post hoc test).

5.3.4. *Timp3*-deficiency Increased Intimal Permeability in AAA, and Increased Peri-adventitial Vascularization in TAA

Having found that inflammation is heightened in *Timp3*$^{-/-}$ mice post-AAA and -TAA, we first examined whether this could be due to impaired endothelial cell (EC) barrier integrity in the absence of TIMP3 which would promote the infiltration of inflammatory cells into the extravascular space. At 3 days post aneurysm induction, Evans blue was injected in the animals (i.p), and the aorta was harvested after 1 hour to evaluate endothelial permeability *in vivo.* Aorta from *Timp3*$^{-/-}$-AAA mice exhibited a markedly more visible Evans Blue permeation (blue color) compared to WT- and *Timp4*$^{-/-}$-AAA mice **(Figure 5.8 A)**, which was more localized to the subintima, and medial regions as detected by the red autofluorescence of Evans Blue in the aorta cross-section **(Figure 5.8 A)**, consistent with the pattern of inflammatory cell infiltration in *Timp3*$^{-/-}$-AAA aortas **(Figure 5.7 A)**. Vascular endothelial cadherin (VE-Cadherin) is the predominant adhesion molecule in maintaining the EC-EC junctions and the intimal barrier. *En face* immunofluorescence staining of the luminal (intimal) surface of the abdominal aorta for VE-cadherin showed a markedly greater impairment of the density and organization of the VE-cadherin staining in *Timp3*$^{-/-}$-AAA compared to WT- and *Timp4*$^{-/-}$-AAA **(Figure 5.8 B)**. Consistently, an *in vitro* EC permeability assay showed that knocking down *Timp3* (by siRNA) increased the permeability of elastase-incubated EC monolayer more severely compared to *Timp4-siRNA* or control siRNA **(Figure 5.8 C).**

Similar analysis in TAA groups revealed a different pattern of endothelial permeability. Evans Blue permeation was observed mainly in the adventitial region in *Timp3*$^{-/-}$-TAA compared to WT- and *Timp4*$^{-/-}$-TAA mice **(Figure 5.9 A)**, which is similar to the pattern of inflammatory cell presence in the adventitia of *Timp3*$^{-/-}$-TAA mice **(Figure 5.7 C)**. Meanwhile, VE-cadherin staining of the luminal (intimal) surface of the TAA aortas showed comparable impairment of VE-cadherin arrangement and density in all three genotypes (**Figure 5.10 A**). These data collectively suggest increased permeability through the vasa vasorum in *Timp3*$^{-/-}$-TAA mice. We assessed the vascular density in the thoracic aortic wall and found a significantly greater density for CD31, an EC-specific surface protein, in the *Timp3*$^{-/-}$-TAA aortas **(Figure 5.9 B)**, showing a more extensive vasa vasorum branching in these mice compared to *Timp4*$^{-/-}$- and WT-TAA aortas. In AAA samples, however, CD31 staining showed comparable vascular density in the adventitia of the abdominal among genotypes (**Figure 5.10 B**).

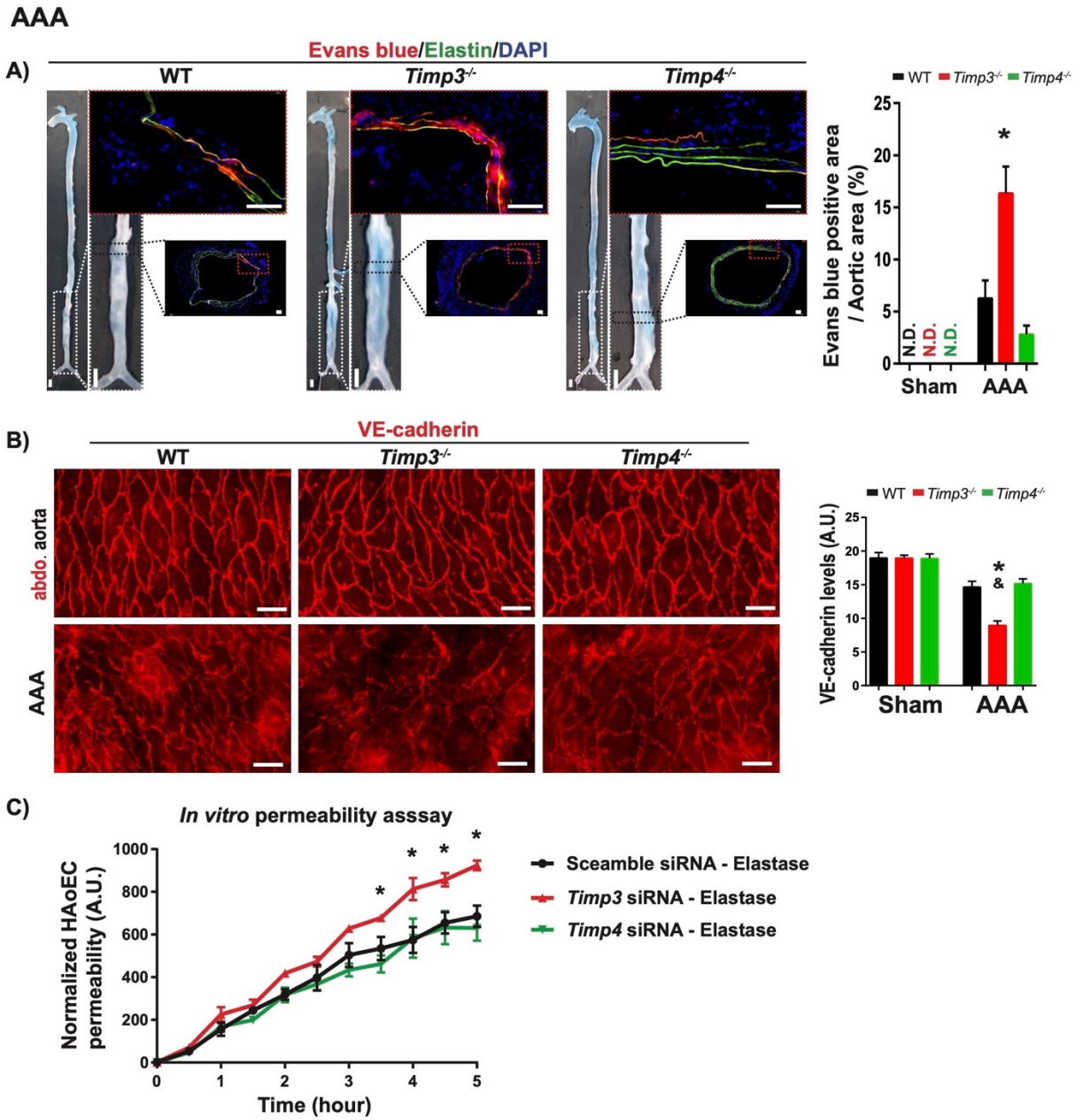

FIGURE 5. 8 *TIMP3*-DEFICIENCY COMPROMISED THE ENDOTHELIAL BARRIER IN ANEURYSMAL ABDOMINAL AORTA.

A) Representative whole aorta and cross-section images showing Evans blue dye permeation (red autofluorescence) mainly concentrated in the intima and media of abdominal aortic wall in mice 3 days post-AAA (Media elastin fibers show green autofluorescence; n=6/group). **B)** *En face* view of the endothelial layer in abdominal aorta immuno-stained with anti-VE-cadherin (red) 3 days post-AAA or post-sham in the indicated genotypes (n=10/group; Scale bars=50 μm). **C)** *In vitro* permeability assay for primary human aortic ECs (HAoECs) monolayers, transfected with *Timp3* or *Timp4* small interfering RNA [siRNA], or scrambled siRNA (control) after incubation with elastase. Averaged values are presented as Mean ± SEM. N.D.=not detected. AAA/TAA, abdominal/thoracic aortic aneurysm. VE-Cadherin, endothelial specific adhesion molecule; Timp3/4, tissue inhibitor of metalloproteinase -3/4. **P*<0.05 vs corresponding WT group or scramble siRNA group; &*P*<0.05 vs corresponding Sham group (2-way ANOVA followed by the Tukey post hoc test).

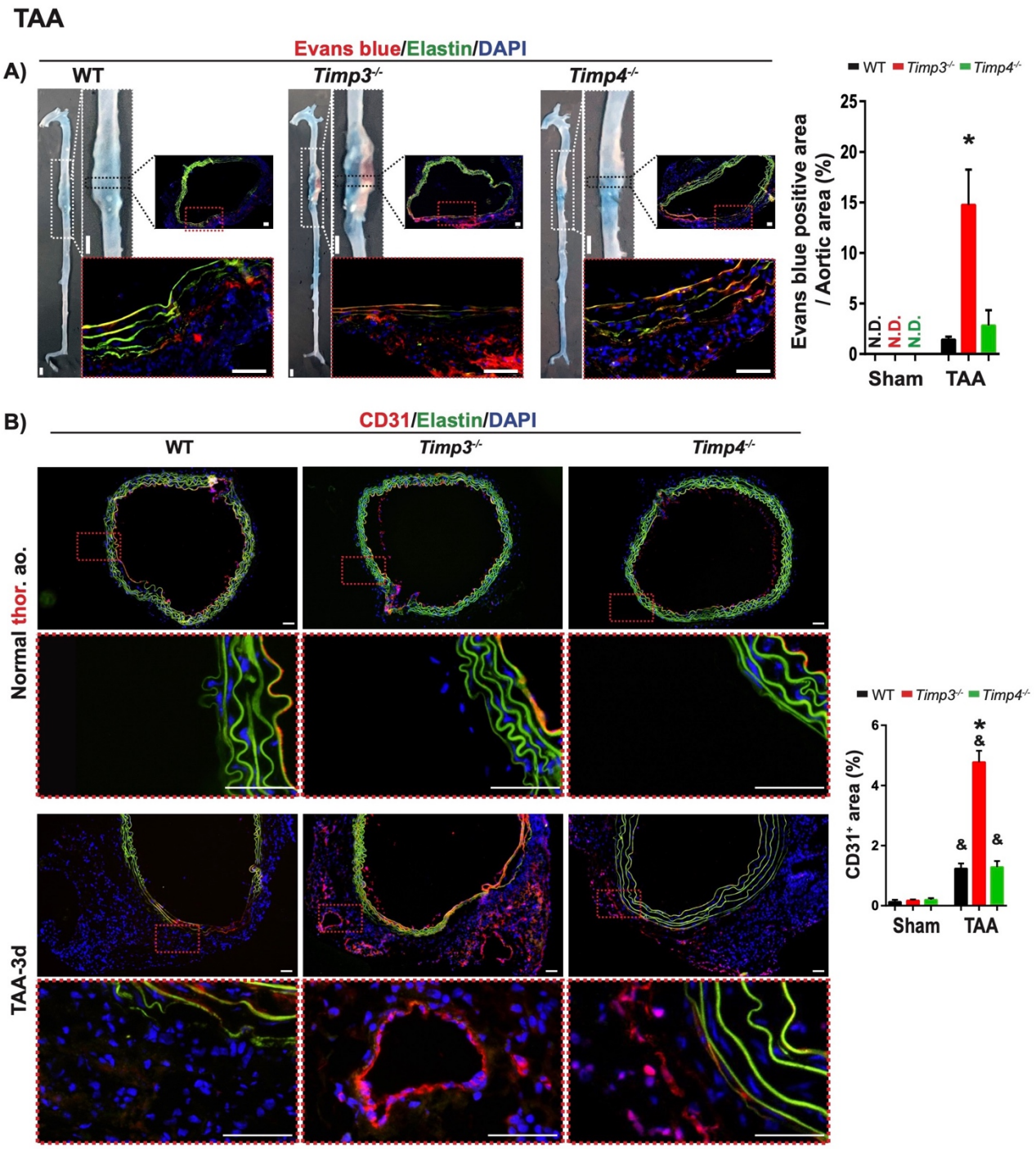

FIGURE 5. 9 INCREASED DENSITY OF ADVENTITIAL VASA VASORUM IN *TIMP3*$^{-/-}$-TAA.

A) Representative whole aorta and cross-section images showing Evans blue dye (red autofluorescence) permeation mainly in the adventitia of thoracic aortic wall in mice 3 days post-TAA (Media elastin fiber shows green autofluorescence; n=6/group). **B)** Cryosections of aorta showing vascular branching in the adventitia (CD31-stained, red), elastin (green, autofluorescence) and DAPI (blue) in 3 day-post TAA in indicated groups. n=10/group. *P<0.05 vs corresponding WT group; Scale bars: 50 μm. Averaged values are presented as Mean ± SEM. N.D.=not detected.

AAA/TAA, abdominal/thoracic aortic aneurysm. Timp3/4, tissue inhibitor of metalloproteinase -3/4. &P<0.05 vs corresponding Sham group (2-way ANOVA followed by the Tukey post hoc test).

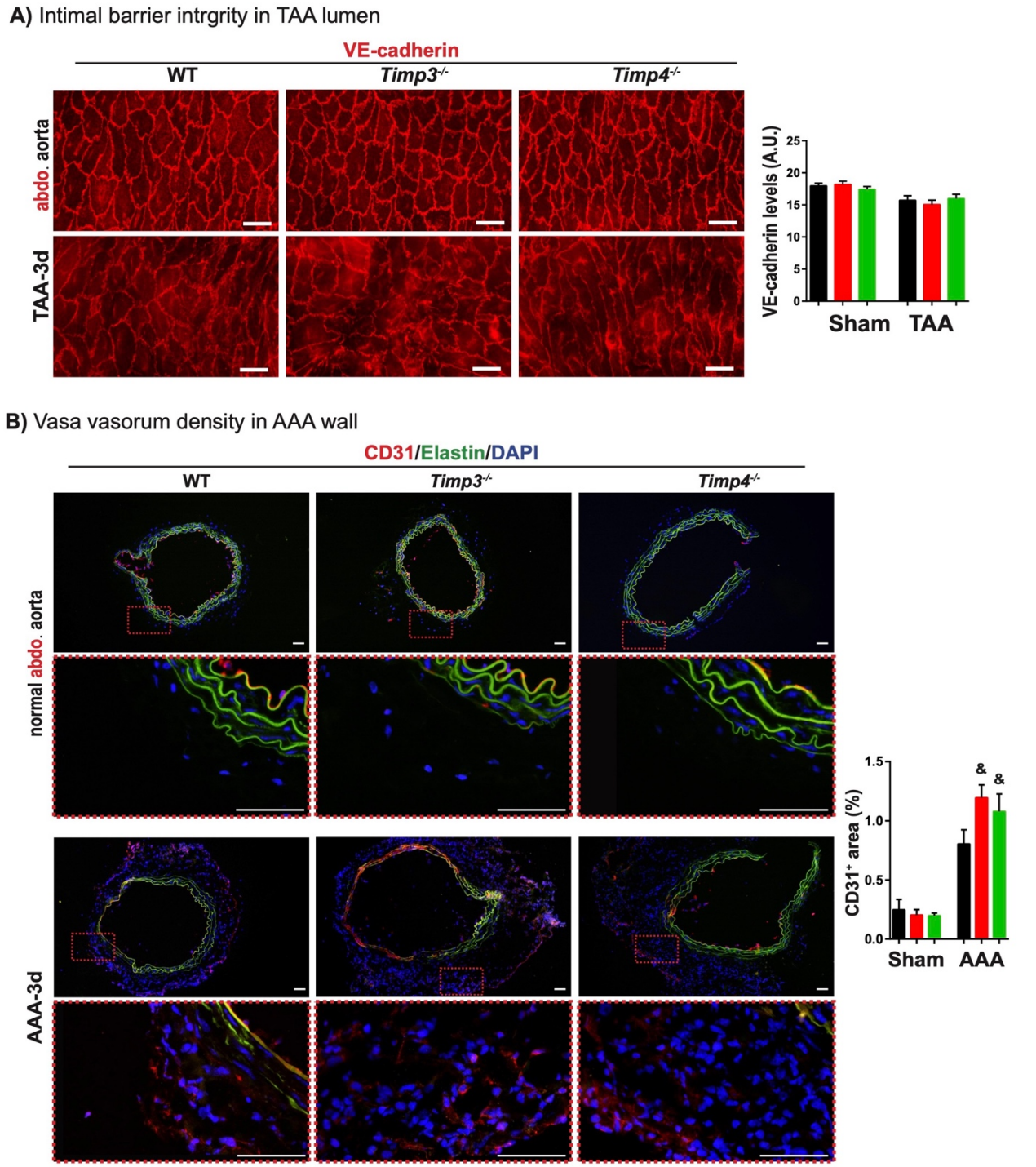

FIGURE 5. 10 TIMP3 DEFECT DID NOT AFFECT THE ENDOTHELIAL PERMEABILITY OF TAA AND THE ADVENTITIAL VASCULARIZATION OF AAA.

A) *En face* view of the integrity of endothelial layer immuno-stained with anti-VE-cadherin (red, endothelial specific adhesion molecule) in mice 3 days post-TAA and their normal abdominal aorta. n=10/group. Scale bars: 50 µm. **B)**

Cryosections of aortic tissue showing neo vessel in the adventitia stained by CD31 (red), elastin (green, autofluorescence) and DAPI (blue) in 3 day-post AAA in indicated groups. n=10/group. Scale bars: 100 μm. AAA/TAA, abdominal/thoracic aortic aneurysm. Timp3/4, tissue inhibitor of metalloproteinases 3/4. &P<0.05 vs corresponding Sham group (2-way ANOVA followed by the Tukey post hoc test).

5.3.5. TIMP3 is Significantly Decreased in AAA, but Increased in TAA Specimens from Patients

Next, we examined how TIMP3 and TIMP4 levels are altered in the aorta specimens from patients with AAA (non-atherosclerotic) and TAA (bicuspid aortic valve) compared to non-aneurysmal controls of the corresponding aortic regions. TIMP3 was detected primarily in intima and media of healthy abdominal aorta and was significantly reduced in AAA specimens from patients **(Figure 5.11 A)**. Interestingly, in the healthy thoracic aorta specimens, TIMP3 was highly expressed in the adventitial region and was decreased in TAA specimens, but TIMP3 levels were markedly increased in the medial layer **(Figure 5.11 A)**. TIMP4 expression was detected more in the abdominal compared to the thoracic aorta specimens in healthy specimens. TIMP4 levels were moderately reduced in AAA specimens, the low level of TIMP4 levels the thoracic aorta remained unchanged in TAA specimens **(Figure 5.11 B)**.

next examined how TIMP3 and TIMP4 protein levels are altered in the aortic specimens from patients with AAA (nonatherosclerotic, non-hypertensive), and TAA (bicuspid aortic valves or Marfan) compared to non-aneurysmal controls of the corresponding aortic regions. TIMP3 was detected primarily in intima and media of control (non-diseased) abdominal aorta, and it was significantly reduced in AAA human specimens in these regions **(Figure 5.11 A)**. Interestingly, in the control thoracic aorta, TIMP3 was also highly expressed in the adventitial region, which was markedly reduced in TAA specimens but increased in the medial layer **(Figure 5.11 A)**. On the other hand, TIMP4 expression remained comparable in TAA and AAA specimens compared to the corresponding non-aneurysmal specimens **(Figure 5.11 B)**.

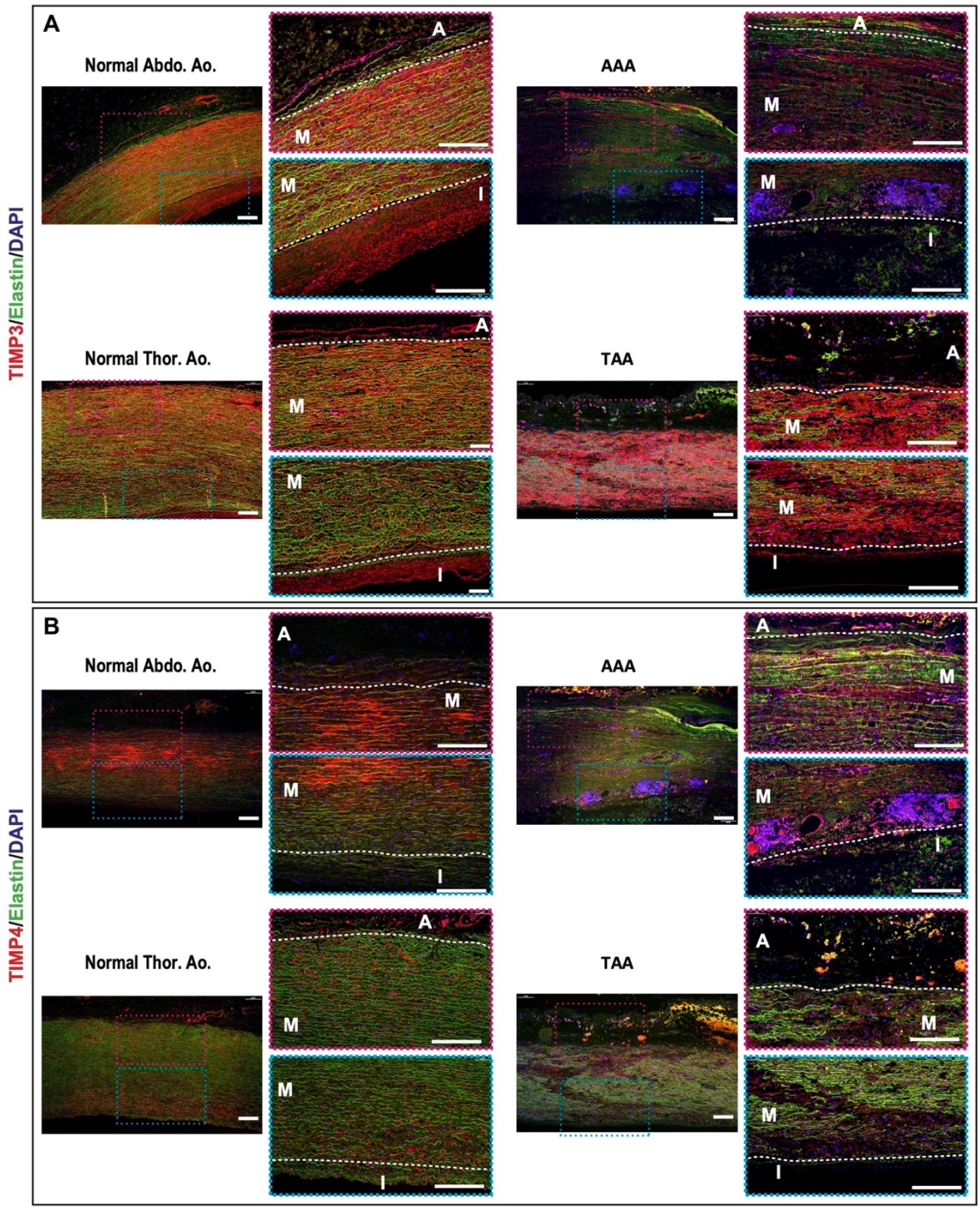

FIGURE 5. 11 DIFFERENTIAL EXPRESSION PATTERN OF TIMP3 & TIMP4 IN HEALTHY & ANEURYSMAL ABDOMINAL AND THORACIC AORTA SPECIMENS FROM PATIENTS.

A) Representative immunofluorescent images for TIMP3 in healthy & aneurysmal aorta specimens. **B)** Representative immunofluorescent images for TIMP4 in healthy & aneurysmal aorta specimens. White dotted line divides the aortic

tunica into 3 different layers of the intima (I), media (M), and adventitia (A). Scale bars: 200 μm. AAA, abdominal aortic aneurysm. TAA, thoracic aortic aneurysm. Timp3/4, tissue inhibitor of metalloproteinase -3/4.

Therefore, since the aortic wall in the thoracic regions is thicker than that in the abdominal aorta, and since TIMP3 is present primarily in the adventitia in the thoracic aorta, but more in the medial aortic wall in the abdominal aorta, loss of TIMP3 would trigger an adventitia-centered response in TAA but a media-centered response in AAA. TIMP4 appears to not be a key player in these processes.

5.4. Discussion

AAA and TAA are distinct pathologies of the aorta with different etiologies and risk factors [348]. We and others have reported on heterogeneity of the aorta [44], as well as region-specific functions of TIMPs [306, 343] and MMPs [133] in aortic aneurysm and other aortic pathologies. In this study we report that loss of TIMP3, but not TIMP4, increases susceptibility to both AAA and TAA, but results in different aortic remodeling and through different mechanisms. Loss of TIMP3 resulted in aberrant proteinase activity and structural remodeling of the aorta in TAA and AAA, but it mediated a distinct pattern of inflammation with a greater presence of inflammatory cells in the subintimal and medial layers in AAA, compared to the adventitial layer in TAA. *Timp3*$^{-/-}$-AAA samples showed marked loss and disarray of VE-cadherin in the intima (of abdominal aorta) indicating impaired intimal barrier integrity, whereas in *Timp3*$^{-/-}$-TAA samples, increased vasa vasorum branching in the adventitia indicates a different path for invasion of inflammatory cells into the aortic vacation. In aorta specimens from patients, TIMP3 was detected in the intima and medial regions of the abdominal aorta, and mainly in the adventitia of the thoracic region. This regional distribution is consistent with the pattern of inflammation in AAA versus

TAA providing evidence for region-dependent function of TIMP3 in the abdominal versus the thoracic aorta.

Both TIMP3 and TIMP4 are potent inhibitors of MMPs [349, 355], therefore the observed changes in gelatinase activity are a combination of increased MMP expression and loss of inhibitory function of these TIMPs in their corresponding groups. However, loss TIMP3 exacerbated the severity of TAA and AAA, whereas loss of TIMP4 did not worsen these pathologies. TIMP4 has been reported to suppress smooth muscle cell migration in a mechanical injury model (in the carotid) [322], and its loss resulted in increased formation of atherosclerotic plaques in the abdominal aorta [343]. However, in the peri-adventitial elastase model of aortic aneurysm, loss TIMP4 appears to be non-consequential, suggesting its lack of contribution to the events that underlie aneurysm formation.

Timp3-deficiency exacerbated SMC loss and transformation and increased proteolysis following AAA and TAA compared to *Timp4*$^{-/-}$ or WT mice. SMC phenotypic switching, from contractile to synthetic state, has been reported in AAA and TAA [299, 356], and can underlie the increase in MMP production by SMCs, which in turn can result in adverse ECM remodeling since MMPs can promote collagen production and fibrotic build up [133, 349]. The disrupted ECM structure along with the heightened inflammation and proteolysis can lead to SMC death as found in the aneurysmal *Timp3*$^{-/-}$ aortas.

Inflammation is a key feature of aortic aneurysm, and we found that loss of TIMP3 exacerbates the inflammation in distinct regions of the aortic wall, primarily in the adventitial layer in TAA, and in the subintimal and medial layer in AAA. Since majority of the inflammatory cells migrate from the blood to the interstitial regions, assessment of the intimal barrier showed severe loss and disarray of VE-cadherin, the predominant endothelial junction protein, in the abdominal aorta of *Timp3*$^{-/-}$-AAA, but not *Timp3*$^{-/-}$-TAA compared to parallel *Timp4*$^{-/-}$ and WT mice. In healthy

aorta, inter-endothelial junctions are well-controlled adhesion molecules to ensure strict management of vascular endothelial permeability. Hydrolysis of the adhesion molecules disrupts the EC barrier and allows transmigration and infiltration of leukocytes into the aortic wall, which is a key pathological process in AAA formation and dilatation [357], as re-establishing the EC lining reduced the progression of experimental AAA [304]. The severe impairment in endothelial intimal barrier in *Timp3*$^{-/-}$-AAA mice is consistent with previous report of similar observation in *Timp3*$^{-/-}$ mice in response to sepsis, attributed to increased proteolytic activities in the absence of TIMP3 [358]. The role of TIMP3 in endothelial proliferation, angiogenesis, and endothelial permeability is controversial with reports on its overexpression being anti-angiogenic *in vitro* [285], but pro-angiogenic *in vivo* [350], and appears to dependent on the tissue, as well as the type and state of pathology. In the heart, overexpression of TIMP3 following ischemic injury increased vascularization and limited infarct expansion [350]. In tumor cells, overexpression of TIMP3 increased endothelial proliferation but decreased VE-cadherin expression resulting in dysfunctional endothelial tubules [359]. In the kidneys, increased microvascular phenotype was observed in mice lacking TIMP3 due to overactivated pericytes and their overexpression of metalloproteinases [360].

Our observation that loss of TIMP3 impaired the intimal barrier in the abdominal aneurysmal aorta but increased vasa vasorum branching in the thoracic aneurysmal aorta highlights the regional heterogeneity of the aorta and the region-specific functions of TIMP3. One explanation for this heterogeneity is the greater number of the lamellar units in the thoracic aorta forming a thicker aortic wall which accommodates formation of extensive vasa vasorum branching that can allow extravasation of the inflammatory cells in the adventitial layer in TAA, which could explain why in vivo deletion of TIMP3 resulted in increased vascularization in the adventitia post-TAA.

TIMP3 inhibits a large spectrum of metalloproteinases including both MMPs and a disintegrin and metalloproteinase (ADAMs) which can cleave endothelial adhesion molecules from the cell surface. Specifically, MMP7, ADAM15 and ADAM17 have been shown to cleave VE-cadherin [299, 314, 361], resulting in increased EC permeability and EC barrier dysfunction. These metalloproteinases could also contribute to the complexity of vascular integrity and remodeling. For instance, MMPs can promote angiogenesis by releasing the pro-angiogenic factor vascular endothelial growth factor (VEGF) through matrix hydrolysis [362, 363], but can also exert anti-angiogenic effects by generating angiogenic inhibitors (i.e. angiostatin and endostatin) [364-366]. Recombinant TIMP3 can repair the adherens junction breakdown induced by VEGF and recapitulate the endothelial barrier function in *vitro* [367]. Therefore, TIMP3 has diverse functions in different cell types and different disease models, and it is critical to recognize that role can not be generalized across the field.

In summary, our study demonstrates that TIMP3 plays a protective role in both AAA and TAA, whereas loss of TIMP4 has minimal impact on the severity of aneurysm formation. Loss of TIMP3 triggers different cellular events in TAA versus AAA, where its impact is primarily in the adventitia compared to the subintimal and medial layers, respectively. This study provides new information on the role of TIMP3 in regional heterogeneity of the aorta in response to aneurysm-inducing stimulus.

CHAPTER 6

DISCUSSION

6.1. Important findings

In the present dissertation, I studied the role of TIMP4 in atherosclerosis and aortic aneurysm as well as the role of TIMP3 in aortic aneurysms. To explore the role of TIMP4 in atherosclerotic plaque deposition, atherogenic mice lacking *Timp4* were fed HFD for 3 or 6 months. We used *in vivo* and *in vitro* approaches to decipher the function of TIMP4 in the regional susceptibility of the aorta to plaque deposition. Additionally, since loss of TIMP4 did not enhance susceptibility to atherosclerosis-associated aortic aneurysm, we investigated if *Timp4*-deficiency reduced susceptibility to aortic aneurysm by subjecting the *Timp4*$^{-/-}$ mice to a different model of aortic aneurysm, peri-adventitial elastase-induced aortic aneurysm model, and used *Timp3*-deficient mice in parallel to compare the impact of TIMP4 loss to the absence of another TIMP in these models. We performed *in vivo* and *in vitro* studies using primary mouse and human aortic cell cultures, to unravel the region-specific functions of these two TIMPs in development of AAA versus TAA. I discuss the main findings from the studies as follows.

6.1.1. Plasma cholesterol levels are not the sole indicator of atherosclerosis risk

Diets with a high content of saturated fat and cholesterol increase plasma lipoprotein levels, primarily LDL, and these alterations result in the transport of cholesterol from LDLs to cells in the arterial walls [368]. Atherosclerosis occurs when the influx of cholesterol into the arterial wall exceeds the amount of cholesterol that is excreted from the tissue [369]. Plasma cholesterol levels are thus considered to be a high-risk factor for atherosclerosis. Our study has shown that compared to *Ldlr*$^{-/-}$-HFD mice, *Ldlr*$^{-/-}$*/Timp4*$^{-/-}$-HFD mice exhibit lower increases in total plasma triglyceride and cholesterol levels which maintain higher HDL levels and lower VLDL levels. These data reveal

that increased plaque density in the abdominal aorta of *Ldlr*$^{-/-}$/*Timp4*$^{-/-}$ mice is not due to a higher plasma cholesterol level. This is consistent with reports from human biopsies published in the 1960s which showed that serum cholesterol levels did not always correlate with the amount and severity of atherosclerosis in patients [332, 333], a concept that has not received sufficient attention since then [335]. Our findings thus suggest that TIMP4 may be a key player in the divergence between atherosclerosis and cholesterol levels.

6.1.2. TIMP4 protects abdominal aorta SMCs from transforming to macrophage-like cells in hyperlipidemic conditions

VSMC plays a critical role in all stages of atherosclerosis, and VSMC-derived cells are a major source of advanced plaque cells [337], mainly composed of macrophage-like cells with a phagocytic phenotype that can become foam cells, whose necrosis is characterized by increased plaque vulnerability. VSMCs that have undergone phenotypic switching metabolize lipids, in part by increased levels of the cholesterol uptake and decreased the levels of the cholesterol efflux transporter, leading to an increased propensity to transform into foam cells. We found a higher population of macrophage-like SMCs in *Ldlr*$^{-/-}$/*Timp4*$^{-/-}$ mice following high fat feeding. This phenotype switching has been identified *in vitro* in cultured VSMC [320], *in vivo* in experimental mouse model [319], in coronary plaques in human [19], and confirmed by lineage-tracing studies [319, 338, 370]. In fact, the hypothesis that a subset of the foam cells in atherosclerotic plaques are derived from VSMCs was proposed as early as 1968 [371]; however, the mechanism underlying SMC transdifferentiation is not fully understood yet.

We found that after *in vitro* oxidized LDL treatment, ABCA1 protein expression was significantly lower in the abdominal aortic SMC of *Ldlr*$^{-/-}$/*Timp4*$^{-/-}$ mice than in the *Ldlr*$^{-/-}$ SMC,

whereas no significant changes were observed in the macrophage or thoracic aortic SMC, indicating that *Timp4* deletion in the abdominal aorta is associated with decreased ABCA1 protein levels. However, ABCA1 mRNA levels in SMC did not show a decrease, suggesting that the reduced ABCA1 protein levels may be due to post-transcriptional regulation, which has been previously reported [372]. Reduced ABCA1 protein decreases cholesterol efflux from SMCs, thus leading to the transition of SMCs into foam cells as well as lipid accumulation within the aortic wall. This is consistent with data from SMCs in human coronary artery, where ABCA1 was reduced in the sub-intimal SMCs compared with myeloid lineage cells [19]. ABCA1 expression in arterial intima SMC was also diminished after *in vitro* loading with excess cholesterol [373]. Overall, TIMP4 protects the abdominal aortic SMCs from transforming to macrophage-like cells under hyperlipidemic conditions, revealing a novel function of TIMP4 that is particularly critical in the progression of atherosclerosis.

6.1.3. TIMP4 is one of the factors underlying the regional heterogeneity of the aorta

Accumulating evidence suggests variations exist between the thoracic and abdominal aorta, underlying the regional heterogeneity of the aorta [5, 44, 374]. Regional heterogeneity of the aorta is manifested by the unique response of the distinct aortic structures above and below the diaphragm to biochemical, molecular as well as genetic factors [374]. Neural crest cell precursors of thoracic aortic VSMCs and mesodermal progenitors of abdominal aortic VSMCs exhibit distinct responses to cytokines and growth factors [44]. For instance, SMC-specific blockade of TGFβ had a negligible effect on experimental AAA progression yet accelerated the TAA pathology [375]. Compared to the thoracic aorta, the abdominal aorta has thinner lamellar units (composed of VSMCs and elastin) and avascular nature, impairing its resistance to the flow changes and media

degradation and thus increasing the risk of aneurysm as well as atherosclerosis formation in this region [44, 48, 376, 377].

My study determined that *Timp4*-deficiency increased the susceptibility of the abdominal aorta to atherosclerotic plaque deposition. TIMP4, unlike other TIMPs, is expressed at a much higher level in the abdominal aorta than in the thoracic aorta, which may indicate that the presence of this TIMP in the abdominal aorta is more critical (compared to other aortic regions) and therefore its loss selectively increases the susceptibility of the abdominal aorta to excess plaque deposition. Moreover, TIMP4 expression was significantly increased in abdominal aortic VSMC compared to that in VSMC from thoracic aorta, suggesting that the special importance of TIMP4 in the abdominal aorta tissue could mainly be reflected in its effect on VSMC function. We further demonstrate that absence of TIMP4 increases the susceptibility of the abdominal aorta SMCs (but not thoracic SMCs) to trans-differentiation to macrophage-like cells and foam cells in hyperlipidemic conditions. Thus, TIMP4 is one of the factors contributing to regional heterogeneity in the aorta, and its role is more important in the abdominal aorta, especially in its SMCs, compared to other aortic regions.

6.1.4. TIMP3 maintains aortic EC barrier integrity by preserving adhesion molecules in aortic aneurysm

In healthy aorta, inter-EC junctions are well-controlled adhesion molecules such as VE-cadherin to ensure strict management of vascular endothelial permeability. Disruption of the endothelial cell barrier by hydrolysis of the adhesion molecules allows transmigration and infiltration of leukocytes into the aortic wall, which is a critical pathological process AAA formation and dilatation, as re-establishing the EC lining reduced the progression of experimental AAA [304]. We found *Timp3*$^{-}$

$^{/-}$ mice following AAA had significantly higher Evans blue dye-labeled albumin leaks and lower VE-cadherin expression in the abdominal aneurysmal aorta compared to WT mice, it suggests TIMP3 deficiency in *Timp3*$^{-/-}$ mice was associated with significant EC barrier dysfunction. This was further demonstrated by an *in vitro* EC permeability assay that knocking down Timp3 (by siRNA) increased the permeability of elastase-treated EC monolayer. Mechanistically, compromised EC barrier associated with TIMP3 deficiency could be mediated by loss of TIMP3-dependent MMP inhibition, resulting in cleavage of EC surface VE-cadherin and disruption of EC junctions.

Adjacent endothelial cells are connected by two types of intercellular junctions: adherens junctions and tight junctions. Endothelial junction integrity is regulated by proteins that form adherens junctions and tight junctions [11]. VE-cadherin is the main component of endothelial junctions. VE-cadherin is composed of extracellular cadherin motifs, a transmembrane domain, and an intracellular domain that mediates interactions with β-catenin, p120-catenin, and γ-catenin. β-catenin and γ-catenin in turn connect to actin-binding α-catenin and other proteins [11]. TIMP3 inhibits a large spectrum of metalloproteinases including both MMPs and ADAMs which can cleave endothelial adhesion molecules from the cell surface. Specifically, MMP7, MMP9, ADAM15 and ADAM17 have been shown to actively cleave VE-cadherin [299, 314, 361, 378], resulting in EC barrier dysfunction via increased EC permeability. Additionally, the intracellular complex of VE-cadherin and catenin is essential for junctional stability. TIMP3 was reported to shelter the cadherin/β-catenin complex from proteolytic processing in hepatocytes and inhibit apoptosis after hepatic IRI (ischemia/reperfusion injury) [379]. It also functions to alter beta-catenin signaling [380]. Thus, TIMP3 can preserve adhesion molecules or adhesion molecule/catenin complex function by inhibiting the proteolytic activity of MMPs/ADAMs on EC adhesion molecules, thereby maintaining EC barrier function and even affecting EC fate.

6.1.5. TIMP3 has a region-specific function in the aorta

Our observation that loss of TIMP3 impaired the intimal barrier in the abdominal aneurysmal aorta but increased vasa vasorum branching in the thoracic aneurysmal aorta highlights the regional heterogeneity of the aorta and the region-specific functions of TIMP3. One explanation for this heterogeneity is the greater number of the lamellar units in the thoracic aorta forming a thicker aortic wall which accommodates formation of extensive vasa vasorum branching that can allow extravasation of the inflammatory cells in the adventitial layer in TAA, which could explain why *in vivo* deletion of TIMP3 resulted in increased vascularization in the adventitia post-TAA. Loss of TIMP3 triggers different cellular events in TAA versus AAA, where its impact is primarily in the adventitia compared to the subintimal and medial layers, respectively. This study provides new information on the role of TIMP3 in regional heterogeneity of the aorta in response to aneurysm-inducing stimulus.

6.2. Clinical significance of abdominal aortic atherosclerosis

As coronary artery disease (CAD) is more strongly associated with plaque in the ascending aorta and arch, atherosclerosis studies may be subject to selection bias and neglect the clinical significance of abdominal aortic atherosclerosis. Current detection of abdominal aortic atherosclerosis in patients aims to improve the predictive value of risk of future cardiovascular events. The prevalence of abdominal aortic plaque was found to be higher in patients with CAD than in those without CAD by ultrasonography measurements and thus could be an independent factor related to the presence and severity of CAD [381]. Also, plaque formation in the infrarenal abdominal aorta in human is associated with aortic enlargement and reduced media thickness.

These chronic changes may predispose the abdominal aorta to subsequent aneurysmal dilation [382]. Atherosclerotic plaque burden in the abdominal aorta can also lead to an increased risk of non-fatal extracardiac events, such as intermittent claudication or signs of distal embolization [383-385]. Penetrating atherosclerotic ulcer of the abdominal aorta, is a rare entity but has a high risk of life-threatening rupture [386, 387]. Despite all these, clinical studies on the abdominal aortic atherosclerosis are limited because screening for abdominal aortic plaque is time-consuming and impractical [388]. Therefore, animal research on multi-site atherosclerosis should be encouraged and strengthened to lay the foundation for various clinical risk predictions of atherosclerotic complications [389].

6.3. Perspectives of developing TIMP3 or TIMP4 mutants as potential therapeutic strategies for vascular diseases

Although TIMPs have attracted a lot of attention as endogenous inhibitors of MMPs, the drug development of TIMPs per se as region-specific inhibitors of MMPs is an unexplored area. The progress of broadly effective small molecule inhibitors targeting MMPs has been halted by failed clinical trials and unknown unavoidable side effects; therefore, engineering of endogenous inhibitors should be proposed as an alternative approach while the next generation of more specific small molecule MMP inhibitors is developed [390, 391].

Ideally, increasing TIMP4 expression or preventing its downregulation in specific regions such as the abdominal aorta could improve atherosclerotic plaque deposition and reduce ischemic peripheral disease due to abdominal aortic stenosis. The use of some gene therapies, for example, intervening in the effects of TIMP deficiency at a specific region by regional placement of the endostents [392, 393] can improve efficacy and narrow the potential side effects. The use of

electroporation-mediated intramuscular or intradermal injection of TIMP4 expression plasmid [394] may inhibit plaque accumulated in abdominal aorta due to lack of TIMP4. In addition, delivery of the TIMP to specific aortic sites will not reverse the dilation of the aortic wall but may prevent the progression of the dilation. For example, cellular or viral-based site-specific delivery of TIMP3 could be used to intervene in further progression of aneurysms at different regions. Last but not least, an in-depth and comprehensive understanding of the underlying mechanisms of TIMPs in regional heterogeneous vascular diseases is a prerequisite for such gene therapy.

CHAPTER 7

LIMITATIONS AND FUTURE DIRECTIONS

7.1. Limitations

7.1.1. Limitations of mouse models for understanding human atherosclerosis

Most current understanding of the mechanisms underlying atherosclerosis comes from studies in mouse models. Apolipoprotein E (*ApoE*) or low-density lipoprotein receptor (*Ldlr*) gene knockout mice are the most commonly used murine models of atherosclerosis. They develop significant atherosclerosis with some vascular characteristics like those in humans [395, 396]. Double knockouts and transgenics have also been developed to explore the effects of certain genes on plaque development and treatment strategies. However, the relevance of mouse models for human atherosclerotic disease remains elusive, leading to limitations in the study of atherosclerosis [397]. First, the plaque morphology in mice differs from that in humans, including the plaque burden, plaque thickness, and the amount of the vessel walls eroded by plaque as well as significant differences in the relative composition of plaques [398]. These may also account for the acute events (e.g., luminal thrombosis and evident plaque rupture) rarely observed in the mouse model. Second, clinical disease manifestations such as coronary artery disease or ischemic stroke in mice are rare or absent. Third, it is controversial whether a complete knockout of a gene in mice can correspond to a mutation with altered expression in humans [399]. Finally, gene redundancy at the pathway level also complicates the interpretation of results in animal models [399, 400]. Nonetheless, mice have many advantages in studying atherosclerosis, and studies in mice will continue to advance the understanding of its mechanisms. In addition, focusing on pathogenic pathways and pathological mechanisms rather than individual genes may be a more fruitful way to translate information from animal models into human studies.

7.1.2. Experimental TAA and AAA model

The AAA and TAA models used in the current study are the most commonly used models that well mimic the morphology of human aneurysms, it is also the best choice for studying the heterogeneity of aneurysms in different regions of the aorta. However, the model still has limitations. There is limited evidence that aneurysms in this model continue to enlarge in the long term, and they tend to plateau over time in the absence of sustained injury [144]. This is not conducive to studying advanced AAA pathology that occurs in patients. Studies have demonstrated the application of chemicals in combination with periaortic elastase, such as TGFβ monoclonal antibodies or BAPN (β-aminopropionitrile), can establish a model of chronic advanced AAA [144, 146]. This BAPN + elastase-induced aneurysm has a diameter progression that can last up to 100 days and is accompanied by thrombosis and spontaneous rupture, better mimicking chronic progression of human AAA and promoting a comprehensive undertraining of the pathophysiology of aortic aneurysm [144].

7.2. Future Directions

7.2.1. To further validate the cell-specific function of TIMP4 in vascular disease

Timp4$^{-/-}$ mice harbor a global deficiency which complicates exploration of its cell-specific functions. Next, we can generate the *Timp4*$^{flox/flox}$ mice which will be cross-bred with mice expressing cell-specific Cre-recombinase to induce *Timp4* deletion in SMC or macrophage or even EC as we have described before [299]. The role of TIMP4 in atherosclerosis can then be further validated using SMC- or macrophage- or EC-specific *Timp4* knockout mice. Although TIMP4 is a

soluble and diffusible protein secreted into plasma or extracellular environment, it shows the highly selective pattern of tissue localization, being expressed predominately in cell-surface of the heart, brain, kidney, and aorta [51, 401]. TIMP4 has also been reported to have an intracellular function, tumor growth is suppressed by the internalization of exogenous recombinant TIMP4 [394]. Therefore, it is of interest to further explore the cell-specific functions of TIMP4 in atherosclerosis.

7.2.2. To further explore the underlying mechanism by which *Timp4*-deficiency impedes Ang II induced-AAA

We found Ang II-induced AAA was alleviated in atherogenic mice lacking TIMP4 after HFD feeding but did not investigate the underlying mechanisms by which *Timp4*-deficiency impeded Ang II induced-AAA. Future studies could be conducted by addressing the following objectives: i) To determine whether TIMP4 loss similarly affects the blood lipid levels in atherosclerotic mouse after Ang II perfusion; ii) To determine whether Ang II intervention affects the expression profiles of TIMP4 in abdominal aorta and thoracic aorta; iii) To determine the impact of TIMP4 on VSMC behaviors (migration, proliferation and apoptosis) and EC functions (production of reactive oxygen species and inflammatory cell infiltration) in response to Ang II treatment *in vivo*; iv) To determine the impact of TIMP4 on the Ang II-mediated adventitial fibrosis in abdominal aorta and thoracic aorta.

REFERENCES

Uncategorized References

1. Roth, G.A., et al., *Global Burden of Cardiovascular Diseases and Risk Factors, 1990-2019: Update From the GBD 2019 Study.* J Am Coll Cardiol, 2020. **76**(25): p. 2982-3021.
2. Golledge, J., et al., *Lack of an effective drug therapy for abdominal aortic aneurysm.* J Intern Med, 2020. **288**(1): p. 6-22.
3. Lindeman, J.H. and J.S. Matsumura, *Pharmacologic Management of Aneurysms.* Circ Res, 2019. **124**(4): p. 631-646.
4. Reimann, C., et al., *Molecular imaging of the extracellular matrix in the context of atherosclerosis.* Adv Drug Deliv Rev, 2017. **113**: p. 49-60.
5. Jana, S., et al., *Extracellular matrix, regional heterogeneity of the aorta, and aortic aneurysm.* Exp Mol Med, 2019. **51**(12): p. 1-15.
6. Zaltsman, A.B., S.J. George, and A.C. Newby, *Increased secretion of tissue inhibitors of metalloproteinases 1 and 2 from the aortas of cholesterol fed rabbits partially counterbalances increased metalloproteinase activity.* Arterioscler Thromb Vasc Biol, 1999. **19**(7): p. 1700-7.
7. Fabunmi, R.P., et al., *Expression of tissue inhibitor of metalloproteinases-3 in human atheroma and regulation in lesion-associated cells: a potential protective mechanism in plaque stability.* Circ Res, 1998. **83**(3): p. 270-8.
8. Goodall, S., et al., *Ubiquitous elevation of matrix metalloproteinase-2 expression in the vasculature of patients with abdominal aneurysms.* Circulation, 2001. **104**(3): p. 304-9.
9. Allaire, E., et al., *Local overexpression of TIMP-1 prevents aortic aneurysm degeneration and rupture in a rat model.* J Clin Invest, 1998. **102**(7): p. 1413-20.
10. Komarova, Y. and A.B. Malik, *Regulation of endothelial permeability via paracellular and transcellular transport pathways.* Annu Rev Physiol, 2010. **72**: p. 463-93.
11. Claesson-Welsh, L., E. Dejana, and D.M. McDonald, *Permeability of the Endothelial Barrier: Identifying and Reconciling Controversies.* Trends Mol Med, 2021. **27**(4): p. 314-331.
12. Pober, J.S. and W.C. Sessa, *Evolving functions of endothelial cells in inflammation.* Nat Rev Immunol, 2007. **7**(10): p. 803-15.
13. Sutton, N.R., A. Baek, and D.J. Pinsky, *Endothelial Cells and Inflammation*, in *Encyclopedia of Medical Immunology: Autoimmune Diseases*, I.R. Mackay, et al., Editors. 2014, Springer New York: New York, NY. p. 367-381.
14. Thompson, M.M., et al., *Angiogenesis in abdominal aortic aneurysms.* Eur J Vasc Endovasc Surg, 1996. **11**(4): p. 464-9.
15. Choke, E., et al., *Abdominal aortic aneurysm rupture is associated with increased medial neovascularization and overexpression of proangiogenic cytokines.* Arterioscler Thromb Vasc Biol, 2006. **26**(9): p. 2077-82.
16. Kessler, K., et al., *Angiogenesis and remodelling in human thoracic aortic aneurysms.* Cardiovasc Res, 2014. **104**(1): p. 147-59.
17. Camaré, C., et al., *Angiogenesis in the atherosclerotic plaque.* Redox Biol, 2017. **12**: p. 18-34.
18. Shi, N., X. Mei, and S.Y. Chen, *Smooth Muscle Cells in Vascular Remodeling.* Arterioscler Thromb Vasc Biol, 2019. **39**(12): p. e247-e252.
19. Allahverdian, S., et al., *Contribution of intimal smooth muscle cells to cholesterol accumulation and macrophage-like cells in human atherosclerosis.* Circulation, 2014. **129**(15): p. 1551-9.
20. Ravikanth, M., et al., *Heterogenecity of fibroblasts.* J Oral Maxillofac Pathol, 2011. **15**(2): p. 247-50.
21. Shi, Y., et al., *Adventitial myofibroblasts contribute to neointimal formation in injured porcine coronary arteries.* Circulation, 1996. **94**(7): p. 1655-64.
22. Forte, A., et al., *Role of myofibroblasts in vascular remodelling: focus on restenosis and aneurysm.* Cardiovasc Res, 2010. **88**(3): p. 395-405.
23. Gibb, A.A., M.P. Lazaropoulos, and J.W. Elrod, *Myofibroblasts and Fibrosis: Mitochondrial and Metabolic Control of Cellular Differentiation.* Circ Res, 2020. **127**(3): p. 427-447.

24. Kuwabara, J.T. and M.D. Tallquist, *Tracking Adventitial Fibroblast Contribution to Disease: A Review of Current Methods to Identify Resident Fibroblasts.* Arterioscler Thromb Vasc Biol, 2017. **37**(9): p. 1598-1607.
25. Li, B.L., et al., *Single-Cell Transcriptome Profiles Reveal Fibrocytes as Potential Targets of Cell Therapies for Abdominal Aortic Aneurysm.* Frontiers in Cardiovascular Medicine, 2021. **8**.
26. Di Carlo, S.E. and L. Peduto, *The perivascular origin of pathological fibroblasts.* J Clin Invest, 2018. **128**(1): p. 54-63.
27. Jiang, L., et al., *Different Roles of Stem/Progenitor Cells in Vascular Remodeling.* Antioxid Redox Signal, 2021. **35**(3): p. 192-203.
28. Zhang, L., et al., *Role of Resident Stem Cells in Vessel Formation and Arteriosclerosis.* Circulation Research, 2018. **122**(11): p. 1608-1624.
29. Heinz, A., *Elastic fibers during aging and disease.* Ageing Res Rev, 2021. **66**: p. 101255.
30. Yanagisawa, H. and J. Wagenseil, *Elastic fibers and biomechanics of the aorta: Insights from mouse studies.* Matrix Biology, 2020. **85-86**: p. 160-172.
31. Theocharis, A.D., et al., *Extracellular matrix structure.* Adv Drug Deliv Rev, 2016. **97**: p. 4-27.
32. Manou, D., et al., *The Complex Interplay Between Extracellular Matrix and Cells in Tissues.* Methods Mol Biol, 2019. **1952**: p. 1-20.
33. Clyman, R.I., K.A. McDonald, and R.H. Kramer, *Integrin receptors on aortic smooth muscle cells mediate adhesion to fibronectin, laminin, and collagen.* Circ Res, 1990. **67**(1): p. 175-86.
34. Li, D.Y., et al., *Elastin is an essential determinant of arterial morphogenesis.* Nature, 1998. **393**(6682): p. 276-280.
35. Mochizuki, S., B. Brassart, and A. Hinek, *Signaling pathways transduced through the elastin receptor facilitate proliferation of arterial smooth muscle cells.* Journal of Biological Chemistry, 2002. **277**(47): p. 44854-44863.
36. Pozzi, A., et al., *Integrin alpha1beta1 mediates a unique collagen-dependent proliferation pathway in vivo.* J Cell Biol, 1998. **142**(2): p. 587-94.
37. Patil, M.S., S.P. Cartland, and M.M. Kavurma, *TRAIL signals, extracellular matrix and vessel remodelling.* Vasc Biol, 2020. **2**(1): p. R73-R84.
38. To, W.S. and K.S. Midwood, *Plasma and cellular fibronectin: distinct and independent functions during tissue repair.* Fibrogenesis Tissue Repair, 2011. **4**: p. 21.
39. Rachev, A., S. Greenwald, and T. Shazly, *Are geometrical and structural variations along the length of the aorta governed by a principle of "optimal mechanical operation"?* J Biomech Eng, 2013. **135**(8): p. 81006.
40. Wolinsky, H., *Comparison of medial growth of human thoracic and abdominal aortas.* Circ Res, 1970. **27**(4): p. 531-8.
41. Wolinsky, H. and S. Glagov, *Comparison of abdominal and thoracic aortic medial structure in mammals. Deviation of man from the usual pattern.* Circ Res, 1969. **25**(6): p. 677-86.
42. Cheng, J.K. and J.E. Wagenseil, *Extracellular matrix and the mechanics of large artery development.* Biomech Model Mechanobiol, 2012. **11**(8): p. 1169-86.
43. Wolinsky, H. and S. Glagov, *Nature of species differences in the medial distribution of aortic vasa vasorum in mammals.* Circ Res, 1967. **20**(4): p. 409-21.
44. Ruddy, J.M., et al., *Regional heterogeneity within the aorta: relevance to aneurysm disease.* J Thorac Cardiovasc Surg, 2008. **136**(5): p. 1123-30.
45. Gadson, P.F., Jr., et al., *Differential response of mesoderm- and neural crest-derived smooth muscle to TGF-beta1: regulation of c-myb and alpha1 (I) procollagen genes.* Exp Cell Res, 1997. **230**(2): p. 169-80.
46. Thieszen, S.L., et al., *Embryonic lineage of vascular smooth muscle cells determines responses to collagen matrices and integrin receptor expression.* Exp Cell Res, 1996. **227**(1): p. 135-45.
47. Majesky, M.W., *Developmental basis of vascular smooth muscle diversity.* Arterioscler Thromb Vasc Biol, 2007. **27**(6): p. 1248-58.

48. Strong, J.P., et al., *Prevalence and extent of atherosclerosis in adolescents and young adults: implications for prevention from the Pathobiological Determinants of Atherosclerosis in Youth Study.* JAMA, 1999. **281**(8): p. 727-35.
49. Brew, K. and H. Nagase, *The tissue inhibitors of metalloproteinases (TIMPs): an ancient family with structural and functional diversity.* Biochim Biophys Acta, 2010. **1803**(1): p. 55-71.
50. Docherty, A.J., et al., *Sequence of human tissue inhibitor of metalloproteinases and its identity to erythroid-potentiating activity.* Nature, 1985. **318**(6041): p. 66-9.
51. Murphy, G., *Tissue inhibitors of metalloproteinases.* Genome Biology, 2011. **12**(11).
52. Lotz, M. and P.A. Guerne, *Interleukin-6 induces the synthesis of tissue inhibitor of metalloproteinases-1/erythroid potentiating activity (TIMP-1/EPA).* J Biol Chem, 1991. **266**(4): p. 2017-20.
53. Mann, J.S., et al., *Hormonal regulation of matrix metalloproteinase inhibitors in rat granulosa cells and ovaries.* Endocrinology, 1991. **128**(4): p. 1825-32.
54. Weber, B.H., et al., *Mutations in the tissue inhibitor of metalloproteinases-3 (TIMP3) in patients with Sorsby's fundus dystrophy.* Nat Genet, 1994. **8**(4): p. 352-6.
55. Lee, M.H., S. Atkinson, and G. Murphy, *Identification of the extracellular matrix (ECM) binding motifs of tissue inhibitor of metalloproteinases (TIMP)-3 and effective transfer to TIMP-1.* J Biol Chem, 2007. **282**(9): p. 6887-98.
56. Itoh, Y., *Membrane-type matrix metalloproteinases: Their functions and regulations.* Matrix Biol, 2015. **44-46**: p. 207-23.
57. Nagase, H., *Cell surface activation of progelatinase A (proMMP-2) and cell migration.* Cell Res, 1998. **8**(3): p. 179-86.
58. Liu, X.W., et al., *Tissue inhibitor of metalloproteinase-1 protects human breast epithelial cells against intrinsic apoptotic cell death via the focal adhesion kinase/phosphatidylinositol 3-kinase and MAPK signaling pathway.* J Biol Chem, 2003. **278**(41): p. 40364-72.
59. Jung, K.K., et al., *Identification of CD63 as a tissue inhibitor of metalloproteinase-1 interacting cell surface protein.* Embo j, 2006. **25**(17): p. 3934-42.
60. Seo, D.W., et al., *TIMP-2 mediated inhibition of angiogenesis: an MMP-independent mechanism.* Cell, 2003. **114**(2): p. 171-80.
61. Brew, K., *Reflections on the evolution of the vertebrate tissue inhibitors of metalloproteinases.* Faseb j, 2019. **33**(1): p. 71-87.
62. Vanhoutte, D. and S. Heymans, *TIMPs and cardiac remodeling: 'Embracing the MMP-independent-side of the family'.* J Mol Cell Cardiol, 2010. **48**(3): p. 445-53.
63. Chirco, R., et al., *Novel functions of TIMPs in cell signaling.* Cancer Metastasis Rev, 2006. **25**(1): p. 99-113.
64. Stetler-Stevenson, W.G., *Tissue inhibitors of metalloproteinases in cell signaling: metalloproteinase-independent biological activities.* Sci Signal, 2008. **1**(27): p. re6.
65. Mimuro, J., R.R. Schleef, and D.J. Loskutoff, *The Extracellular-Matrix (Ecm) of Cultured Bovine Aortic Endothelial-Cells (Baes) Contains Functionally Active Type-I Plasminogen-Activator Inhibitor (Pai-1).* Thrombosis and Haemostasis, 1987. **58**(1): p. 445-445.
66. Knudsen, B.S., P.C. Harpel, and R.L. Nachman, *Plasminogen-Activator Inhibitor Is Associated with the Extracellular-Matrix of Cultured Bovine Smooth-Muscle Cells.* Journal of Clinical Investigation, 1987. **80**(4): p. 1082-1089.
67. Lijnen, H.R., *Plasmin and matrix metalloproteinases in vascular remodeling.* Thromb Haemost, 2001. **86**(1): p. 324-33.
68. Wang, X. and R.A. Khalil, *Matrix Metalloproteinases, Vascular Remodeling, and Vascular Disease.* Adv Pharmacol, 2018. **81**: p. 241-330.
69. Raffetto, J.D. and R.A. Khalil, *Matrix metalloproteinases and their inhibitors in vascular remodeling and vascular disease.* Biochemical Pharmacology, 2008. **75**(2): p. 346-359.
70. Sternlicht, M.D. and Z. Werb, *How matrix metalloproteinases regulate cell behavior.* Annual Review of Cell and Developmental Biology, 2001. **17**: p. 463-516.
71. Lee, H.S., et al., *Complete regression of coronary atherosclerosis.* Eur Heart J, 2020. **41**(2): p. 332.

72. Barrett, T.J., et al., *Apolipoprotein AI) Promotes Atherosclerosis Regression in Diabetic Mice by Suppressing Myelopoiesis and Plaque Inflammation.* Circulation, 2019. **140**(14): p. 1170-1184.
73. Ward, N.C., G.F. Watts, and R.H. Eckel, *Statin Toxicity.* Circ Res, 2019. **124**(2): p. 328-350.
74. Tsimikas, S., et al., *Statin therapy increases lipoprotein(a) levels.* Eur Heart J, 2020. **41**(24): p. 2275-2284.
75. Ridker, P.M., et al., *Antiinflammatory Therapy with Canakinumab for Atherosclerotic Disease.* N Engl J Med, 2017. **377**(12): p. 1119-1131.
76. Engelen, S.E., et al., *Therapeutic strategies targeting inflammation and immunity in atherosclerosis: how to proceed?* Nat Rev Cardiol, 2022. **19**(8): p. 522-542.
77. Reidy, M.A. and D.E. Bowyer, *Scanning electron microscopy of arteries. The morphology of aortic endothelium in haemodynamically stressed areas associated with branches.* Atherosclerosis, 1977. **26**(2): p. 181-94.
78. Gimbrone, M.A., Jr., et al., *Endothelial dysfunction, hemodynamic forces, and atherogenesis.* Ann N Y Acad Sci, 2000. **902**: p. 230-9; discussion 239-40.
79. Nordestgaard, B.G. and A. Varbo, *Triglycerides and cardiovascular disease.* The Lancet, 2014. **384**(9943): p. 626-635.
80. Bornfeldt, K.E., *The Remnant Lipoprotein Hypothesis of Diabetes-Associated Cardiovascular Disease.* Arterioscler Thromb Vasc Biol, 2022. **42**(7): p. 819-830.
81. Tsimikas, S., *A Test in Context: Lipoprotein(a): Diagnosis, Prognosis, Controversies, and Emerging Therapies.* J Am Coll Cardiol, 2017. **69**(6): p. 692-711.
82. Huang, L., et al., *SR-B1 drives endothelial cell LDL transcytosis via DOCK4 to promote atherosclerosis.* Nature, 2019. **569**(7757): p. 565-569.
83. Kraehling, J.R., et al., *Genome-wide RNAi screen reveals ALK1 mediates LDL uptake and transcytosis in endothelial cells.* Nature Communications, 2016. **7**.
84. Ramirez, C.M., et al., *Caveolin-1 Regulates Atherogenesis by Attenuating Low-Density Lipoprotein Transcytosis and Vascular Inflammation Independently of Endothelial Nitric Oxide Synthase Activation.* Circulation, 2019. **140**(3): p. 225-239.
85. Skalen, K., et al., *Subendothelial retention of atherogenic lipoproteins in early atherosclerosis.* Nature, 2002. **417**(6890): p. 750-754.
86. Boren, J., et al., *Identification of the principal proteoglycan-binding site in LDL - A single-point mutation in apo-B100 severely affects proteoglycan interaction without affecting LDL receptor binding.* Journal of Clinical Investigation, 1998. **101**(12): p. 2658-2664.
87. Moore, K.J., F.J. Sheedy, and E.A. Fisher, *Macrophages in atherosclerosis: a dynamic balance.* Nat Rev Immunol, 2013. **13**(10): p. 709-21.
88. Wang, Y., et al., *Smooth Muscle Cells Contribute the Majority of Foam Cells in ApoE (Apolipoprotein E)-Deficient Mouse Atherosclerosis.* Arterioscler Thromb Vasc Biol, 2019. **39**(5): p. 876-887.
89. Speer, M.Y., et al., *Smooth Muscle Cells Give Rise to Osteochondrogenic Precursors and Chondrocytes in Calcifying Arteries.* Circulation Research, 2009. **104**(6): p. 733-U65.
90. Gistera, A. and G.K. Hansson, *The immunology of atherosclerosis.* Nature Reviews Nephrology, 2017. **13**(6).
91. Ouimet, M., T.J. Barrett, and E.A. Fisher, *HDL and Reverse Cholesterol Transport Basic Mechanisms and Their Roles in Vascular Health and Disease.* Circulation Research, 2019. **124**(10): p. 1505-1518.
92. Shen, W.J., S. Azhar, and F.B. Kraemer, *SR-B1: A Unique Multifunctional Receptor for Cholesterol Influx and Efflux.* Annual Review of Physiology, Vol 80, 2018. **80**: p. 95-116.
93. Westerterp, M., et al., *Deficiency of ATP-binding cassette transporters A1 and G1 in macrophages increases inflammation and accelerates atherosclerosis in mice.* Circ Res, 2013. **112**(11): p. 1456-65.
94. Van Eck, M., et al., *Leukocyte ABCA1 controls susceptibility to atherosclerosis and macrophage recruitment into tissues.* Proceedings of the National Academy of Sciences of the United States of America, 2002. **99**(9): p. 6298-6303.
95. Yvan-Charvet, L., et al., *Combined deficiency of ABCA1 and ABCG1 promotes foam cell accumulation and accelerates atherosclerosis in mice.* J Clin Invest, 2007. **117**(12): p. 3900-8.

96. Zhang, Y.Z., et al., *Hepatic expression of scavenger receptor class B type I (SR-BI) is a positive regulator of macrophage reverse cholesterol transport in vivo.* Journal of Clinical Investigation, 2005. **115**(10): p. 2870-2874.
97. Zhang, W.W., et al., *Inactivation of macrophage scavenger receptor class B type I promotes atherosclerotic lesion development in apolipoprotein E-deficient mice.* Circulation, 2003. **108**(18): p. 2258-2263.
98. Kim, J.B., et al., *Risk of rupture or dissection in descending thoracic aortic aneurysm.* Circulation, 2015. **132**(17): p. 1620-9.
99. Lederle, F.A., et al., *Rupture rate of large abdominal aortic aneurysms in patients refusing or unfit for elective repair.* JAMA, 2002. **287**(22): p. 2968-72.
100. Golledge, J., *Abdominal aortic aneurysm: update on pathogenesis and medical treatments.* Nat Rev Cardiol, 2019. **16**(4): p. 225-242.
101. Golledge, J. and P.E. Norman, *Current status of medical management for abdominal aortic aneurysm.* Atherosclerosis, 2011. **217**(1): p. 57-63.
102. Ghansah, J.N. and J.T. Murphy, *Complications of major aortic and lower extremity vascular surgery.* Semin Cardiothorac Vasc Anesth, 2004. **8**(4): p. 335-61.
103. Hoel, A.W., *Aneurysmal disease: thoracic aorta.* Surg Clin North Am, 2013. **93**(4): p. 893-910, ix.
104. Lederle, F.A., et al., *Immediate repair compared with surveillance of small abdominal aortic aneurysms.* N Engl J Med, 2002. **346**(19): p. 1437-44.
105. Klink, A., et al., *Diagnostic and therapeutic strategies for small abdominal aortic aneurysms.* Nat Rev Cardiol, 2011. **8**(6): p. 338-47.
106. Sughimoto, K., et al., *Effects of arterial blood flow on walls of the abdominal aorta: distributions of wall shear stress and oscillatory shear index determined by phase-contrast magnetic resonance imaging.* Heart and Vessels, 2016. **31**(7): p. 1168-1175.
107. Petriceks, A.H., J.C. Olivas, and D. Salmi, *Educational Case: Symptomatic but Unruptured Abdominal Aortic Aneurysm.* Acad Pathol, 2018. **5**: p. 2374289518798560.
108. Li, X., et al., *Prevalence and trends of the abdominal aortic aneurysms epidemic in general population--a meta-analysis.* PLoS One, 2013. **8**(12): p. e81260.
109. Lederle, F.A., et al., *Prevalence and associations of abdominal aortic aneurysm detected through screening. Aneurysm Detection and Management (ADAM) Veterans Affairs Cooperative Study Group.* Ann Intern Med, 1997. **126**(6): p. 441-9.
110. Klarin, D., et al., *Genetic Architecture of Abdominal Aortic Aneurysm in the Million Veteran Program.* Circulation, 2020. **142**(17): p. 1633-1646.
111. Lindeman, J.H., et al., *Distinct defects in collagen microarchitecture underlie vessel-wall failure in advanced abdominal aneurysms and aneurysms in Marfan syndrome.* Proc Natl Acad Sci U S A, 2010. **107**(2): p. 862-5.
112. Dobrin, P.B. and R. Mrkvicka, *Failure of elastin or collagen as possible critical connective tissue alterations underlying aneurysmal dilatation.* Cardiovasc Surg, 1994. **2**(4): p. 484-8.
113. Michel, J.B., G. Jondeau, and D.M. Milewicz, *From genetics to response to injury: vascular smooth muscle cells in aneurysms and dissections of the ascending aorta.* Cardiovasc Res, 2018. **114**(4): p. 578-589.
114. López-Candales, A., et al., *Decreased vascular smooth muscle cell density in medial degeneration of human abdominal aortic aneurysms.* Am J Pathol, 1997. **150**(3): p. 993-1007.
115. Golledge, J. and P.E. Norman, *Atherosclerosis and abdominal aortic aneurysm: cause, response, or common risk factors?* Arterioscler Thromb Vasc Biol, 2010. **30**(6): p. 1075-7.
116. Eliason, J.L., et al., *Neutrophil depletion inhibits experimental abdominal aortic aneurysm formation.* Circulation, 2005. **112**(2): p. 232-40.
117. Raffort, J., et al., *Monocytes and macrophages in abdominal aortic aneurysm.* Nat Rev Cardiol, 2017. **14**(8): p. 457-471.
118. Sun, J., et al., *Mast cells modulate the pathogenesis of elastase-induced abdominal aortic aneurysms in mice.* J Clin Invest, 2007. **117**(11): p. 3359-68.

119. Tsuruda, T., et al., *Adventitial mast cells contribute to pathogenesis in the progression of abdominal aortic aneurysm.* Circ Res, 2008. **102**(11): p. 1368-77.
120. Zhang, J., et al., *Mast cell tryptase deficiency attenuates mouse abdominal aortic aneurysm formation.* Circ Res, 2011. **108**(11): p. 1316-27.
121. Meijer, C.A., et al., *Doxycycline for stabilization of abdominal aortic aneurysms: a randomized trial.* Ann Intern Med, 2013. **159**(12): p. 815-23.
122. Isselbacher, E.M., *Thoracic and abdominal aortic aneurysms.* Circulation, 2005. **111**(6): p. 816-28.
123. Clouse, W.D., et al., *Improved prognosis of thoracic aortic aneurysms: a population-based study.* Jama, 1998. **280**(22): p. 1926-9.
124. Mathur, A., et al., *Aortic aneurysm.* J Transl Int Med, 2016. **4**(1): p. 35-41.
125. Cury, M., F. Zeidan, and A.C. Lobato, *Aortic disease in the young: genetic aneurysm syndromes, connective tissue disorders, and familial aortic aneurysms and dissections.* Int J Vasc Med, 2013. **2013**: p. 267215.
126. Quintana, R.A. and W.R. Taylor, *Cellular Mechanisms of Aortic Aneurysm Formation.* Circ Res, 2019. **124**(4): p. 607-618.
127. Renard, M., et al., *Clinical Validity of Genes for Heritable Thoracic Aortic Aneurysm and Dissection.* J Am Coll Cardiol, 2018. **72**(6): p. 605-615.
128. Pinard, A., G.T. Jones, and D.M. Milewicz, *Genetics of Thoracic and Abdominal Aortic Diseases.* Circ Res, 2019. **124**(4): p. 588-606.
129. Neptune, E.R., et al., *Dysregulation of TGF-beta activation contributes to pathogenesis in Marfan syndrome.* Nat Genet, 2003. **33**(3): p. 407-11.
130. Li, G., et al., *Chronic mTOR activation induces a degradative smooth muscle cell phenotype.* J Clin Invest, 2020. **130**(3): p. 1233-1251.
131. Tang, P.C., et al., *Hyperplastic cellular remodeling of the media in ascending thoracic aortic aneurysms.* Circulation, 2005. **112**(8): p. 1098-105.
132. Segura, A.M., et al., *Immunohistochemistry of matrix metalloproteinases and their inhibitors in thoracic aortic aneurysms and aortic valves of patients with Marfan's syndrome.* Circulation, 1998. **98**(19 Suppl): p. II331-7; discussion II337-8.
133. Shen, M., et al., *Divergent roles of matrix metalloproteinase 2 in pathogenesis of thoracic aortic aneurysm.* Arterioscler Thromb Vasc Biol, 2015. **35**(4): p. 888-98.
134. Lederle, F.A., et al., *Open versus Endovascular Repair of Abdominal Aortic Aneurysm.* N Engl J Med, 2019. **380**(22): p. 2126-2135.
135. Chung, J., et al., *Sex differences in thoracic aortic disease: A review of the literature and a call to action.* J Thorac Cardiovasc Surg, 2020. **160**(3): p. 656-660.
136. Li, B., et al., *Sex Differences in Outcomes Following Ruptured Abdominal Aortic Aneurysm Repair.* JAMA Netw Open, 2022. **5**(5): p. e2211336.
137. Portilla-Fernandez, E., et al., *Genetic and clinical determinants of abdominal aortic diameter: genome-wide association studies, exome array data and Mendelian randomization study.* Hum Mol Genet, 2022.
138. Daugherty, A., M.W. Manning, and L.A. Cassis, *Angiotensin II promotes atherosclerotic lesions and aneurysms in apolipoprotein E-deficient mice.* J Clin Invest, 2000. **105**(11): p. 1605-12.
139. Wang, M., et al., *Microsomal prostaglandin E synthase-1 deletion suppresses oxidative stress and angiotensin II-induced abdominal aortic aneurysm formation.* Circulation, 2008. **117**(10): p. 1302-9.
140. Chiou, A.C., B. Chiu, and W.H. Pearce, *Murine aortic aneurysm produced by periarterial application of calcium chloride.* J Surg Res, 2001. **99**(2): p. 371-6.
141. Yamanouchi, D., et al., *Accelerated aneurysmal dilation associated with apoptosis and inflammation in a newly developed calcium phosphate rodent abdominal aortic aneurysm model.* J Vasc Surg, 2012. **56**(2): p. 455-61.
142. Anidjar, S., et al., *Elastase-induced experimental aneurysms in rats.* Circulation, 1990. **82**(3): p. 973-81.
143. Bhamidipati, C.M., et al., *Development of a novel murine model of aortic aneurysms using peri-adventitial elastase.* Surgery, 2012. **152**(2): p. 238-46.

144. Lu, G., et al., *A novel chronic advanced stage abdominal aortic aneurysm murine model.* J Vasc Surg, 2017. **66**(1): p. 232-242 e4.
145. Romary, D.J., A.G. Berman, and C.J. Goergen, *High-frequency murine ultrasound provides enhanced metrics of BAPN-induced AAA growth.* Am J Physiol Heart Circ Physiol, 2019. **317**(5): p. H981-H990.
146. Lareyre, F., et al., *TGFbeta (Transforming Growth Factor-beta) Blockade Induces a Human-Like Disease in a Nondissecting Mouse Model of Abdominal Aortic Aneurysm.* Arterioscler Thromb Vasc Biol, 2017. **37**(11): p. 2171-2181.
147. Maki, J.M., et al., *Inactivation of the lysyl oxidase gene Lox leads to aortic aneurysms, cardiovascular dysfunction, and perinatal death in mice.* Circulation, 2002. **106**(19): p. 2503-9.
148. Huang, J., et al., *Fibulin-4 deficiency results in ascending aortic aneurysms: a potential link between abnormal smooth muscle cell phenotype and aneurysm progression.* Circ Res, 2010. **106**(3): p. 583-92.
149. Judge, D.P., et al., *Evidence for a critical contribution of haploinsufficiency in the complex pathogenesis of Marfan syndrome.* J Clin Invest, 2004. **114**(2): p. 172-81.
150. Pereira, L., et al., *Pathogenetic sequence for aneurysm revealed in mice underexpressing fibrillin-1.* Proc Natl Acad Sci U S A, 1999. **96**(7): p. 3819-23.
151. Gallo, E.M., et al., *Angiotensin II-dependent TGF-beta signaling contributes to Loeys-Dietz syndrome vascular pathogenesis.* J Clin Invest, 2014. **124**(1): p. 448-60.
152. Ye, P., et al., *GM-CSF contributes to aortic aneurysms resulting from SMAD3 deficiency.* J Clin Invest, 2013. **123**(5): p. 2317-31.
153. Ikonomidis, J.S., et al., *A murine model of thoracic aortic aneurysms.* J Surg Res, 2003. **115**(1): p. 157-63.
154. Johnston, W.F., et al., *Inhibition of interleukin-1beta decreases aneurysm formation and progression in a novel model of thoracic aortic aneurysms.* Circulation, 2014. **130**(11 Suppl 1): p. S51-9.
155. Anzai, A., et al., *Adventitial CXCL1/G-CSF expression in response to acute aortic dissection triggers local neutrophil recruitment and activation leading to aortic rupture.* Circ Res, 2015. **116**(4): p. 612-23.
156. Prescott, M.F., et al., *Effect of matrix metalloproteinase inhibition on progression of atherosclerosis and aneurysm in LDL receptor-deficient mice overexpressing MMP-3, MMP-12, and MMP-13 and on restenosis in rats after balloon injury.* Ann N Y Acad Sci, 1999. **878**: p. 179-90.
157. Silence, J., et al., *Persistence of atherosclerotic plaque but reduced aneurysm formation in mice with stromelysin-1 (MMP-3) gene inactivation.* Arterioscler Thromb Vasc Biol, 2001. **21**(9): p. 1440-5.
158. Kanematsu, Y., et al., *Pharmacologically induced thoracic and abdominal aortic aneurysms in mice.* Hypertension, 2010. **55**(5): p. 1267-74.
159. Zhang, P., et al., *Smad4 Deficiency in Smooth Muscle Cells Initiates the Formation of Aortic Aneurysm.* Circ Res, 2016. **118**(3): p. 388-99.
160. Nishijo, N., et al., *Salt-sensitive aortic aneurysm and rupture in hypertensive transgenic mice that overproduce angiotensin II.* Lab Invest, 1998. **78**(9): p. 1059-66.
161. Liu, S., et al., *Mineralocorticoid receptor agonists induce mouse aortic aneurysm formation and rupture in the presence of high salt.* Arterioscler Thromb Vasc Biol, 2013. **33**(7): p. 1568-79.
162. Forsdahl, S.H., et al., *Risk Factors for Abdominal Aortic Aneurysms A 7-Year Prospective Study: The Tromso Study, 1994-2001.* Circulation, 2009. **119**(16): p. 2202-2208.
163. Erbel, R. and M. Budoff, *Improvement of cardiovascular risk prediction using coronary imaging: subclinical atherosclerosis: the memory of lifetime risk factor exposure.* European Heart Journal, 2012. **33**(10): p. 1201-+.
164. Ward, M.R., et al., *Arterial remodeling. Mechanisms and clinical implications.* Circulation, 2000. **102**(10): p. 1186-91.
165. Johnsen, S.H., et al., *Atherosclerosis in abdominal aortic aneurysms: a causal event or a process running in parallel? The Tromso study.* Arterioscler Thromb Vasc Biol, 2010. **30**(6): p. 1263-8.
166. Agmon, Y., et al., *Is aortic dilatation an atherosclerosis-related process? Clinical, laboratory, and transesophageal echocardiographic correlates of thoracic aortic dimensions in the population with implications for thoracic aortic aneurysm formation.* J Am Coll Cardiol, 2003. **42**(6): p. 1076-83.

167. Maurice, P., et al., *Elastin fragmentation and atherosclerosis progression: The elastokine concept.* Trends in Cardiovascular Medicine, 2013. **23**(6): p. 211-221.
168. Adiguzel, E., et al., *Collagens in the progression and complications of atherosclerosis.* Vasc Med, 2009. **14**(1): p. 73-89.
169. Wight, T.N., *A role for proteoglycans in vascular disease.* Matrix Biol, 2018. **71-72**: p. 396-420.
170. Fischer, J.W., *Role of hyaluronan in atherosclerosis: Current knowledge and open questions.* Matrix Biol, 2019. **78-79**: p. 324-336.
171. Pedicino, D., et al., *Alterations of Hyaluronan Metabolism in Acute Coronary Syndrome: Implications for Plaque Erosion.* J Am Coll Cardiol, 2018. **72**(13): p. 1490-1503.
172. Kolodgie, F.D., et al., *Differential accumulation of Proteoglycans and hyaluronan in culprit lesions - Insights into plaque erosion.* Arteriosclerosis Thrombosis and Vascular Biology, 2002. **22**(10): p. 1642-1648.
173. Botnar, R.M., et al., *In vivo assessment of aortic aneurysm wall integrity using elastin-specific molecular magnetic resonance imaging.* Circ Cardiovasc Imaging, 2014. **7**(4): p. 679-89.
174. Xu, J. and G.P. Shi, *Vascular wall extracellular matrix proteins and vascular diseases.* Biochim Biophys Acta, 2014. **1842**(11): p. 2106-2119.
175. Milewicz, D.M., et al., *Marfan syndrome.* Nature Reviews Disease Primers, 2021. **7**(1).
176. Lee, V.S., et al., *Loss of function mutation in LOX causes thoracic aortic aneurysm and dissection in humans.* Proc Natl Acad Sci U S A, 2016. **113**(31): p. 8759-64.
177. Guo, D.C., et al., *LOX Mutations Predispose to Thoracic Aortic Aneurysms and Dissections.* Circ Res, 2016. **118**(6): p. 928-34.
178. Cikach, F.S., et al., *Massive aggrecan and versican accumulation in thoracic aortic aneurysm and dissection.* JCI Insight, 2018. **3**(5).
179. Herman, M.P., et al., *Expression of neutrophil collagenase (matrix metalloproteinase-8) in human atheroma: a novel collagenolytic pathway suggested by transcriptional profiling.* Circulation, 2001. **104**(16): p. 1899-904.
180. Sukhova, G.K., et al., *Evidence for increased collagenolysis by interstitial collagenases-1 and -3 in vulnerable human atheromatous plaques.* Circulation, 1999. **99**(19): p. 2503-9.
181. Molloy, K.J., et al., *Unstable carotid plaques exhibit raised matrix metalloproteinase-8 activity.* Circulation, 2004. **110**(3): p. 337-43.
182. Loftus, I.M., et al., *Increased matrix metalloproteinase-9 activity in unstable carotid plaques. A potential role in acute plaque disruption.* Stroke, 2000. **31**(1): p. 40-7.
183. Peeters, W., et al., *Collagenase matrix metalloproteinase-8 expressed in atherosclerotic carotid plaques is associated with systemic cardiovascular outcome.* European Heart Journal, 2011. **32**(18): p. 2314-2325.
184. Libby, P., *Molecular bases of the acute coronary syndromes.* Circulation, 1995. **91**(11): p. 2844-50.
185. Galis, Z.S., et al., *Increased expression of matrix metalloproteinases and matrix degrading activity in vulnerable regions of human atherosclerotic plaques.* J Clin Invest, 1994. **94**(6): p. 2493-503.
186. Kaartinen, M., et al., *Mast cell infiltration in acute coronary syndromes: implications for plaque rupture.* J Am Coll Cardiol, 1998. **32**(3): p. 606-12.
187. Moreau, M., et al., *Interleukin-8 mediates downregulation of tissue inhibitor of metalloproteinase-1 expression in cholesterol-loaded human macrophages: relevance to stability of atherosclerotic plaque.* Circulation, 1999. **99**(3): p. 420-6.
188. Silence, J., *Reduced Atherosclerotic Plaque but Enhanced Aneurysm Formation in Mice With Inactivation of the Tissue Inhibitor of Metalloproteinase-1 (TIMP-1) Gene.* Circulation Research, 2002. **90**(8): p. 897-903.
189. Cheng, M., et al., *Relationships of adiponectin and matrix metalloproteinase-9 to tissue inhibitor of metalloproteinase-1 ratio with coronary plaque morphology in patients with acute coronary syndrome.* Can J Cardiol, 2008. **24**(5): p. 385-90.
190. Rouis, M., et al., *Adenovirus-mediated overexpression of tissue inhibitor of metalloproteinase-1 reduces atherosclerotic lesions in apolipoprotein E-deficient mice.* Circulation, 1999. **100**(5): p. 533-40.

191. Johnson, J.L., et al., *Suppression of atherosclerotic plaque progression and instability by tissue inhibitor of metalloproteinase-2: involvement of macrophage migration and apoptosis.* Circulation, 2006. **113**(20): p. 2435-44.
192. Di Gregoli, K., et al., *Differential effects of tissue inhibitor of metalloproteinase (TIMP)-1 and TIMP-2 on atherosclerosis and monocyte/macrophage invasion.* Cardiovasc Res, 2016. **109**(2): p. 318-30.
193. Barth, J.L., et al., *Oxidised, glycated LDL selectively influences tissue inhibitor of metalloproteinase-3 gene expression and protein production in human retinal capillary pericytes.* Diabetologia, 2007. **50**(10): p. 2200-8.
194. Cardellini, M., et al., *TIMP3 Is Reduced in Atherosclerotic Plaques From Subjects With Type 2 Diabetes and Increased by SirT1.* Diabetes, 2009. **58**(10): p. 2396-2401.
195. Stohr, R., et al., *Loss of TIMP3 exacerbates atherosclerosis in ApoE null mice.* Atherosclerosis, 2014. **235**(2): p. 438-43.
196. Casagrande, V., et al., *Overexpression of tissue inhibitor of metalloproteinase 3 in macrophages reduces atherosclerosis in low-density lipoprotein receptor knockout mice.* Arterioscler Thromb Vasc Biol, 2012. **32**(1): p. 74-81.
197. Menghini, R., et al., *TIMP3 overexpression in macrophages protects from insulin resistance, adipose inflammation, and nonalcoholic fatty liver disease in mice.* Diabetes, 2012. **61**(2): p. 454-62.
198. Menghini, R., et al., *Tissue inhibitor of metalloproteinase 3 deficiency causes hepatic steatosis and adipose tissue inflammation in mice.* Gastroenterology, 2009. **136**(2): p. 663-72 e4.
199. Goodall, S., et al., *Enhanced invasive properties exhibited by smooth muscle cells are associated with elevated production of MMP-2 in patients with aortic aneurysms.* Eur J Vasc Endovasc Surg, 2002. **24**(1): p. 72-80.
200. Wilson, W.R.W., et al., *Matrix metalloproteinase 8 (neutrophil collagenase) in the pathogenesis of abdominal aortic aneurysm.* British Journal of Surgery, 2005. **92**(7): p. 828-833.
201. Longo, G.M., et al., *Matrix metalloproteinases 2 and 9 work in concert to produce aortic aneurysms.* Journal of Clinical Investigation, 2002. **110**(5): p. 625-632.
202. Longo, G.M., et al., *MMP-12 has a role in abdominal aortic aneurysms in mice.* Surgery, 2005. **137**(4): p. 457-462.
203. Mao, D.L., et al., *Expression of collagenase-3 (MMP-13) in human abdominal aortic aneurysms and vascular smooth muscle cells in culture.* Biochemical and Biophysical Research Communications, 1999. **261**(3): p. 904-910.
204. Xiong, W., et al., *Membrane-type 1 matrix metalloproteinase regulates macrophage-dependent elastolytic activity and aneurysm formation in vivo.* J Biol Chem, 2009. **284**(3): p. 1765-71.
205. Brophy, C.M., et al., *Decreased tissue inhibitor of metalloproteinases (TIMP) in abdominal aortic aneurysm tissue: a preliminary report.* J Surg Res, 1991. **50**(6): p. 653-7.
206. Defawe, O.D., et al., *TIMP-2 and PAI-1 mRNA levels are lower in aneurysmal as compared to athero-occlusive abdominal aortas.* Cardiovasc Res, 2003. **60**(1): p. 205-13.
207. Nakamura, M., et al., *Circulating biochemical marker levels of collagen metabolism are abnormal in patients with abdominal aortic aneurysm.* Angiology, 2000. **51**(5): p. 385-92.
208. Wilson, W.R., et al., *Matrix metalloproteinase 8 (neutrophil collagenase) in the pathogenesis of abdominal aortic aneurysm.* Br J Surg, 2005. **92**(7): p. 828-33.
209. Thompson, R.W., et al., *Production and localization of 92-kilodalton gelatinase in abdominal aortic aneurysms. An elastolytic metalloproteinase expressed by aneurysm-infiltrating macrophages.* J Clin Invest, 1995. **96**(1): p. 318-26.
210. Higashikata, T., et al., *Application of real-time RT-PCR to quantifying gene expression of matrix metalloproteinases and tissue inhibitors of metalloproteinases in human abdominal aortic aneurysm.* Atherosclerosis, 2004. **177**(2): p. 353-360.
211. Eskandari, M.K., et al., *Enhanced abdominal aortic aneurysm in TIMP-1-deficient mice.* J Surg Res, 2005. **123**(2): p. 289-93.

212. Koullias, G.J., et al., *Increased tissue microarray matrix metalloproteinase expression favors proteolysis in thoracic aortic aneurysms and dissections.* Ann Thorac Surg, 2004. **78**(6): p. 2106-10; discussion 2110-1.
213. Xiong, W., et al., *Effects of tissue inhibitor of metalloproteinase 2 deficiency on aneurysm formation.* J Vasc Surg, 2006. **44**(5): p. 1061-6.
214. Aoki, T., et al., *Role of TIMP-1 and TIMP-2 in the progression of cerebral aneurysms.* Stroke, 2007. **38**(8): p. 2337-45.
215. Wang, Z., R. Juttermann, and P.D. Soloway, *TIMP-2 is required for efficient activation of proMMP-2 in vivo.* J Biol Chem, 2000. **275**(34): p. 26411-5.
216. Schmoker, J.D., et al., *Matrix metalloproteinase and tissue inhibitor expression in atherosclerotic and nonatherosclerotic thoracic aortic aneurysms.* Journal of Thoracic and Cardiovascular Surgery, 2007. **133**(1): p. 155-161.
217. de Vries, M.R., et al., *Plaque rupture complications in murine atherosclerotic vein grafts can be prevented by TIMP-1 overexpression.* PLoS One, 2012. **7**(10): p. e47134.
218. Ikonomidis, J.S., et al., *Effects of deletion of the tissue inhibitor of matrix metalloproteinases-1 gene on the progression of murine thoracic aortic aneurysms.* Circulation, 2004. **110**(11 Suppl 1): p. II268-73.
219. Lemaitre, V., P.D. Soloway, and J. D'Armiento, *Increased medial degradation with pseudo-aneurysm formation in apolipoprotein E-knockout mice deficient in tissue inhibitor of metalloproteinases-1.* Circulation, 2003. **107**(2): p. 333-8.
220. Basu, R., et al., *Loss of Timp3 gene leads to abdominal aortic aneurysm formation in response to angiotensin II.* J Biol Chem, 2012. **287**(53): p. 44083-96.
221. Vandenbroucke, R.E. and C. Libert, *Is there new hope for therapeutic matrix metalloproteinase inhibition?* Nature Reviews Drug Discovery, 2014. **13**(12): p. 904-927.
222. George, S.J., et al., *Adenovirus-mediated gene transfer of the human TIMP-1 gene inhibits smooth muscle cell migration and neointimal formation in human saphenous vein.* Human Gene Therapy, 1998. **9**(6): p. 867-877.
223. Cheng, L., et al., *Adenovirus-mediated gene transfer of the human tissue inhibitor of metalloproteinase-2 blocks vascular smooth muscle cell invasiveness in vitro and modulates neointimal development in vivo.* Circulation, 1998. **98**(20): p. 2195-2201.
224. George, S.J., et al., *Inhibition of late vein graft neointima formation in human and porcine models by adenovirus-mediated overexpression of tissue inhibitor of metalloproteinase-3.* Circulation, 2000. **101**(3): p. 296-304.
225. Baker, A.H., et al., *Divergent effects of tissue inhibitor of metalloproteinase-1, -2, or -3 overexpression on rat vascular smooth muscle cell invasion, proliferation, and death in vitro. TIMP-3 promotes apoptosis.* J Clin Invest, 1998. **101**(6): p. 1478-87.
226. Pulukuri, S.M., et al., *Epigenetic inactivation of the tissue inhibitor of metalloproteinase-2 (TIMP-2) gene in human prostate tumors.* Oncogene, 2007. **26**(36): p. 5229-37.
227. Jackson, H.W., et al., *TIMPs: versatile extracellular regulators in cancer.* Nat Rev Cancer, 2017. **17**(1): p. 38-53.
228. Greene, J., *Molecular Cloning and Characterization of Human Tissue Inhibitor of Metalloproteinase 4.* THE JOURNAL OF BIOLOGICAL CHEMISTRY, 1996.
229. Leco, K.J., et al., *Murine tissue inhibitor of metalloproteinases-4 (Timp-4): cDNA isolation and expression in adult mouse tissues.* FEBS Lett, 1997. **401**(2-3): p. 213-7.
230. Young, D.A., et al., *Identification of an initiator-like element essential for the expression of the tissue inhibitor of metalloproteinases-4 (Timp-4) gene.* Biochem J, 2002. **364**(Pt 1): p. 89-99.
231. Donnini, S., et al., *Peroxynitrite inactivates human-tissue inhibitor of metalloproteinase-4.* FEBS Lett, 2008. **582**(7): p. 1135-40.
232. Liu, Y.E., et al., *Preparation and characterization of recombinant tissue inhibitor of metalloproteinase 4 (TIMP-4).* J Biol Chem, 1997. **272**(33): p. 20479-83.

233. Tunuguntla, R., et al., *Expression of matrix metalloproteinase-26 and tissue inhibitors of metalloproteinases TIMP-3 and -4 in benign endometrium and endometrial cancer.* Gynecol Oncol, 2003. **89**(3): p. 453-9.
234. Bigg, H.F., et al., *Tissue inhibitor of metalloproteinases-4 inhibits but does not support the activation of gelatinase A via efficient inhibition of membrane type 1-matrix metalloproteinase.* Cancer Res, 2001. **61**(9): p. 3610-8.
235. Mochizuki, S., et al., *ADAM28 is activated by MMP-7 (matrilysin-1) and cleaves insulin-like growth factor binding protein-3.* Biochem Biophys Res Commun, 2004. **315**(1): p. 79-84.
236. Zou, J., et al., *Catalytic activity of human ADAM33.* J Biol Chem, 2004. **279**(11): p. 9818-30.
237. Hernandez-Barrantes, S., et al., *Differential roles of TIMP-4 and TIMP-2 in pro-MMP-2 activation by MT1-MMP.* Biochem Biophys Res Commun, 2001. **281**(1): p. 126-30.
238. Radomski, A., et al., *Identification, regulation and role of tissue inhibitor of metalloproteinases-4 (TIMP-4) in human platelets.* Br J Pharmacol, 2002. **137**(8): p. 1330-8.
239. Jiang, Y., et al., *Stimulation of mammary tumorigenesis by systemic tissue inhibitor of matrix metalloproteinase 4 gene delivery.* Cancer Res, 2001. **61**(6): p. 2365-70.
240. Wang, M., *Inhibition of tumor growth and metastasis of human breast cancer cells transfected with tissue inhibitor of metalloproteinase 4.* Oncogene, 1997.
241. Zhao, Y.G., et al., *Endometase/matrilysin-2 in human breast ductal carcinoma in situ and its inhibition by tissue inhibitors of metalloproteinases-2 and -4: a putative role in the initiation of breast cancer invasion.* Cancer Res, 2004. **64**(2): p. 590-8.
242. Melendez-Zajgla, J., et al., *Tissue inhibitor of metalloproteinases-4. The road less traveled.* Mol Cancer, 2008. **7**: p. 85.
243. Rahkonen, O.P., et al., *Characterization of the murine Timp4 gene, localization within intron 5 of the synapsin 2 gene and tissue distribution of the mRNA.* Biochim Biophys Acta, 2002. **1577**(1): p. 45-52.
244. Hoit, B.D., et al., *Remodeling of the left atrium in pacing-induced atrial cardiomyopathy.* Mol Cell Biochem, 2002. **238**(1-2): p. 145-50.
245. Li, H., et al., *MMP/TIMP expression in spontaneously hypertensive heart failure rats: the effect of ACE- and MMP-inhibition.* Cardiovasc Res, 2000. **46**(2): p. 298-306.
246. Koskivirta, I., et al., *Tissue inhibitor of metalloproteinases 4 (TIMP4) is involved in inflammatory processes of human cardiovascular pathology.* Histochem Cell Biol, 2006. **126**(3): p. 335-42.
247. Li, Y.Y., et al., *Differential expression of tissue inhibitors of metalloproteinases in the failing human heart.* Circulation, 1998. **98**(17): p. 1728-34.
248. Weir, R.A., et al., *Plasma TIMP-4 predicts left ventricular remodeling after acute myocardial infarction.* J Card Fail, 2011. **17**(6): p. 465-71.
249. Koskivirta, I., et al., *Mice with tissue inhibitor of metalloproteinases 4 (Timp4) deletion succumb to induced myocardial infarction but not to cardiac pressure overload.* J Biol Chem, 2010. **285**(32): p. 24487-93.
250. Schulze, C.J., et al., *Imbalance between tissue inhibitor of metalloproteinase-4 and matrix metalloproteinases during acute myocardial [correction of myoctardial] ischemia-reperfusion injury.* Circulation, 2003. **107**(19): p. 2487-92.
251. Takawale, A., et al., *Myocardial recovery from ischemia-reperfusion is compromised in the absence of tissue inhibitor of metalloproteinase 4.* Circ Heart Fail, 2014. **7**(4): p. 652-62.
252. Dollery, C.M., et al., *TIMP-4 is regulated by vascular injury in rats.* Circulation Research, 1999. **84**(5): p. 498-504.
253. Wu, J., et al., *Progressive Aortic Dilation Is Regulated by miR-17-Associated miRNAs.* J Am Coll Cardiol, 2016. **67**(25): p. 2965-77.
254. Ketsawatsomkron, P., et al., *Protective Role for Tissue Inhibitor of Metalloproteinase-4, a Novel Peroxisome Proliferator-Activated Receptor-gamma Target Gene, in Smooth Muscle in Deoxycorticosterone Acetate-Salt Hypertension.* Hypertension, 2016. **67**(1): p. 214-22.

255. Oikonen, M., et al., *Tissue inhibitor of matrix metalloproteinases 4 (TIMP4) in a population of young adults relations to cardiovascular risk markers and carotid artery intima-media thickness. The Cardiovascular Risk in Young Finns Study.* Scand J Clin Lab Invest, 2012. **72**(7): p. 540-6.
256. Guo, Y.H., et al., *Tissue inhibitor of metalloproteinases-4 suppresses vascular smooth muscle cell migration and induces cell apoptosis.* Life Sci, 2004. **75**(20): p. 2483-93.
257. Sakamuri, S., et al., *Absence of Tissue Inhibitor of Metalloproteinase-4 (TIMP4) ameliorates high fat diet-induced obesity in mice due to defective lipid absorption.* Sci Rep, 2017. **7**(1): p. 6210.
258. Harrison, S.C., et al., *Genetic Association of Lipids and Lipid Drug Targets With Abdominal Aortic Aneurysm: A Meta-analysis.* JAMA Cardiol, 2018. **3**(1): p. 26-33.
259. Salata, K., et al., *Statins Reduce Abdominal Aortic Aneurysm Growth, Rupture, and Perioperative Mortality: A Systematic Review and Meta-Analysis.* J Am Heart Assoc, 2018. **7**(19): p. e008657.
260. Lutshumba, J., et al., *BMAL1/Timp4 & AAAs.* Arterioscler Thromb Vasc Biol, 2018. **38**(5): p. 1063-1075.
261. Gestrich, C., et al., *Activation of Endocannabinoid System Is Associated with Persistent Inflammation in Human Aortic Aneurysm.* Biomed Res Int, 2015. **2015**: p. 456582.
262. Spano, D.P. and S.D. Scilabra, *Tissue Inhibitor of Metalloproteases 3 (TIMP-3): In Vivo Analysis Underpins Its Role as a Master Regulator of Ectodomain Shedding.* Membranes, 2022. **12**(2).
263. Leco, K.J., et al., *Tissue Inhibitor of Metalloproteinases-3 (Timp-3) Is an Extracellular Matrix-Associated Protein with a Distinctive Pattern of Expression in Mouse Cells and Tissues.* Journal of Biological Chemistry, 1994. **269**(12): p. 9352-9360.
264. Wilde, C.G., et al., *Cloning and Characterization of Human Tissue Inhibitor of Metalloproteinases-3.* DNA and Cell Biology, 1994. **13**(7): p. 711-718.
265. Qureshi, H.Y., et al., *TGF-beta-induced expression of tissue inhibitor of metalloproteinases-3 gene in chondrocytes is mediated by extracellular signal-regulated kinase pathway and Sp1 transcription factor.* J Cell Physiol, 2005. **203**(2): p. 345-52.
266. Yan, D.Y., et al., *Bovine lactoferricin induces TIMP-3 via the ERK1/2-Sp1 axis in human articular chondrocytes.* Gene, 2013. **517**(1): p. 12-18.
267. Qureshi, H.Y., G. Ricci, and M. Zafarullah, *Smad signaling pathway is a pivotal component of tissue inhibitor of metalloproteinases-3 regulation by transforming growth factor beta in human chondrocytes.* Biochim Biophys Acta, 2008. **1783**(9): p. 1605-12.
268. Su, C.W., et al., *TIMP-3 as a therapeutic target for cancer.* Therapeutic Advances in Medical Oncology, 2019. **11**.
269. Shi, J., et al., *miR-17-3p Contributes to Exercise-Induced Cardiac Growth and Protects against Myocardial Ischemia-Reperfusion Injury.* Theranostics, 2017. **7**(3): p. 664-676.
270. Di Gregoli, K., et al., *MicroRNA-181b Controls Atherosclerosis and Aneurysms Through Regulation of TIMP-3 and Elastin.* Circ Res, 2017. **120**(1): p. 49-65.
271. Son, D.J., et al., *The atypical mechanosensitive microRNA-712 derived from pre-ribosomal RNA induces endothelial inflammation and atherosclerosis.* Nat Commun, 2013. **4**: p. 3000.
272. Kim, C.W., et al., *Prevention of abdominal aortic aneurysm by anti-microRNA-712 or anti-microRNA-205 in angiotensin II-infused mice.* Arterioscler Thromb Vasc Biol, 2014. **34**(7): p. 1412-21.
273. Scilabra, S.D., et al., *Dissecting the interaction between tissue inhibitor of metalloproteinases-3 (TIMP-3) and low density lipoprotein receptor-related protein-1 (LRP-1): Development of a "TRAP" to increase levels of TIMP-3 in the tissue.* Matrix Biology, 2017. **59**: p. 69-79.
274. Moore, L., et al., *Tissue inhibitor of metalloproteinases (TIMPs) in heart failure.* Heart Fail Rev, 2012. **17**(4-5): p. 693-706.
275. Kassiri, Z., et al., *Combination of tumor necrosis factor-alpha ablation and matrix metalloproteinase inhibition prevents heart failure after pressure overload in tissue inhibitor of metalloproteinase-3 knock-out mice.* Circ Res, 2005. **97**(4): p. 380-90.
276. Leco, K.J., et al., *Spontaneous air space enlargement in the lungs of mice lacking tissue inhibitor of metalloproteinases-3 (TIMP-3).* J Clin Invest, 2001. **108**(6): p. 817-29.

277. Amour, A., et al., *TNF-alpha converting enzyme (TACE) is inhibited by TIMP-3.* FEBS Lett, 1998. **435**(1): p. 39-44.
278. Black, R.A., et al., *A metalloproteinase disintegrin that releases tumour-necrosis factor-alpha from cells.* Nature, 1997. **385**(6618): p. 729-33.
279. Smookler, D.S., et al., *Tissue inhibitor of metalloproteinase 3 regulates TNF-dependent systemic inflammation.* J Immunol, 2006. **176**(2): p. 721-5.
280. Borland, G., G. Murphy, and A. Ager, *Tissue inhibitor of metalloproteinases-3 inhibits shedding of L-selectin from leukocytes.* J Biol Chem, 1999. **274**(5): p. 2810-5.
281. Fitzgerald, M.L., et al., *Shedding of syndecan-1 and -4 ectodomains is regulated by multiple signaling pathways and mediated by a TIMP-3-sensitive metalloproteinase.* J Cell Biol, 2000. **148**(4): p. 811-24.
282. Mohammed, F.F., D.S. Smookler, and R. Khokha, *Metalloproteinases, inflammation, and rheumatoid arthritis.* Ann Rheum Dis, 2003. **62 Suppl 2**: p. ii43-7.
283. Murthy, A., et al., *Ectodomain shedding of EGFR ligands and TNFR1 dictates hepatocyte apoptosis during fulminant hepatitis in mice.* J Clin Invest, 2010. **120**(8): p. 2731-44.
284. Monteleone, I., et al., *Tissue inhibitor of metalloproteinase-3 regulates inflammation in human and mouse intestine.* Gastroenterology, 2012. **143**(5): p. 1277-1287 e4.
285. Qi, J.H., et al., *A novel function for tissue inhibitor of metalloproteinases-3 (TIMP3): inhibition of angiogenesis by blockage of VEGF binding to VEGF receptor-2.* Nat Med, 2003. **9**(4): p. 407-15.
286. Janssen, A., et al., *Abnormal vessel formation in the choroid of mice lacking tissue inhibitor of metalloprotease-3.* Invest Ophthalmol Vis Sci, 2008. **49**(7): p. 2812-22.
287. Baker, A.H., et al., *Inhibition of invasion and induction of apoptotic cell death of cancer cell lines by overexpression of TIMP-3.* Br J Cancer, 1999. **79**(9-10): p. 1347-55.
288. Ahonen, M., et al., *Antitumor activity and bystander effect of adenovirally delivered tissue inhibitor of metalloproteinases-3.* Mol Ther, 2002. **5**(6): p. 705-15.
289. Carrell, T.W.G., *Stromelysin-1 (Matrix Metalloproteinase-3) and Tissue Inhibitor of Metalloproteinase-3 Are Overexpressed in the Wall of Abdominal Aortic Aneurysms.* Circulation, 2002.
290. Ogata, T., et al., *Genetic analysis of polymorphisms in biologically relevant candidate genes in patients with abdominal aortic aneurysms.* J Vasc Surg, 2005. **41**(6): p. 1036-42.
291. Tsarouhas, K., et al., *Transcriptional regulation of TIMPs in ascending aorta aneurysms.* Thromb Res, 2010. **126**(5): p. 399-405.
292. Montezano, A.C., et al., *Angiotensin II and vascular injury.* Curr Hypertens Rep, 2014. **16**(6): p. 431.
293. Satoh, H., et al., *Expression and localization of tumour necrosis factor-alpha and its converting enzyme in human abdominal aortic aneurysm.* Clin Sci (Lond), 2004. **106**(3): p. 301-6.
294. Xiong, W., et al., *Blocking TNF-alpha attenuates aneurysm formation in a murine model.* J Immunol, 2009. **183**(4): p. 2741-6.
295. Kawai, T., et al., *Vascular ADAM17 (a Disintegrin and Metalloproteinase Domain 17) Is Required for Angiotensin II/beta-Aminopropionitrile-Induced Abdominal Aortic Aneurysm.* Hypertension, 2017. **70**(5): p. 959-963.
296. Hans, C.P., et al., *Inhibition of Notch1 signaling reduces abdominal aortic aneurysm in mice by attenuating macrophage-mediated inflammation.* Arterioscler Thromb Vasc Biol, 2012. **32**(12): p. 3012-23.
297. Thatcher, S.E., et al., *Angiotensin-converting enzyme 2 decreases formation and severity of angiotensin II-induced abdominal aortic aneurysms.* Arterioscler Thromb Vasc Biol, 2014. **34**(12): p. 2617-23.
298. Kaneko, H., et al., *Tumor necrosis factor-α converting enzyme is a key mediator of abdominal aortic aneurysm development.* Atherosclerosis, 2011. **218**(2): p. 470-8.
299. Shen, M., et al., *Cell-Specific Functions of ADAM17 Regulate the Progression of Thoracic Aortic Aneurysm.* Circ Res, 2018. **123**(3): p. 372-388.
300. Ni, X.Q., et al., *Inhibition of Notch1-mediated inflammation by intermedin protects against abdominal aortic aneurysm via PI3K/Akt signaling pathway.* Aging (Albany NY), 2021. **13**(4): p. 5164-5184.

301. Tedesco, M.M., et al., *Analysis of in situ and ex vivo vascular endothelial growth factor receptor expression during experimental aortic aneurysm progression.* Arterioscler Thromb Vasc Biol, 2009. **29**(10): p. 1452-7.
302. Xu, B., et al., *Inhibition of VEGF (Vascular Endothelial Growth Factor)-A or its Receptor Activity Suppresses Experimental Aneurysm Progression in the Aortic Elastase Infusion Model.* Arterioscler Thromb Vasc Biol, 2019. **39**(8): p. 1652-1666.
303. Bazzoni, G. and E. Dejana, *Endothelial cell-to-cell junctions: molecular organization and role in vascular homeostasis.* Physiol Rev, 2004. **84**(3): p. 869-901.
304. Franck, G., et al., *Reestablishment of the endothelial lining by endothelial cell therapy stabilizes experimental abdominal aortic aneurysms.* Circulation, 2013. **127**(18): p. 1877-87.
305. Koenen, R.R., et al., *Regulated release and functional modulation of junctional adhesion molecule A by disintegrin metalloproteinases.* Blood, 2009. **113**(19): p. 4799-809.
306. Basu, R., et al., *TIMP3 is the primary TIMP to regulate agonist-induced vascular remodelling and hypertension.* Cardiovasc Res, 2013. **98**(3): p. 360-71.
307. Andres-Manzano, M.J., V. Andres, and B. Dorado, *Oil Red O and Hematoxylin and Eosin Staining for Quantification of Atherosclerosis Burden in Mouse Aorta and Aortic Root.* Methods Mol Biol, 2015. **1339**: p. 85-99.
308. Seimon, T.A., et al., *Macrophage deficiency of p38alpha MAPK promotes apoptosis and plaque necrosis in advanced atherosclerotic lesions in mice.* J Clin Invest, 2009. **119**(4): p. 886-98.
309. Matyash, V., et al., *Lipid extraction by methyl-tert-butyl ether for high-throughput lipidomics.* J Lipid Res, 2008. **49**(5): p. 1137-46.
310. Xie, W., et al., *Krüppel-like factor 14 inhibits atherosclerosis via mir-27a-mediated down-regulation of lipoprotein lipase expression in vivo.* Atherosclerosis, 2019. **289**: p. 143-161.
311. Jin, X., et al., *Macrophages Shed Excess Cholesterol in Unique Extracellular Structures Containing Cholesterol Microdomains.* Arterioscler Thromb Vasc Biol, 2018. **38**(7): p. 1504-1518.
312. Zhang, M., et al., *MicroRNA-27a/b regulates cellular cholesterol efflux, influx and esterification/hydrolysis in THP-1 macrophages.* Atherosclerosis, 2014. **234**(1): p. 54-64.
313. Weischenfeldt, J. and B. Porse, *Bone Marrow-Derived Macrophages (BMM): Isolation and Applications.* CSH Protoc, 2008. **2008**: p. pdb prot5080.
314. Jana, S., et al., *ADAM (a Disintegrin and Metalloproteinase) 15 Deficiency Exacerbates Ang II (Angiotensin II)-Induced Aortic Remodeling Leading to Abdominal Aortic Aneurysm.* Arterioscler Thromb Vasc Biol, 2020: p. ATVBAHA120314600.
315. Mathers, C.D., A. Lopez, and C.J.L. Murray, *Global Burden of Disease and Risk Factors.*, ed. A. Lopez, et al. 2006, New York: Oxford University Press.
316. Herrington, W., et al., *Epidemiology of Atherosclerosis and the Potential to Reduce the Global Burden of Atherothrombotic Disease.* Circ Res, 2016. **118**(4): p. 535-46.
317. Libby, P., K.E. Bornfeldt, and A.R. Tall, *Atherosclerosis: Successes, Surprises, and Future Challenges.* Circ Res, 2016. **118**(4): p. 531-4.
318. Ruddy, J.M., J.S. Ikonomidis, and J.A. Jones, *Multidimensional Contribution of Matrix Metalloproteinases to Atherosclerotic Plaque Vulnerability: Multiple Mechanisms of Inhibition to Promote Stability.* J Vasc Res, 2016. **53**(1-2): p. 1-16.
319. Feil, S., et al., *Transdifferentiation of vascular smooth muscle cells to macrophage-like cells during atherogenesis.* Circ Res, 2014. **115**(7): p. 662-7.
320. Rong, J.X., et al., *Transdifferentiation of mouse aortic smooth muscle cells to a macrophage-like state after cholesterol loading.* Proc Natl Acad Sci U S A, 2003. **100**(23): p. 13531-6.
321. Zeller, I. and S. Srivastava, *Macrophage functions in atherosclerosis.* Circ Res, 2014. **115**(12): p. e83-5.
322. Dollery, C.M., et al., *TIMP-4 is regulated by vascular injury in rats.* Circ Res, 1999. **84**(5): p. 498-504.
323. Guo, Y.H., et al., *Tissue inhibitor of metalloproteinases-4 suppresses vascular smooth muscle cell migration and induces cell apoptosis.* Life Sciences, 2004. **75**(20): p. 2483-2493.
324. Libby, P., et al., *Atherosclerosis.* Nat Rev Dis Primers, 2019. **5**(1): p. 56.

325. Ruddy, J.M., et al., *Differential hypertensive protease expression in the thoracic versus abdominal aorta.* J Vasc Surg, 2017. **66**(5): p. 1543-1552.
326. Patel, V.B., et al., *Angiotensin-converting enzyme 2 is a critical determinant of angiotensin II-induced loss of vascular smooth muscle cells and adverse vascular remodeling.* Hypertension, 2014. **64**(1): p. 157-64.
327. Getz, G.S. and C.A. Reardon, *Diet and murine atherosclerosis.* Arterioscler Thromb Vasc Biol, 2006. **26**(2): p. 242-9.
328. Johnson, J.L., et al., *Relationship of MMP-14 and TIMP-3 expression with macrophage activation and human atherosclerotic plaque vulnerability.* Mediators Inflamm, 2014. **2014**: p. 276457.
329. Chen, Q.J., et al., *Polymorphisms of MMP-3 and TIMP-4 genes affect angiographic coronary plaque progression in non-diabetic and type 2 diabetic patients.* Clin Chim Acta, 2009. **405**(1-2): p. 97-103.
330. Nordestgaard, B.G., *Triglyceride-Rich Lipoproteins and Atherosclerotic Cardiovascular Disease: New Insights From Epidemiology, Genetics, and Biology.* Circ Res, 2016. **118**(4): p. 547-63.
331. Wolf, D. and K. Ley, *Immunity and Inflammation in Atherosclerosis.* Circ Res, 2019. **124**(2): p. 315-327.
332. Mathur, K.S., et al., *Serum cholesterol and atherosclerosis in man.* Circulation, 1961. **23**: p. 847-52.
333. Paterson, J.C., L. Dyer, and E.C. Armstrong, *Serum cholesterol levels in human atherosclerosis.* Can Med Assoc J, 1960. **82**: p. 6-11.
334. Cabin, H.S. and W.C. Roberts, *Relation of serum total cholesterol and triglyceride levels to the amount and extent of coronary arterial narrowing by atherosclerotic plaque in coronary heart disease. Quantitative analysis of 2,037 five mm segments of 160 major epicardial coronary arteries in 40 necropsy patients.* Am J Med, 1982. **73**(2): p. 227-34.
335. Ravnskov, U., *Is atherosclerosis caused by high cholesterol?* QJM, 2002. **95**(6): p. 397-403.
336. Ruddy, J.M., J.A. Jones, and J.S. Ikonomidis, *Pathophysiology of thoracic aortic aneurysm (TAA): is it not one uniform aorta? Role of embryologic origin.* Prog Cardiovasc Dis, 2013. **56**(1): p. 68-73.
337. Basatemur, G.L., et al., *Vascular smooth muscle cells in atherosclerosis.* Nat Rev Cardiol, 2019. **16**(12): p. 727-744.
338. Shankman, L.S., et al., *KLF4-dependent phenotypic modulation of smooth muscle cells has a key role in atherosclerotic plaque pathogenesis.* Nat Med, 2015. **21**(6): p. 628-37.
339. Diehm, N., et al., *Novel insight into the pathobiology of abdominal aortic aneurysm and potential future treatment concepts.* Prog Cardiovasc Dis, 2007. **50**(3): p. 209-17.
340. Toghill, B.J., A. Saratzis, and M.J. Bown, *Abdominal aortic aneurysm-an independent disease to atherosclerosis?* Cardiovasc Pathol, 2017. **27**: p. 71-75.
341. Lutshumba, J., et al., *Deletion of BMAL1 in Smooth Muscle Cells Protects Mice From Abdominal Aortic Aneurysms.* Arterioscler Thromb Vasc Biol, 2018. **38**(5): p. 1063-1075.
342. Maguire, E.M., et al., *Matrix Metalloproteinase in Abdominal Aortic Aneurysm and Aortic Dissection.* Pharmaceuticals (Basel), 2019. **12**(3).
343. Hu, M., et al., *Loss of TIMP4 (Tissue Inhibitor of Metalloproteinase 4) Promotes Atherosclerotic Plaque Deposition in the Abdominal Aorta Despite Suppressed Plasma Cholesterol Levels.* Arterioscler Thromb Vasc Biol, 2021. **41**(6): p. 1874-1889.
344. Golledge, J., S.M. Krishna, and Y. Wang, *Mouse models for abdominal aortic aneurysm.* Br J Pharmacol, 2020.
345. Daugherty, A. and L.A. Cassis, *Mouse models of abdominal aortic aneurysms.* Arterioscler Thromb Vasc Biol, 2004. **24**(3): p. 429-34.
346. Senemaud, J., et al., *Translational Relevance and Recent Advances of Animal Models of Abdominal Aortic Aneurysm.* Arterioscler Thromb Vasc Biol, 2017. **37**(3): p. 401-410.
347. Laser, A., et al., *Differential gender- and species-specific formation of aneurysms using a novel method of inducing abdominal aortic aneurysms.* J Surg Res, 2012. **178**(2): p. 1038-45.
348. Liu, B., et al., *Pathogenic mechanisms and the potential of drug therapies for aortic aneurysm.* Am J Physiol Heart Circ Physiol, 2020. **318**(3): p. H652-H670.

349. Takawale, A., S.S. Sakamuri, and Z. Kassiri, *Extracellular matrix communication and turnover in cardiac physiology and pathology.* Compr Physiol, 2015. **5**(2): p. 687-719.
350. Takawale, A., et al., *Myocardial overexpression of TIMP3 after myocardial infarction exerts beneficial effects by promoting angiogenesis and suppressing early proteolysis.* Am J Physiol Heart Circ Physiol, 2017. **313**(2): p. H224-H236.
351. Kilic, T., et al., *Disintegrin and Metalloproteinases (ADAMs [A Disintegrin and Metalloproteinase] and ADAMTSs [ADAMs With a Thrombospondin Motif]) in Aortic Aneurysm.* Hypertension, 2022. **79**(7): p. 1327-1338.
352. Chen, P.Y., et al., *Smooth Muscle Cell Reprogramming in Aortic Aneurysms.* Cell Stem Cell, 2020. **26**(4): p. 542-557 e11.
353. Yuan, Z., et al., *Abdominal Aortic Aneurysm: Roles of Inflammatory Cells.* Front Immunol, 2020. **11**: p. 609161.
354. Pisano, C., et al., *Cardiovascular Disease in Ageing: An Overview on Thoracic Aortic Aneurysm as an Emerging Inflammatory Disease.* Mediators of Inflammation, 2017. **2017**.
355. Fan, D. and Z. Kassiri, *Biology of Tissue Inhibitor of Metalloproteinase 3 (TIMP3), and Its Therapeutic Implications in Cardiovascular Pathology.* Front Physiol, 2020. **11**: p. 661.
356. Farrell, K., et al., *Alterations in phenotype and gene expression of adult human aneurysmal smooth muscle cells by exogenous nitric oxide.* Exp Cell Res, 2019. **384**(1): p. 111589.
357. Mikolajczyk, K., et al., *The Important Role of Endothelium and Extracellular Vesicles in the Cellular Mechanism of Aortic Aneurysm Formation.* Int J Mol Sci, 2021. **22**(23).
358. Arpino, V., et al., *Tissue inhibitor of metalloproteinases 3-dependent microvascular endothelial cell barrier function is disrupted under septic conditions.* Am J Physiol Heart Circ Physiol, 2016. **310**(11): p. H1455-67.
359. Spurbeck, W.W., et al., *Enforced expression of tissue inhibitor of matrix metalloproteinase-3 affects functional capillary morphogenesis and inhibits tumor growth in a murine tumor model.* Blood, 2002. **100**(9): p. 3361-8.
360. Schrimpf, C., et al., *Pericyte TIMP3 and ADAMTS1 modulate vascular stability after kidney injury.* J Am Soc Nephrol, 2012. **23**(5): p. 868-83.
361. Ichikawa, Y., et al., *Matrilysin (MMP-7) degrades VE-cadherin and accelerates accumulation of beta-catenin in the nucleus of human umbilical vein endothelial cells.* Oncol Rep, 2006. **15**(2): p. 311-5.
362. Deryugina, E.I., L. Soroceanu, and A.Y. Strongin, *Up-regulation of vascular endothelial growth factor by membrane-type 1 matrix metalloproteinase stimulates human glioma xenograft growth and angiogenesis.* Cancer Res, 2002. **62**(2): p. 580-8.
363. Bergers, G., et al., *Matrix metalloproteinase-9 triggers the angiogenic switch during carcinogenesis.* Nat Cell Biol, 2000. **2**(10): p. 737-44.
364. Dong, Z., et al., *Macrophage-derived metalloelastase is responsible for the generation of angiostatin in Lewis lung carcinoma.* Cell, 1997. **88**(6): p. 801-10.
365. Pozzi, A., W.F. LeVine, and H.A. Gardner, *Low plasma levels of matrix metalloproteinase 9 permit increased tumor angiogenesis.* Oncogene, 2002. **21**(2): p. 272-81.
366. Wen, W., et al., *The generation of endostatin is mediated by elastase.* Cancer Res, 1999. **59**(24): p. 6052-6.
367. Menge, T., et al., *Mesenchymal stem cells regulate blood-brain barrier integrity through TIMP3 release after traumatic brain injury.* Sci Transl Med, 2012. **4**(161): p. 161ra150.
368. Mahley, R.W., *Atherogenic hyperlipoproteinemia. The cellular and molecular biology of plasma lipoproteins altered by dietary fat and cholesterol.* Med Clin North Am, 1982. **66**(2): p. 375-402.
369. Spady, D.K., *Reverse cholesterol transport and atherosclerosis regression.* Circulation, 1999. **100**(6): p. 576-8.
370. Gomez, D., et al., *Detection of histone modifications at specific gene loci in single cells in histological sections.* Nat Methods, 2013. **10**(2): p. 171-7.
371. Wissler, R.W., *The arterial medial cell, smooth muscle, or multifunctional mesenchyme?* Circulation, 1967. **36**(1): p. 1-4.

372. Oram, J.F. and J.W. Heinecke, *ATP-binding cassette transporter A1: a cell cholesterol exporter that protects against cardiovascular disease.* Physiol Rev, 2005. **85**(4): p. 1343-72.
373. Choi, H.Y., et al., *ATP-binding cassette transporter A1 expression and apolipoprotein A-I binding are impaired in intima-type arterial smooth muscle cells.* Circulation, 2009. **119**(25): p. 3223-31.
374. Ruddy, J.M., J.A. Jones, and J.S. Ikonomidis, *Pathophysiology of Thoracic Aortic Aneurysm (TAA): Is It Not One Uniform Aorta? Role of Embryologic Origin.* Progress in Cardiovascular Diseases, 2013. **56**(1): p. 68-73.
375. Angelov, S.N., et al., *TGF-beta (Transforming Growth Factor-beta) Signaling Protects the Thoracic and Abdominal Aorta From Angiotensin II-Induced Pathology by Distinct Mechanisms.* Arterioscler Thromb Vasc Biol, 2017. **37**(11): p. 2102-2113.
376. Kuivaniemi, H., et al., *Understanding the pathogenesis of abdominal aortic aneurysms.* Expert Rev Cardiovasc Ther, 2015. **13**(9): p. 975-87.
377. Homma, S., et al., *Histological topographical comparisons of atherosclerosis progression in juveniles and young adults.* Atherosclerosis, 2008. **197**(2): p. 791-8.
378. Muradashvili, N., et al., *Fibrinogen-induced increased pial venular permeability in mice.* J Cereb Blood Flow Metab, 2012. **32**(1): p. 150-63.
379. Fujii, T., et al., *Tissue Inhibitor of Metalloproteinase 3 Deficiency Disrupts the Hepatocyte E-Cadherin/beta-Catenin Complex and Induces Cell Death in Liver Ischemia/Reperfusion Injury.* Liver Transpl, 2020. **26**(1): p. 113-126.
380. Hojilla, C.V., et al., *Metalloproteinase axes increase beta-catenin signaling in primary mouse mammary epithelial cells lacking TIMP3.* J Cell Sci, 2007. **120**(Pt 6): p. 1050-60.
381. Li, W., et al., *Association between abdominal aortic plaque and coronary artery disease.* Clin Interv Aging, 2016. **11**: p. 683-8.
382. Zarins, C.K., C. Xu, and S. Glagov, *Atherosclerotic enlargement of the human abdominal aorta.* Atherosclerosis, 2001. **155**(1): p. 157-64.
383. West, C.A., Jr., et al., *A contemporary experience of open aortic reconstruction in patients with chronic atherosclerotic occlusion of the abdominal aorta.* J Vasc Surg, 2010. **52**(5): p. 1164-72.
384. Brewster, D.C., *Clinical and anatomical considerations for surgery in aortoiliac disease and results of surgical treatment.* Circulation, 1991. **83**(2 Suppl): p. I42-52.
385. Maroules, C.D., et al., *Abdominal aortic atherosclerosis at MR imaging is associated with cardiovascular events: the Dallas heart study.* Radiology, 2013. **269**(1): p. 84-91.
386. Batt, M., et al., *Penetrating atherosclerotic ulcers of the infrarenal aorta: life-threatening lesions.* Eur J Vasc Endovasc Surg, 2005. **29**(1): p. 35-42.
387. Tsuji, Y., et al., *Endovascular stent-graft repair for penetrating atherosclerotic ulcer in the infrarenal abdominal aorta.* J Vasc Surg, 2003. **38**(2): p. 383-8.
388. Buhk, J.H., et al., *Screening for atherosclerotic plaques in the abdominal aorta in high-risk patients with multicontrast-weighted MRI: a prospective study at 3.0 and 1.5 tesla.* Br J Radiol, 2011. **84**(1006): p. 883-9.
389. Tison, G.H., M.J. Blaha, and K. Nasir, *Atherosclerosis imaging in multiple vascular beds--enough heterogeneity to improve risk prediction?* Atherosclerosis, 2011. **214**(2): p. 261-3.
390. Raeeszadeh-Sarmazdeh, M., L.D. Do, and B.G. Hritz, *Metalloproteinases and Their Inhibitors: Potential for the Development of New Therapeutics.* Cells, 2020. **9**(5).
391. Raeeszadeh-Sarmazdeh, M., et al., *Engineering of tissue inhibitor of metalloproteinases TIMP-1 for fine discrimination between closely related stromelysins MMP-3 and MMP-10.* J Biol Chem, 2022. **298**(3): p. 101654.
392. Alferiev, I.S., et al., *Stent-Based Gene Delivery for Coronary Disease.* Methods Mol Biol, 2022. **2573**: p. 217-233.
393. Feldman, M.D., et al., *Stent-based gene therapy.* J Long Term Eff Med Implants, 2000. **10**(1-2): p. 47-68.
394. eliker, M.C., *Inhibition of Wilms' tumor growth by intramuscular administration of tissue inhibitor of metalloproteinases-4 plasmid DNA.* Oncogene, 2001.

395. Plump, A.S., et al., *Severe hypercholesterolemia and atherosclerosis in apolipoprotein E-deficient mice created by homologous recombination in ES cells.* Cell, 1992. **71**(2): p. 343-53.
396. Ishibashi, S., et al., *Massive xanthomatosis and atherosclerosis in cholesterol-fed low density lipoprotein receptor-negative mice.* J Clin Invest, 1994. **93**(5): p. 1885-93.
397. von Scheidt, M., et al., *Applications and Limitations of Mouse Models for Understanding Human Atherosclerosis.* Cell Metab, 2017. **25**(2): p. 248-261.
398. Campbell, I.C., et al., *Biomechanical modeling and morphology analysis indicates plaque rupture due to mechanical failure unlikely in atherosclerosis-prone mice.* Am J Physiol Heart Circ Physiol, 2013. **304**(3): p. H473-86.
399. Pasterkamp, G., et al., *Human Validation of Genes Associated With a Murine Atherosclerotic Phenotype.* Arterioscler Thromb Vasc Biol, 2016. **36**(6): p. 1240-6.
400. Kitami, T. and J.H. Nadeau, *Biochemical networking contributes more to genetic buffering in human and mouse metabolic pathways than does gene duplication.* Nat Genet, 2002. **32**(1): p. 191-4.
401. Peeney, D., et al., *Single cell profiling of the Timp gene family.* bioRxiv, 2021.

APPENDIX A

OFF TARGET EFFECT OF SM22α-CRE IN ATHEROSCLEROSIS MODEL

IMPLICATIONS OF SM22α-CRE EXPRESSION IN KERATINOCYTES AND UNANTICIPATED INFLAMMATORY SKIN LESION IN A MODEL OF ATHEROSCLEROSIS

Mei Hu, MD/MSc[1], Sho Hiroyasu, MD/PhD[2,3], David J. Granville, PhD[3], Zamaneh Kassiri, PhD[1]

[1] Department of Physiology, Cardiovascular Research Center, Faculty of Medicine and Dentistry, University of Alberta, Edmonton, AB, Canada

[2] Department of Dermatology, Osaka Metropolitan University Graduate School of Medicine, Osaka, Japan.

[3] ICORD Centre and Department of Pathology and Laboratory Medicine, Vancouver Coastal Health Research Institute, University of British Columbia, Vancouver, BC, Canada

Contributions:

MH: Conceived and designed experiments, performed all experiments on human specimens, performed all the in vivo and in vitro murine experiments, collected and analyzed the data, prepared figures, interpreted the results, wrote and revise manuscript, and responsed the reviewers.

SH: Contributed to data interpretation and edited the manuscript.

DJG: Contributed to data interpretation and edited the manuscript.

ZK: Corresponding author. Conceived hypothesis, analyzed data, wrote, and revised the manuscript.

***** A version of this section has been published. *Hu M, Hiroyasu S, Granville DJ, Kassiri Z. Implications of SM22α-Cre expression in keratinocytes and un-anticipated inflammatory skin lesions in a model of atherosclerosis. Am J Physiol Heart Circ Physiol. 2022 Aug 5. doi: 10.1152/ajpheart.00325.2022. Epub ahead of print. PMID: 35930445*.

Introduction

Atherosclerosis continues to be one of the leading risk factors for cardiovascular disease and stroke worldwide (1). Animal studies have been instrumental in unraveling the underlying mechanisms of atherosclerosis, however, many unanswered questions remain. Commonly used mouse models of atherosclerosis are mice lacking low-density lipoprotein receptor (*Ldlr*$^{-/-}$) or apolipoprotein E (*ApoE*$^{-/-}$) along with high fat or high cholesterol diet. This model can be used with various genetic modifications, for instance, whole body or cell-specific targeting of a gene of interest, or pharmacological treatments to understand the molecular and cellular mechanisms of atherosclerosis or associated arterial remodeling. Owing to the remarkable phenotypic plasticity, smooth muscle cells (SMCs) are considered to be the major source of the macrophage-like cells in the plaque and are recognized as an important contributor to plaque formation (10, 19).

Mice expressing Cre recombinase under the control of SMC promoters, *Sm22α* (*transgelin*) or *Mhy11* (myosin heavy chain-11), have been used to target the expression of the gene of interest. *Sm22α*-Cre driver has been reported to also express in other cell types, such as embryonic heart (13), myeloid cells (17), and perivascular adipocytes (18). However, this has not hindered investigators from continuing to use this SMC-driver mice in various studies (2, 4-7, 11, 14, 16) mainly because in most cases no side-effects presented. A disintegrin and metalloproteinase 17 (ADAM17) is a transmembrane proteinase with reported functions in vascular remodeling and pathologies (15, 16). In this study we report that deletion of ADAM17 in SMCs using the *Sm22α*-Cre driver in a model of hyperlipidemia and atherosclerosis (*Ldlr*$^{-/-}$/*Adam17*$^{fl/fl}$/*Sm22α*-Cre) resulted in severe skin lesions that prevented from completion of the study. We report a high level of expression of *Sm22α* in keratinocytes, which could explain the observed side-effect in the skin of these mice with hyperlipidemia.

Materials and Methods

Animals and treatment

Mice used for this study included male and female low-density lipoprotein receptor-deficient (*Ldlr*$^{-/-}$, Stock No: 002207), *Adam17*$^{flox/flox}$ (*Adam17*$^{fl/fl}$, Stock No: 009597), *Sm22α*-Cre (Stock No: 017491) and *Myh11*-CreER^{T2} (Stock No: 019079) purchased from The Jackson

Laboratory. *Myh11*-CreER^{T2} incorporates into the Y chromosome and therefore is only expressed in male mice. All mice are in C57Bl/6 background and were cross-bred to generate: *Ldlr*$^{-/-}$*/Adam17*^{Sm22Cre}, *Ldlr*$^{-/-}$*/Adam17*^{Myh11Cre}, *Ldlr*$^{-/-}$*/Adam17*$^{fl/fl}$, *Ldlr*$^{-/-}$, *Adam17*^{Sm22Cre}, and *Adam17*^{Myh11Cre}. The CreER^{T2}-recombinase was activated by tamoxifen (Sigma-Aldrich, olive oil as solvent) at 80 mg/kg/d, i.p. injection for 5 days starting at six weeks of age. At 8 weeks of age, mice started to receive a high fat diet (HFD) (# TD.88137 from Envigo) or continued to receive a regular laboratory diet for 12 weeks. All experiments were performed according to the guidelines of the University of Alberta Animal Care and Use Committee (ACUC) and the Canadian Council of Animal Care (CCAC).

Tissue collection, histology and immunofluorescence

Animals were euthanized after 3 months of HFD/chow feeding (or earlier if skin lesion was too severe to complete the 3-month period). The ventral and dorsal neck skin tissue were resected, and fixed (30% sucrose/ 4% paraformaldehyde solution) and embedded in paraffin, or frozen in optimal cutting temperature (OCT) medium for histological and immunofluorescent staining. Hematoxylin and eosin (H&E) staining and immuno-staining were performed on 5μm fixed tissue sections as described before (10). Primary antibodies targeting CD68 (MCA 5709, AbD Serotec; 1:50 dilution), SM22α (ab155272, Abcam; 1:100) and pan-keratin (ab8068, Abcam; 1:200) were used for immunofluorescence staining. Briefly, 5 μm cryosections (of skin) were used for the immunofluorescence staining. The cryosections were first fixed in 4% formaldehyde (20 mins, room temperature), permeabilized in 0.1% Triton-X100 (10 mins), blocked with 1% BSA (in 1× Tris-buffered saline with 0.1% Tween 20) for 1 hour, then incubated with the primary antibody (diluted in 1% BSA, overnight, 4°C), followed by incubation with fluorophore-conjugated secondary antibody (1 hour, room temperature). Counter-staining was done with Prolong Gold Antifade Reagent with DAPI (Invitrogen, P36935) to stain the nuclei. IgG isotype controls were used as negative control and no background signal was detected.

Beads-based multiplex cytokine protein array

Skin tissue from neck were send to Eve Technologies for the measurement of cytokine and chemokine profiles (MD31; Eve Technologies, Calgary, AB). Fluorescence intensity values were

recorded as relative fluorescent units (RFU) and converted to protein concentration (pg/ml) based on a protein standard linear curve consisting of purified cytokines at known concentrations included in each batch run. The individual cytokine/chemokine concentrations were further converted to pg per mg tissue protein.

Primary mouse keratinocytes and smooth muscle cell isolation and culture

Primary mouse keratinocytes were isolated from the tail skin of adult wild type mice described as before (12), and cultured in keratinocyte growth medium with defined growth supplements (dGS, Zenbio Advanced Cell Solution and Services) in collagen-coated culture plates.

Primary mouse aortic smooth muscle cells (SMCs) were isolated from wild type mice as described (15). The entire aorta was dissected, surrounding connective tissue was cleared, briefly incubated in digestion buffer (1×HBSS, 2 mg/ml BSA, 1 mg/ml collagenase type II, 0.774 U/ml elastase, and 1 mg/ml soybean trypsin inhibitor) at 37 °C to detach the adventitial layer from the medial layer. Next, the medial layer was cut into small pieces and further incubated in the digestion buffer (@37°C, 1.5 hours), the cell pellet was collected and resuspended in DMEM/F12 culture medium (Gibco™) supplemented with 10% fetal bovine serum (FBS, Gibco™), and plated on a gelatin-coated plates.

RNA extraction and quantitative real-time PCR

The total RNA was extracted from the keratinocytes and SMCs using TRIzol™ reagent according to the manufacturer's protocol. Quantitative TaqMan real time-PCR was carried out on a LightCycler 480 II system (Roche) using the LightCycler 480 Probes Master kit (Roche, 04887301001) and 18s was used as the housekeeping (internal control) gene. Primers for *Sm22α* (Assay ID: Mm00724260_g1) and *Myh11* (Assay ID: Mm00443013_m1) were purchased from Invitrogen. The gene expression levels were normalized to 18s expression for the corresponding samples and are presented as relative gene expression for each gene.

Statistics

All data were analyzed using IBM SPSS software (Version 21). Error bars represent the standard error of the mean. The Kolmogorov-Smirnov test was performed to test for normality.

Comparisons between any two groups were performed with the unpaired student's *t*-test. Comparison among multiple groups (>3) with two main factor (diet and genotype) was performed by two-way ANOVA followed by Bonferroni post-hoc test. Averaged values are presented as mean ± SEM. In the analysis of cytokine and chemokine profiles, each n value corresponds to an individual mouse. In TaqMan analyses, each n value corresponds to an independent experiment. *p* values of ≤0.05 were considered to indicate statistical significance.

Results

Ldlr$^{-/-}$/Adam17^{Sm22Cre} Mice Developed Unexpected Skin Lesions when Fed a High Fat Diet

To investigate the role of SMC ADAM17 in atherosclerosis *Ldlr$^{-/-}$/Adam17^{Sm22Cre}*, and parallel controls received regular chow or HFD for a 12-week period. However, after about 8 weeks of HFD, *Ldlr$^{-/-}$/Adam17^{SM22Cre}* mice started to exhibit severe skin lesions primarily in the dorsal and ventral regions of the neck which in some cases extended to the rump or to the face **(Figure 1Ai-ii)**. The affected mice failed to gain weighted (and had minimal plaque deposition) compared to other genotypes receiving the same HFD. This was likely due to the discomfort resulting from the skin lesions that interfered with their feeding. As such, they had to be terminated prior to the 12-week feeding endpoint. The histological analysis of the skin from these mice showed marked thickening of the epidermis and infiltration of a large number of inflammatory cells in the dermis **(Figure 1A-ii)**. The insets in Figure 1A show higher magnification images of the selected epidermis (cyan box) and dermis (green box) regions. This was observed in both, male and female *Ldlr$^{-/-}$/Adam17^{SM22Cre}* mice (~70% and 60% prevalence, respectively), compared to <10% of *Ldlr$^{-/-}$* mice that developed a very mild skin irritation (hair loss but skin remained intact without redness) which was not considered a morbidity by the Institutional Animal Care and Use Committee **(Figure 1B)**. Moreover, *Adam17* deletion in SMC by a different Cre driver, *Myh11*-Cre, did not have any adverse effects on *Ldlr$^{-/-}$/Adam17^{Myh11Cre}* mice did not develop skin lesions following 12 weeks of HFD **(Figure 1A-iii, 1B)**. Similarly, no skin lesion was observed in the HFD-fed mice of control genotypes (*Ldlr$^{-/-}$*, *Ldlr$^{-/-}$/Adam17$^{fl/fl}$*, *Adam17^{SM22Cre}*, or *Adam17^{Myh11Cre}*, data not shown).

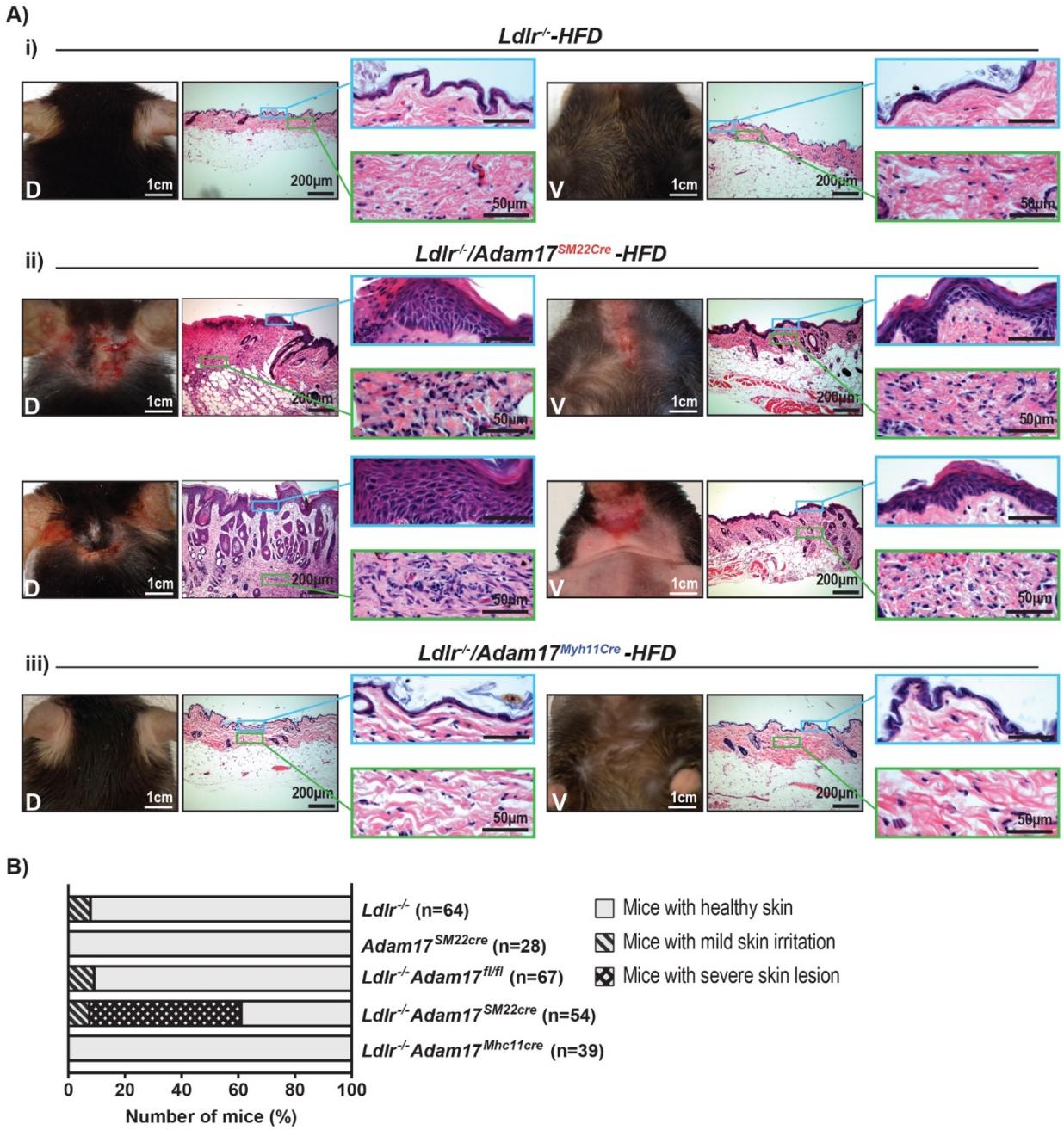

FIGURE 1. *LDLR*$^{-/-}$/*ADAM17*^{SM22CRE} MICE EXHIBIT SEVERE SKIN LESIONS FOLLOWING HIGH-FAT DIET (HFD) FEEDING. **A**: representative photographs and H&E-stained tissue sections of dorsal and ventral neck skin after 3 mo of HFD showing varying degrees of skin lesions in Ldlr-/-/Adam17SM22Cre mice (ii), but not in *Ldlr*$^{-/-}$ (i), and *Ldlr*$^{-/-}$/*Adam17*^{Mhy11Cre} (iii) mice. Higher magnification H&E images show increased epidermal thickness (cyan box) and abundant inflammatory cell infiltration in dermis (green box) in *Ldlr*$^{-/-}$/*Adam17*^{SM22Cre} mice, but not in *Ldlr*$^{-/-}$ mice and *Ldlr*$^{-/-}$/*Adam17*^{Mhy11Cre} mice. **B**: frequency of severe skin lesions (hair loss, redness, and broken skin barrier that led to termination of the animal) and mild skin irritation (hair loss, but intact skin barrier and no redness; did not require intervention) in mice of indicated genotypes following HFD. D, dorsal neck; H&E, hematoxylin and eosin; HFD, high-fat diet; V, ventral neck.

Severe Inflammation in the Skin from HFD-fed Ldlr$^{-/-}$*/Adam17*^{SM22Cre}

Immunofluorescent staining revealed a marked accumulation of macrophages in the epidermis and dermis of the HFD-fed *Ldlr*$^{-/-}$/*Adam17*^{SM22Cre} mice, which was not observed in the *Ldlr*$^{-/-}$ nor the *Ldlr*$^{-/-}$/*Adam17*^{Myh11Cre} following HFD **(Figure 2A)**. The extent of inflammation was further determined by measuring the protein levels of cytokines and chemokines in the skin tissue. Consistent with immunofluorescent staining, levels of inflammatory cytokines and chemokines: interleukins (IL-6, IL-17), TNFα (tumor necrosis factor-α), LIF (Leukemia inhibitory factor), CCL3 (Chemokine C-C motif ligand)-3, CCL11, C-X-C motif chemokine ligand (CXCL)-1 and CXCL2); IL-3 and IL-4 that are involved in the adaptive immune response, and colony-stimulating factors (CSFs), such as granulocyte CSF (G-CSF) and macrophage CSF (M-CSF), that are essential for the activity of monocyte- or macrophage-derived pro-inflammatory cytokines {Hamilton, 2008 #4481}, were elevated in the HFD-fed *Ldlr*$^{-/-}$/*Adam17*^{SM22Cre} mice but not in any other HFD-fed genotypes (*Ldlr*$^{-/-}$, *Adam17*^{SM22Cre} and *Ldlr*$^{-/-}$/*Adam17*$^{fl/fl}$) nor in any chow-fed group **(Figure 2A)**.

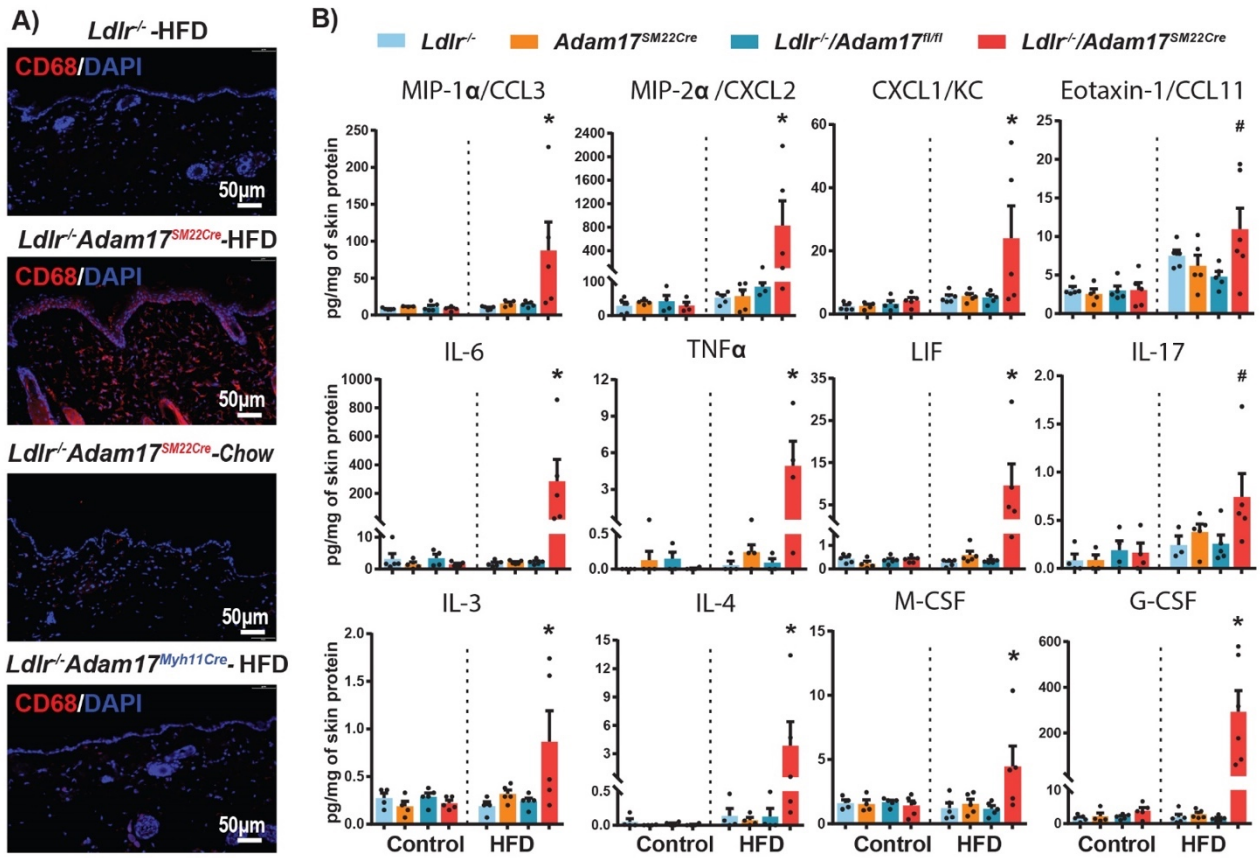

FIGURE 2. HEIGHTENED SKIN INFLAMMATION IN HIGH-FAT DIET (HFD)-FED *LDLR*$^{-/-}$/*ADAM17*^{SM22CRE} MICE.
A: immunostaining of neck skin tissue showing markedly higher population of macrophages (CD68, red) in *Ldlr*$^{-/-}$/*Adam17*^{SM22Cre} mice after HFD compared with the chow-fed mice of the same genotype and the other groups (n = 3

mice/group/genotype). **B**: cytokine protein levels in the skin (homogenate) from mice of indicated genotypes following regular laboratory diet (control) or high-fat diet (HFD). All averaged values are presented as means ± SE; n = 5 or 6 mice/group/genotype. * P<0.05 vs all group, # P<0.05 vs. control groups. Kolmogorov–Smirnov test was performed to test for normality of data. Two-way ANOVA followed by Bonferroni post hoc test was performed to determine statistical significance. CXCL1/KC, C-X-C motif chemokine ligand 1 or keratinocytes-derived chemokine; Eotaxin-1/CCL11, C-C motif chemokine 11 or eosinophil chemotactic protein; G/M-CSF, granulocyte/macrophage colony-stimulating factor; IL, interleukin; LIF, leukemia inhibitory factor; MIP-1/2α, macrophage inflammatory protein 1/2-α; TNF-α, tumor necrosis factor α.

SM22α is Highly Expressed in Keratinocytes

To investigate the mechanism underlying the off-target effect of *Sm22α* promoter under hyperlipidemic conditions we first examined expression of SM22α in the skin tissue. Immunofluorescent staining revealed that SM22α immunoreactivity was widely localized to the epidermal keratinocytes as the staining for SM22α and pan-keratin closely overlapped **(Figure 3A)**. To confirm the expression of *Sm22α* in keratinocytes, we used the in vitro primary culture of mouse keratinocytes and aortic SMCs and measured the expression of *Sm22α* compared to *Myh11*. We found that while both genes are expressed in SMCs, *Sm22α* shows a markedly higher expression in keratinocytes **(Figure 3B-i)**, while a significant ADAM17 expression is also detected in the keratinocytes compared to SMCs **(Figure 3B-ii)**.

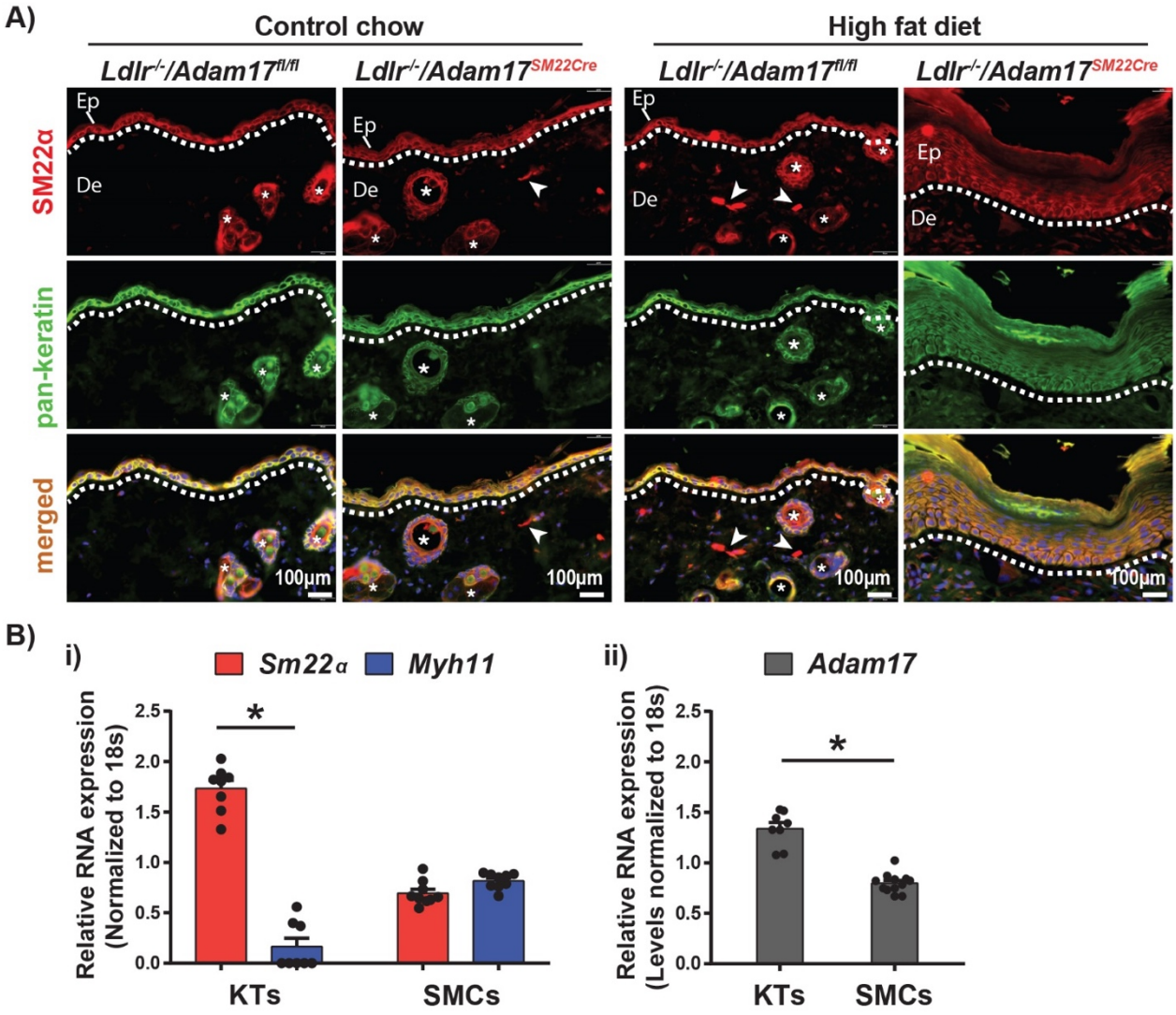

FIGURE 3. SM22A IS HIGHLY EXPRESSED IN MOUSE SKIN KERATINOCYTES.
A: coimmunostaining for SM22a and keratin in the skin tissue showing colocalization of SM22a (red) and pan-keratin (green) in indicated groups. White dotted line separates the epidermis (EP) and dermis (De); * hair follicles; arrows indicate arrector pili. n = 5 mice/genotype/group. **B**: TaqManmRNA expression of *Sm22a*, *Myh11* (i), and *Adam17* (ii) in keratinocytes (KTs) and smooth muscle cells (SMCs) from wild-type mice. All averaged values are presented as means ± SE. *P < 0.05 determined by unpaired Student's *t* test.

Discussion and Conclusion

Genetically modified mice have been valuable tools in uncovering the role of various proteins in different disease models. The cre-lox system has further allowed for investigating the cell-specific function of a gene and its corresponding protein in an organ physiology or pathology. The aortic wall is comprised of endothelial cells, smooth muscle cells and fibroblasts. Targeting ADAM17 in the SMCs has revealed novel functions for this ADAM in vascular physiology and

different pathologies (11, 15, 16). Therefore, although expression of *Sm22α* in cell types other than SMCs has been reported (3, 13, 17), SMC-targeted gene deletion using *Sm22α* -Cre mice has continued to be used, mainly because no detectable side effects that would interfere with a study has been reported. This is the first report demonstrating that *Sm22α* driven Adam17 deletion in SMCs led to severe skin lesions following HFD which significantly interfered with studying atherosclerosis in these mice and led to study disruption. This finding will be most valuable to investigators considering using *Sm22α*-Cre mice in atherosclerosis models.

Another experimental model for atherosclerosis is $ApoE^{-/-}$ mice and HFD. $ApoE^{-/-}$ mice are more susceptible to atherosclerotic plaque deposition compared to $Ldlr^{-/-}$ mice, and are often found to develop skin irritations following HFD feeding. However, this observation is significantly less prevalent in $Ldlr^{-/-}$ mice as we have found minimal skin irritations in these mice for up to 6 months of HFD feeding (10).

ADAM17 is a transmembrane proteinase with a diverse proteolytic substrate profile. Keratinocyte-specific *Adam17*-deficiency ($Adam17^{flox/flox}$/*Krt14*-Cre) impaired the epidermal barrier resulting in chronic dermatitis and heightened epidermal inflammation in adult mice (8). This was linked to the reduced ADAM17-mediated shedding of transforming growth factor-alpha, and reduced activity of epidermal growth factor receptor (EGFR) and its downstream signaling pathway since mice with keratinocyte loss of EGFR exhibited the same phenotype (8). The detected high levels of *Sm22a* expression in keratinocytes indicates that *Sm22a*-drived *Adam17* loss resulted in a significant *Adam17* loss in keratinocytes. In our study, the epidermal lesion in *Sm22α*-drived *Adam17*-deficient mice became evident following HFD, suggesting that a secondary trigger was required for the manifestation of this side-effect in $Ldlr^{-/-}/Adam17^{SM22Cre}$ mice. Importantly, *Adam17* deletion in SMC by a different driver, *Myh11*-Cre, with very low expression in keratinocytes, did not result in skin lesions following HFD. Therefore, the epidermal lesions $Ldlr^{-/-}/Adam17^{SM22Cre}$ mice are not due to ADAM17 loss in SMCs, but due to its loss in keratinocytes.

In summary, despite the non-specific expression pattern of *Sm22a*-Cre driver, no reports of significant side-effects have been reported to date, and therefore, the *Sm22a*-Cre driver mouse continues to be used in various studies. Here, we report that the high expression of *Sm22a* in

keratinocytes can lead to severe epidermal side-effects when studying proteins with potential roles in keratinocytes, which can lead to study disruption.

References

1. Bjorkegren JLM, and Lusis AJ. Atherosclerosis: Recent developments. *Cell* 185: 1630-1645, 2022.
2. Cai Z, Ding Y, Zhang M, Lu Q, Wu S, Zhu H, Song P, and Zou MH. Ablation of Adenosine Monophosphate-Activated Protein Kinase alpha1 in Vascular Smooth Muscle Cells Promotes Diet-Induced Atherosclerotic Calcification In Vivo. *Circ Res* 119: 422-433, 2016.
3. Chakraborty R, Saddouk FZ, Carrao AC, Krause DS, Greif DM, and Martin KA. Promoters to Study Vascular Smooth Muscle. *Arterioscler Thromb Vasc Biol* 39: 603-612, 2019.
4. Colijn S, Muthukumar V, Xie J, Gao S, and Griffin CT. Cell-specific and athero-protective roles for RIPK3 in a murine model of atherosclerosis. *Dis Model Mech* 13: 2020.
5. Ding Y, Zhang M, Zhang W, Lu Q, Cai Z, Song P, Okon IS, Xiao L, and Zou MH. AMP-Activated Protein Kinase Alpha 2 Deletion Induces VSMC Phenotypic Switching and Reduces Features of Atherosclerotic Plaque Stability. *Circ Res* 119: 718-730, 2016.
6. Doddapattar P, Dev R, Jain M, Dhanesha N, and Chauhan AK. Differential Roles of Endothelial Cell-Derived and Smooth Muscle Cell-Derived Fibronectin Containing Extra Domain A in Early and Late Atherosclerosis. *Arterioscler Thromb Vasc Biol* 40: 1738-1747, 2020.
7. Doring Y, Noels H, van der Vorst EPC, Neideck C, Egea V, Drechsler M, Mandl M, Pawig L, Jansen Y, Schroder K, Bidzhekov K, Megens RTA, Theelen W, Klinkhammer BM, Boor P, Schurgers L, van Gorp R, Ries C, Kusters PJH, van der Wal A, Hackeng TM, Gabel G, Brandes RP, Soehnlein O, Lutgens E, Vestweber D, Teupser D, Holdt LM, Rader DJ, Saleheen D, and Weber C. Vascular CXCR4 Limits Atherosclerosis by Maintaining Arterial Integrity: Evidence From Mouse and Human Studies. *Circulation* 136: 388-403, 2017.
8. Franzke CW, Cobzaru C, Triantafyllopoulou A, Loffek S, Horiuchi K, Threadgill DW, Kurz T, van Rooijen N, Bruckner-Tuderman L, and Blobel CP. Epidermal ADAM17 maintains the skin barrier by regulating EGFR ligand-dependent terminal keratinocyte differentiation. *J Exp Med* 209: 1105-1119, 2012.
9. Hamilton JA. Colony-stimulating factors in inflammation and autoimmunity. *Nat Rev Immunol* 8: 533-544, 2008.

10. Hu M, Jana S, Kilic T, Wang F, Shen M, Winkelaar G, Oudit GY, Rayner K, Zhang DW, and Kassiri Z. Loss of TIMP4 (Tissue Inhibitor of Metalloproteinase 4) Promotes Atherosclerotic Plaque Deposition in the Abdominal Aorta Despite Suppressed Plasma Cholesterol Levels. *Arterioscler Thromb Vasc Biol* 41: 1874-1889, 2021.
11. Kawai T, Takayanagi T, Forrester SJ, Preston KJ, Obama T, Tsuji T, Kobayashi T, Boyer MJ, Cooper HA, Kwok HF, Hashimoto T, Scalia R, Rizzo V, and Eguchi S. Vascular ADAM17 (a Disintegrin and Metalloproteinase Domain 17) Is Required for Angiotensin II/beta-Aminopropionitrile-Induced Abdominal Aortic Aneurysm. *Hypertension* 70: 959-963, 2017.
12. Li FW, Adase CA, and Zhang LJ. Isolation and Culture of Primary Mouse Keratinocytes from Neonatal and Adult Mouse Skin. *Jove-J Vis Exp* 2017.
13. Li L, Miano JM, Cserjesi P, and Olson EN. SM22 alpha, a marker of adult smooth muscle, is expressed in multiple myogenic lineages during embryogenesis. *Circ Res* 78: 188-195, 1996.
14. Osonoi Y, Mita T, Azuma K, Nakajima K, Masuyama A, Goto H, Nishida Y, Miyatsuka T, Fujitani Y, Koike M, Mitsumata M, and Watada H. Defective autophagy in vascular smooth muscle cells enhances cell death and atherosclerosis. *Autophagy* 14: 1991-2006, 2018.
15. Shen M, Hu M, Fedak PWM, Oudit GY, and Kassiri Z. Cell-Specific Functions of ADAM17 Regulate the Progression of Thoracic Aortic Aneurysm. *Circ Res* 123: 372-388, 2018.
16. Shen M, Morton J, Davidge ST, and Kassiri Z. Loss of smooth muscle cell disintegrin and metalloproteinase 17 transiently suppresses angiotensin II-induced hypertension and end-organ damage. *J Mol Cell Cardiol* 103: 11-21, 2017.
17. Shen Z, Li C, Frieler RA, Gerasimova AS, Lee SJ, Wu J, Wang MM, Lumeng CN, Brosius FC, 3rd, Duan SZ, and Mortensen RM. Smooth muscle protein 22 alpha-Cre is expressed in myeloid cells in mice. *Biochem Biophys Res Commun* 422: 639-642, 2012.
18. Sui Y, Park SH, Xu J, Monette S, Helsley RN, Han SS, and Zhou C. IKKbeta links vascular inflammation to obesity and atherosclerosis. *J Exp Med* 211: 869-886, 2014.
19. Wang Y, Dubland JA, Allahverdian S, Asonye E, Sahin B, Jaw JE, Sin DD, Seidman MA, Leeper NJ, and Francis GA. Smooth Muscle Cells Contribute the Majority of Foam Cells in ApoE (Apolipoprotein E)-Deficient Mouse Atherosclerosis. *Arterioscler Thromb Vasc Biol* 39: 876-887, 2019.

APPENDIX B

FUNCTION OF TGFβ RECEPTOR IN THE VEIN IS NOT IN VAIN

FUNCTION OF TGF β (TRANSFORMING GROWTH FACTOR-β) RECEPTOR IN VEIN IS NOT IN VAIN

Mei Hu[1], Zamaneh Kassiri[1]

[1] Department of Physiology, Cardiovascular Research Center, University of Alberta, Edmonton, AB, Canada

* A version of this section has been published. *Hu M, Kassiri Z. Function of TGFβ (Transforming Growth Factor-β) Receptor in the Vein Is Not in Vain. Arterioscler Thromb Vasc Biol. 2022 Jul;42(7):884-885. doi: 10.1161/ATVBAHA.122.317861. Epub 2022 May 26. PMID: 35616032.*

Hemodialysis is a critical procedure in patients with renal failure. An arteriovenous fistula (AVF) is created to gain vascular access that can be repetitively used for effective and efficient hemodialysis. Subsequent to AVF formation, the vein undergoes maturation and structural remodeling that accommodates sufficient blood flow during dialysis and repetitive access. Maturation failure of AVF, or excess remodeling of the venous wall causing stenosis, are significant causes of morbidity and hospitalization in dialysis patients. This prompts the need for understanding the cellular and molecular mechanism underlying the AVF maturation process.

In this issue of Arteriosclerosis, Thrombosis, and Vascular Biology, Taniguchi *et al.* [ref] report that targeting the TGFβ pathway can improve AVF patency. This study disrupted the TGFβ pathway by a pharmacological agent, and by implementing cell specific deletion of TGFβ receptor in smooth muscle cells (SMCs, *Tgfbr2*$^{flx/flx}$/*Myh11-CreER*^{T2}) or endothelial cells (ECs, *Tgfbr2*$^{flx/flx}$/*Cdh5-CreER*^{T2}) **(Figure 1)**. Pharmacological inhibition of TGFβ receptor (TGFBR) improved overall remodeling of the vein and improved patency of the AVF as assessed by ultrasound, although the long-term functional efficacy of the fistula, with repeated vascular access, was not assessed. This study further identifies the ECs as a more effective target for inhibition of TGFβ pathway compared to SMCs since deletion of TGFBR2 in ECs suppressed SMC proliferation, collagen deposition, medial wall thickness and improved outward remodeling, whereas in SMCs, TGFBR2 deletion only reduced collagen synthesis without decreasing SMC proliferation nor wall thickness. AVF stenosis has been linked to neointimal hyperplasia, characterized by excessive accumulation of SMCs and extracellular matrix (ECM), and/or inadequate outward remodeling of the venous wall.[1] The findings by Taniguchi et al. also suggest an important paracrine function of TGFβ pathway such that its inhibition in ECs can regulate proliferation and function of SMCs. The underlying mechanism of this paracrine function of TGFβ receptor requires further investigation.

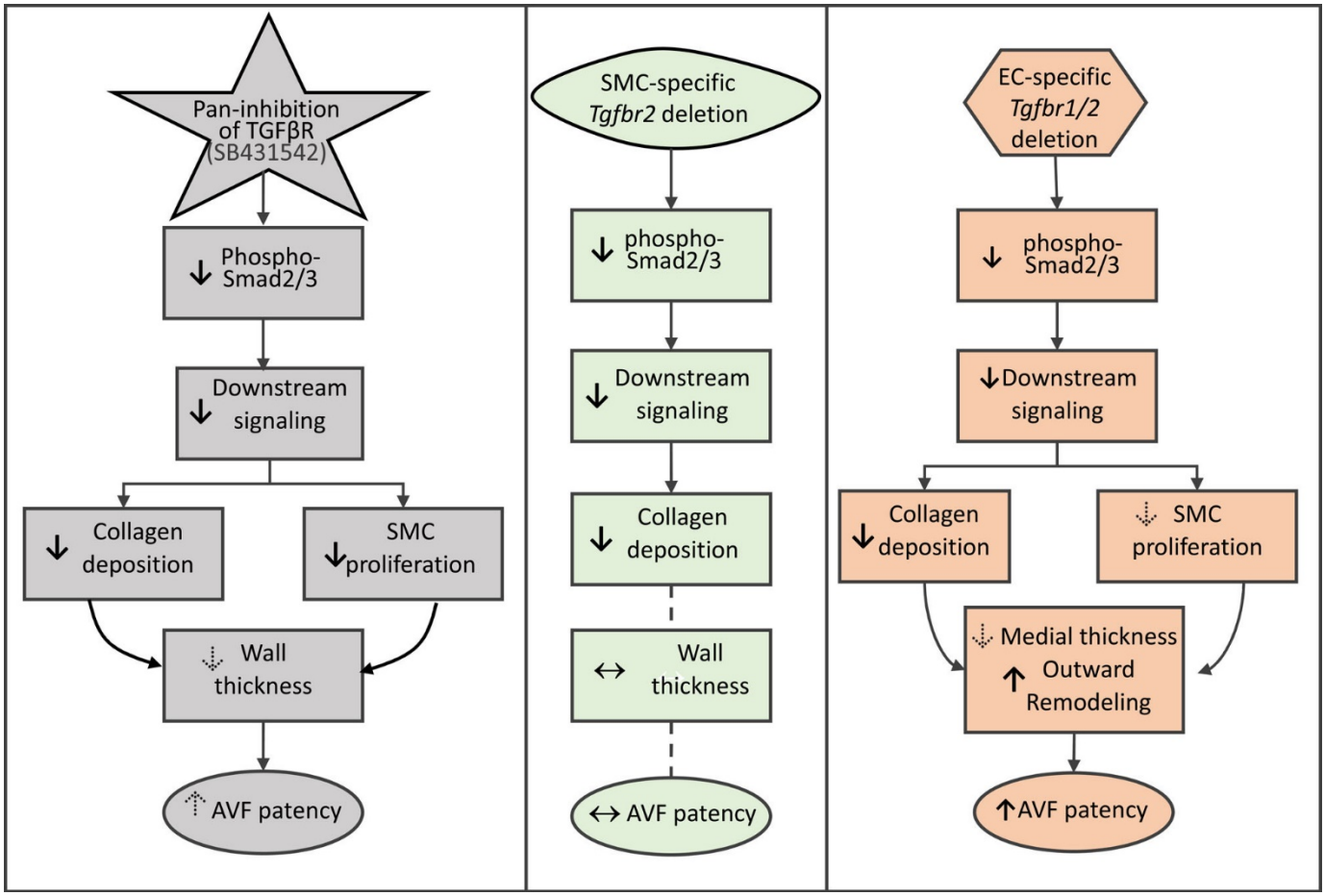

Figure. Pharmacological and cell-specific inhibition of TGFβ (transforming growth factor β) receptors, in smooth muscle cells (SMCs) or endothelial cells (ECs) in remodeling of venous wall in arteriovenous fistula (AVF). The dotted arrows show where there was an increase or decrease but it did not reach statistical significance.

TGFβ is a well-studied anti-inflammatory cytokine best known for its pro-fibrotic functions, and has also been reported to be important in a number of vascular pathologies such as aortic aneurysm,[2, 3] atherosclerosis,[4] and vein graft remodeling,[5] while TGFβ expression is increased in both mouse and human AVF.[6-8] Bioavailability of TGFβ (ligand) involves a number of steps including synthesis by various cells (primarily fibroblasts and smooth muscle cells), release into the extracellular space non-covalently bound to LAP (latency associated proprotein) forming the small latent complex (SLC), which is sequestered in the extracellular matrix bound to LTBP (latent TGFβ-binding protein) forming the large latent complex (LLC). Activation of the latent TGFβ requires cleavage of the LTBP by a proteinase, usually a matrix metalloproteinase (MMP), release of SLC and subsequently the release of the TGFβ dimer that binds to TGFβ receptor II (TGFBR2) triggering its dimerization with TGFBR1 and activation of the downstream pathways, the canonical

Smad 2/3 pathway, or the non-canonical MAPK pathway through TGFβ-activated Kinase (TAK-1).[9] In the study by Taniguchi *et al*, authors targeted the TGFβ receptor, rather than its ligand (TGFβ) which can be a more direct approach in disrupting the TGFβ-mediated pathways. However, it is important to note that other ligands, including bone morphogenic proteins (BMPs) and activin, that are members of the TGFβ superfamily, can also bind to and activate the TGFβ receptor. As such, the impact of targeting TGFBR2 may not be limited to inhibition of TGFβ pathway. This is not necessarily a limitation of this study, but could imply involvement of other molecules in addition to TGFβ.

Taniguchi *et al.* identify the ECs as the key cell type in regulating venous remodeling in an AVF. Using a similar mouse AVF model, an earlier study reported that AVF formation resulted in a significant increase in the vein due to its exposure to the aortic flow.[10] Exposure of mouse ECs to laminar shear stress equivalent to that in the arterial flow increased activation of the non-canonical TGFβ signaling pathway including phosphorylation of TGFβ–activated kinase 1 (TAK1).[11] These studies further support the involvement of the TGFβ pathway in AVF maturation, although through the non-canonical pathway downstream of TGFβ receptors rather than the canonical Smad2/3 pathway reported by Taniguchi *et al*.

In summary, the study by Taniguchi *et al.* provides evidence on how disruption of the TGFBR2-related signaling pathway in ECs can positively impact venous remodeling in the AVF. Therefore, targeted drug delivery to inhibit TGFBR2 in ECs at the AVF site could be a viable treatment option for dialysis patients. However, AVF is created in patients with renal failure who often suffer from uremia that itself can cause vascular complications, such as calcification, and as such the beneficial impact of TGFBR2 inhibition in AVF stability should be confirmed in the presence of co-morbidities such as uremia.

This study was supported by Project Grant from Canadian Institute for Health Research (PJT- 153306) to Z.K.

References

1. Viecelli AK, Mori TA, Roy-Chaudhury P, Polkinghorne KR, Hawley CM, Johnson DW, Pascoe EM and Irish AB. The pathogenesis of hemodialysis vascular access failure and systemic therapies for its prevention: Optimism unfulfilled. *Semin Dial*. 2018;31:244-257.

2. Shen M, Lee J, Basu R, Sakamuri SS, Wang X, Fan D and Kassiri Z. Divergent roles of matrix metalloproteinase 2 in pathogenesis of thoracic aortic aneurysm. *Arterioscler Thromb Vasc Biol*. 2015;35:888-898.

3. Lareyre F, Clement M, Raffort J, Pohlod S, Patel M, Esposito B, Master L, Finigan A, Vandestienne M, Stergiopulos N, Taleb S, Trachet B and Mallat Z. TGFbeta (Transforming Growth Factor-beta) Blockade Induces a Human-Like Disease in a Nondissecting Mouse Model of Abdominal Aortic Aneurysm. *Arterioscler Thromb Vasc Biol*. 2017;37:2171-2181.

4. Chen PY, Qin L, Li G, Wang Z, Dahlman JE, Malagon-Lopez J, Gujja S, Cilfone NA, Kauffman KJ, Sun L, Sun H, Zhang X, Aryal B, Canfran-Duque A, Liu R, Kusters P, Sehgal A, Jiao Y, Anderson DG, Gulcher J, Fernandez-Hernando C, Lutgens E, Schwartz MA, Pober JS, Chittenden TW, Tellides G and Simons M. Endothelial TGF-beta signalling drives vascular inflammation and atherosclerosis. *Nat Metab*. 2019;1:912-926.

5. Cooley BC, Nevado J, Mellad J, Yang D, St Hilaire C, Negro A, Fang F, Chen G, San H, Walts AD, Schwartzbeck RL, Taylor B, Lanzer JD, Wragg A, Elagha A, Beltran LE, Berry C, Feil R, Virmani R, Ladich E, Kovacic JC and Boehm M. TGF-beta signaling mediates endothelial-to-mesenchymal transition (EndMT) during vein graft remodeling. *Sci Transl Med*. 2014;6:227ra234.

6. Stracke S, Konner K, Kostlin I, Friedl R, Jehle PM, Hombach V, Keller F and Waltenberger J. Increased expression of TGF-beta1 and IGF-I in inflammatory stenotic lesions of hemodialysis fistulas. *Kidney Int*. 2002;61:1011-1019.

7. Ikegaya N, Yamamoto T, Takeshita A, Watanabe T, Yonemura K, Miyaji T, Ohishi K, Furuhashi M, Maruyama Y and Hishida A. Elevated erythropoietin receptor and transforming growth factor-beta1 expression in stenotic arteriovenous fistulae used for hemodialysis. *J Am Soc Nephrol*. 2000;11:928-935.

8. Cai C, Kilari S, Singh AK, Zhao C, Simeon ML, Misra A, Li Y and Misra S. Differences in Transforming Growth Factor-beta1/BMP7 Signaling and Venous Fibrosis Contribute to Female Sex Differences in Arteriovenous Fistulas. *J Am Heart Assoc*. 2020;9:e017420.

9. Takawale A, Sakamuri SS and Kassiri Z. Extracellular matrix communication and turnover in cardiac physiology and pathology. *Compr Physiol*. 2015;5:687-719.

10. Yamamoto K, Protack CD, Tsuneki M, Hall MR, Wong DJ, Lu DY, Assi R, Williams WT, Sadaghianloo N, Bai H, Miyata T, Madri JA and Dardik A. The mouse aortocaval fistula recapitulates human arteriovenous fistula maturation. *Am J Physiol Heart Circ Physiol*. 2013;305:H1718-1725.
11. Hu H, Lee SR, Bai H, Guo J, Hashimoto T, Isaji T, Guo X, Wang T, Wolf K, Liu S, Ono S, Yatsula B and Dardik A. TGFbeta (Transforming Growth Factor-Beta)-Activated Kinase 1 Regulates Arteriovenous Fistula Maturation. *Arterioscler Thromb Vasc Biol*. 2020;40:e203-e213.